Axially and Peripherally Substituted Phthalocyanine and Azaphthalocyanine Complexes for Heterojunction Design

Dissertation

zur

Erlangung des Doktorgrades der Naturwissenschaften

(Dr. rer. nat.)

dem

Fachbereich Chemie

Philipps-Universität Marburg

vorgelegt von

Ahmed Bayoumi Mohamed Ibrahim (M.Sc.)

aus

Assiut, Ägypten

Marburg 2015

Vom Fachbereich Chemie der Philipps-Universität Marburg (Hochschulkennziffer 1180) als Dissertation angenommen

Erstgutachter: Prof. Dr. Jörg Sundermeyer

Zweitgutachter: Prof. Dr. Stefanie Dehnen

Tag der Disputation: 04.05.2015

Vom Fachbereich Chemie

Der Philipps-Universität Marburg

angenommen am: 07.04.2015

Acknowledgement

I dedicate this thesis to my father:
To whom I owe being who I am

Posters and an oral lecture belong to this work

Posters

1. Highly Soluble Isomerically Pure Metalloazaphthalocyanines [Ppz*MX$_n$] of the 3d Metals, YoungChem2013 in Poznan (Poland), 9-13th October 2013.

2. Ahmed B. Ibrahim, Christian Prinzisky, Lars H. Finger, Jörg Sundermeyer, Highly Soluble Metallophthalocyanines [Pc*MX$_n$] of the 3d Metals, the Royal Australian Chemical Institute's Inorganic Chemistry Divisional conference in Brisbane (Australia), 8-12th December 2013.

3. Ahmed B. Ibrahim, Christian Prinzisky, Jörg Sundermeyer, Synthesis, Structural Characterization and Electrochemistry of Highly Soluble Phthalocyanines, 5th EuCheMS in Istanbul (Turkey), 31st August – 4th September (2014).

4. Ahmed B. Ibrahim, Lars H. Finger, Jörg Sundermeyer, A New series of highly soluble Pyrazinoporphyrazines: Structural Characterization and Electrochemistry, YoungChem2014 in Szczecin (Poland), 8-12th October 2014.

Lecture

1. Axially and peripherally substituted phthalocyanine and azaphthalocyanine complexes for heterojunction design of different electronic systems, The European Yousef Jameel Summer School (Cardiff, 23rd June 2014)

Zusammenfassung

Es war das Ziel dieser Arbeit, neue Phthalocyanine und Pyrazinoporphyrazine mit Hauptgruppenelementen und Übergangsmetallen als Zentralatom zu synthetisieren. Die konformative Starrheit und sterische Hinderung ihrer peripher angeordneten Cyclohexen-Ringe führen zu einem tendenziell verringerten Aggregationsausmaß und erhöhen somit die Löslichkeit dieser 42 π – Hückel aromatischen Systeme ohne ihre Tendenz zur Bildung kristalliner Phasen zu beeinträchtigen. Bei Zentralmetallen mit einem Oxidationszustand > II wurde untersucht, ob anionische axiale Liganden L_{ax} am Metallzentrum eingebracht werden können. Die optischen Eigenschaften dieser Chromophore wurden untersucht. Zusätzlich zu ihrer hohen Löslichkeit konnten einige der synthetisierten Chromophore sublimiert werden. Phthalocyanine und verwandte Verbindungen sind interessante Materialien für optoelektronische Anwendungen. Daher wird ein Überblick über eine Studie der elektronischen HOMO und LUMO Anpassung und Kopplung dieser neuen Chromophore an Heterogrenzflächen gegeben.

[Pc*ML$_{ax}$]   [Ppz*ML$_{ax}$]
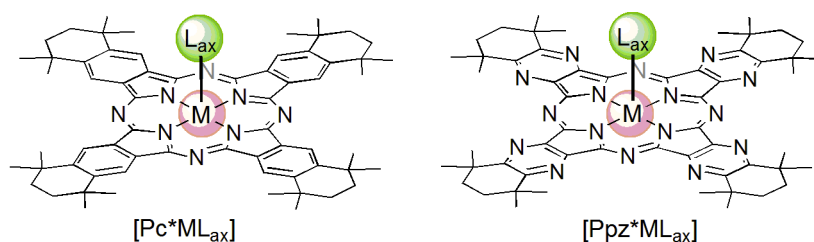
Die Synthese von vier substituierten Phthalonitrilen und Pyrazin-Dinitrilen als chromophore Bausteine wird diskutiert.

PDN*   PzDN*   PzDN#   CatPzDN*
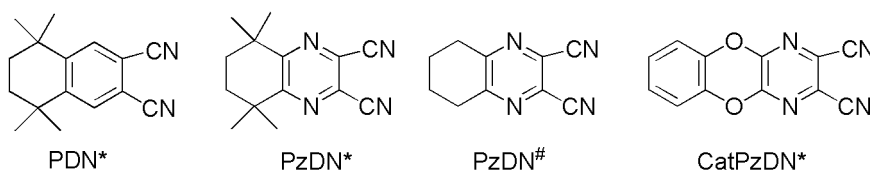
Während CatPzDN* nicht tetramerisiert, ist der Nutzen von PzDn# stark begrenzt durch die geringen Ausbeuten und geringe Löslichkeit seiner Komplexe. Die Verwendung von PDN* und PzDN* als Vorstufen führte dagegen zur Bildung sehr gut löslicher Makrozyklen, die durch ^{1}H-NMR- und manchmal durch ^{13}C-NMR-Spektroskopie analysiert werden konnten. Darüber hinaus erleichtert die Isomerenreinheit der Chromophore ihre Kristallisierung und die Analyse ihrer Kristallstrukturen.

3d Metallkomplexe

Mit Ausnahme von Scandium wurden Pc*-/Ppz*-Komplexe mit allen 3d-Elementen hergestellt:
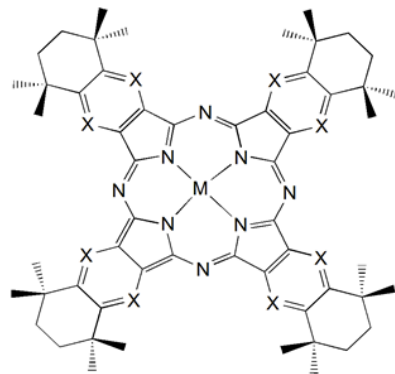
X=CH	X=N
[Pc*TiO]	[Ppz*TiO]
[Pc*VO]	[Ppz*VO]
[Pc*Cr]	[Ppz*Cr]
[Pc*CrCl]	[Ppz*CrCl]
[Pc*MnCl]	[Ppz*MnCl]
[Pc*Fe]	[Ppz*Fe]
[Pc*FeCl]	[Ppz*FeCl]
[Pc*Co]	[Ppz*Co]
[Pc*Ni]	[Ppz*Ni]
[Pc*Cu]	[Ppz*Cu]
[Pc*Zn]	[Ppz*Zn]

Bei Pc*- und Ppz*-Komplexen mit Chrom und Eisen konnte das Metallzentrum entweder mit der Oxidationsstufe II oder III eingefügt werden. Ausgenommen von [Pc*Fe] und [Pc*FeCl] sind alle anderen 3d-Metallkomplexe sehr luft- und lichtstabil. Die metallfreien Liganden (Pc*H$_2$ und Ppz*H$_2$) sowie die Kupferkomplexe ([Pc*Cu] und [Ppz*Cu]) konnten ohne Zersetzung sublimiert werden. Die Metallkomplexe wurden vollständig charakterisiert und von den 3d-Metallkomplexen wurden die molekularen und die Gitterstrukturen von sechs Chromophoren bestimmt. Repräsentative Molekül- und Gitter-Strukturen werden unten gezeigt:
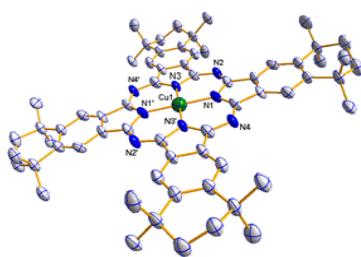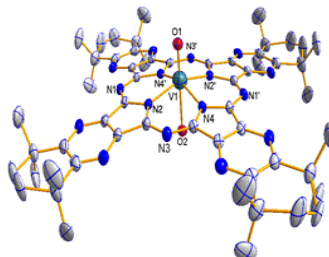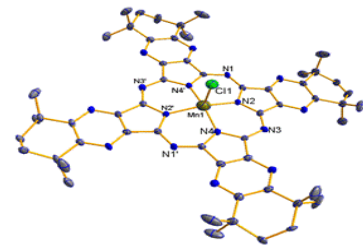
[Pc*Cu]　　　　　　[Ppz*VO(OH$_2$)]　　　　　　[Ppz*MnCl]
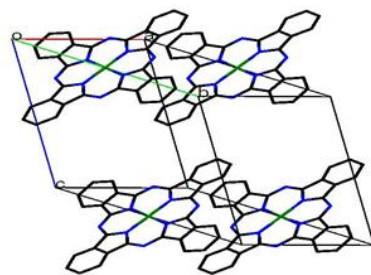
Gitter-Strukturen　　　　[Pc*Co]　　　　　　[Ppz*VO(OH$_2$)]
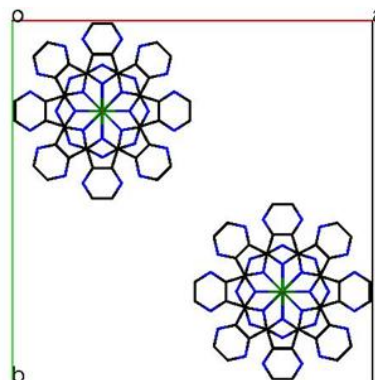
Während [Pc*VO] Wasser nicht koordiniert, stellte sich heraus, dass das korrespondierende [Ppz*VO] einen Aqualiganden in einem oktaedrisch konfigurierten Komplex koordiniert. Dies resultiert aus der geringeren Lewis-Säurestärke des Pc*-Komplexes verglichen mit der des Ppz*-Gegenstücks. Um zwischen dem d^1-Komplex [Ppz*VO(OH$_2$)] und dem d^0-Komplex [Ppz*VO(OH)] zu unterscheiden, wurden die paramagnetischen Eigenschaften des Komplexes durch SQUID-Untersuchungen bestätigt, und es zeigte sich, dass die magnetische Suszeptibilität des Komplexes temperaturabhängig ist.
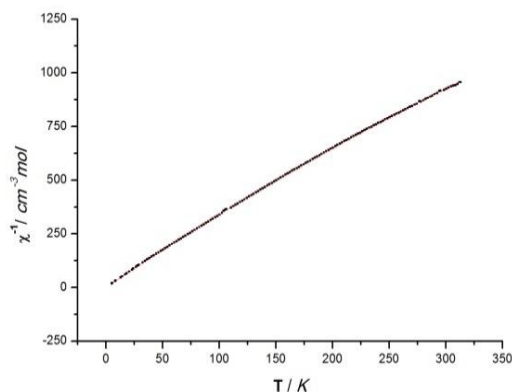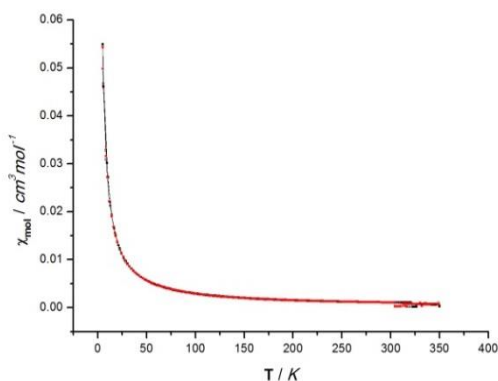
Wegen des größeren HOMO-LUMO Abstands bei Ppz*-Komplexen verglichen mit den Pc*-Gegenstücken zeigten die Pc*-Komplexe rot verschobene Q-Banden. Die Q-Bandenergien der 3d-Metallkomplexe folgen nahezu dem Trend Mn > Ti ≈ V > Cr > Zn ≈ Cu > Co ≈ Ni ≈ Fe. Die Lagen der Q-Absorptionsbanden bei Pc*/Ppz* mit Cr und Fe werden nicht durch die

Metalloxidationsstufe beeinflusst. Jedoch wird eine breite, schwache Bande, die in den Spektren von [Pc*FeCl] und [Ppz*FeCl] bei 878 nm beobachtet wurde und Ladungs-transferübergängen von $a_{lu}(\pi)$ oder $a_{2u}(\pi)$ auf $e_g(d_{\pi*})$ bei high-spin Eisen (III)-Komplexen zugerechnet wird, dazu verwendet zwischen, den Fe(II)- und den Fe(III)-Komplexen zu unterscheiden.
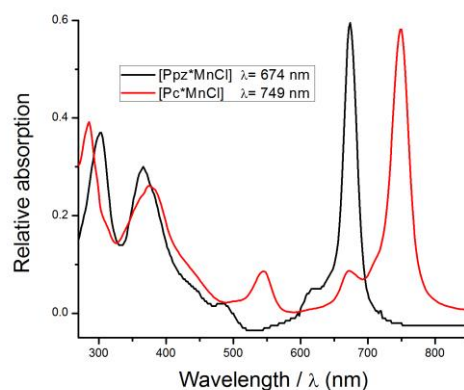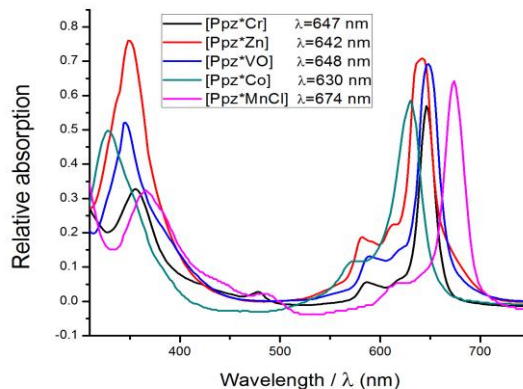
Komklexe von Hauptgruppenelementen (Gruppe 13 & 14)

Die Pc*-/Ppz*-Komplexe der Gruppe-13- (Al, Ga und In) und Gruppe-14-Elemente (Si und Ge) wurden ebenfalls hergestellt und vollständig charakterisiert. Lösungen von [Pc*InCl] sind lichtempfindlich und zerfallen bei Licht schnell, während die anderen Komplexe eine hohe Stabilität aufweisen.

X=CH	X=N
[Pc*AlCl]	[Ppz*AlCl]
[Pc*AlF]	[Ppz*AlF]
[Pc*GaCl]	[Ppz*GaCl]
[Pc*GaMe]	[Ppz*InCl]
[Pc*Ga(n-butyl)]	[Ppz*SiCl$_2$]
[Pc*Ga(n-hexyl)]	[Ppz*Ge(OH)$_2$]
[Pc*GaPh]	
[Pc*InCl]	

Bei Gruppe-13 und weiterem Vorrücken zu schwereren Atomen (Al→Ga→In) wurde eine Rotverschiebung der Q-Bande beobachtet; dies könnte der geringeren Lewis-Säurestärke der Gruppe-13-Elemente in dieser Sequenz zugeschrieben werden. Jedoch wird im Falle von Si- und Ge-Komplexen ein gegenteiliger Trend beobachtet, d. h. die Q-Bande von [Ppz*Ge(OH)$_2$] zeigt eine Blauverschiebung verglichen mit der von [Ppz*SiCl$_2$]. Es wird angenommen, dass verschiedene strukturelle Konfigurationen der beiden Komplexe für den umgekehrten Trend verantwortlich sind: Chemisch nicht äquivalente Methyl- und Methylenprotonen wurden im ^{1}H-NMR-Spektrum von *cis*-[Ppz*Ge(OH)$_2$] beobachtet, was auf einen Komplex mit einem stärker verzerrten π-System hinweist, während [Ppz*SiCl$_2$] äquivalente Protonen (1a/b und 2a/b) in Übereinstimmung mit einem *trans*-Komplex mit einem absolut planaren aromatischen System zeigt.
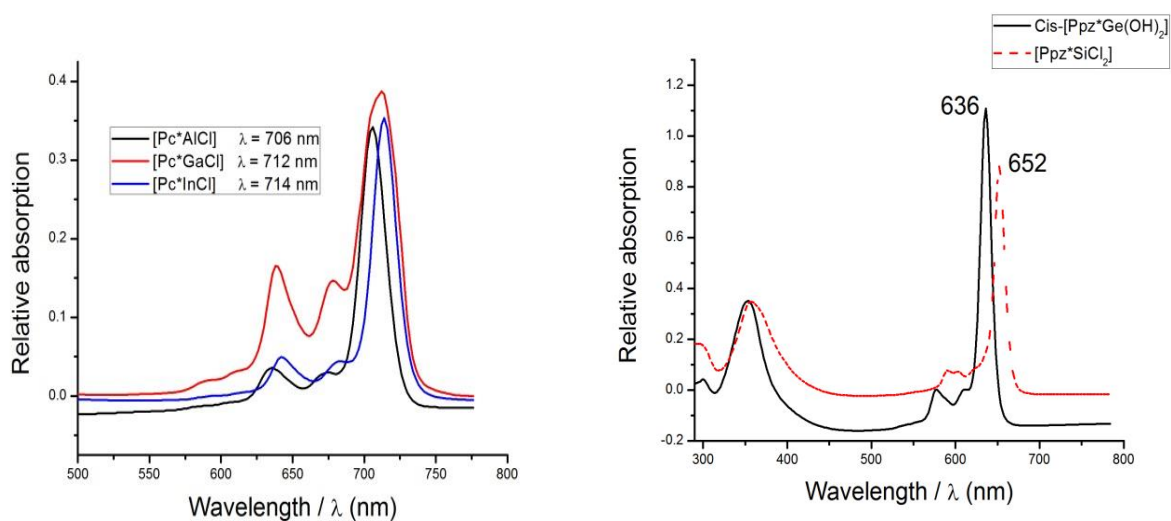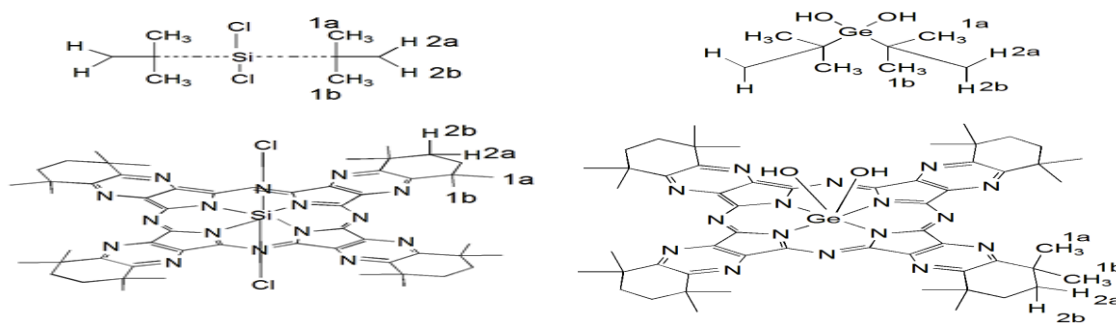
Die M-Cl Bindungen bei [Pc*AlCl]- und [Pc*GaCl]-Komplexen stellten sich als reaktionsfreudiger als die der Ppz*-Gegenstücke heraus. Während APCI⁺-MS-Messungen von [Ppz*AlCl] und [Ppz*GaCl] aus THF-Lösungen die erwarteten Molkülionen [MH]⁺ zeigten, wiesen die zugehörigen [Pc*AlCl]- und [Pc*GaCl]-Verbindungen Pseudo-Molekülionen [PcM(thf)]⁺ auf. Diese Spezies wurden möglicherweise während des Ionisationsprozesses gebildet.

Die Funktionalisierung der drei- und vierwertigen Metallkomplexe wurde durchgeführt. Wegen der leichten Abbaubarkeit des Ppz*-Gerüsts zerstörten Reaktionen mit Reduktionsmitteln wie beispielsweise Kaliumgraphit das Ringsystem. Des Weiteren zersetzen sich die Ppz*-Chromophore sehr schnell in Anwesenheit von Organolithium-Reagenzien oder in refluxierenden polaren aprotischen Lösungsmitteln wie z. B. Aceton und THF. Jedoch sind Ppz*-Lösungen ziemlich stabil in unpolaren Lösungsmitteln wie beispielsweise Toluol und Chloroform, sogar in Anwesenheit von Licht und bei erhöhten Temperaturen. Andererseits sind Pc*-Komplexe stabiler gegenüber nukleophilen oder reduzierenden Reagenzien.

Die interessanten Chromophore [Pc*AlF] und [Ppz*AlF] wurden aus den analogen Chloro-Komplexen in refluxierenden wässrigen KF-Lösungen erzeugt . Wegen der starken Metall-Fluor-Bindung erwarten wir, dass diese Chromophore bei geordneter Anbringung an einer Metall-Halbleiter-Schnittstelle die Exzitonendissoziation fördern könnten und es damit erlauben würden, die Ladungstransferdynamiken am Heteroübergang des Halbleiters zu untersuchen.
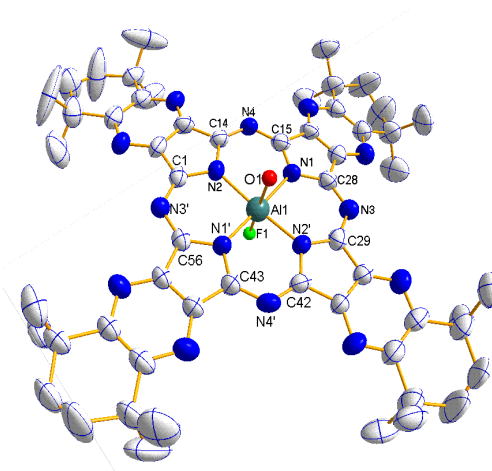
Es wurden auch Versuche unternommen, axiale Amido-, Alkyl- und Phenyl-Al/Ga-Komplexe von Pc* und Ppz* unter Verwendung von Lithium- oder Grignard-Reagenzien herzustellen. Generell wurden die axialen *n*-Alkyl (Methyl, Butyl und Hexyl) und Phenyl-Gallium Phthalocyanine, [Pc*GaR] erfolgreich erhalten. Die elektronischen Spektren

dieser Komplexe wiesen nur eine sehr geringe Blauverschiebung von 2 nm des Q-Bande bezüglich [Pc*GaCl] auf.
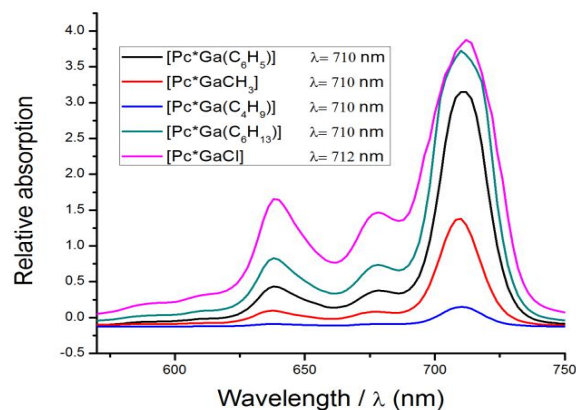
Fluoreszenzspektren

Die Ppz*-Komplexe zeigen eine starke Fluoreszenz, die sogar mit bloßem Auge beobachtet werden kann. Die Fluoreszenzspektren einiger Ppz*-Komplexe ([[Ppz*TiO], [Ppz*VO], [Ppz*CrCl], [Ppz*AlCl], [Ppz*GaCl] and [Ppz*InCl]) wurden gemessen. Die Stokes-Verschiebung wurde für jeden Komplex bestimmt. Die kleinste Verschiebung wurde bei [Ppz*TiO] ≈ 2 nm gemessen, die größte Verschiebung wurde bei [Ppz*VO] ≈ 13 nm beobachtet.
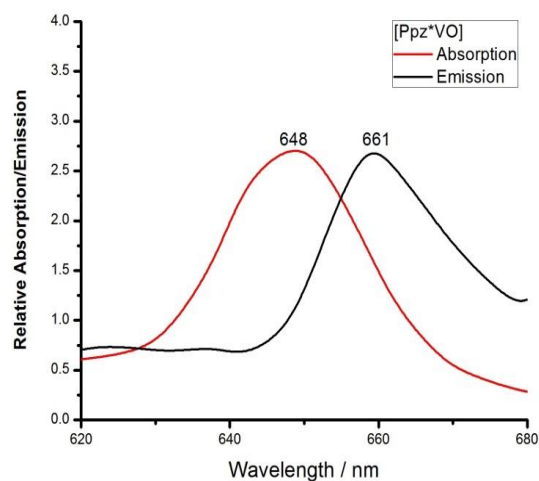
Zyklische Voltammetrie

Es wurden zyklische Voltammogramme der Pc*/Ppz*-Komplexe gemessen. Die Redoxprozesse können am Liganden und am Metallzentrum lokalisiert werden. Die Reduktion des Liganden ([M(II)Pc(−2)] + e ⇔[M(II)Pc(−3)]⁻) wird mit der Position des LUMOs in Verbindung gebracht, während die Oxidation des Liganden (M(II)Pc(−2) ⇔ [(M(II)Pc(−1)]⁻ +e) mit der Position des HOMOs in Verbindung gebracht wird. Es ist möglich, zwei aufeinander folgende Ein-Elektronen-Oxidationen des Pc-Rings zu beobachten, die eventuell der Entnahme von Elektronen aus dem a_{1u} Orbital zugeschrieben werden können, weiterhin vier aufeinander folgende Ein-Elektronen-Reduktionen in die beiden e_g Orbitale. Falls Metallorbitale mit Energien zwischen dem HOMO und LUMO des

Makrozyklus liegen, kann Oxidation oder Reduktion am Zentralmetall auftreten. Dies ist der Fall bei Pc*-/Ppz*-Komplexen von Cr, Ti, Mn, Co und Fe.

Einige Metalle, wie z. B. Ni, Cu und V stellten sich elektronisch inaktiv heraus bezogen auf das Potenzialfenster des Liganden. Im Allgemeinen wird Ppz* leichter reduziert verglichen mit dem Pc*-System, aber es ist schwieriger zu oxidieren. Daher ist innerhalb des gleichen Potenzialfensters die Anzahl der Reduktionsprozesse für Ppz* gleich oder größer der entsprechenden Anzahl für Pc*. Auch müssen ähnliche Reduktionsprozesse von Ppz* bei weniger negativem Potenzial stattfinden als bei Pc*. Repräsentative Voltammogramme von [Pc*Cu] und [Ppz*Cu] werden unten gezeigt. Der Pc*-Komplex wies einen Oxidations- und einen Reduktionsprozess auf, während der Ppz*-Komplex zwei Oxidations- und einen Reduktionsprozess zeigte. Abgesehen vom Oxidationsprozess von [Ppz*Cu] sind alle anderen Prozesse reversibel. Jedoch ist wegen der Tendenz des Komplexes an den Platinelektroden zu adsorbieren der anodische Strom des Oxidationsprozesses der CuPcs gewöhnlich viel höher als der kathodische Strom. In diesem Fall wurde der HOMO-LUMO Abstand durch CV gemessen. Je elektronenreicher der Ligand ist, desto kleiner war der HOMO-LUMO Abstand: z. B. ist der Abstand 1.664 V für [Pc*Cu] und 1.924 V für [Ppz*Cu].
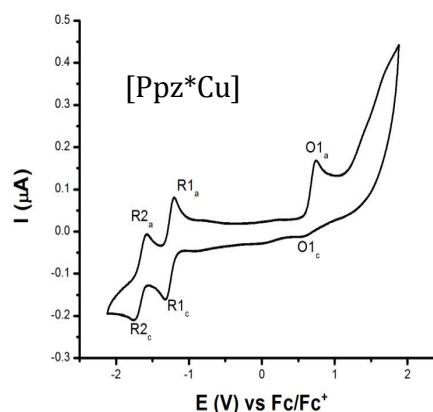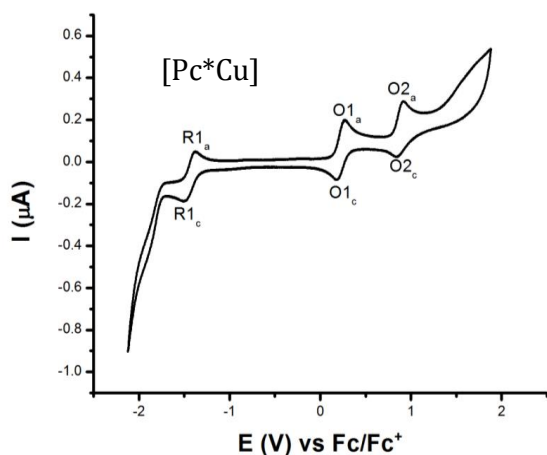
Das elektrochemische Verhalten der Pc* / Ppz*-Komplexe mit elektroaktiven Metallen ist komplizierter. So zeigt beispielsweise [Pc*Co] drei Oxidations- und einen Reduktionsübergang. Laut Literatur ist der Reduktionsprozess metallzentriert. Dagegen werden die Oxidationsprozesse O1, O2 und O3 den Pc^{2-}/Pc^-, Co^{2+}/Co^{3+} bzw. Pc^-/Pc^0 Redoxpaaren zugeschrieben.
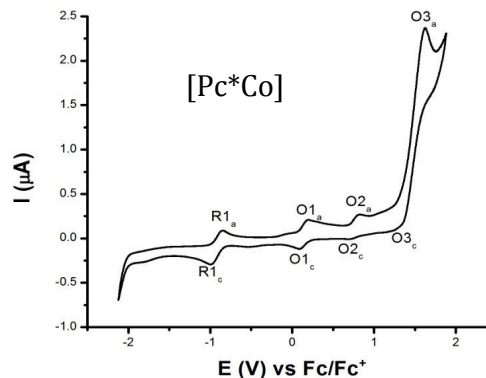
Zusammenfassend kann gesagt werden, dass die Bildung löslicher, isomerenreiner Pc*- und Ppz*-Komplexe der 3d-Metalle sowie der Gruppe-13 und Gruppe-14 Elemente untersucht wurde. Die Komplexe wurden in relativ hohen Ausbeuten gebildet verglichen mit den typischen Ausbeuten für ring-substituierte Pc-Komplex-Synthesen. Die Struktur von sieben Komplexen wurde bestimmt unter Verwendung von XRD-Messungen. Die optischen und elektrochemischen Eigenschaften der Komplexe, die für ihre Anwendung in Halbleiter-Heteroübergängen wichtig sind, wurden systematisch untersucht.

List of symbols and abbreviations

A	Electrode Area
Abs.	Absorbance
Ac	Acetyl
amu	Atomic Mass Units
APCI	Atmospheric Pressure Chemical Ionization
Aq.	Aqueous
Ar	Aryl
ATR	Attenuated Total Reflection
ax	Axial
Bu	Butyl
C	Material-Specific Curie Constant
Cat	Catechol
CB	Conduction Band
CNP	1-Chlornaphthalene
CRC	Colorectal Cancer
CV	Cyclic Voltammetry
D	Diffusion Coefficient
DAMN	Diaminomaleonitrile
dba	Tris(dibenzylideneacetone)dipalladium
DBU	1,8-Diazabicyclo[5,4,0]undec-7-ene
DCM	Dichlormethane
DMA	Dimethylacetamide
DMF	Dimethylformamide
DMSO	Dimethylsulfoxide
DN	Dinitrile
DNA	Deoxyribonucleic Acid
DPEP	Deoxophylloerythroetioporphyrin
DPPF	1,1$'$-Bis(diphenylphosphino)ferrocene
DSSC	Dye Sensitized Solar Cell
e	Elementary Charge
E_a	Activation Energy
$E_{p,a}$	Anodic Peak Potential
$E_{p,c}$	Cathodic Peak Potential
$E_{1/2}$	Half-Wave Potential
EGFR	Epidermal Growth Factor Receptor

EI	Electron Impact
Em	Emission
eq	Equivalent
EQE	External Quantum Efficiency
Ex	Excitation
F	Faraday Constant
Fc	Ferrocene
FDA	Food and Drug Administration
FF	Fill Factor
FT-IR	Fourier transform infrared spectroscopy
FTO	Fluorine Doped Tin Oxide
g	Landé g-Factor
h	Hour, Planck's Constant
HOMO	Highest Occupied Molecular Orbital
HRMS	High Resolution Mass Spectrometry
I	Photocurrent
i_a	Anodic Current
I_c	Cathodic Current
I_{SC}	Short Circuit Current
IPCE	Incident Photon to Current Conversion Efficiency
ISC	Intersystem Crossing
ITO	Indium Tin Oxide
k_B	Boltzmann's constant
L	Ligand
LHE	Light Harvesting Efficiency of Active Materials
LUMO	Lowest Unoccupied Molecular Orbital
M	Metal
[M]	Molecular ion
MALDI-TOF	Matrix-Assisted Laser Desorption Ionization - Time of Flight
Me	Methyl
MPP	Maximum Power Point
MS	Mass Spectroscopy
n	Number of Mols
NEt_3	Triethylamine
NHE	Normal Hydrogen Electrode
NLO	Nonlinear Optics
NMR	Nuclear Magnetic Resonance
O	Oxidation Process
OL	Optical Limiter
OTFT	Organic Thin-Film Transistor

P	Incident Light Power
Pc	Phthalocyanine
PCE	Power Conversion Efficiency
PDT	Photodynamic Therapy
PE	Pentane
Ph	Phenyl
PMHS	Polymethylhydrosiloxane
Por	Porphyrin
ppm	Parts Per Million
Ppz	Pyrazinoporphyrazine
i-Pr	Isopropyl
PTCBI	3,4,9,10-Perylenetetracarboxylic-bis-benzimidazole
Py	Pyridine
Pz	Porphyrazine
R	Alkyl Group, Gas Constant or Reduction Process
ROS	Reactive Oxygen Species
RT	Room Temperature
SCE	Saturated Calomel Electrode
Sec.	Second
SQUID	Superconducting Quantum Interference Device
T	Temperature
TBA	Tetrabutylammonium
TLC	Thin Layer Chromatography
THF	Tetrahydrofuran
TMS	Trimethylsilyl
p-TMP	p-(trifluoromethyl)phenyl
TPP	meso-Tetraphenylporphyrinate
p-TsOH	p-Toluenesulphonic Acid
UV/Vis	Ultraviolet and Visible Light
V	Scan Rate
V_{OC}	Open Circuit Voltage
XRD	X-ray Diffraction
α	Transfer Coefficient
η	Overall Photon to Current Conversion Efficiency
σ	Electrical Conductivity
λ	Wavelength
δ	Chemical Shift
χ	Magnetic Susceptibility

Contents

1 Introduction

Phthalocyanines (Pcs) and porphyrazines (Pzs) are important dyes containing a 16-membered aromatic macrocycle.[1-3] Structurally, Pzs are similar to naturally occuring porphyrins (Pors), except that methine bridges (=CH- groups) between the five membered pyrrole rings in the porphyrin core are replaced by nitrogen atoms (Figure 1). In turn, Pcs are Pz chromophores with extended conjugation as four benzene rings are anellated to the pyrroles, thus four isoindole rings are formed. Pyrazinoporphyrazines (Ppzs) are also analogous to the Pcs where the four benzene rings of a Pc are replaced by pyrazines. Pyrazinoporphrzyines are symmetrical octaazaphthalocyanines: eight =CH- groups are replaced by =N- moieties. According to Gouterman's model,[319] the nitrogen Pπ- electrons contribute very little to the conjugation, and 18 π-electrons (shown in red, Figure 1) form the shortest cyclic conjugation path of these compounds. However, the total delocalized π-electrons are twenty-six for porphyrins and porphrazines, and fourty-two for phthalocyanines and pyrazinoporphyrazines.

[PorM]   [PzM]

[PcM]   [PpzM]
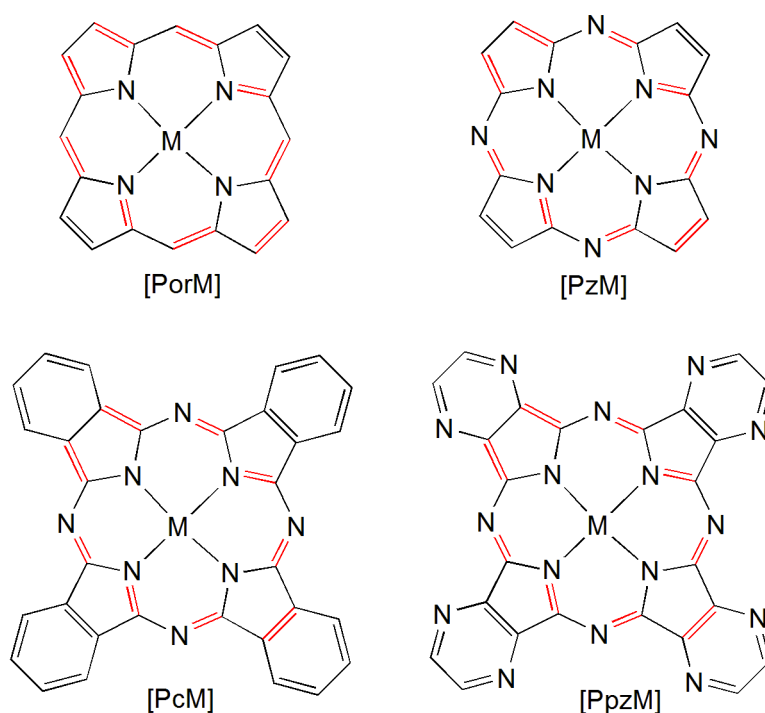
Figure 1: Structures of porphyrin, porphyrazine, phthalocyanine and pyrazinoporphyrazine.

The first metal free macrocycle, PcH$_2$, was obtained in 1907 as a blue by-product in the production of 2-cyanobenzamide; further investigations were not conducted at this

time.[4] In 1927, Swiss researchers accidentally synthesized copper phthalocyanine in an attempted conversion of o-dibromobenzene into phthalonitrile in presence of CuCN. They remarked on the enormous stability of these blue complexes, but did not further characterize them.[5] However the macrocyclic nature of the product was only determined in 1934 through the work of Linstead et al.[6]

1.1 Phthalocyanines

1.1.1 Synthesis of Phthalocyanines

According to literature, several strategies can be applied to synthesize the Pcs (Figure 2). Generally, Pcs form upon heating phthalic acid derivatives that contain nitrogen functional groups *via* a reductive cyclotetramerization process.[3] Classical precursors are phthalonitriles and diiminoisoindoles. However, even phthalic acid, phthalic anhydride, phthalimide, o-cyanobenzamide or dibromobenzene can be used as starting materials as the implementation of these substances leads usually to *in situ* formation of phthalonitrile and diiminoisoindoles, which are the actual precursors for the cyclotetramerization process.[7]
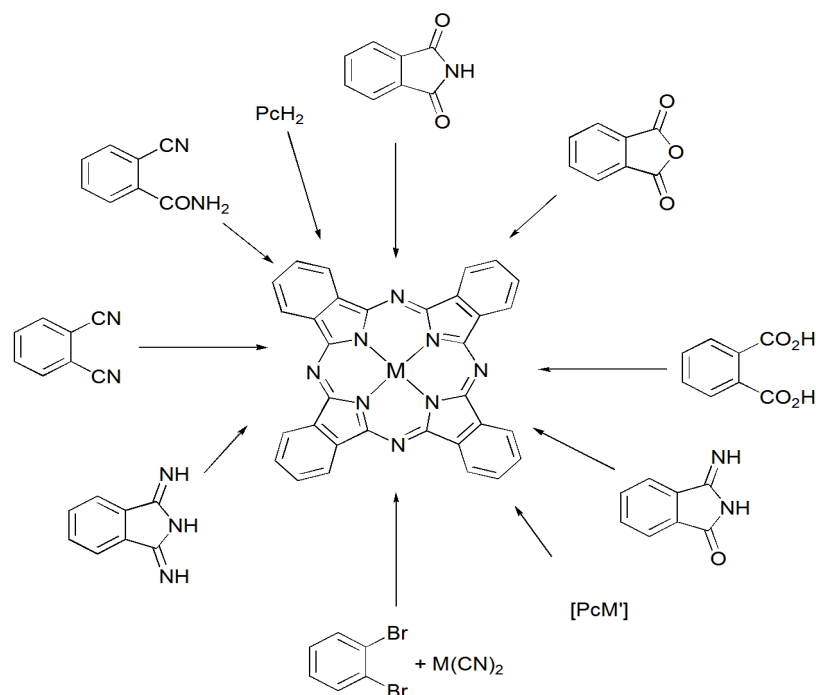
Figure 2: Different synthetic routes of MPcs.

In each reaction, typically four equivalents of a phthalic acid derivative react with an equivalent of a metal / metal salt at temperatures above 150°C, either in melt or in a high boiling solvent. Addition of an ammonia source, such as urea, is often desirable as it promotes the *in situ* formation of the diiminoisoindoles. Other than the

cyclotetramerization of a dinitrile, MPcs could also be prepared by metalation of the metal free chromophore, PcH_2, or from its salts, i.e. $[PcLi_2]$ or $[PcK_2]$.

Christie et al.[8] studied the formation mechanism of the Pcs (Figure 3). It is assumed that in the first step, a negative particle (X) nucleophilically attacks the dinitrile carbon to form the anion (A), where X is the counter ion of the metal cation in melt or an alkoxide in a basic solution of a high boiling alcohol. Once A is obtained, it attacks another dinitrile molecule (B) to form the dimeric complex (C), which is converted in a further step to (D). The addition of two more dinitrile molecules follows the same mechanism. Structure (E) indicates that the coordination of the precursor with the metal template favors the subsequent cyclization to (F). By elimination of X and transfer of two electrons, [PcM] then results.
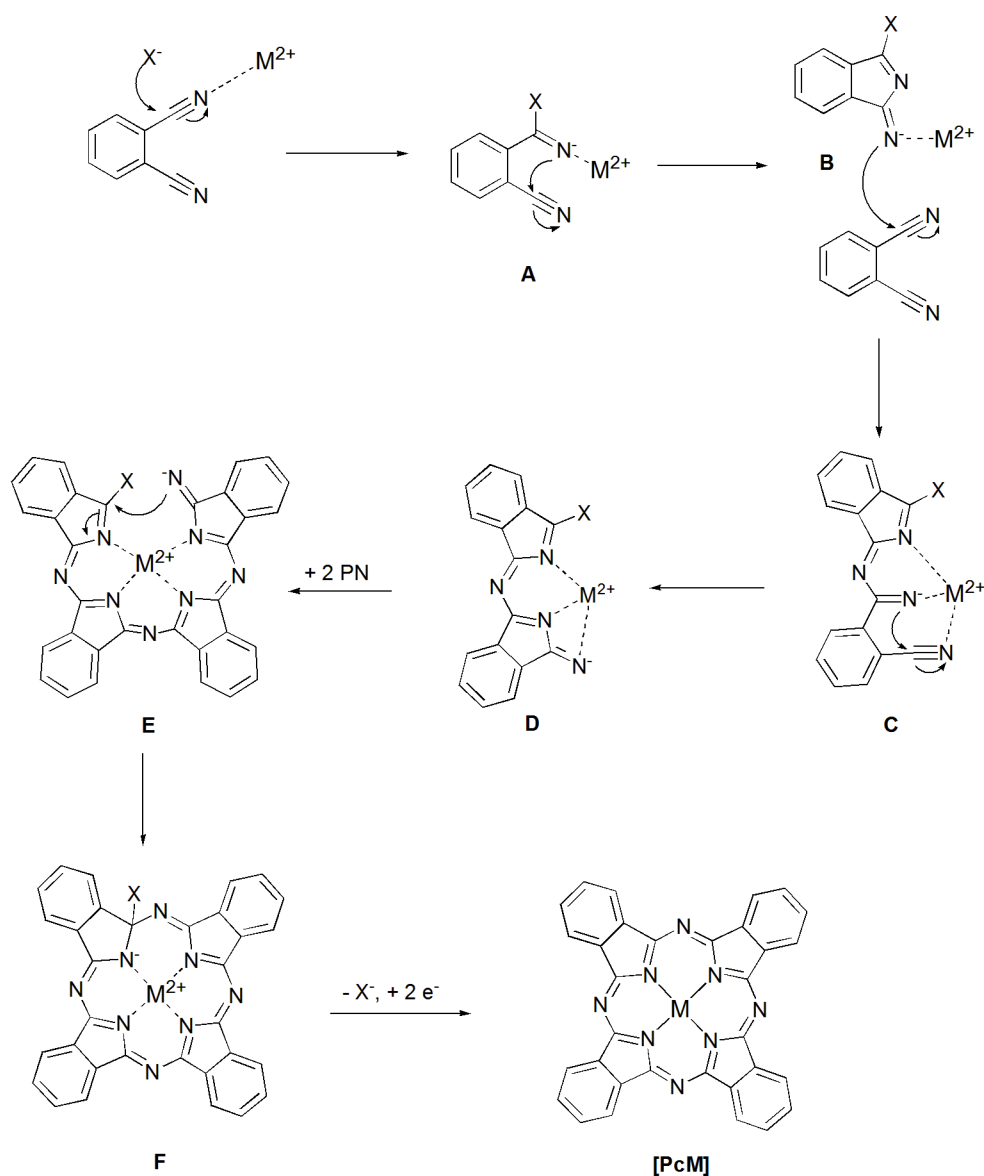
Figure 3: The proposed mechanism of cyclotetramerization.

The required electrons are supplied by different reagents depending on the nature of the starting materials. Most commonly, the electrons come from the oxidation of a high boiling alcohol, $RCH_2OH \rightarrow RCHO + 2H^+ + 2e$, under basic conditions. However, the electrons could also be provided by a low-valent metal precursor, e.g. $TiCl_3$ for the synthesis of $PcTiCl_2$. Additionally, electrons can also be provided by X, originating from the metal template MX_n.

1.1.2 Structural Variations of Phthalocyanines

The class of Pcs includes a large structural diversity[3] with a manifold of variations possible at the metal or on the ligand. Figure 4 summarizes the possible structures obtainable. The most common structure type, among all the divalent metal complexes, is Type G. Substitution of the ring could occur at either a peripheral or at a non-peripheral position, and up to sixteen H-atoms can be substituted on one Pc molecule. Another variation possibe is for the dimeric complexes [PcM-MPc], where metal-metal bonds exist. Examples including molybdenum and rhenium complexes [PcM ≡ MPc][9] (M = Mo, Re) in which the low oxidation of the heavy metal cation is stabilized by formation of metal-metal quadruple bonds.
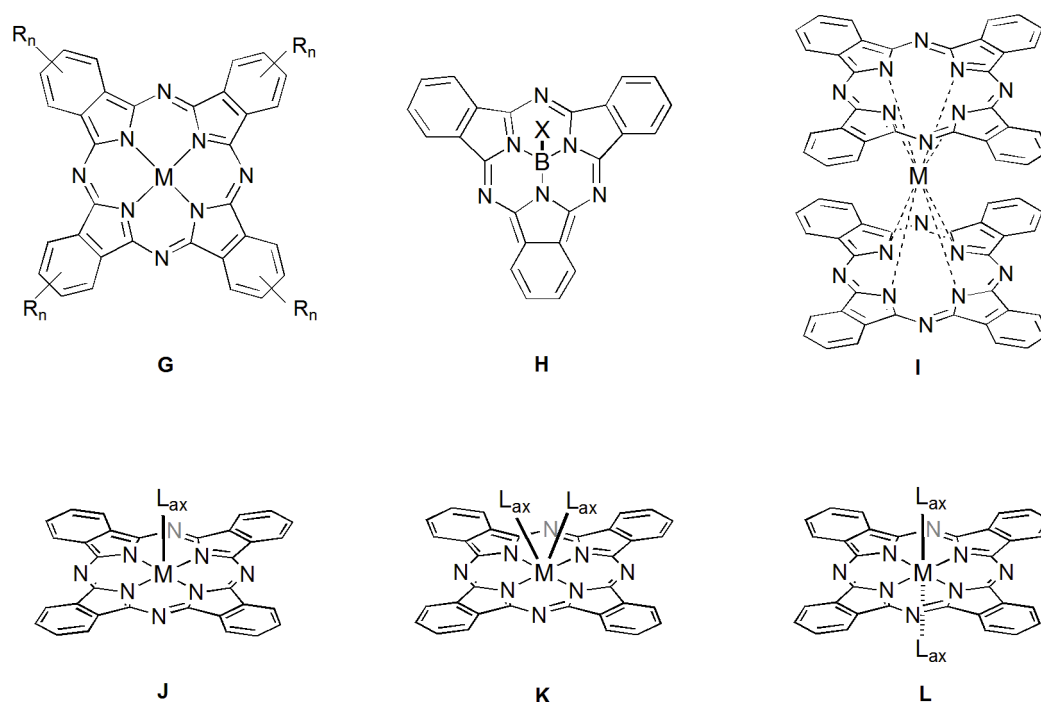
Figure 4: Structural variations of MPcs.

Owing to its small atomic radius, the template-cyclization of the dinitriles with boron (III) compounds results in formation of subphthalocyanines, Type H, containing only three isoindole groups.[10] On the other hand, a comparatively large atom such as

uranium is templating the synthesis of superphthalocyanines, which contain five isoindole moieties.[11]

For the large metal cations that do not fit into the ligand central cavity, double decker complexes [Pc₂M] (Type I, M = rare earth (III)) can be obtained, where a monoanionic radical (Pc⁻) is present.[12] These complexes have been intensively studied because of their unique electrochromic property[13–16], intrinsic semiconductivity[17–21] and single-molecule magnetism.[316]

To obtain neutral, mononuclear high valent MPcs, at least one anionic substituent in an axial position has to be present (Type J). This type is best described by the widely known titanyl phthalocyanine [PcTiO].[22, 23] In a special position within the complexes of this type, the dimers [PcM-μ-X-MPc] (e.g. M = Cr, Mn; X = O), in which the axial ligand bridges two MPc fragments, are described.[24] Structures of MPcs with two anionic axial ligands, depending on steric and geometrical factors, can lead to structures of Type K or Type L, e.g. the complex [PcTiCl₂] shows a *cis*-arrangement of the dichloro substituents Type K[25] whereas the bulky OSiPh₃ groups in [PcTi(OSiPh₃)₂] display a *trans*-coordination to each other Type L.[26] In some cases, high-valent metal cations, such as tantalum, take up to four axial ligands.[27]

1.1.3 Symmetrical and Asymmetrical Phthalocyanines

Generally, when a dinitrile is involved in a reductive cyclization reaction, its structure has a large impact on the products formed. Depending on the substitution and the symmetry of the precursor, a large number of symmetrically and asymmetrically substituted Pcs of type G could be obtained.[3] For example, cyclization of a mono-substituted dinitrile could possibly lead to four regioisomers of different symmetries (Figure 5).[28]
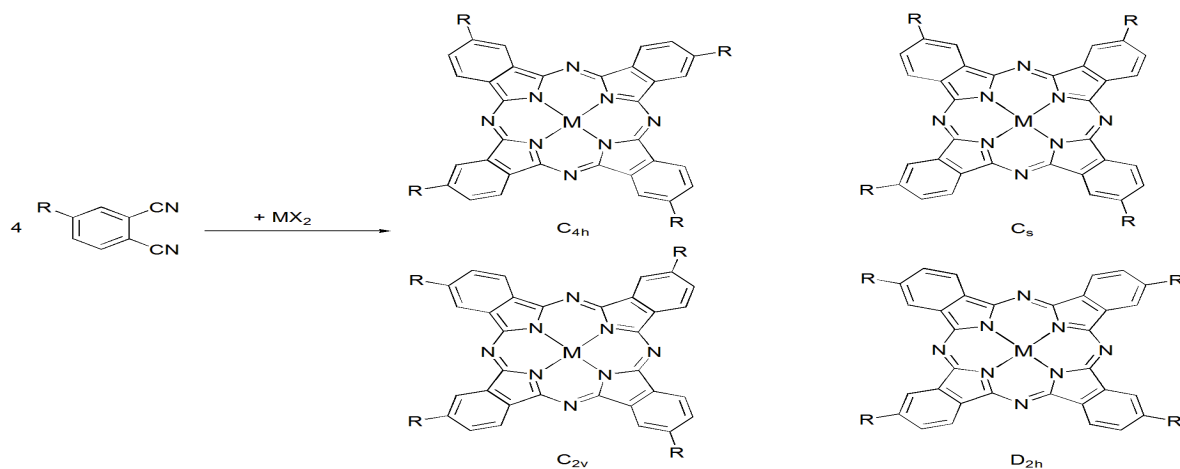
Figure 5: Regioisomers of tetrasubstituted MPcs.

The different symmetries of the isomers affect the Pcs' lattice structures, and thus their optical properties. Additionally, if any axial ligand coordinates to the metal, the symmetry is further reduced (Types J and K), as various enantiomers could be present due to their planar chirality. However, it is generally difficult, or impossible, to separate such isomers due to their identical molecular weight and similar physical polarities.

If a reaction involves two different nitriles, A and B, in addition to the standard A_4 and B_4 systems, other macrocycles of different symmetries might form (Figure 6).[28, 29] The asymmetric introduction of substituents provides several advantages, such as the solubility enhancement due to reduced aggregation. Furthermore, sometimes, it is necessary to introduce a certain number of asymmetric units into the chromophore, e.g. A_3B systems are highly attractive materials in nonlinear optics (NLO).[30]
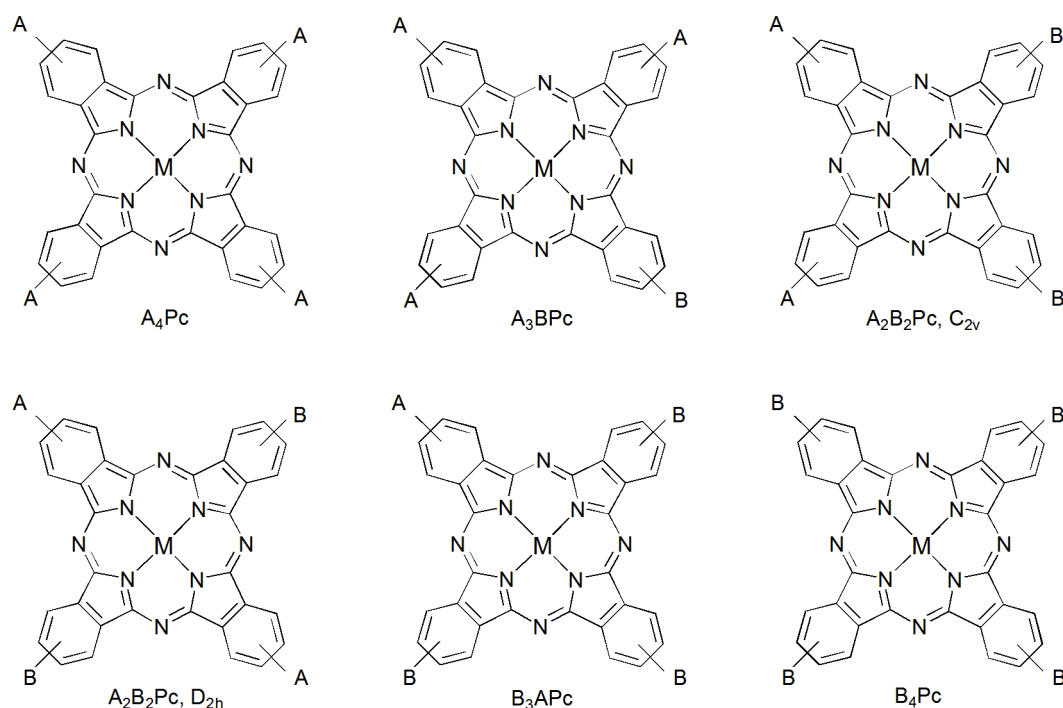
Figure 6: Different A_nB_m Pcs.

The separation of these systems might be achieved by column chromatography; however, selective synthesis of an A_3B system by the ring expansion of subphthalocyanines by diiminoisoindoline (Figure 7) is also possible.[31] It should be noted that only selective methods could be used to synthesize insoluble Pcs, as chromatographic purification is not possible. In the case of soluble Pcs, the chromatographic separation of the products is often less expensive than the preparation and purification of the corresponding subphthalocyanine and diiminoisoindoline.
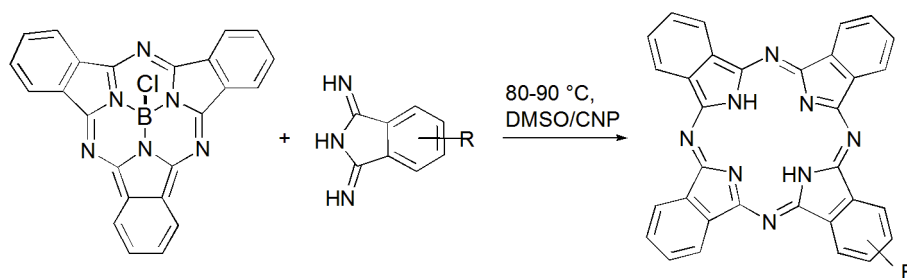
Figure 7: Selective synthesis of an A₃B complex by ring expansion of a subphthalocyanine.

Also, polymer support can assist to obtain an A_3B system.[32] In this method, a dinitrile or 1,3-diiminoisoindoline is anchored to a polymer support. Afterwards, a second dinitrile is added and allowed to react; thereby obtaining a mixture of A_4 Pc and a polymer supported A_3B Pc. After isolating the A_4 system, both the polymer support and the A_3B Pc can be obtained.

As the chromatographic separation of the C_{2v} and D_{2h} isomers of the A_2B_2 system is usually not possible, selective methods were developed to prepare a particular isomer, e.g. Young et al.[33] showed the synthesis of substituted D_{2h} Pcs by the reaction of 1,1,3-trichloroisoindoline and diiminoisoindoline derivatives at a relatively low temperature (Figure 8). 1,1,3-Trichlorisoindolines do not tetramerize, additionally the reaction temperature is too low to cyclize the diiminoisoindoline. Therefore, after elimination of NEt_3HCl, only two different units can react together leading to selective formation of the D_{2h} isomer.
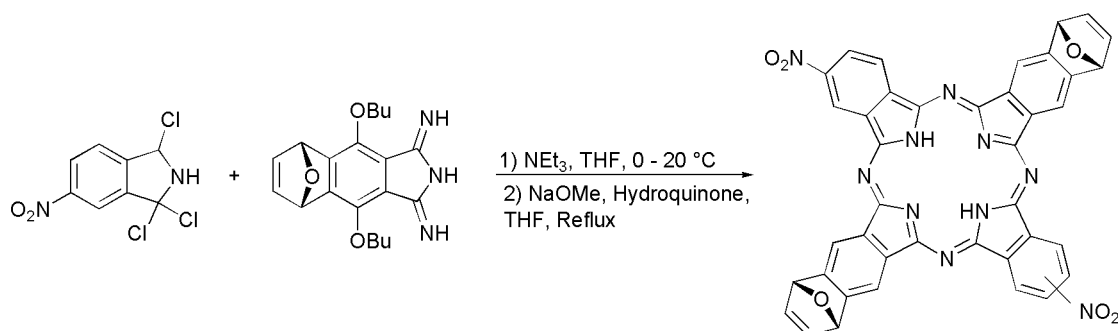
Figure 8: Selective synthesis of an ABAB phthalocyanine.

The C_{2v} A_2B_2 system, due to its polarizability, is a potential candidate for NLO applications. Nolan et al. therefore developed a selective synthetic strategy starting from "Half-a phthalocyanine" (Figure 9)[34], which could be prepared from the corresponding phthalonitrile and LiOMe in methanol. Subsequently, it is added to an excess of a second dinitrile in dimethylaminoethanol in the presence of a metal salt at 60°C. The low reaction temperature in this case prevents the cyclotetramerization of the second dinitrile so that a C_{2v} symmetrical A_2B_2 Pc is obtained.
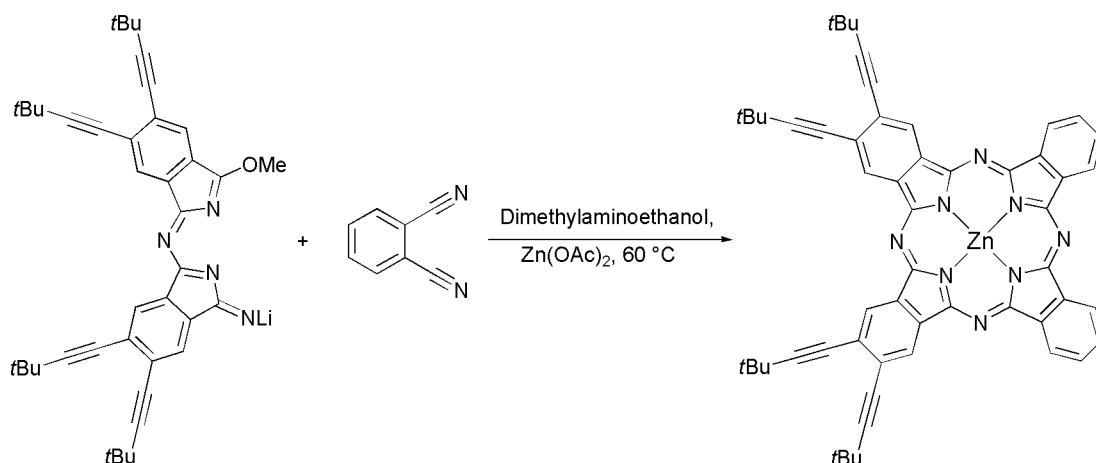
Figure 9: Selective synthesis of an A_2B_2 Phthalocyanine.

1.1.4 Synthetic Strategies towards axially substituted metal phthalocyanines

Usually, cyclization of a dinitrile precursor in the presence of a divalent metal cation e.g. Co^{2+}, Ni^{2+}, Cu^{2+} or Zn^{2+}, results in neutral complexes without any axial functionalities. However, macrocycles of high-valent metals, e.g. Ti, V, Cr, Mn, Fe, Al, Ga, In, Si or Ge, containing one or more axially coordinating ligands, are of particular interest, as the variation of the axial ligand opens the possibility to change the complex structure and, hence, its reactivity.
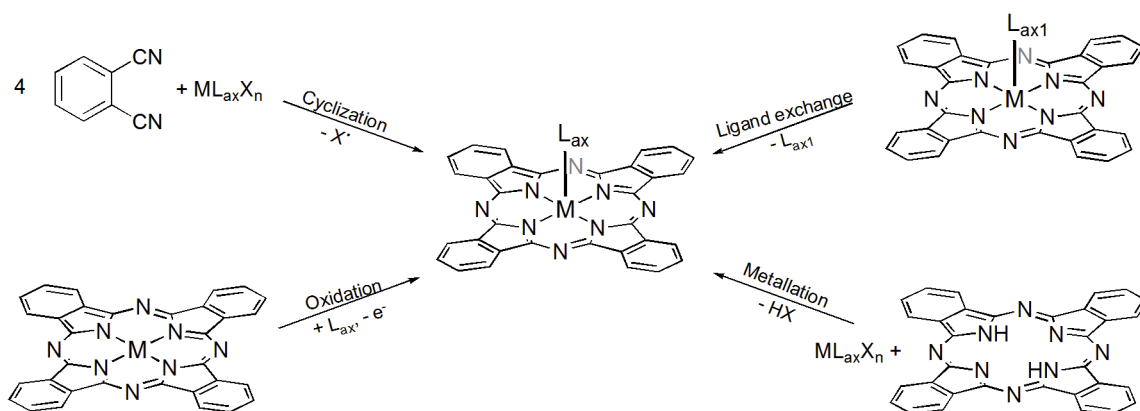
Figure 10: Different synthetic routes to the axially functionalized Pcs.

When M (oxidation state > II) is involved in the tetramerization reaction, an MPc with at least one axial ligand can be obtained (Figure 10). Additionally, the metal precursors could react with either a free or a deprotonated ligand to form the axially substituted macrocycles. Furthermore, the axially functionalized Pcs might be accessible by substituting an existing axial ligand or by using oxidative addition procedures.

8

1.2 Pyrazinoporphyrazine

Pyrazinoporphyrazines (Ppzs; X=N, Figure 11) are compounds where the carbon atoms in the non-peripheral positions of a phthalocyanine are substituted by N-atoms, i.e. the positions 1,4,8,11,15,18,22 and 25 of a Pc are known as non-peripheral, or α- positions, while positions 2,3,9,10,16,17,23 and 24 are known as peripheral, or β- positions (Figure 11).[140]
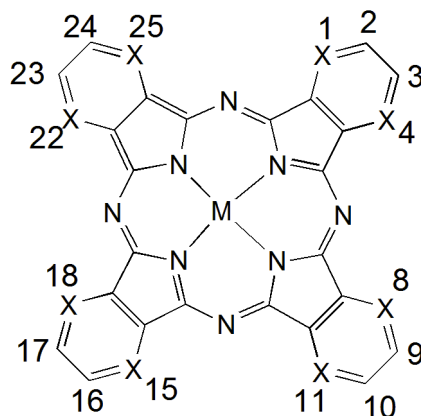
Figure 11: Potential sites for Pc (X=CH) and Ppz (X=N) substitution (numbering used for nomenclature).

Linstead et al[49] introduced the class of Ppz compounds for the first time in 1937, just three years after the structural elucidation of the Pcs. These chromophores could form upon reductive cyclotetramerization of a pyrazinedinitrile precursor using similar strategies to those used for the synthesis of the Pcs; however the pyrazinedinitriles could be easily obtained by condensation of 1,2-diketones and diaminomaleonitrile (DAMN) (Figure 12). Owing to their structural similarities, both Pcs and Ppzs have similar optical properties and comparable stability.
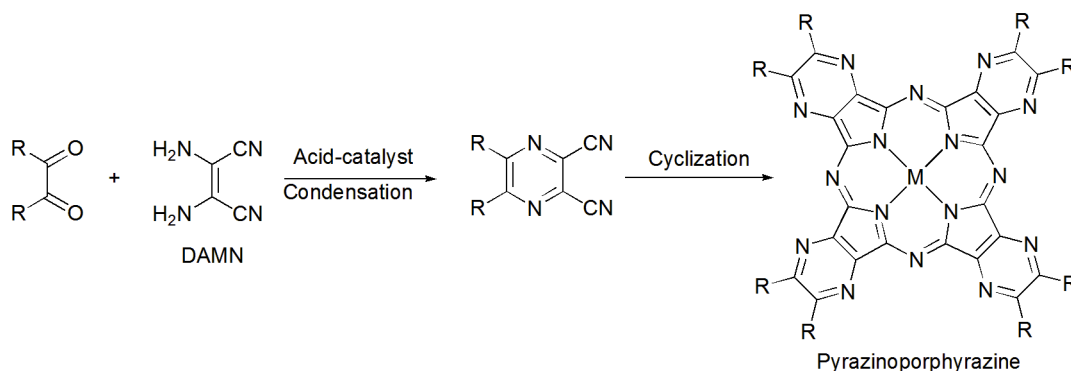
Figure 12: Synthesis of pyrazinoporphyrazines (Ppzs).

Synthesis of different dinitrile templates starting from 1,2-diketones allows for the introduction of different substituents by a simple synthetic approach, as a large number of 1,2-diketo compounds are commercially available or intensively studied.[50-52] The

condensation usually works in good yield, however, this reaction is acid catalyzed since a catalytic amount of an acid e.g. p-toluenesulphonic acid, must be added.[49]

Compared to the phthalonitriles, pyrazinenitriles are more electron-deficient as a result of the substitution of carbon atoms with nitrogen atoms in the non-peripheral positions. For this reason, the cyclization is enhanced, and hence reductive cyclotetrameritzation of the pyrazinenitriles can occur at temperatures above 150 °C, even in absence of any metal template or ammonia source.[53]

Also, in comparison to the Pc aromatic system, and due to the large contribution of the atomic orbitals to the HOMO at the positions where the N-atoms are located[55], the energy of the HOMO level is influenced, while the energy of the LUMO is remarkably unaffected.[54] This leads to a larger HOMO-LUMO gap and a blue shift of 60-70 nm, of the Q band is observed.

Pcs and Ppzs posses comparable properties and have been almost examined in terms of similar applications. It is worthwhile to mention that Ppzs could be used as optical limiters (OL), since they have a higher efficiency compared to that obtained from the Pc homologues. Moreover, fluorescence of a Ppz solution shifts hypsochromically with respect to an analogous Pc, and its orange-red color could usually be seen with the eye. Furthermore, Ppzs were intensively studied regarding the singlet oxygen production.[57] However, Ppz complexes are less favored for the use in solar cells due to its energetically lower HOMO in comparison to their Pc counterparts, as the electron poor ligand can scavenge the charge carriers by the trapping effect, and thus the charge separation becomes more difficult.[56]

1.3   Properties of Phthalocyanines

The Pcs are known for their unique optical properties, as well as their chemical and thermal stabilities, e.g. the unsubstituted Pcs decompose at temperatures above 600°C[3], and are relatively stable against acids and alkalis. Thus they could be possibly purified by sublimation, or by crystallization from a concentrated sulfuric acid solution.[1] Owing to their geometry and their planar π–system, the Pcs experience strong π- π interaction, resulting in practical insolubility in the most common organic solvents. However, the solubility is increased by means of bulky substituents attached to the Pc core.

Owing to the aromatic, 18 π - electron system, Pcs are extensively used as pigments and in different areas of optoelectronics. The allowed $\pi \to \pi^*$ transitions, which are responsible for the intense color of the chromophores, lie partly in the visible range.[28, 35] It was reported[1] the unsubstituted Pcs display Q band transitions in the range of 650-700 nm, corresponding to the HOMO- LUMO gap of the chromophore, while the higher energy B-band is observed at 200-350 nm.[1]

Literature[130-132] counted on modeling and experimental evaluation of the electronic properties of Pcs and MPcs. Gouterman's model describes the origin of the main spectral features of the Pcs in terms of four orbitals, HOMO-1, HOMO, LUMO, and LUMO+1.[133, 134] In Pcs, due to the large energy gap between the $1a_{1u}$ and $1a_{2u}$ orbitals resulting from the presence of aza bridges, the Q and B bands appear in different regions.[135, 136] Generally, the Q and B bands are assigned respectively to the $a_{1u}(\pi)$ to $e_g(\pi^*)$ and $a_{2u}(\pi)$ or $b_{1u}(\pi)$ to $eg(\pi^*)$ transitions. For metal free Pcs, Q band splitting is indicative of D_{2h} symmetry with lifted orbital degeneracy, while the symmetry of MPcs is generally D_{4h}.[137] Owing to the ligand cavity size, accommodation of some metals may result in doming or ring expansion of the macrocycle, causing distortion of the symmetry of the molecule.[138] Additionally, mixing the transition metal d-orbitals and the π-orbitals of the chromophore may change the electronic features of the complex. The metal macrocycle orbital interaction has been analyzed in detail by Rosa et al.[139]

Fluorescence of Phthalocyanines

Fluorescence spectroscopy has been considered as a significant achievement over the past years, as it has permitted the exploration of new avenues in molecular dynamics.[36-38] As a result of its specificity, high sensitivity to small modifications in the structural dynamics, and the ability to detect very low concentrations, it has become a primary analytical tool in the disciplines of chemistry and biochemistry.[37, 39, 40] Stokes and Förster demonstrated the usefulness of fluorescence spectroscopy in important applications, including cell identification and detection for DNA sequencing.[41-45]

Fluorescence is a short-lived type of luminescence created by electromagnetic excitation. It is generated when a substance absorbs light energy at a short wavelength and then emits at a longer one as it relaxes to the ground state.[36, 46] The span of time between the absorption and emission processes is relatively brief, $\approx 10^{-9}$ to 10^{-8} sec. However, the emission rate depends on the nature of the excited state. To understand the fate of an excited molecule, a general Jablonski diagram is shown (Figure 13).

The electronic singlet states are S_0, S_1, and S_2, in which all electrons are paired (multiplicity = 1), while the triplet states are those in which two electrons have parallel spins. Also, each electronic state is subdivided into vibrational states represented by horizontal lines. First, the molecule occupies the lowest energy singlet state S_0. After absorption of a photon, the molecule is excited to occupy a vibrational level of an excited singlet state (e.g. S_2); then the excited molecule partially loses some of its absorbed energy, creating a relaxed singlet state S_1. This process, called internal conversion, takes place in about 10^{-11} sec. Fluorescence emission occurs when the molecule further relaxes to the ground state, S_0, from the lowest excited singlet state S_1, radiating energy in the form of light.[37,46,47] The emission process lasts approximately 10^{-8} sec. Also, when

a molecule is in the excited singlet state, an electron might change its spin, resulting in a transfer of the excited molecule to an excited triplet state through intersystem crossing.[37] The molecule then rapidly relaxes to the lowest vibrational level of the first excited triplet state, then to the ground state and emission is observed in the form of phosphorescence, which occurs in 10^{-4} to 10 s. In addition to fluorescence and phosphorescence, other non-radiative pathways, including intramolecular charge transfer and intermolecular processes, such as electron transfer and excimer formation, dimers associated with excited electronic states, could occur.[48]
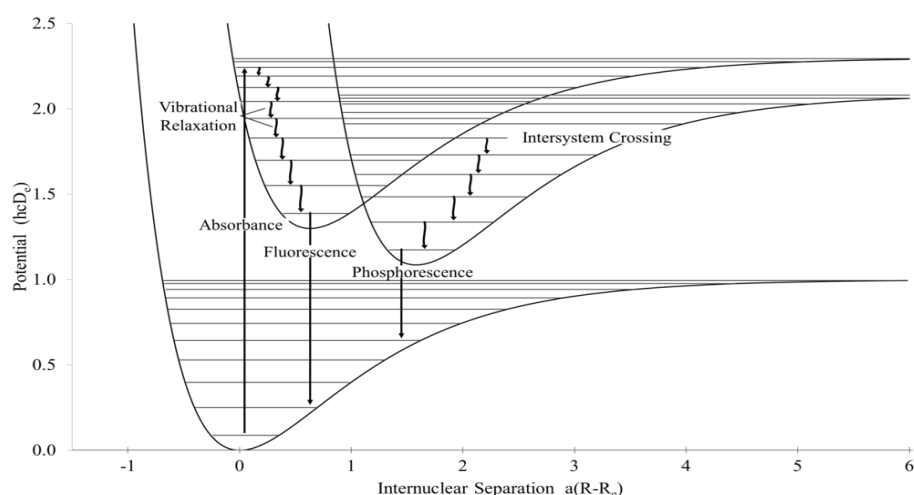
Figure 13: Simple diagram showing the excitation of a molecule and the relaxation process of the excited molecule.

1.4 Applications of Phthalocyanines

Generally, Pcs have been utilized in many fields, including: gas sensors[58], semiconducting materials[59], photovoltaic cells[60, 61], liquid crystals[62, 63], optical limiting devices[64-66], molecular electronics[67], non-linear optics[68], fibrous assemblies[69] and photodynamic therapy[70-73]. A brief overview on the use of different Pcs in selected applications is given below.

1.4.1 Photosensitizers in PDT

Photodynamic therapy (PDT) is a rapidly advancing treatment modality with diverse clinical applications. It involves exposure of tissues to a photosensitizing drug, followed by irradiation with light of an appropriate wavelength.[74,75] In the presence of molecular oxygen, triplet oxygen is generated from the introduced light energy. Transfer of this energy allows for the generation of singlet oxygen. This is termed the Type II redox reaction. Singlet oxygen is extremely toxic, and unlike other reactive species, has a

relatively long half-life time being measured in microseconds.[76] Current photosensitizers are designed to achieve high activity of this pathway with the generation of singlet oxygen. Therefore, singlet oxygen generation is regarded as the most important characteristic of a successful sensitizer. An activated sensitizer may also generate a Type I redox reaction. Here, rather than the triplet oxygen state being created, the energy transfer from the sensitizer may generate other reactive oxygen species (ROS). Should water be the target, this will create toxic hydroxyl radicals or superoxide ions. Potentially, a Type III, oxygen independent pathway may be followed. Here, the activated sensitizer directly destroys the target.[76]

Photofrin®, the first US FDA-approved porphyrin photosensitizer, is administered intravenously, prior to irradiation of the tumor or pathologic tissue with 633 nm light. Because Photofrin® remains in tissues for up to several weeks, patients are advised to avoid natural sunlight or any intense artificial light to minimize the likelihood of developing photosensitive side reactions.[77, 78] Occasionally, side reactions may occur in patients who have compliance issues.

Another example, Photosens® (Sulfonated AlPc), offered excellent clinical response and fluorescence in naturally occurring veterinary tumors.[79] It has had extensive use for both tumors and infections.[80, 81] This photosensitizer can be formulated for intravenous use, direct lesion injection and aerosol formulation. Treatment for early stage and recurrent lip, pharynx, larynx and tongue lesions was successful, as well as, for primary lung, recurrent lung and esophageal tumors.[82—85] Also, a SiPc photosensitizer has shown minimal toxicity in phase I/II clinical studies, with both intravenous and topical application.[86]

Moreover, resulting from their physiological applications, Pcs and Ppzs with Zn, Mg, Al or Ga metal centers are extensively studied.[57] The fluorescence quantum yield of these complexes is about 0.2, while the quantum yield of the singlet oxygen production is about 0.7.[57, 87, 88]

1.4.2   Applications in Bioimaging

Pcs, due to their hydrophobicity, tend to aggregate in aqueous medium. To be used for bioimaging applications, they have to possess a reactive group for bioconjugation purposes. La Jolla Blue (Figure 14) was the first commercially available Pc dye having two axial polyethylene glycol moieties and two carboxylic acid groups free for bioconjugation.[141] The glycol moieties make the chromophore water soluble, and thus attractive as a biomarker. Therefore, different biomolecules, e.g. peptides and proteins, can bind to the dyes in bioimaging and bioanalytical fields.[142-145] Renzoni et al.[146], also synthesized MPcs containing both water soluble groups and another reactive group

bound to the benzo-ring (Figure 14). If the copper in this structure is replaced by silicon, this allows the chromophore to bear two axial ligands.
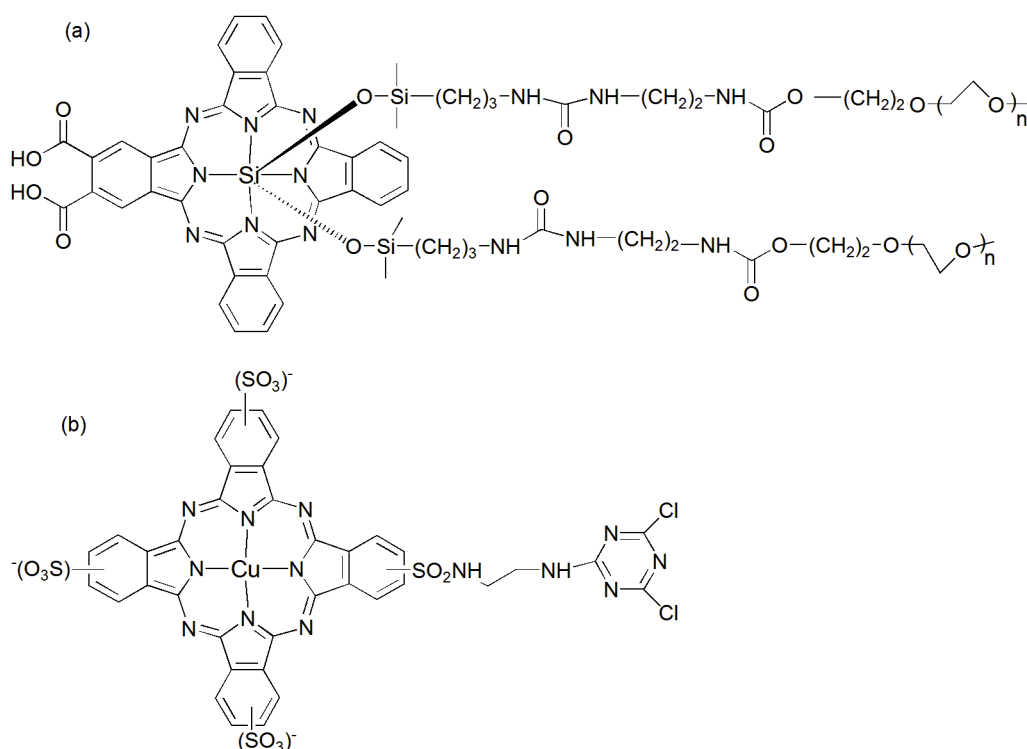
Figure 14: Structure of a) La Jolla Blue dye and b) Copper sulfophthalocyanine dye.

The conjugation of Pcs with peptides of specific receptors or antibodies that are overexpressed in cancer cells, such as the human epidermal growth factor receptor (EGFR), is a remarkable strategy for increasing their biological efficiency.[147-151] EGFR is over-expressed in various cancers, including small cancers (< 5 mm) and the flat, dysplastic and aberrant crypt foci, which are believed to precede the development of cancer.[152-154] To selectively deliver the cytotoxic drugs to the tumor sites[155-161], two small peptides[160-161] have proved attractive as a result of their availability, low immunogenicity, ease of conjugation to other molecules and a relatively superior EGFR-targeting ability. Pc-peptide conjugates *via* various linkers for colorectal cancer (CRC) diagnostic applications have been evaluated *in vitro* and *in vivo*[162]. Polyethylene glycols have also been used as delivery vehicles[163,164], and may be covalently bound[165,166] to the Pcs to improve the delivery to specific target tissues. Moreover, pegylation of photosensitizers enhances their water solubility, serum life, tumor accumulation and also reduces their uptake by the reticuloendothelial system.[167,168] Investigations were carried out to identify potential ZnPcs that serve as photosensitizers with enhanced biological selectivity and effectiveness.

1.4.3 Nonlinear Optics

Generally, optical limiting (OL) is a nonlinear effect consisting of a decrease in the sample transmittance under high intensity or fluence illumination. Ideally the transmitted intensity should remain constant above a certain illumination threshold. Consequently, the initial constant transmittance should linearly decrease to zero above the threshold. This effect finds useful applications for sensor protection, including the human eye.

Optical limiting by Pcs was first reported by Coulter et al.[89] as they demonstrated the optical limiting effect of [PcAlCl]. Subsequently, a large number of other Pcs has been investigated, e.g. [PcInCl] and [t-Bu$_4$PcIn(p-TMP)], where p-TMP is p-(trifluoromethyl)phenyl).[90] Perry et al.[64] prepared a practical optical limiting device using a tetra-substituted chloro-InPc in an inhomogeneous distribution along the beam path. This device was able to attenuate nanosecond irradiation by factors of up to 540.

It has been suggested[92] that asymmetrically substituted Pcs with suitable donor/acceptor groups capable of displaying efficient intramolecular charge transfer should exhibit interesting NLO responses. Thus, some research has been carried out to develop non-centrosymmetric, peripherally susbstituted Pcs, e.g. A$_2$B$_2$ and A$_3$B systems. By applying an external electric field, a polarization can be induced, which alters the optical properties of the material as a function of the field strength.

Most of the OL experiments on Pcs are discussed with respect to Figure 15. Under illumination, at around 550 nm, a photon is absorbed at the ground state level S$_o$. Therefore the molecule is excited to a higher vibrational level of a singlet electronic excited state S$_1$ (corresponding to the Q-band). This state rapidly decays via ISC into a lower triplet energy level, T$_1$ state, that may absorb another photon so that the system is excited to a higher level, T$_2$. Moreover, transitions from S$_1$ to a higher singlet state S$_2$, are also possible. Generally, short pulse processes are dominated by singlet-singlet absorption before a significant population of the triplet has developed. In this case, if the cross section of the S$_1$-S$_2$ transition is larger than that of S$_o$-S$_1$, reverse saturation behavior occurs. Under these conditions, the simplest three levels, S$_o$, S$_1$ and S$_2$, can be used to interpret the electronic dynamics of the system. On the other hand, the processes occurring under long pulse illumination are dominated by T$_1$-T$_2$ transitions. If this cross-section is larger than that of S$_o$-S$_1$ transition, then optical limiting also takes place.

In general, among the transition metal Pcs, VPcs display the fastest intersystem crossing, hence they are the best suited to OL applications.[55] Furthermore, Ppzs generally show enhanced OL properties compared to the analogous Pcs.[55]
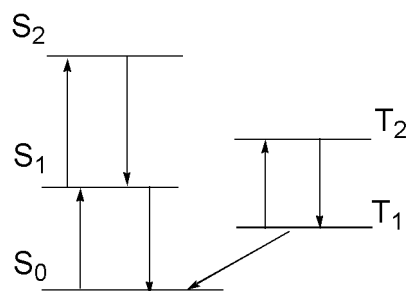
Figure 15: Schematic diagram showing the levels and relevant transitions for optical limiting action.

1.4.4 Applications as Optical Semiconducting Materials

Unsubstituted MPcs are classical p-type, or hole, conductors. However, appropriate substitution can allow for fine tuning of the HOMO-LUMO levels.[93, 98] For example, Bao et al. explored a variety of MPcs as channels in n-type organic thin-film transistors (OTFTs).[94] It was shown that the introduction of electron withdrawing groups results in lowering of the LUMO level. Optimum results were obtained with a perfluorinated CuPc [$F_{16}CuPc$], as the introduction of the fluorine atoms resulted in a 1.6 eV drop in the energy of the LUMO level.[98]

Basically, the morphology of the Pc macrocycles affects their optoelectronic properties. To achieve good conducting properties, a special, spatial arrangement of the macrocycles is necessary.[99] Assuming a suitable distance between confacially arranged planar macrocycles possessing an extended π-electron system, electron delocalization by π-π overlap of the perpendicular orbitals in the stacked arrangement is possible.

Intrinsically, electrically conductive MPcs could be prepared *via* bridging of the central metals with an axial ligand;[99] for example, the fluoro bridged MPcs [$PcMF$]$_n$ with Al, Ga or Cr.[95-97] Generally, all the known [$PcMF$]$_n$ complexes can be doped with iodine, and their conductivities rise with an increasing iodine content. However the highest conductivity observed was for [$(PcAlF)I_{3.3}$]$_n$ (σ_{RT} = 5 S/cm, activation energy E_a = 0.017 eV).[99]

1.4.5 Application in Solar Cells[122]

Energy will remain one of the most important factors influencing human society in the 21st century[100, 101] as the cost, availability and sustainability of energy have a significant impact on the quality of our lives and the environment. Researchers are now focusing on the development of renewable energies[102] generated from natural resources, such as sunlight, wind, rain, tides and geothermal heat. Of these, the sun has the potential to make the largest energy contribution; only one hour of sunshine (3.8 × 1023 kW) is needed to satisfy the highest human demand for energy for an entire year (1.6 × 1010

kW in 2005).[103-106] Solar cells, also called photovoltaics,[107] are devices designed to convert sunlight into electricity *via* the photovoltaic effect.

In 1954, the first silicon-based solar cell was developed with an efficiency, η, of 6 %.[108] Nowadays, values of η ~ 20 % can be achieved.[109] For optimal functioning of a Si solar cell, high-purity monocrystalline silicon is required. Although silicon is regarded as the second most abundant element in the earth's crust,[110] the production of highly pure silicon starting from SiO_2 is an energy consuming process, which in turn leads to a high cost for the production of silicon solar cells.

1.4.5.1   Heterojunction Solar Cells

In 1986, Tang developed the first bilayer heterojunction solar cell based on [PcCu] as a donor material and a perylene derivative PTCBI as an acceptor (Figure 16).[112] After excitation of the Pc dye, migration of excitons takes place, leading to charge separation at the interface of the bilayer heterojunction.[111, 113] Based on this principle, different donor and acceptor materials have been developed.[111, 114, 115]
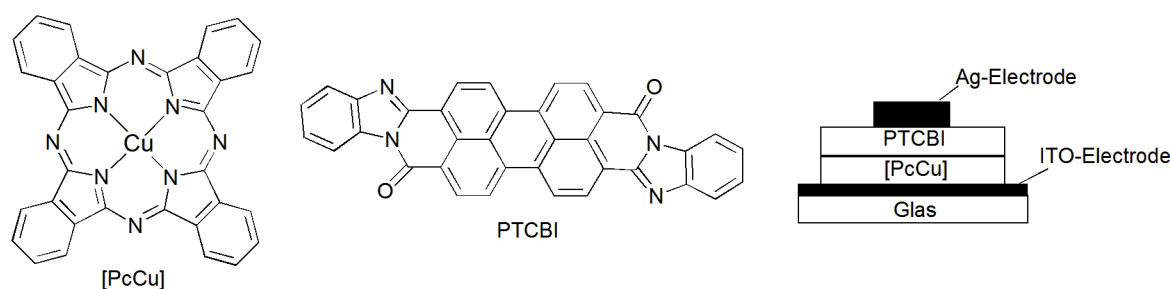
Figure 16: Structure of the bilayer heterojunction solar cell.

A disadvantage of this cell is its low efficiency.[111] This is a result of the low diffusion length of the excitons, as the donor and the acceptor must be of sufficient thickness to effectively collect light. When the diffusion length is insufficient, the excitons formed can not diffuse to the interface, and no efficient charge separation occurs. To resolve this problem, bulk heterojunction solar cells have been developed, in which a blend of a donor and an acceptor is employed. The achieved efficiency for a [PcCu] / C60-based bulk heterojunction solar cell is η = 2.56 % [116], which is clearly enhanced compared to that achieved by Tang (η = 0.95%).[112] Nevertheless, the efficiencies are significantly below those achieved by Grätzel cells (η ~ 11%).

1.4.5.2   Operation of Grätzel Cell

Dye-sensitized solar cells (DSSCs), known as Grätzel cells, where invented by Grätzel and O'Regan.[117] As a result of their high efficiency and stability, DSSCs were the first organic photovoltaic products to reach the market. G24 Innovations Limited (G24i), a

U.K. company founded in 2006, uses DSSCs technology to manufacture and design solar modules. The cells are extremely lightweight and ideal for integration or embedding into a wide array of products, such as mobile electronic devices, tents, and building materials.

A DSSC (Figure 17) is composed of a fluorine-doped tin oxide (SnO_2:F, FTO) covered glass anode, a thin wide-band gap oxide semiconductor mesoporous film, such as TiO_2, a dye monolayer deposited on the surface of the TiO_2 layer, an electrolyte (hole transport material) fully covering the TiO_2/dye surface and a counter electrode, e.g. platinum on glass for electrolyte-containing DSSCs, or a silver or gold electrode for cells using organic hole conducting materials.[118, 119] Under irradiation, an electron is injected from the excited dye into the conduction band (CB) of the oxide. The electrons migrate across the inorganic semiconductor nanoparticle network to the current collector (FTO). After traversing the electrical load, the electrons proceed to the counter electrode. The organic electrolyte (the hole conductor) serves to regenerate the sensitizer and transport the positive charges to the counter electrode, where they recombine with the electrons. Liquid electrolyte DSSCs, with an iodide/triiodide redox couple, are the most efficient organic solar cells (up to 11%) till present.[120, 121]
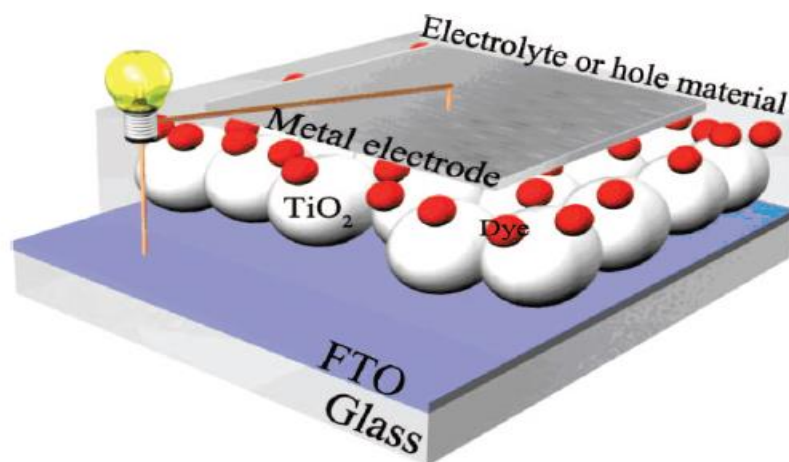
Figure 17: Construction of a DSSC.[122]

1.4.5.2.1 Determination of Photovoltaic Performance[122]

In addition to the overall photon to current conversion efficiency η, the photovoltaic performance is determined according to other parameters, including the incident photon to current conversion efficiency (IPCE), the short circuit current (I_{sc}), the open circuit voltage (V_{oc}) and the fill factor (FF).

Incident Photon to Current Conversion Efficiency (IPCE)

The photocurrent action spectrum of solar cells provides important information about the character of new materials in a device. It represents the ratio of the observed photocurrent divided by the incident photon flux as a function of the excitation wavelength, and is referred to as the incident photon to current conversion efficiency (IPCE). Because normally the measured photocurrent is obtained outside the solar cell device, IPCE can also be called as external quantum efficiency (EQE), i.e. the current obtained outside the photovoltaic device per incoming photon:

$$IPCE(\lambda) = \frac{n(electrons)}{n(Photons)} = \frac{I/e}{P/h\upsilon} = \frac{I}{P} x \frac{hc}{e\lambda} = \frac{I(1240)}{P(\lambda nm)}$$

Where, I, is the photocurrent in A m^{-2} and P is the incident light power in W m^{-2}, e is the elementary charge 1.602×10^{-19} columb, c is the speed of light 3×10^{8} m/sec. and h is Planck's constant (6.626×10^{-34} m^{2}kg/s). By recording the photocurrent response while varying the incident light wavelength, the conversion efficiency of photons to electrons (IPCE) can be determined.

The IPCE value is also given by:

$$IPCE(\lambda) = LHE(\lambda) x \phi_{onj} x \phi_{coI}$$

Where LHE(λ) is the light harvesting efficiency of active materials, Φ_{inj} is the charge injection efficiency between the active materials and Φ_{coI} is the charge collection efficiency at the external electrodes. The maximum IPCE value (IPCE$_{max}$) is a key parameter for describing the device and correlating its performance to the dye absorption, and thereby its molecular structure. The higher the IPCE$_{max}$ and the broader the spectrum, the higher the photocurrent will be.

Power Conversion Efficiency (I-V Curve)

The photocurrent action spectrum is used to assess the ability of the solar cells to convert photons efficiently. To determine whether or not a solar cell has the potential to be commercialized, the photocurrent and photovoltage under the simulated AM 1.5 solar light (the standard intensity of spectral irradiance used for testing) must be measured. A typical solar cell I-V curve is shown in Figure 18.
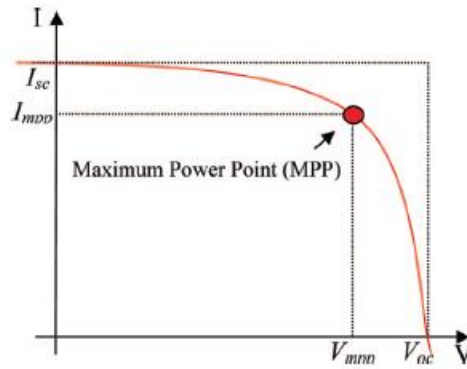
Figure 18: Typical I-V curve of solar cells.[122]

The overall power conversion efficiency (PCE), η, is given by:

$$\eta = \frac{P(out)}{P(in)} = FF \frac{V_{oc}I_{sc}}{P(in)}$$

Where P(out) is the maximum output electrical power (W m^{-2}) of the device under illumination, P(in) is the light intensity incident on the device (W m^{-2}), V_{oc} is the open circuit voltage and I_{sc} is the short circuit current in A m^{-2}.

The parameter FF, the fill factor, is defined as

$$FF = \frac{V_{mpp}I_{mpp}}{V_{oc}I_{sc}}$$

Where V_{mpp} and I_{mpp} are the maximum power point voltage and current in the I-V curve, respectively.

The maximum rectangular area, given by $V_{mpp} \times I_{mpp}$ under the I-V curve, corresponds to the maximum output power of the device. An ideal device would have a rectangular shaped I-V curve, therefore a fill factor FF ≈ 1. The overall efficiency is an important parameter for evaluating the performance of the device.

1.4.5.2.2 Efficient Dyes in DSSCs

An efficient sensitizer has to fulfill several requirements including[118, 169-176]:

- Broad and strong absorption, preferably extending from the visible to the near-infrared region.
- Minimal deactivation of its excited state through emission of light or heat.
- Firm and irreversible adsorption (chemisorption) to the semiconductor surface, and presence of strong electronic coupling between its excited state and the semiconductor conduction band.
- Chemical stability in its ground, excited and oxidized states so that the resulting DSSCs will be stable over many years of exposure to sunlight.

- Reduction potential sufficiently higher (by ~ 150–200 mV) than that of the semiconductor conduction band edge (Fermi level), in order to achieve an effective electron injection. Also, the oxidation potential should be sufficiently lower (by ~ 200–300 mV) than the redox potential of the electron mediator species for rapid regeneration processes.
- Low cost.

Among the Pc dyes, ZnPcs have been involved in both liquid and solid state DSSCs. Unfortunately, the power efficiencies achieved with the Pc based DSSCs is η < 1%. This poor performance has been mainly ascribed to the general tendency of Pcs to aggregate on the surface of the metal oxide nanocrystals[123-125, 177] and to the lack of directionality of the excited state of symmetrically substituted Pcs. However, these limitations could be countered by substitution of the Pcs with bulky groups and by introducing electron withdrawing carboxylic acid groups at selected positions of the Pc macrocycle, thus leading to an efficient electron transfer from the excited dye to the TiO_2 conduction band by improving the electronic overlap between the LUMO of the dye and the Ti 3d orbital.

Examples of unsymmetrical ZnPcs designed for favorable push-pull and steric effects have been recently reported. Although contrasting results have been described,[126] a promising η = 4.6 % was achieved with DSSCs based on ZnPcs having carboxylated aryl groups and six electron donating 2,6-diphenylphenoxy groups (Figure 19).[127]

To suppress aggregation and recombination, the possible benefits offered by unsymmetrical fluorous ZnPcs were explored, since organic compounds characterized by the presence of extended, saturated fluorocarbon domains can lead to self-assembled nanoarchitectures where a fluid like hydro- and organophobic fluorous barrier surrounds nonfluorinated molecular moieties.

The two fluorous ZnPcs[128] (Figure 20) contain one or two electron withdrawing carboxylic moieties directly linked to a benzene unit of the Pc ring, whereas appropriate insulating spacers between the Pc ring and the highly electronegative C_nF_{2n+1} groups were introduced to counter the inductive effect of the fluorocarbon substituents, which would actually counteract the pull effect of the carboxylic groups and disfavor the electron transfer from the photoexcited dye to the TiO_2 conduction band. DFT calculations showed that both the mono- and the dicarboxylic ZnPc derivatives display a perfectly planar geometry of the aromatic macrocycle. The calculated spectrum was in good agreement with the experimental one and the presence of transitions, in which the electronic density was shifted in the proximity of the carboxylic binding groups, thereby guaranting favourable electronic coupling with the acceptor states of TiO_2, was confirmed.
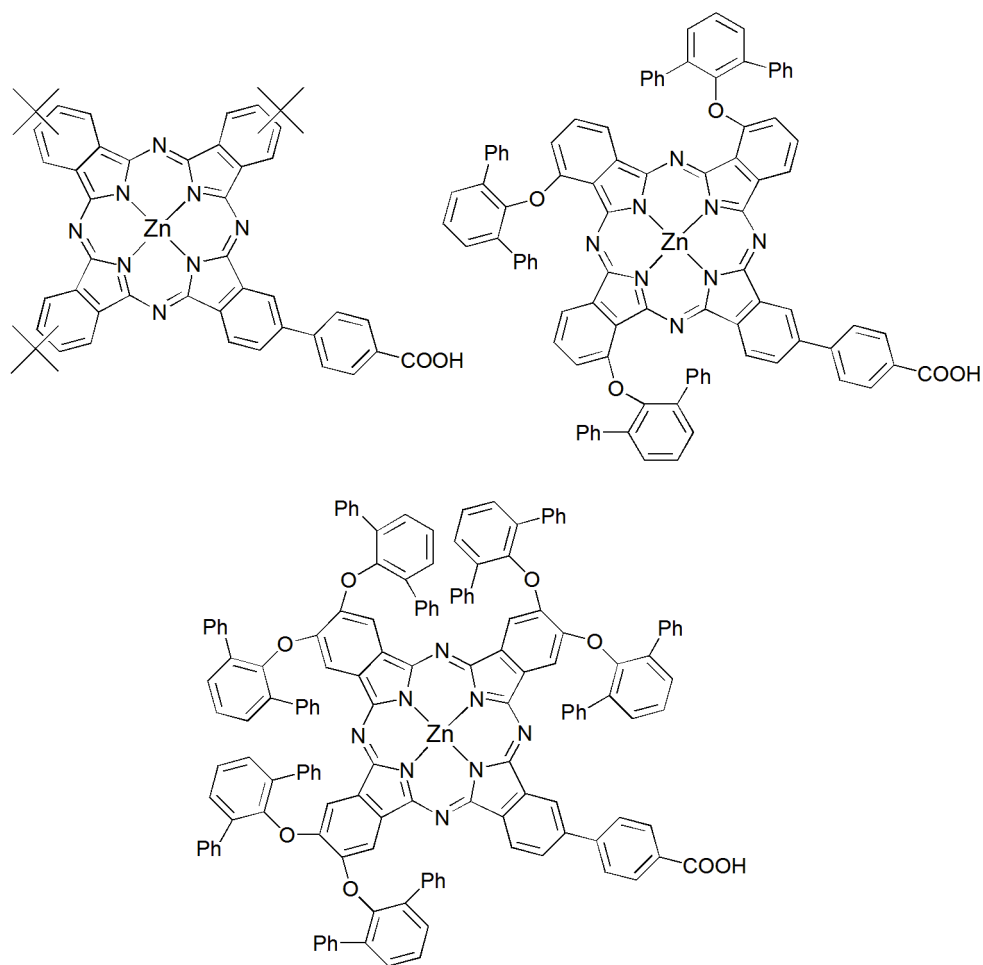
Figure 19: Strucure of some ZnPcs used in DSSC.

The dicarboxylated dye was found to be considerably more effective than the monocarboxylated one, due to a combination of factors mainly resulting from the presence of the twin anchor groups, which allowed for an improved surface coverage, and thus enhanced light absorption and passivation of the surface against electron recapture by $(I_3)^-$.[128]

1, X=H. Y=COOH
2, X= Y= COOH
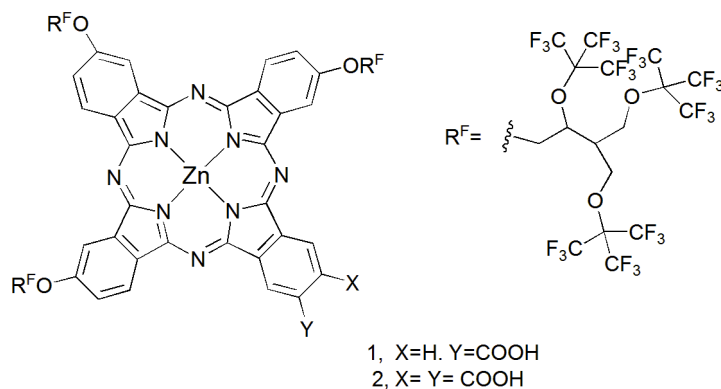
Figure 20: Molecular Structures of fluorous ZnPcs with carboxylate anchors.

Although the sterically hindered fluorous chains may help in shielding the titania surface and the dye itself against the back recombination involving I_2 or $(I_3)^-$, the existence of specific fluorophilic interactions preventing electron recombination is not yet confirmed. Nevertheless, this basic information obtained is useful for the development of new Pc sensitizers for DSSCs with improved photoelectrochemical properties. Recently, Torres et al. confirmed the importance of an appropriate number of linkers for achieving an efficient and stable cell operation with unsymmetrical ZnPc dyes. Indeed, efficiencies approaching 4% have been recorded by using Pcs functionalized with two carboxylic acid groups directly attached to the ring [129] as in ZnPc(COOH)$_2$ (Figure 21), or a mono carboxylic acid moiety conjugated to the Pc ring *via* vinyl groups (Figure 21).[91] The improved, long term stability of the dicarboxylated species compared to analogous, monocarboxylated derivatives is a further indication of the improvement seen by a more complete and stable surface coverage limiting the amount of exposed TiO$_2$ surface that could act as an active recombination center.
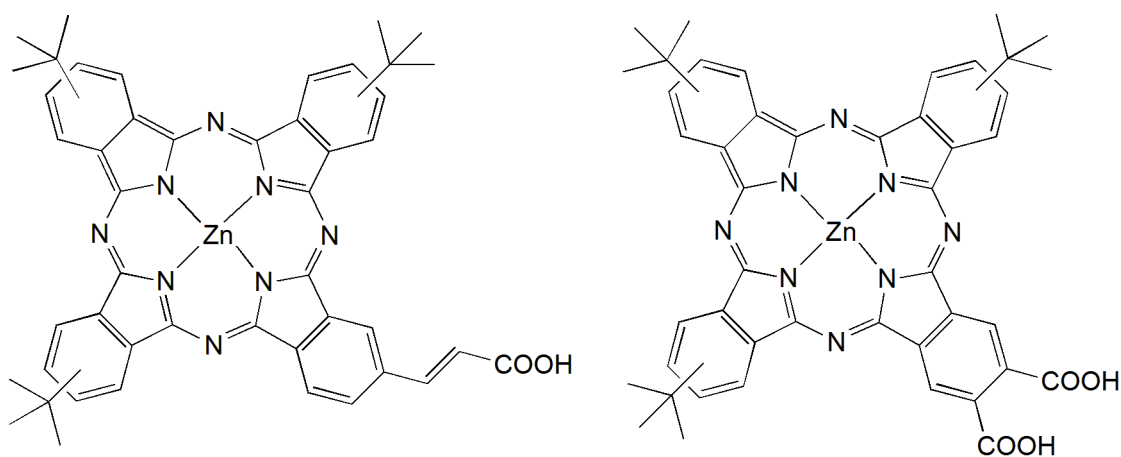
Figure 21: Molecular Structures of ZnPcs achieving efficiencies of 4 % in DSSCs.

1.5 Motivation for phthalocyanines

Although phthalocyanines make up a quarter of the industrial synthetic organic pigments[330] with a worldwide production of 80,000 tons per year (over one billion US$),[331] the usefulness of the phthalocyanines is limited due to their practical insolubility. Pyrazinoporphrazines also have similar characteristics, but as non-sublimable materials, they have not been considered attractive.

Owing to the limited solubility of the phthalocyanines and pyrazinoporphyrazines, reserarchers are focusing on having substituted complexes, and, although many soluble phthalocyanines were reported, none reported on the sublimability of these compounds.

Thus, the aim of this work is to find alternative complexes to the unsubstituted phthalocyanines that are highly soluble, isomerically pure and sublimable. The targeted pyrazinoporphyrazines mentioned in this thesis should also have these characterstics, but at the same time different absolute HOMO and LUMO levels.

2 Results and Discussion

The results section is subdivided into several subsections. Section 2.1 deals with synthesis of the organic precursors, which were building blocks for macrocyclic complexes. Section 2.2 represents some testing conditions for unsuccessful tetramerization of CatPzDN*. In section 2.3, synthetic strategies for the preparation of different metal phthalocyanines and pyrazinoporphyrazines (including, for example, metals of 3d and elements of Group 13 & Group 14) are displayed. This section also includes some successful and unsuccessful testing conditions for the preparation of axially functionalized phthalocyanines, with focus on Group 13 complexes. Section 2.4 describes the Ppz# complexes. Section 2.5 gives a short study on the fluorescence spectroscopy of some complexes. In section 2.6, the electrochemistry of the Pc* and Ppz* complexes was studied by cyclic voltammetry.

2.1 Organic building blocks

The focus of this work was to synthesize substituted MPcs and MPpzs of different metals as well as to axially functionalize the trivalent and tetravalent metal complexes. Hence, the reactions of metal templates with different building blocks for reductive cyclization were studied. The dinitriles used in this work are shown in Figure 22.
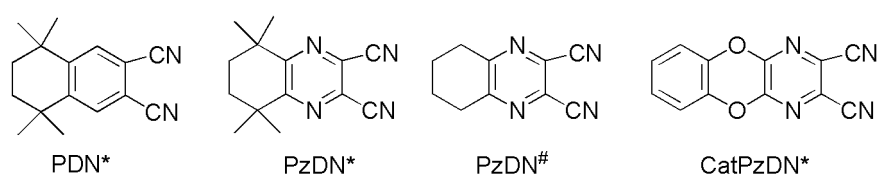
Figure 22: Structure of the dinitriles.

Synthesis of PDN* starting from 2,5-dimethyl-2,5-hexanediol is shown in Figure 23.[189, 190] The starting dihydroxy compound reacted with hydrochloric acid to give the dichloro analog. Friedel-Crafts alkylation with o-xylene formed 1,1,4,4,6,7-hexamethyltetraline. The latter, when oxidized by potassium permanganate in aqueous pyridine, 1,1,4,4-tetramethyltetraline-6,7-dicarboxylic acid was obtained. In turn, treating the acid with acetyl chloride led to formation of the corresponding anhydride. The imide formed upon reacting the anhydride with ammonium acetate in acetic acid. Stirring the product for two days in an ammonia solution led to formation of the diamide. This amide was finally dehydrated and converted to the dinitrile precursor

PDN* using phosphorous oxychloride in DMF. The overall reaction yield *via* these seven steps is ≈ 6 %.
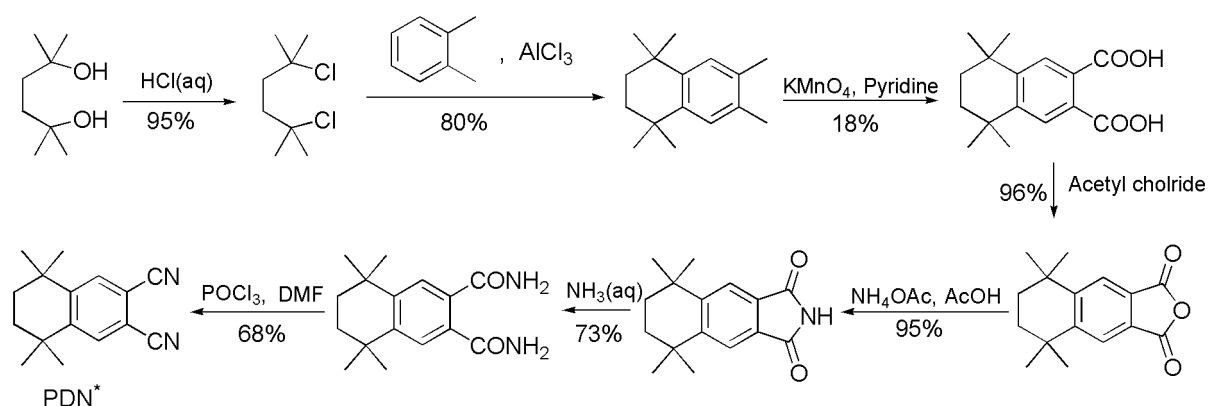
Figure 23: Synthesis of PDN*.

The precursor PDN* was also accessible using different procedures (Figure 24).[314] Once the dichloro compound was obtained, it can react with benzene in the presence of AlCl$_3$ to give 1,1,4,4-tetramethyltetraline. Afterwards, the latter compound reacted with bromine in the prescence of trace amounts of iodine and iron powder to afford 1,1,4,4-tetramethyl-6,7-dibromotetraline. Finally, using CuCN, the bromo subistituents were exchanged with cyano groups and PDN* was formed. The overall reaction yield of these procedures is ≈ 21 %.
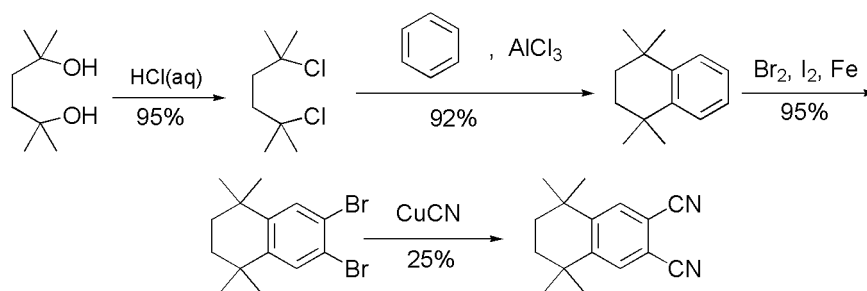
Figure 24: Shorter route for synthesis of PDN*.

While all the products were confirmed by ^{1}H-NMR, a crystal structure of the intermediate 1,1,4,4-tetramethyl-6,7-dibromotetraline was also obtained (Figure 25). The compound crystallizes free of any solvent molecules as colourless plates in the monoclinic space group P 2$_1$/c.

The bond lengths and angles (Table 1) fit well with the expected results. However, as no unique structural parameters are observed, the molecular structure is not discussed in detail.
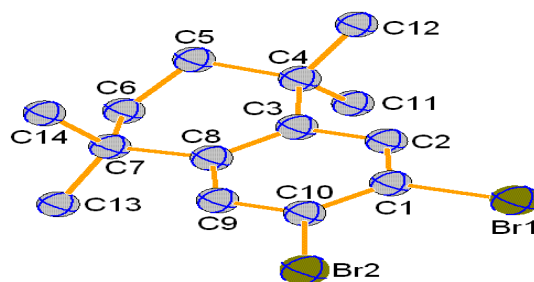
Figure 25: Molecular structure of 1,1,4,4-tetramethyl-6,7-dibromotetraline.

Table 1: Selected Bond Lengths (Å) and Angles (°) of
1,1,4,4-tetramethyl-6,7-dibromotetraline.

Bond lengths/ Å		Angles/ °	
C1-Br1	1.888(3)	C2-C1-Br1	118.8(2)
C10-Br2	1.893(3)	C10-C1-Br1	121.6(2)
C1-C2	1.378(4)	C9-C10-Br2	119.3(2)
C1-C10	1.388(4)	C1-C10-Br2	121.5(2)
C2-C3	1.399(4)	C6-C7-C13	108. 1(11)

Following literature procedures[191-193], the analogous pyrazindinitrile PzDN* was prepared in five steps (Figure 26) starting from pivalic acid. Pivalic acid underwent dimerization using Fenton's reagent (H_2O_2 + $FeSO_4$) to form 2,2,5,5-tetramethyladipic acid. The reaction yield is highly dependent on the stirring rate, and, although it proceeds (with the highest stirring efficiency) in low yield, the reaction could be, due to the inexpensive starting materials, easily carried out in a large scale (1-1.5 mol). Generally, the dimerization reaction occurs by the action of the hydroxyl radicals generated from Fenton's reagent. A hydroxyl radical attacks the aliphatic acid to remove a hydrogen atom bonded to carbon; the free radicals formed then dimerize. After preparation of an adequate amount of the tetramethyladipic acid, the following steps, starting from the esterification reaction, could be easily performed in high yield. The esterification reaction with ethanol gave 80 % yield. Refluxing the diester with trimethylsilyl chloride and sodium in dry toluene led to the formation of 3,3,6,6-tetramethyl-1,2-bis(trimethylsiloxy)cyclohexene. This product was, in turn, quantitatively oxidized by bromine in tetrachloromethane to form 3,3,6,6-tetramethylcyclohexane-1,2-dione. Although the resulting yellow powder was characterized as the desired dione using ^{1}H-NMR spectroscopy, small amount of a colorless by-product formed as single crystals suitable for XRD measurements. The crystals were manually separated, and surprisingly elucidated as 2-bromo-3,3,6,6-hexamethylcyclohexanone. This compound might be formed upon the bromination of 3,3,6,6-tetramethyl-1-mono(trimethylsiloxy)cyclohexene, which could be obtained by over-reduction of the bis (trimethylsiloxy)cyclohexene. Finally, the dione underwent a condensation reaction with diaminomaleonitrile (DAMN) in ethanol and in the presence of a catalytic amount of p-toluenesulfonic acid to obtain the desired precursor PzDN*.

Owing to the poor yield of the first step, the overall reaction yield was calculated as ≈ 6%.
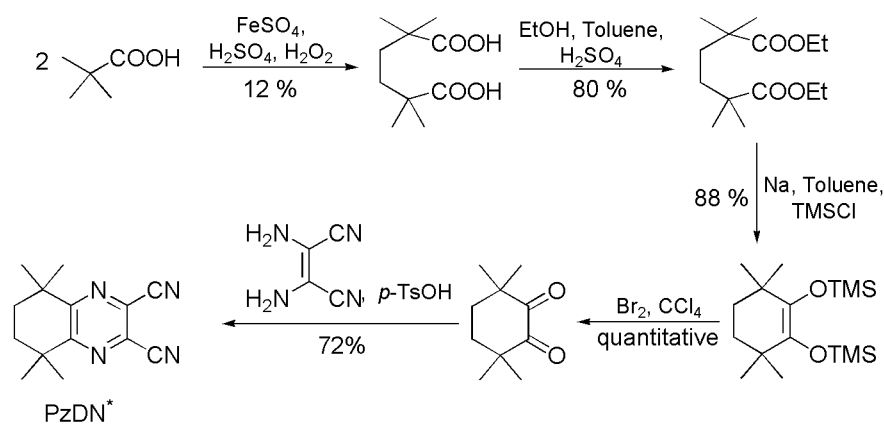
Figure 26: Synthesis of PzDN*.

The molecular structure of 2-bromo-3,3,6,6-hexamethylcyclohexanone is shown in Figure 27. The compound crystallizes free of any solvent molecules as colourless plates in the monoclinic space group P 2_1/c with four molecules per unit cell. The annulated cyclohexene ring adopts a twist-boat conformation. Selected bond lengths and angles are summarized in Table 2. However, the molecular structure is not discussed in detail, as no deviation from the expected bond distances is observed.

Table 2: Selected Bond Lengths (Å) and Angles (°) of 2-bromo-3,3,6,6-hexamethylcyclohexanone.

Bond lengths/ Å		Angles/ °		Angles/ °	
C1-O1	1.2100(15)	C1-C2-C3	112.85(10)	C5-C4-C3	114.10(11)
C2-Br1	1.9560(12)	C1-C2-Br1	109.72(8)	C1-C6-C8	109.85(11)
C1-C2	1.5294(18)	C3-C2-Br1	112.73(8)	C1-C6-C5	108.94((11)
C2-C3	1.5465(17)	C9-C3-C10	109.72(11)	C8-C6-C5	109.85(11)
C3-C4	1.5428(18)	C9-C3-C4	108.71(11)	C1-C6-C7	108.17(11)
C4-C5	1.526(2)	C10-C3-C4	111.31(11)	C8-C6-C7	109.12(12)
C5-C6	1.5425(19)	C9-C3-C2	110.08(10)	C5-C6-C7	110.89(12)
C6-C7	1.5462(19)	C10-C3-C2	111.39(10)	C4-C5-C6	113.45(11)
C6-C8	1.5299(19)	C4-C3-C2	105.54(10)	O1-C1-C2	122.92(11)
C3-C9	1.5294(18)	O1-C1-C6	122.56(12)	O1-C1-C6	114.51(10)
C3-C10	1.5316(18)				
C1-C6	1.5251(17)				

The mechanism of obtaining 2-bromo-3,3,6,6-hexamethylcyclohexanone is proposed (Figure 28). This side product may result from over reduction of the bis-enolate followed by bromination.

It is worthwhile to mention that some reports counted on formation of 2-bromocyclohexanone from (cyclohexenyloxy)trimethylsilane[301-303], but not using bromine.
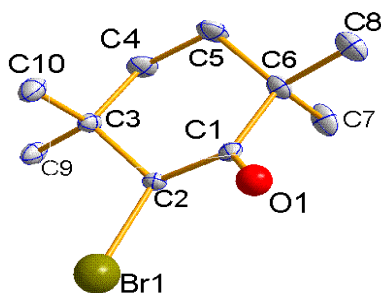
Figure 27: Molecular structure of 2-bromo-3,3,6,6-hexamethylcyclohexanone.
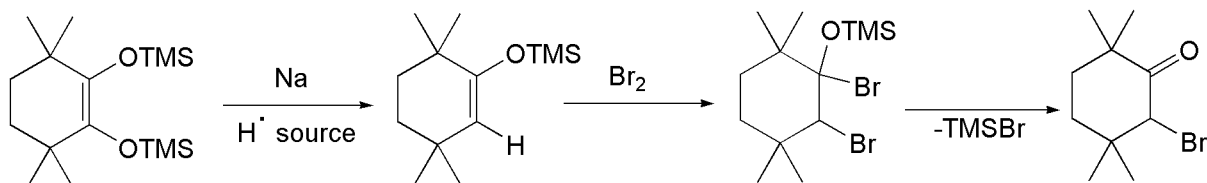
Figure 28: Suggested mechanism for formation of 2-bromo-3,3,6,6-hexamethylcyclohexanone using bromine.

Structurally related to PzDN*, 2, 3-dicyanoquinoxaline (PzDN#) was readily prepared in one step (Figure 29) by refluxing DAMN and 1,2-cyclohexandione with a catalytic amount of p-TsOH in ethanol.[222]
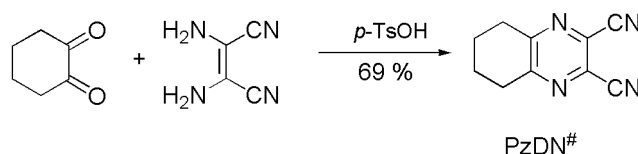
Figure 29: Synthesis of PzDN#.

The new diaza derivative of the already known dibenzo[b,e][1,4]dioxine-2,3-dicarbonitrile[194], 2,3-dicyanopyrazino[6,5-e]benzo[b][1,4]dioxane CatPzDN*, was synthesized for the first time in three steps according to Figure 30. First, by slowly adding the inexpensive, commercially available DAMN to a vigorously stirred oxalyl chloride solution in dioxane; if the addition rate is fast, N,N'-bis[(Z)-3-amino(dinitrilo)but-2-en-yl]oxamide, which could not further react with oxalyl chloride to form 2,3-dioxo-1,2,3,4-tetrahydropyrazine-5,6-dicarbonitrile, would be obtained. Once the desired product was formed, it reacted with thionyl chloride to yield 5,6-dichloropyrazine-2,3-dicarbonitrile.[195] Finally, the precursor was formed upon treating the latter compound with catechol and potassium carbonate in dimethylacetamide (DMA). The last step proceeds only in about 8% yield. The reaction yield was not optimized, as this yellow precursor did not tetramerize under several conditions.
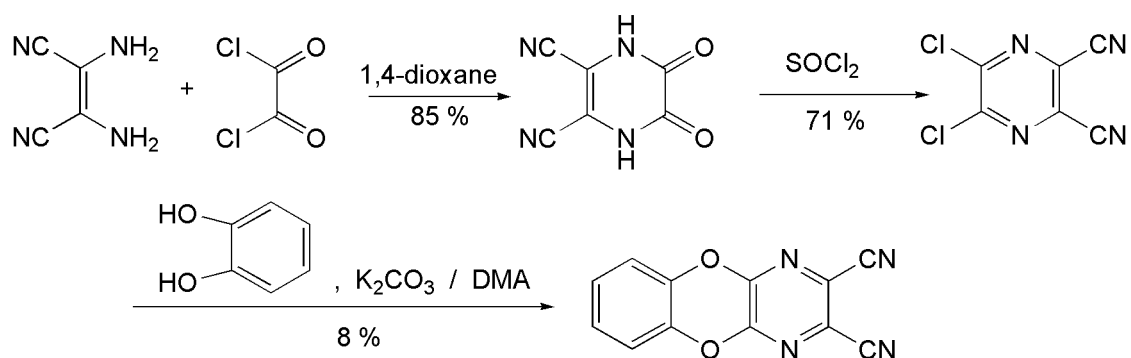
Figure 30: Synthesis of CatPzDN*.

2.2 Attempted Synthesis of [(CatPpz*)Zn]

Several attempts were made to cyclotetrameraize the organic precursor CatPzDN* in the presence of Zn(OAc)$_2$ (Figure 31), however the attempts to prepare [(CatPpz*)Zn] were unsuccessful. Table 3 summarizes all the reaction conditions used in an attempt to prepare the target complex.
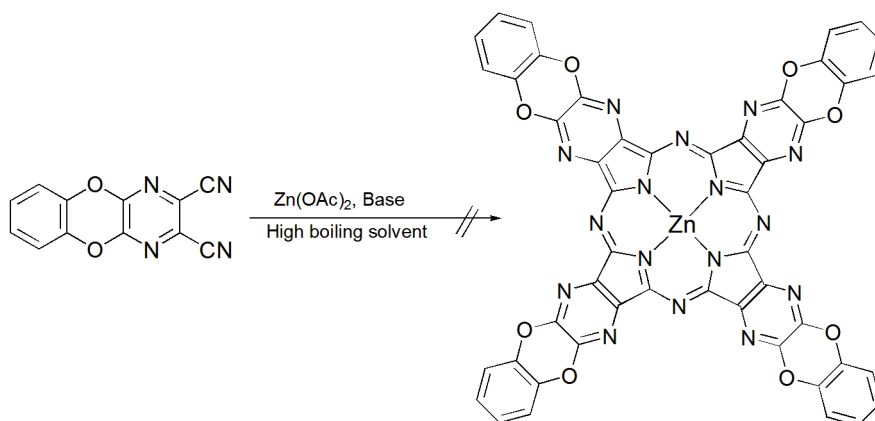
Figure 31: Attempted synthesis of [(CatPpz*)Zn].

Table 3: Unsuccessful attempts to prepare [(CatPpz*)Zn]

Number	Base	Solvent	Temperature	Reaction time
1	Urea	Quinoline	160°C	20 h
2	Urea	-	220°C	45 m
3	DBU	1-Octanol	160°C	18 h
4	Urea	1-CNP	160°C	20 h

Although the selected procedures for the preparation of [(CatPpz*)Zn] have been successfully followed to cyclize other dinitriles, in all cases, the products obtained were not colorful and poorly soluble in the most common organic solvents. Furthermore, EI-

MS measurements did not detect any ion peak assignable to the molecular ion of the expected product [(CatPpz*)Zn].

2.3 Synthesis of Pc* and Ppz* complexes

Since PDN* or PzDN* were first synthesized, many attempts have been made to cyclotetramerize them in the presence of different metal templates.

PDN* was first described by Mikhalenko et al.[190] They prepared [Pc*Co], [Pc*Cu] and [Pc*VO] in 1-bromonaphthalene *via* reacting the organic dinitrile with the corresponding metal chloride in the presence of ammonium molybdate as a source of ammonia. Furthermore, the synthetic procedures of [Pc*Zn] using ZnI_2, as a metal template, were described.[190] However, the authors did not succeed in determining the crystal structure of any complex. Recently in our group, Elisabeth Seikel was able to prepare and elucidate the crystal structure of [Pc*TiO].[197] The titanyl complex formed by reacting the dinitrile with $Ti(On-Bu)_4$ in 1-octanol. Moreover, she obtained and described the crystal structure of the reactive dichloro analog [Pc*TiCl₂].[196]

Elisabeth also succeeded in introducing the pyrazinedinitrile PzDN*, but only its complexes with titanium[198] or molybdenum[193] as central atoms were prepared.

Using PDN* and PzDN* led to three major advantages. First, the obtained symmetrical complexes are substituted in all the peripheral positions making them "isomerically pure", and this facilitated their crystallization. Furthermore, solving their molecular structures using XRD should be much easier. Second, it is simple to characterize the diamagnetic complexes of PDN* and PzDN* using ¹H NMR, as these precursors contain only three and two types of protons, respectively. All the proton types do not couple with each other, thus the respective bands appear as singlets. Finally, the bulky substituents improve the solubility of the macrocyclic complexes in the most common organic solvents.

2.3.1 The Free Ligands Pc*H₂ and Ppz*H₂

Owing to the necessity of using the metal free macrocycles in further reactions, Pc*H₂ and Ppz*H₂ were prepared by treating the dinitrile with a catalytic amount of DBU in 1-pentanol (Figure 32). The reaction requires a high temperature of ≈ 220 °C to proceed in less than 15 minutes. Below this temperature, no reaction takes place. The purification of the crude products was performed using column chromatography (CHCl₃, Al₂O₃), and the products Pc*H₂ and Ppz*H₂ were obtained in 15 % and 24 %.
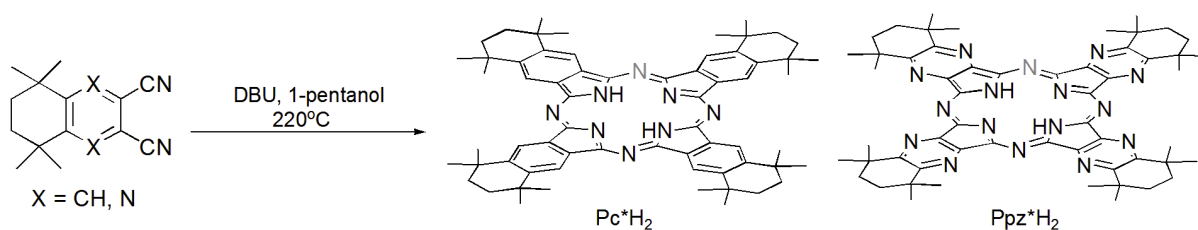
Figure 32: Synthesis of Pc*H_2 and Ppz*H_2.

Formation of Ppz*H_2 in high yield (85 %) by demetalation of [Ppz*Zn] was also successful by heating the complex with pyridine hydrochloride (Figure 33). However, this method is not economically desirable as it depends mainly on adding a large excess of pyridine hydrochloride ($\approx$ 186 eq.).
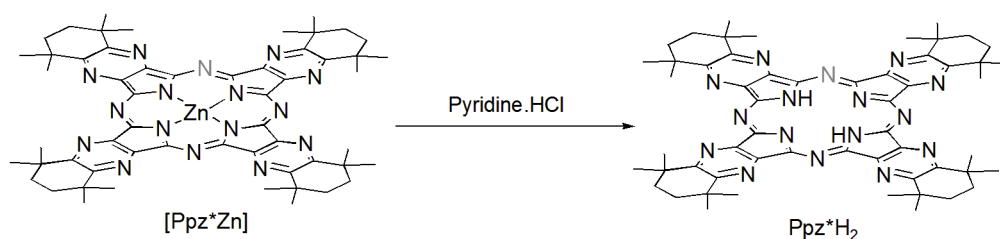
Figure 33: Synthesis of Ppz*H_2 by demetalation of [Ppz*Zn] using pyridine hydrochloride .

The macrocycles are highly soluble in a variety of organic solvents, including $CHCl_3$, DCM, THF and toluene. The chromophores were identified using MS-APCI$^+$ technique, and their spectra displayed protonated molecular ion peaks at 955.8 for Pc*H_2 (Figure 34) and 963.6 for Ppz*H_2.
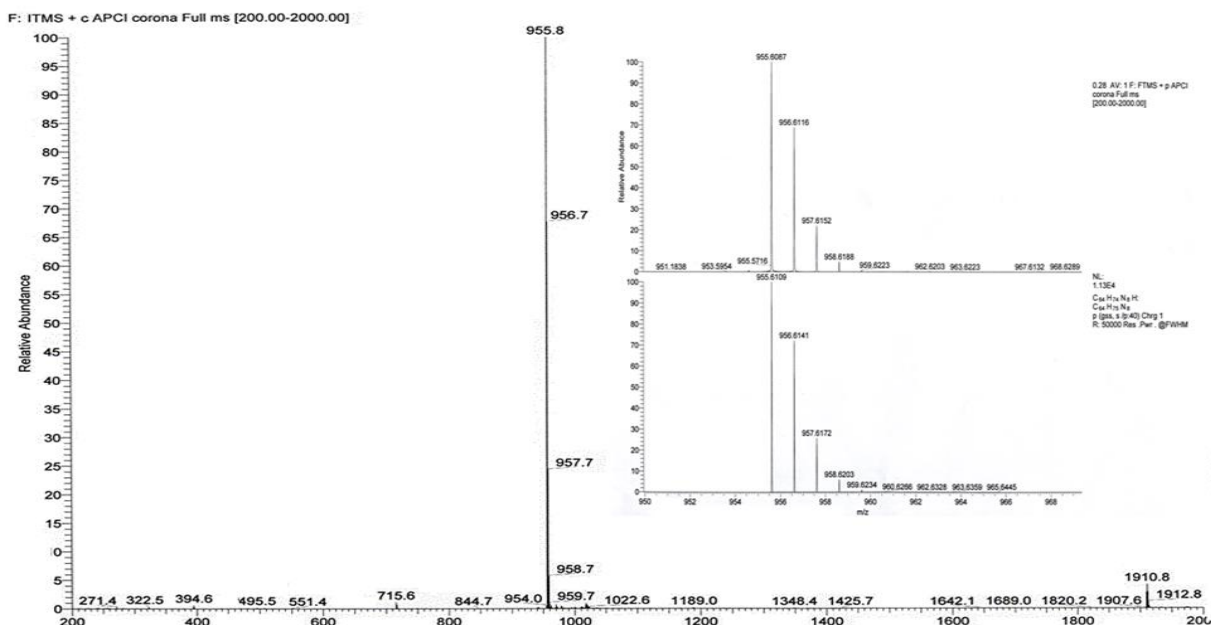
Figure 34: APCI$^+$ Mass Spectrum of Pc*H_2. On the right, a high resolution of the molecular ion peak position is shown compared with its theoretically calculated isotopic pattern.

32

2.3.2   Titanium(IV) Complexes [Pc*TiO] and [Ppz*TiO]

Generally, the oxidation state of titanium in most TiPcs is IV; hence, the titanium central atom coordinates axially to either a dianionic or two monoanionic ligands. However, TiPcs having central Ti(III) atom have been rarely described, e.g. synthesis of [PcTiCl] using TiCl$_3$.[23, 223]

By cyclization of the dinitriles in neat and in the presence of titanium trichloride (TiCl$_3$), we expect the formation of the dichlorotitanium(IV)(aza)phthalocyanines.[196] After 15 minutes from starting the reaction, a purple product of [Pc*TiCl$_2$] or [Ppz*TiCl$_2$] was formed. The obtained complexes could not be sufficiently purified by simple washing under an argon atmosphere, therefore purification using column chromatography (Al$_2$O$_3$, CHCl$_3$) was required. After purifying the complexes, they were no longer purple; rather, a green [Pc*TiO] or a greenish blue [Ppz*TiO] complex was obtained (Figure 35), as the dichloro complexes underwent hydrolysis to form the corresponding oxotitanium(IV) macrocycles. The reaction yield was 52 % and 46 % for [Pc*TiO] and [Ppz*TiO], respectively. This yield of the substituted chromophores is enhanced compared to the previously published results.[197]
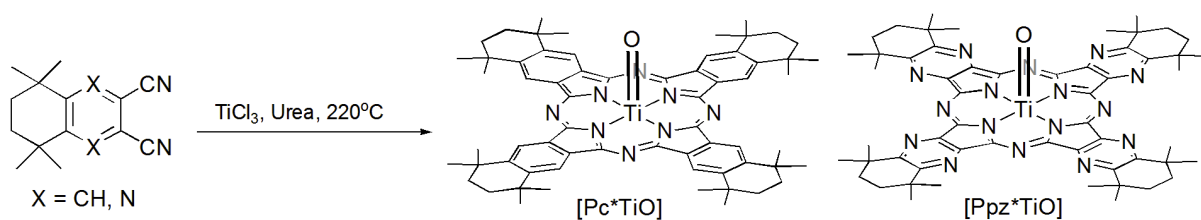
Figure 35: Synthesis of [Pc*TiO] and [Ppz*TiO].

The complexes showed good solubility in most common organic solvents, such as THF, CHCl$_3$, toluene, diethylether and DCM. Their enhanced solubility is due to the presence of methyl groups out of the plane of the macrocycles. These groups hinder the intermolecular interaction between the π-system of the Pc molecules.

APCI$^+$ mass spectral data of [Pc*TiO] and [Ppz*TiO] showed intense protonated molecular ion peaks at 1017.6 and 1025.7, respectively. The mass spectrum of [Ppz*TiO] is shown in Figure 36. In the figure, small peaks were observed at 1039.6 and 1071.6 due to the interaction of the complex with the methanol added during the measurement to form the new species [Ppz*TiOMe+H]$^+$ and [Ppz*Ti(OMe)$_2$+H]$^+$.
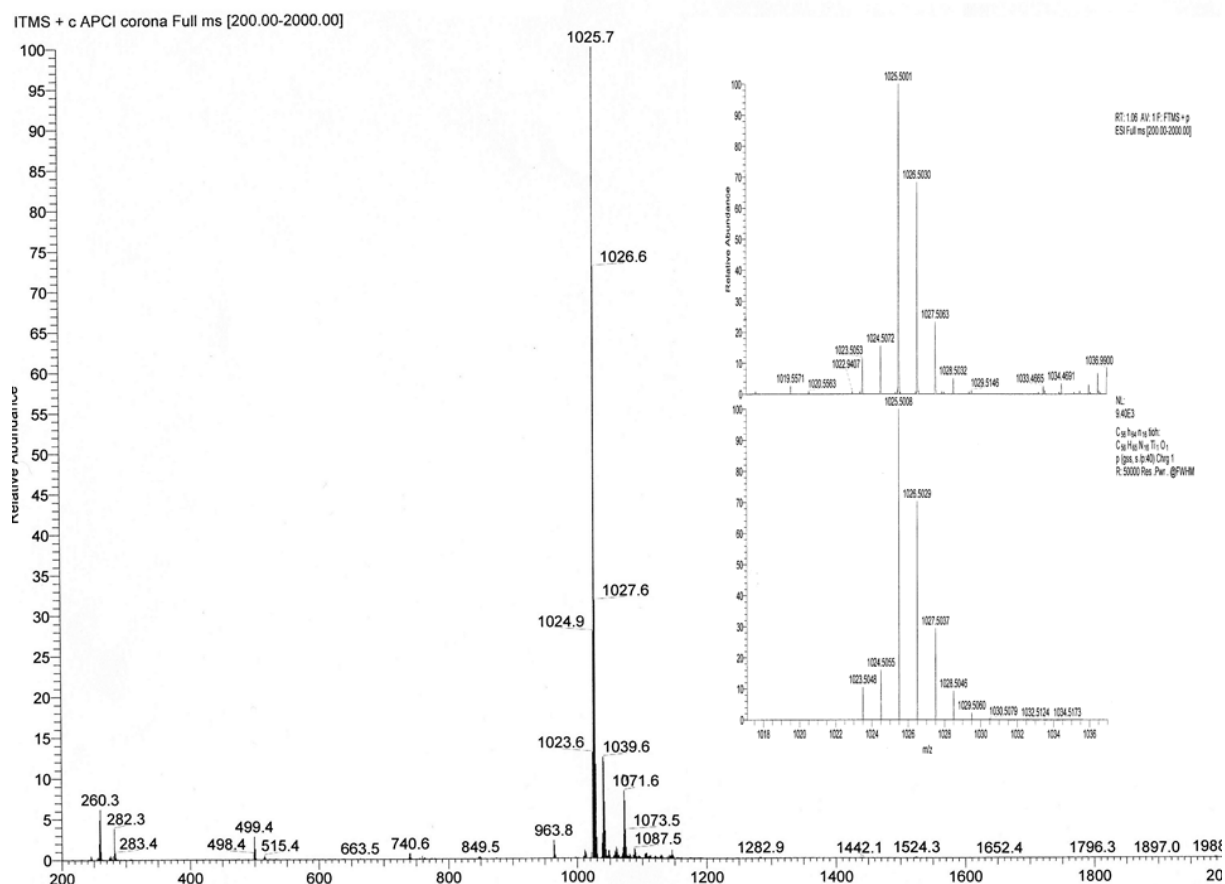
Figure 36: APCI+ Mass Spectrum of [Ppz*TiO]. On the right, a high resolution of the molecular ion peak position is shown compared with its theoretically calculated isotopic pattern .

Figure 37 shows the ^{1}H-NMR spectrum of [Pc*TiO]. As a result of the molecular C_{4v} symmetry, the ^{1}H-NMR spectrum in $CDCl_3$ displayed only four singlets. The signal observed at 9.63 ppm corresponds to the eight aromatic protons. The methyl protons appear as a set of two equivalent singlets at 1.81 and 1.89 ppm, integrated for twenty four protons each. This is not observed in macrocycles without axial ligands. This effect can be explained by the lowering of the molecular symmetry imposed by the axial Ti=O group. The upper and lower hemisphere of the macrocycle become inequivalent, and the methyl groups pointing towards the titanyl moiety (endo) and those pointing away (exo) are located in different chemical environments.[197] The other sixteen aliphatic CH_2 protons are observed at 2.09 ppm. On the other hand, the ^{1}H-NMR spectrum of [Ppz*TiO] in $CDCl_3$ showed its characteristic three singlets. The fourty eight protons of the methyl groups appeared as two singlets at 1.93 and 2.03 ppm and the sixteen CH_2 protons appeared at 2.26 ppm.
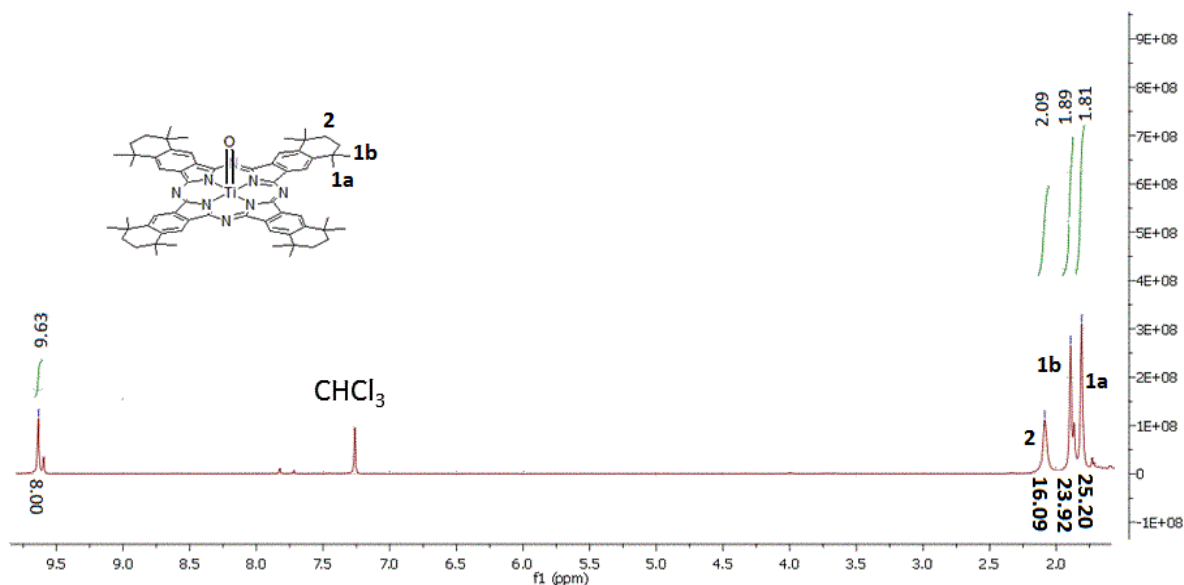
Figure 37: ^{1}H-NMR spectra of [Pc*TiO] in CDCl$_3$ (300 MHz).

The UV/Vis. spectra of the complexes with C$_{4V}$ symmetry [Pc*TiO] and [Ppz*TiO] measured in CHCl$_3$ are shown in Figure 38. The spectra exhibit typical B-bands between 300 to 400 nm and narrow Q-bands in the near infrared region between 716 to 650 nm.[201] This indicates monomeric behavior of the titanium complexes[199], as aggregation in the MPc complexes is typified by a broadened or split Q-band with the high energy band belonging to the aggregate and the low energy band corresponding to the monomer. The Q-absorption band of [Pc*TiO] is red-shifted relative to that of [Ppz*TiO], which has been observed by E. Seikel for [Pc*Mo(Nt-Bu)Cl] and [Ppz*Mo(Nt-Bu)Cl] as well.[193] Furthermore, the main B-band of both [Pc*TiO] and [Ppz*TiO] was observed exactly at 348 nm.
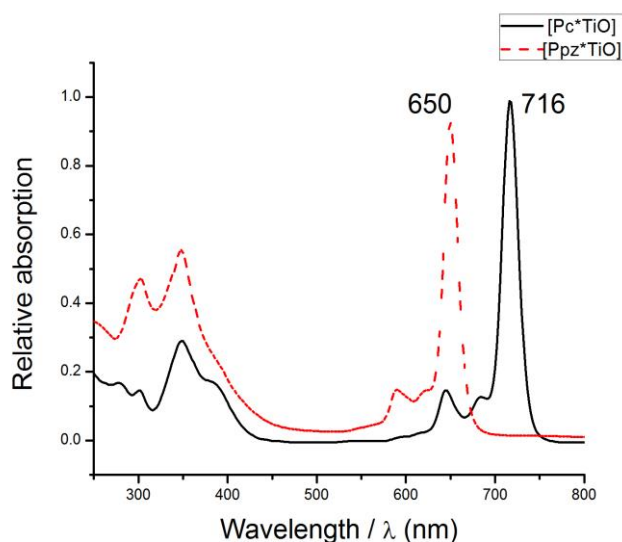
Figure 38: UV/Vis. spectra of [Pc*TiO] and [Ppz*TiO] in CHCl$_3$.

35

Unlike [Ppz*TiO], the B bands of [Pc*TiO] are broadened due to the superimposition of the B1 and B2 bands.[200]   Additionally, in the range of 250-300 nm, the complexes exhibit a rarely observed N-band arising from deeper π levels due to LUMO transitions. However, these bands were usually observed only in UV transparent solvents such as DCM.[202, 203] The Q-band of the soluble [Pc*TiO] is also shifted bathochromically compared to that of the unsubstituted [PcTiO], as a result of the lower HOMO-LUMO gap of the Pc* complex relative to the gap of the unsubstituted Pc one.[198]

2.3.3   Attempted Synthesis of Axially Functionalized Ti(IV)Pcs / Ti(IV)Ppzs

One aim of this work was to synthesize axially functionalized MPcs or MPpzs for various applications as the number of axially substituted complexes is still small. The lack of selective syntheses might be a result of the insolubility of the unsubstituted macrocycles. The sulfur and selenium homologues of [Pc*TiO] and the peroxo complex [Pc*Ti(O_2)], i.e. [Pc*TiS], [Pc*TiSe], [Pc*TiS$_2$] and [Pc*TiSe$_2$], have been already prepared, as the complexes of heavier sulfur and selenium are of particular interest in view of their optoelectronic properties.

In this work, we applied the same synthetic strategy[196, 198] used for these complexes to prepare the corresponding Ppz* macrocycles. We expected that these chromophores could covalently link at different, well-ordered or even single-crystalline model interfaces of classical conductors, e.g. Au(111), Ag(111), Cu(111) or Si(001), and thereby allow us to study their electronic coupling at the heterojunction interface in order to compare their behavior with those of the physically adsorbed (unfunctionalized) parent chromophores.

The reactive complex [Ppz*TiCl$_2$][196] was prepared and kept under an argon atmosphere. Se$_8$ or S$_8$ was then added in the presence of the reducing agent C$_8$K (Figure 39). Unfortunately, attempted reduction in THF led to decomposition to unidentified products, however when toluene was used, no reaction was observed for 24 hours.
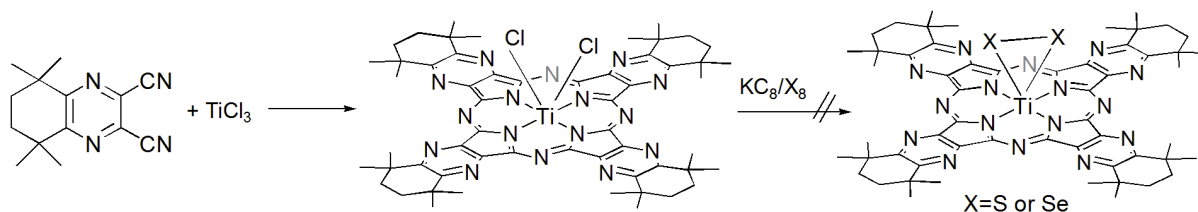
Figure 39: Attempted Synthesis of [Ppz*TiSe$_2$] and [Ppz*TiS$_2$].

Another strategy, described for the unsubstituted complex [PcTiS$_2$][26], was applied to synthesize [Ppz*TiS$_2$] by refluxing [Ppz*TiO] with phosphorous pentasulphide P$_4$S$_{10}$ in dry toluene. This method led to formation of a very colorful blue compound. This compound might be surprisingly [(C$_6$H$_4$N$_2$S$_2$)$_4$TiS$_2$] (Figure 40) confirmed only by high

resolution MS-APCI⁺ results. To confirm this as the product, we tried to grow a single crystal for XRD; however, all the crystals obtained were not suitable for XRD measurements.

Confirmed only by APCI⁺ spectroscopy
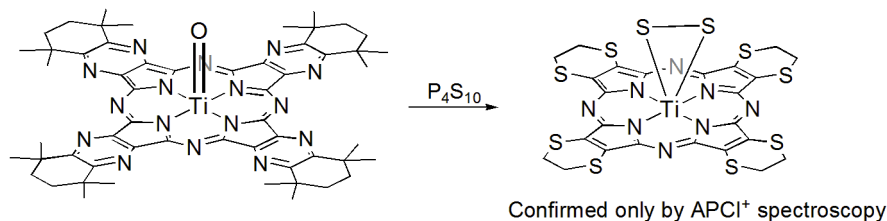
Figure 40: Attempted Synthesis of [Ppz*TiS$_2$] resulted in formation of [(C$_6$H$_4$N$_2$S$_2$)$_4$TiS$_2$] as confirmed by APCI⁺ MS technique.

In addition to the soluble complexes, we tried to develop new strategies for the conversion of ring unsubstituted [PcTiO] to [PcTiS]. Upon using Lawesson's reagent, the monosulphido-complex [PcTiS] was obtained.[320] However, due to the very limited solubilty of the reagent, it was rather difficult to purify the complex. Hence, a structurally similar compound to Lawesson's reagent, but highly soluble in common organic solvents (Figure 41), where phenoxy groups replace the methoxy ones, was prepared.[315] Having the advantage of the high solubility of this reagent in THF at room temperature, the use of this reagent in excess allows for the synthesis of the monosulphido complex [PcTiS]. The molecular ion peak of this complex was detected using both of APCI⁺ and LDI mass spectroscopic measurements. However, the results also indicated the prescence of the oxido complex in small amount (< 5 %).

Previous reports counted on the prescence of stretching vibration of (Ti=S) in the IR spectrum of [PcTiS] at 563 cm⁻¹,[323] however, therein, the methods used to prepare [PcTiS] are known to be non-selective. In our case, the formation of [PcTiS] is accompanied by complete absence of the stretching vibration of (Ti=O), and appearance of a broad band between 900 and 1110 cm⁻¹ . Furthermore, a new peak at 495 cm⁻¹ was observed which might be attributed to a vibration of (Ti=S) bond.
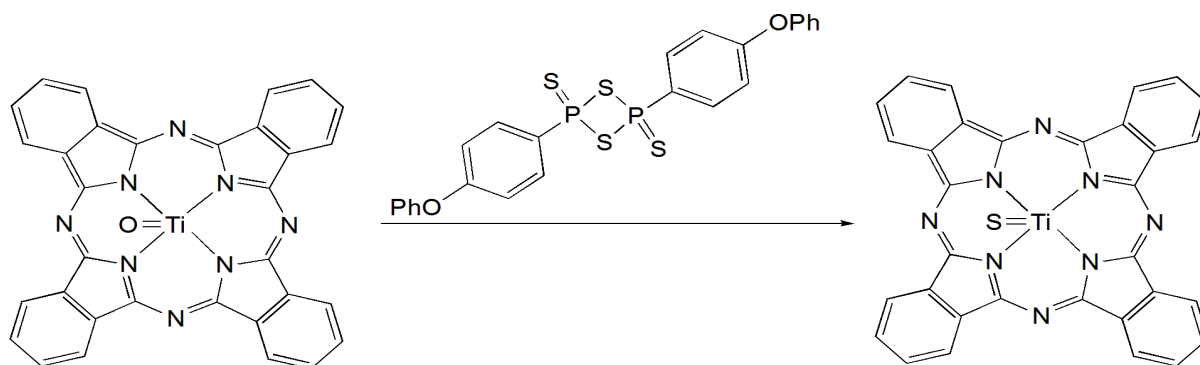
Figure 41: Synthesis of [PcTiS].

37

The structurally similar complex [PcTiSe] was also formed (Figure 42) by the action of Woolins' reagent.[317] However, unlike the APCI+ mass measurements, the molecular ion peak of this complex was only detected by LDI mass spectroscopy. Comparing the IR-spectrum of the product with that of [PcTiO] revealed the absence of the stretching vibration of (Ti=O) at 978 cm^{-1} and appearance of a broad band between 890 and 948 cm^{-1}. Additionally, a new band is observed at 526 cm^{-1}.
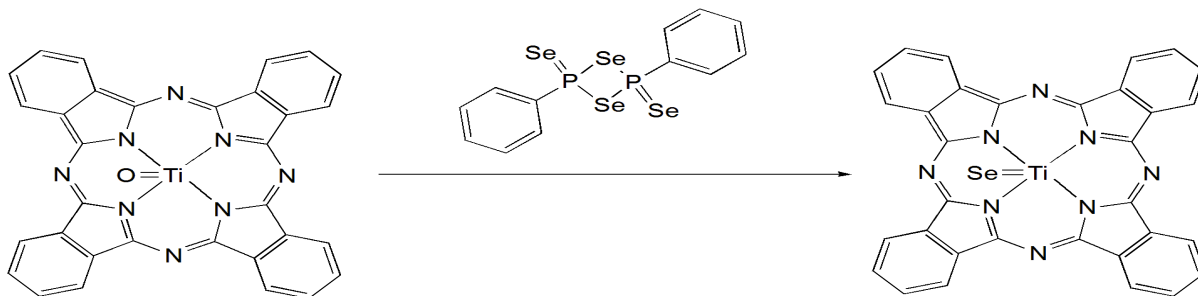
Figure 42: Synthesis of [PcTiSe].

All the previously reported procedures showed low selectivity of substituting the oxido ligand for a sulphido one, as the Q-band of both of [PcTiO] and [PcTiS] was found to be exactly at 692 nm in chlorobenzene. However, upon the action of Lawesson's reagent, a small red-shift of 2 nm was observed, hence [PcTiS] absorbs at 694 nm (Figure 43). Although the starting [PcTiO] was not any more detected by LDI, the Q-band of [PcTiSe] was found at 693 nm. This means that substituting O by S or Se is not affecting the two main absorption peaks of the chromophoric Pc ligands.
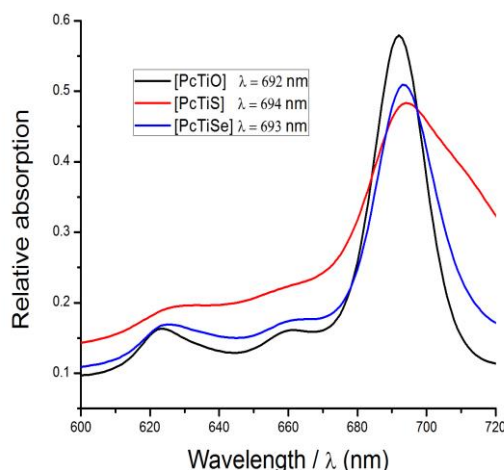
Figure 43: UV / Vis. spectra of [PcTiO], [PcTiS] and [PcTiSe] in chlorobenzene.

To conclude, a new synthesis for [PcTiS] and [PcTiSe] has been described. It leads to higher purity products, as indicated by the absence of the stretching vibration of (Ti=O) at 978 cm^{-1}, detecting a small red-shift regarding the Q-band position of [PcTiS] and

[PcTiSe] compared to that of [PcTiO] and detecting the molecular ion peaks of the complexes [PcTiS] and [PcTiSe].

Other unsuccessful strategies for the formation of [PcTiS] were also attempted (see experimental section).

Pcs functionalized with the acidic anchor –COOH either axially or equatorially are known[198, 211, 212] and commonly used in DSSCs. This moiety allows for an efficient overlapping between the LUMO of the macrocycles and the conduction band of a metal oxide semiconductor surface, e.g. TiO_2. Pcs with equatorial phosphonic acid moieties are also known[226-228, 249], however, attempted preparation of TiPcs with an axial phosphonic acid functionality was unsuccessful.[198] A comparison between the anchoring carboxylic and phosphonic acid moieties has been explored in detail.[249] The results showed that a carboxylic acid function leads to higher levels of dye adsorption than does a phosphonic acid anchoring group, and thus gives a slightly higher solar conversion efficiency. However, the phosphonic acid was shown to have stronger binding properties than the carboxylate anchoring group, which improves the durability of the DSSCs. In this work, we tried to perform a salt elimination reaction between K_2HPO_4 and [LTiCl$_2$] (L=Pc* or Ppz*, Figure 44) in order to obtain TiPcs bearing an axial phosphoric acid functionality. The reactants were suspended and refluxed in dry toluene under an argon atmosphere. Unfortunately, the desired reaction did not proceed, and finally the titanyl complexes [Pc*TiO] and [Ppz*TiO] were obtained.
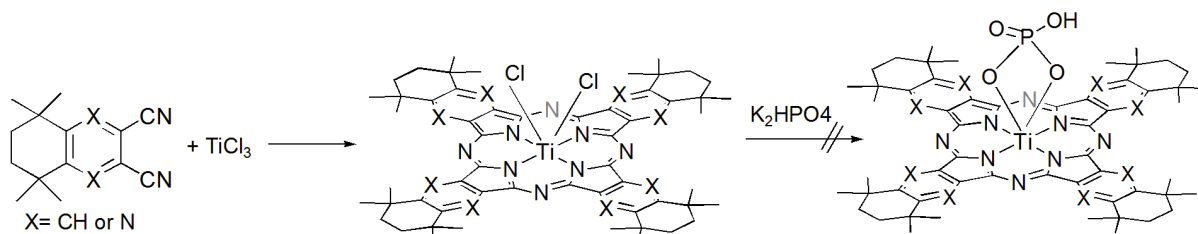
Figure 44: Attempted Synthesis of [Pc*Ti(HPO$_4$)] and [Ppz*Ti(HPO$_4$)].

2.3.4 Vanadium(IV) Complexes [Pc*VO] and [Ppz*VO]

Among all the oxidation states of vanadium, only VPcs containing V(III) and V(IV) are known. The axial ligand is either a halogen[204] or an oxygen[205]; however, the macrocycles of the type [PcVO] are the most common. In this work, we were able to prepare both the substituted [Pc*VO] and [Ppz*VO] complexes (Figure 45). Addition of urea was not essential but only used to increase the reaction yield. After purifying the products using column chromatography (CHCl$_3$, Al$_2$O$_3$), [Pc*VO] and [Ppz*VO], especially the latter were obtained in high yield of 50 % and 84 %, respectively. The complexes are highly soluble in common organic solvents including: CHCl$_3$, THF, DCM and toluene.

[Pc*VO] and [Ppz*VO] were clearly identified using UV-Vis. and APCI+ spectroscopic techniques and elemental analysis.
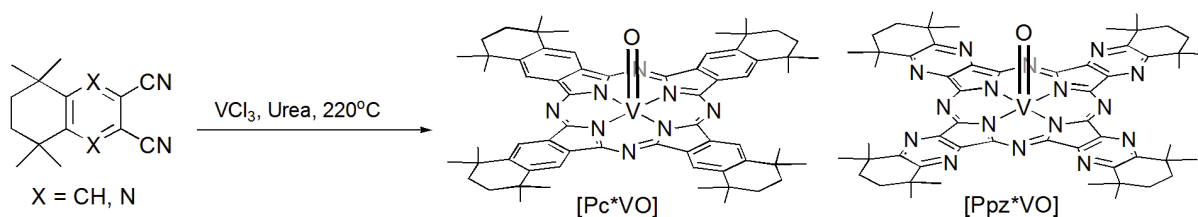
Figure 45: Synthesis of [Pc*VO] and [Ppz*VO].

The APCI+ mass spectra of the complexes showed intense protonated molecular ion peaks at m/z 1020.5 and 1028.7 for [Pc*VO] and [Ppz*VO] (Figure 46), respectively, confirming the proposed molecular structures
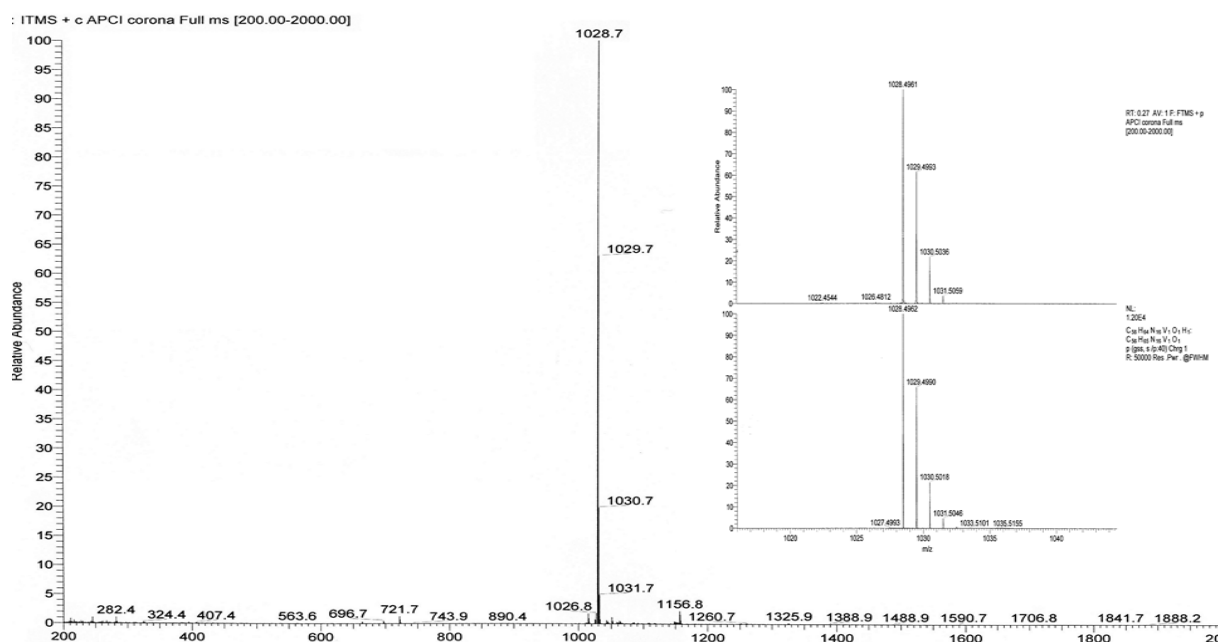
Figure 46: APCI+ Mass Spectrum of [Ppz*VO]. On the right, a high resolution of the molecular ion peak position is shown compared with its theoretically calculated isotopic pattern.

The UV-Vis. spectra of [Pc*VO] and [Ppz*VO] in $CHCl_3$ are quite similar to those of the titanium ones, showing Q-bands at 717 and 648 nm respectively (Figure 47). The B bands lie in the range of 348-298 nm; however, the B bands of [Pc*VO] are not very well separated due to some superimposition.[200] The effect of substituting the benzene rings by pyrazine ones is clearly observable causing blue shifts in the spectra.
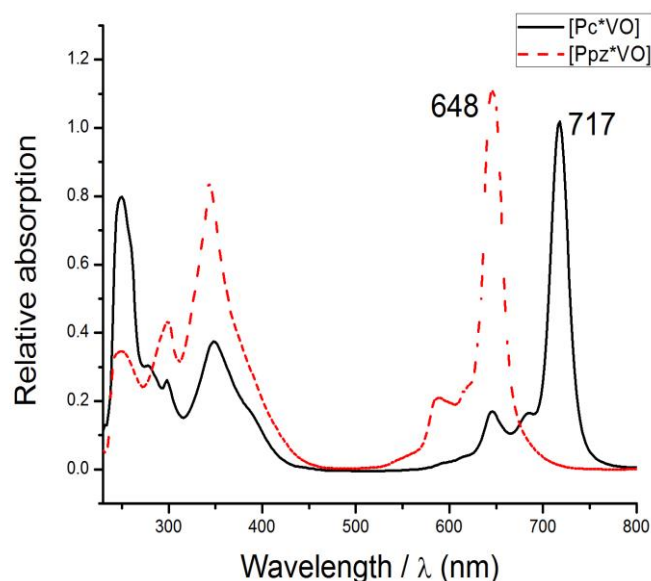
Figure 47: UV / Vis. spectra of [Pc*VO] and [Ppz*VO] in CHCl₃.

In the reaction, it is striking that the complexation process is associated with oxidation of V(III) to V(IV). To prove this, we were able to obtain suitable single crystals for XRD measurements.

Suitable crystals for X-ray diffraction of [Pc*VO] were obtained by controlled diffusion of pentane vapor into a chloroform solution of the complex. The complex crystallizes as [Pc*VO].4CHCl₃ (Figure 48) in the monoclinic space group P2₁/c as a green prism with ten formula units per unit cell. The vanadium atom is too large to occupy the Pc* cavity; it sits 'atop' or 'out-of plane' from the N4 plane, and has a five-coordinate, square-pyramidal configuration. Owing to the C₄ᵥ symmetry of the molecule, all the isoindole rings in the molecule are equivalent. Furthermore, the fused cyclohexene rings adopt a half-chair conformation. Selected structural parameters of the obtained vanadyl complex [Pc*VO].4CHCl₃ are summarized in Table 4.

Table 4: Selected Bond Lengths (Å) and Angles (°) for [Pc*VO].4CHCl₃.

Bond lengths/ Å		Angles/ °	
V1-N2	2.057(3)	N4-V1-N2	84.75(12)
V1-N4	2.058(3)	O1-V1-N2	146.04(8)
V1-N2'	2.016(3)	O1-V1-N4	106.9(2)
V1-N4'	2.035(3)	O1-V1-N2'	107.5(2)
V1-O1	1.587(5)	O1-V1-N4'	106.9(2)
dV(out of plane)	0.600	N2-V-N2'	146.04(8)
d(P₁-P₂)	3.927	N4-V1-N2'	84.90(12)
d(V₁-V₂)	11.849	N4-V1-N4'	146.20(8)

d(P₁-P₂) the distance between two neighboring N₄ planes
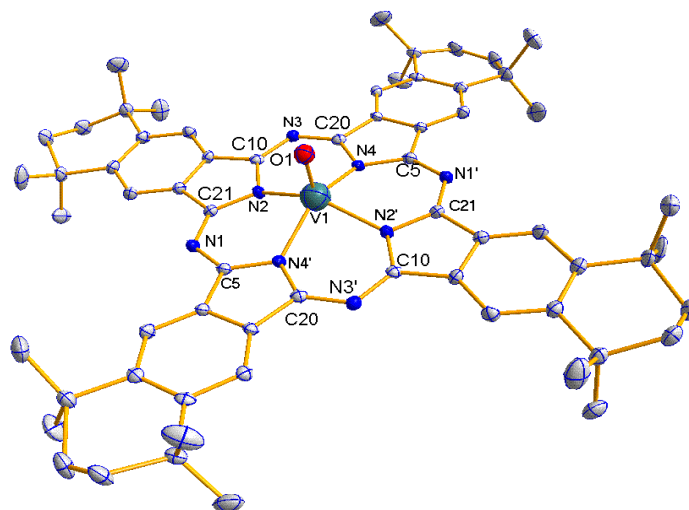
Figure 48: Molecular structure of [Pc*VO].4CHCl$_3$ crystallized from CHCl$_3$. The four solvent molecules and all H atoms are omitted for clarity, Ellipsoids are shown at 50% probability.

The unsubstituted [PcVO], like many MPcs, possesses interesting photoconductor and semiconductor properties. The complex, and its ring-substituted derivatives have found use as pigments, semiconductors, photoconductors, photoreceptors, imaging agents, and catalysts. In a detailed study of the polymorphism in [PcVO] by Griffiths et al, three crystalline phases - α, β, and γ - were identified for the complex[235], but only the β phase was characterized, *via* a single-crystal, X-ray structural determination.[236]

Comparing the β phase of [PcVO] to the substituted [Pc*VO].4CHCl$_3$ crystals reveals closeness of the analogous bond lengths and angles between the two complexes. In [PcVO], the VO^{2+} cation lies perpendicular to the isoindole nitrogen plane, with a V-O distance of 1.580(3) Å, the four N-V-N base angles have a mean value of 85.4(2), the two obtuse N-V-N angles are 146.8(1) and 147.2(1) and the V-N distances do not differ significantly; having a mean length of 2.026(7) Å. The oxovanadium cation of [PcVO] coordinates the four isoindole nitrogens with vanadium lying 0.575(1) Å above the plane formed by the four nitrogen atoms. Furthermore, The shortest centroid-centroid distance in [PcVO] is 5.378 Å and the shortest intermolecular distance between two neighboring N4 planes is 3.208 Å. Comparing to [Pc*VO], the intermolecular distance is 3.927 Å and the closest vanadium-vanadium distance is 11.849 Å. The longer metal-metal distance might be attributed to the prescence of the bulky substituents, which might prevent the coupling between the neighboring molecules.

In the similar oxovanadium(IV)porphyrin ''vanadyldeoxophylloerythroetioporphyrin-l,2-dichloroethane solvate (Vanadyl DPEP)''[324] (Figure 49 (a)), the V-O distance is 1.62(1) Å and the vanadium atom lies 0.48 Å above the isoindole nitrogen plane. The differences, which are marginally significant, correlate with the slightly larger coordination cavity of the porphyrin macrocycle.
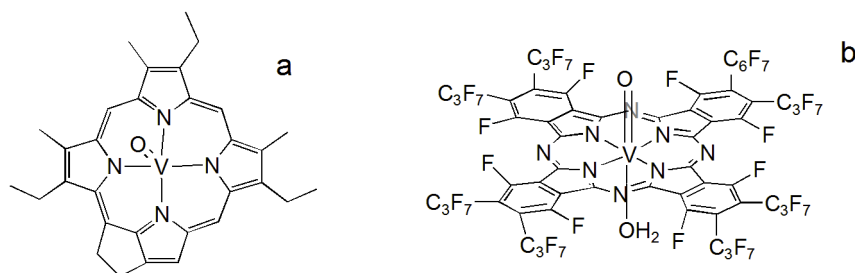
Figure 49: Molecular structure of vanadyl DPEP (a)[324] and [F_{64}PcVO(H_2O)] (b). [237]

The relative arrangement of the molecules to each other in the crystal lattice has a decisive influence on the electrical conductivity of the Pcs. Therefore, the arrangement of the aromatic system of [Pc*VO], with solvent molecules omitted, is shown in Figure 50. Generally, a 50:50 disorder occurrs with respect to the orientation of V = O groups, which could be attributed to the steric shielding of the central metal by the peripheral alkyl groups. The cell packing of [Pc*VO] is composed of sheets of approximately parallel and weakly π-stacked molecules, with no evidence of the presence of a discrete dimer pair in the solid state. Generally, the Pcs can be considered electrically conductive if the π-systems of the adjacent molecules are able to overlap to promote the transfer of electrons or holes. In [Pc*VO], the axial moiety and the prescence of bulky substituents prevent strong aggregation of the π-systems. Furthermore, it has been reported that the formation of dimeric assemblies takes place via intermolecular contact of the benzene rings below the 3.6 Å threshold that is indicative of π-π interactions.[237] Owing to the higher intermolecular distance in this case, dimeric assemblies of the complex can be excluded.
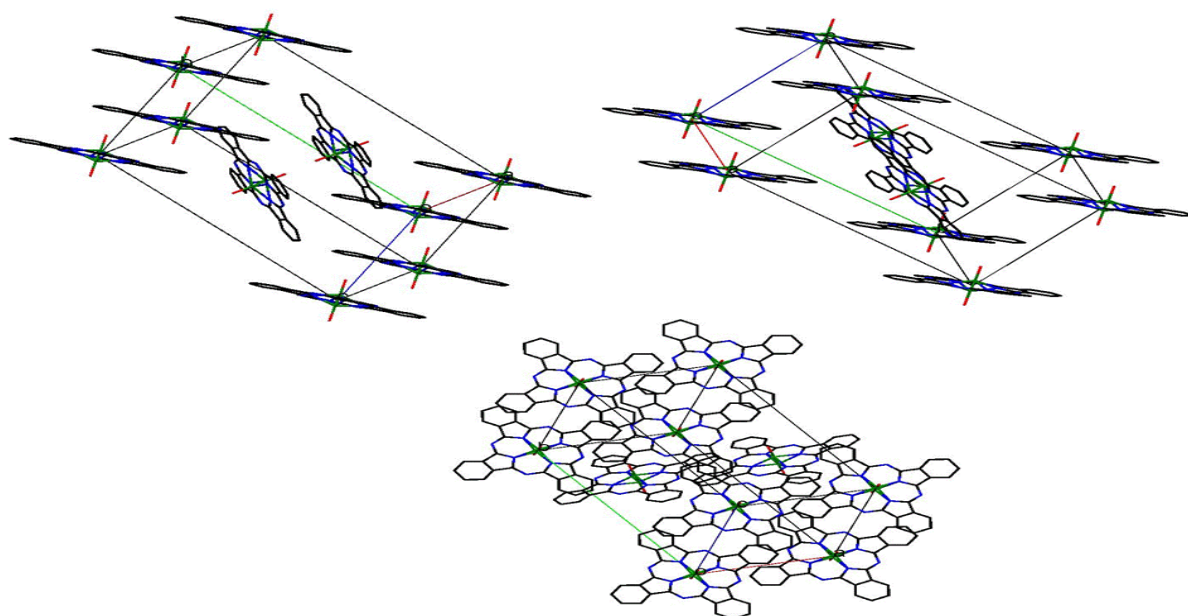
Figure 50: Unit cell packing of the aromatic system of [Pc*VO] molecules in the solid state. All the solvent molecules, H atoms and aliphatic substituents are removed for clarity. The orientation of the V=O moieties is not clear and might be located at both sides with 50% probability.

43

Slightly different results were obtained for the corresponding Ppz* derivative. Blue plates of [Ppz*VO(OH$_2$)].8DCM formed by slow evaporation of DCM from a saturated solution of the complex. The complex crystallizes in the tetragonal space group P4/nmm. The complex molecular structure is shown in Figure 51.
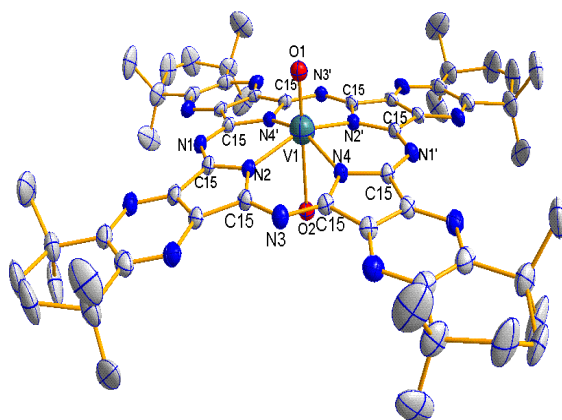
Figure 51: Molecular structure of [Ppz*VO(H$_2$O)].8DCM crystallized from DCM. All the DCM molecules and H atoms are omitted for clarity. Ellipsoids are shown at 50% probability.

All the isoindole rings in the molecule are equivalent, and the fused cyclohexene rings adopt a half-chair conformation. Surprisingly, the vanadium atom in this structure is octahedrally coordinated with the four nitrogen atoms of the four isoindole rings and two oxygen ligands occupying the axial positions. Furthermore, the vanadium atom resides only little above the N4 equatorial plane. To better understand the reason, it is worthwhile comparing the molecular structure of the complex with a molecular structure of an electron deficient vanadyl phthalocyanine, e.g. [F$_{64}$PcVO(H$_2$O)] (Figure 49(b)).[237] Generally, the finding that a metal in a high valence state (IV) can be accommodated in such an electron deficient coordinating environment is surprising, but it can be rationalized by the presence of the axial oxo-ligand and an aqua lgand *trans* to the oxo one, the ligand with lowest thermodynamic *trans* effect. The additional H$_2$O coordination was also postulated to occur in frozen DMSO solutions of t-butyl [PcVO] as a possible alternative to DMSO coordination.[238]

The bond distances and angles of [Ppz*VO(H$_2$O)].8DCM (Table 5) agree well with the reported values of [F$_{64}$PcVO(H$_2$O)]. For [F$_{64}$PcVO(H$_2$O)], the V-N distances are statistically indistinguishable at 2.027(4) Å and close to those obtained for [Ppz*VO(OH$_2$)].8DCM. The doming of [F$_{64}$PcVO(H$_2$O)] is virtually identical, with the V-N4 (coordination plane) distances being 0.36(1) Å shorter than that obtained for [Ppz*VO(H$_2$O)].8DCM. For [F$_{64}$PcVO(H$_2$O)], the V-O (H$_2$O) and V=O distances are 2.359(3) Å and 1.586(3) Å, respectively, and correspond to 2.353(13) Å and 1.594(11) Å for the [Ppz*VO(H$_2$O)].8DCM, while the V=O distance in H$_{16}$PcVO is 1.580(3) Å. The V=O distance is statistically insensitive to changes in the metal coordination environments. The intramolecular structural effects of perfluorinated [F$_{64}$PcVO(H$_2$O)] are apparent in a

comparison with those of the parent nonfluorinated $[H_{16}PcVO]$. Although the V-N distances are quite close, 2.027(4) Å for $[F_{64}PcVO(H_2O)]$ and 2.026(7) Å for $[H_{16}PcVO]$, the V atom is 0.2 Å closer to the N4 coordination plane in $[F_{64}PcVO(H_2O)]$. In our case, the V atom of $[Ppz*VO(H_2O)].8DCM$ deviates less from the planarity compared to $[Pc*VO].4CHCl_3$, i.e the distance between the V atom and the N4 plane is 0.1865 Å closer than in the case of $[Ppz*VO(H_2O)].8DCM$. Generally, this effect could be ascribed to an increase in the ligand coordination sphere and the approximate invariability of the V-N bond lengths.

Table 5: Selected Bond Lengths (Å) and Angles (°) for $[Ppz*VO(H_2O)].8DCM$.

Bond lengths/ Å		Angles/ °		Angles/ °	
V1-N2	2.031(7)	N4-V1-N2	87.62(7)	N4-V1-N4'	156.5(4)
V1-N4	2.031(7)	O1-V1-N2	101.75(18)	O2-V-N2	78.25(18)
V1-N2'	2.031(7)	O1-V1-N4	101.75(18)	O2-V1-N4	78.25(18)
V1-N4'	2.031(7)	O1-V1-N2'	101.75(18)	O2-V1-N2'	78.25(18)
V1-O1	1.594(11)	O1-V1-N4'	101.75(18)	O2-V1-N4'	78.25(18)
V1-O2	2.353(13)	N4-V1-N2'	87.62(7)	O2-V1-O1	180.0
dV(out of plane)	0.4135				
d(P_1-P_2)	6.664				
d(V_1-V_2)	6.654				

d(P_1-P_2) the distance between two neighboring N_4 planes

In Figures 52, the $[Ppz*VO(OH_2)]$ molecules showed columnar packing with four molecules per unit cell. The molecules are regularly packed in a face to back mode. However, surprisingly, the closest intermolecular distance between two neighboring N4 planes and the closest distance between two vanadium atoms in neighboring molecules are very close, i.e. 6.664 Å and 6.654 Å, respectively. That means only a very short distance of 2.7146(2) Å is present between the oxido ligand of a molecule and the water oxygen atom of the neighboring molecule. Thus, in this case, formation of dimeric species (Figure 53) having hydrogen bonds between the adjacent molecules is expected.

Usually coordinated water molecules could be confirmed in the metal complexes by the prescence of a sharp and a broad peak at 726 and 637 cm⁻¹, respectively.[225] However, in this case, due to the absence of any broad peak at around 637 cm⁻¹, the water molecule is supposed to be included during the crystallization process.
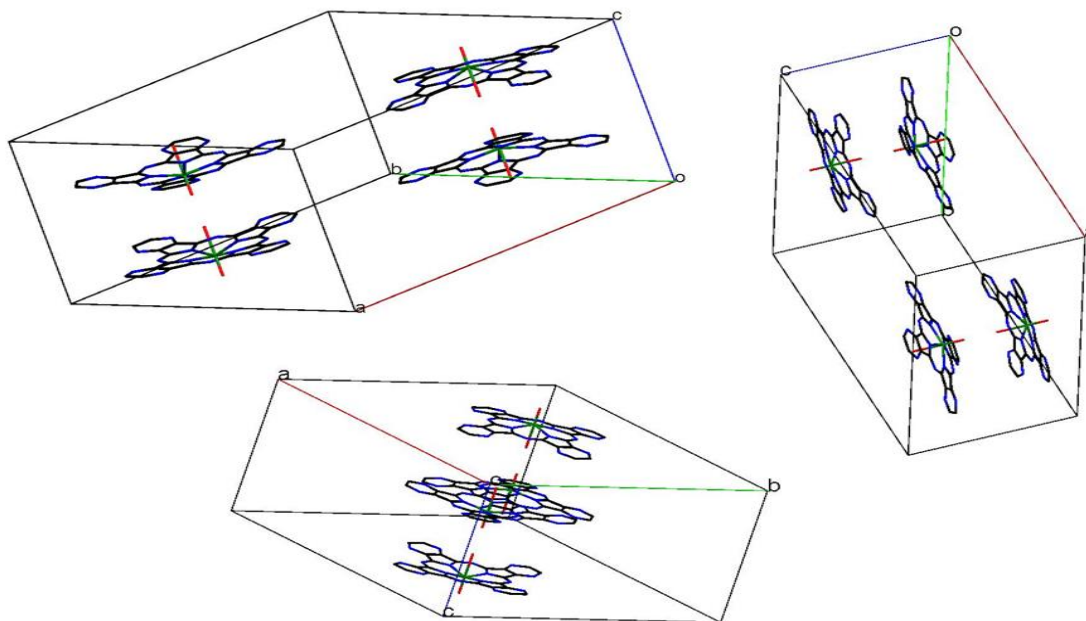
Figure 52: Unit cell packing of the aromatic system of [Ppz*VO(H$_2$O)] molecules in the solid state. All the solvent molecules, H atoms and aliphatic substituents are removed for clarity.
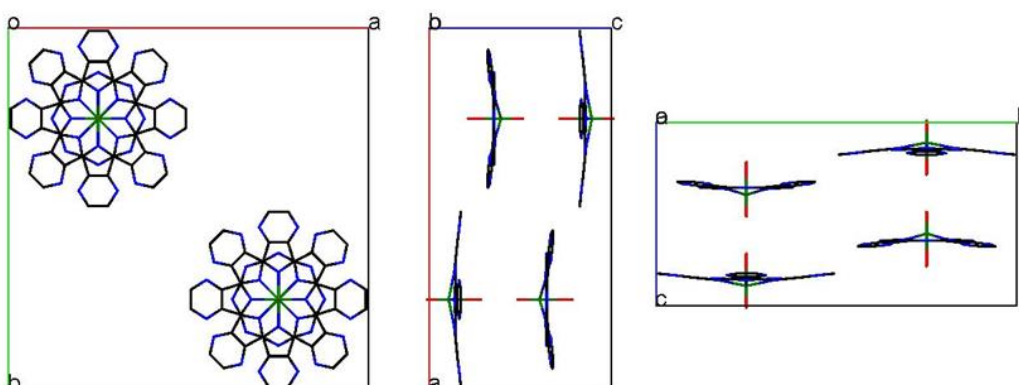
Figure 53: Two dimensional view for a unit cell of [Ppz*VO*(H$_2$O)] showing the stacking probability of the π- system of the molecules. The aliphatic substituents, solvent molecules and H atoms are omitted for clarity.

To further confirm the vanadium oxidation state in [Ppz*VO], i.e. V(IV) or V(V), we studied the magnetic behavior of the complex. In the case of V(V), the complex is diamagnetic and no net magnetic moment should be found for the complex. The other characteristic behavior of diamagnetic materials is that the susceptibility is temperature independent. However, the magnetic susceptibility values of a paramagnetic material change with the temperature following the Curie equation.[247, 248]

$$\chi = \frac{C}{T}, \quad C = J(J+1)g^2\mu_B^2\frac{N}{3k_B}$$

Where χ= the magnetic susceptibility, C= the material-specific Curie constant, T= Absolute temperature, g = the Landé g-factor, J(J+1)= the eigenvalue for eigenstate J^2 for the stationary states within the incomplete atom shells (electrons unpaired), μ$_B$= the

effective magnetic moment, k_B = Boltzmann's constant and N = the number of magnetic atoms (or molecules) per unit volume.

Practically, the data obtained obeyed the Curie equation confirming the paramagnetic nature of the complex (Figure 54). Furthermore, the complex was found to have a magnetic moment of 1.73 Bohr Magneton which is previousely reported for d^1 vanadium complexes.[321]
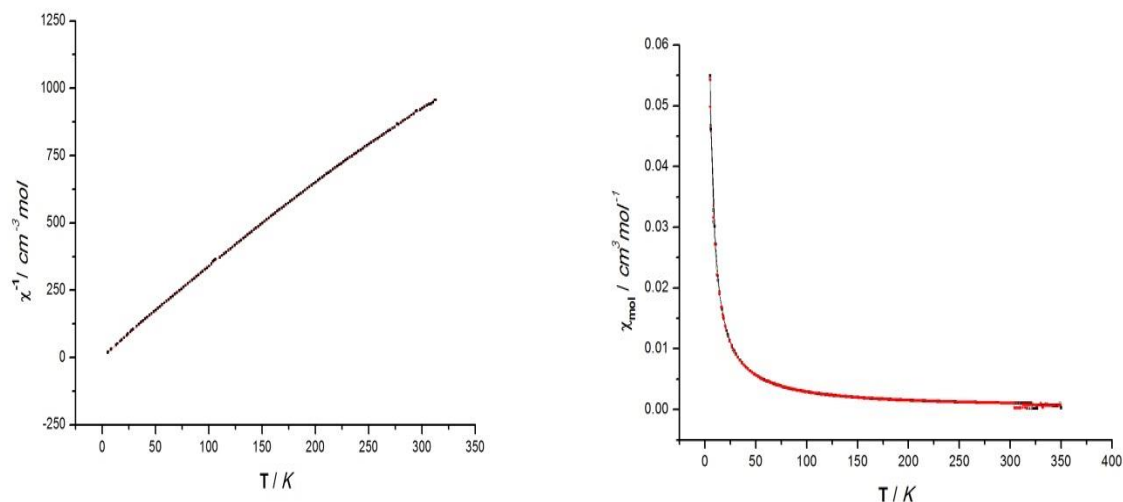
Figure 54: Plots showing the relation bertween the magnetic susceptibility of [Ppz*VO(OH$_2$)] and the absolute temperature. The results indicated the paramagnetic nature of the complex.

2.3.5 Attempted Synthesis of Axially Functionalized Vanadium(IV)Ppz Complexes

To obtain macrocycles able to connect to the surface of a metal oxide semiconductor, we tried to convert [Ppz*VO] to other axially substituted complexes with different acid functionalities, eg. -COOH and -SO$_3$H. Thus, the vanadyl complex was treated with L-phenylalanine or with sulfur containing compounds, such as the aliphatic sulfamic acid and the aromatic sulphanilic acid (Figure 55).
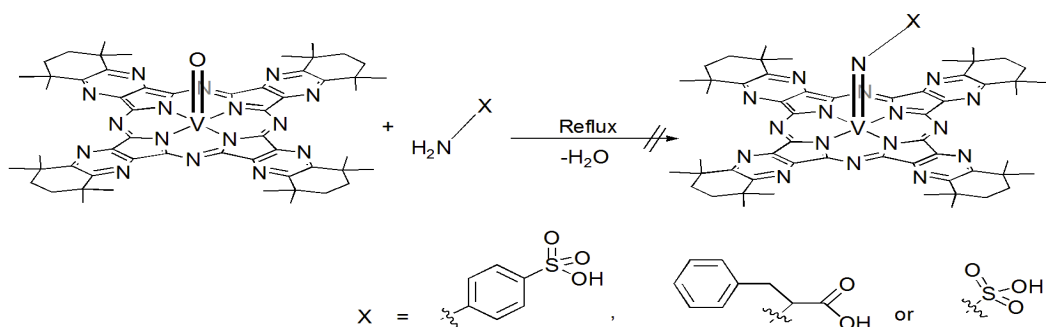
Figure 55: Attempted conversion of [Ppz*VO] to [Ppz*V(NC$_8$H$_8$COOH)], [Ppz*V(NSO$_3$H)], [Ppz*V(NC$_6$H$_4$SO$_3$H)].

While the chromophore decomposed by an unidentified mechanism in the presence of the carboxylic aminoacid, no reaction took place with the acidic sulfur compounds; this is probably due to their zwitterionic nature.

2.3.6 Chromium(II) and Chromium(III) Complexes ([Pc*Cr], [Ppz*Cr], [Pc*CrCl] and [Ppz*CrCl])

Depending on the oxidation state of the Cr template used in the reaction, i.e. either [Cr(CO)$_6$] or CrCl$_3$, we have successfully synthesized chromium complexes of the type [PcCr] or [PcCrCl] (Figure 56). The metal template was mixed with the dinitrile in presence of urea. The whole mixture was then heated at 220°C for 30 minutes under an argon atmosphere. The products were eluted as follows; (CHCl$_3$, Al$_2$O$_3$) for [Pc*CrCl], (EtOAc, Al$_2$O$_3$) for [Ppz*CrCl] and the Cr(II) macrocycles, i.e. [Pc*Cr] and [Ppz*Cr], were eluted using CHCl$_3$ on a short Al$_2$O$_3$ column. In addition to the high solubility of these complexes in CHCl$_3$, THF and toluene, surprisingly, the complexes showed enhanced solubility in the nonpolar solvent diethyl ether. The products, especially the Ppz* complexes, were obtained in good yield, i.e. 38 % for [Pc*CrCl], 43 % for [Ppz*CrCl], 29 % for [Pc*Cr] and 50 % [Ppz*Cr].
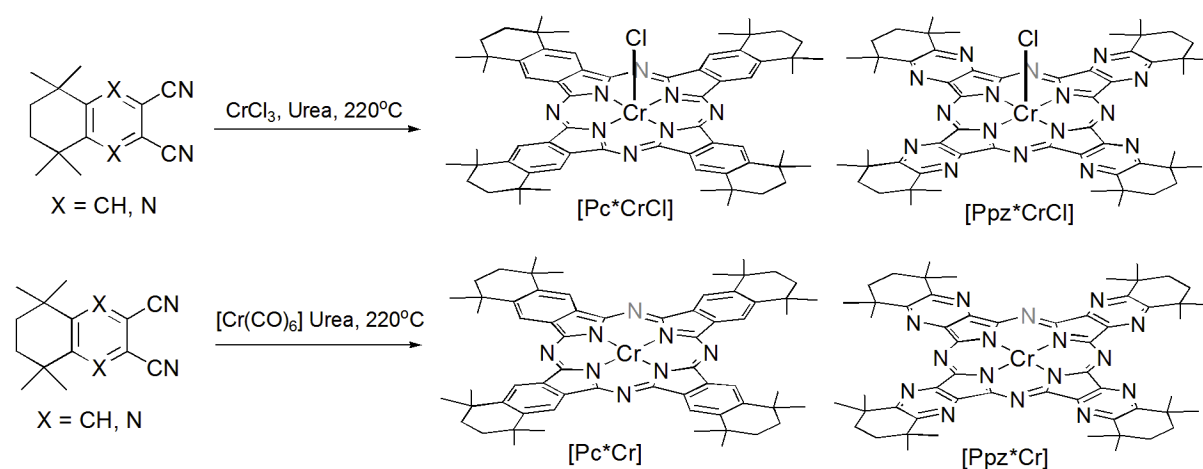
Figure 56: Synthesis of [Pc*Cr], [Ppz*Cr], [Pc*CrCl] and [Ppz*CrCl].

The APCI$^+$ mass spectra of the complexes confirmed the proposed structures. The protonated molecular ion peaks were observed at m/z 1040.6 for [Pc*CrCl] and at 1048.6 for [Ppz*CrCl]. Also, the mass spectra of [Pc*Cr] and [Ppz*Cr] showed intense peaks at m/z 1005.7 and 1013.6, corresponding to their protonated molecular ions. In the mass spectrum of [Pc*Cr] (Figure 57), although an ion peak at m/z = 1040.7 corresponding to [MH+Cl]$^+$ was observed, this species was probably due to an oxidative addition of a chlorine radical transferred from the chlorinated solvent CHCl$_3$ during the APCI$^+$ measurement, as the complex was prepared from starting materials that do not contain any chlorine.
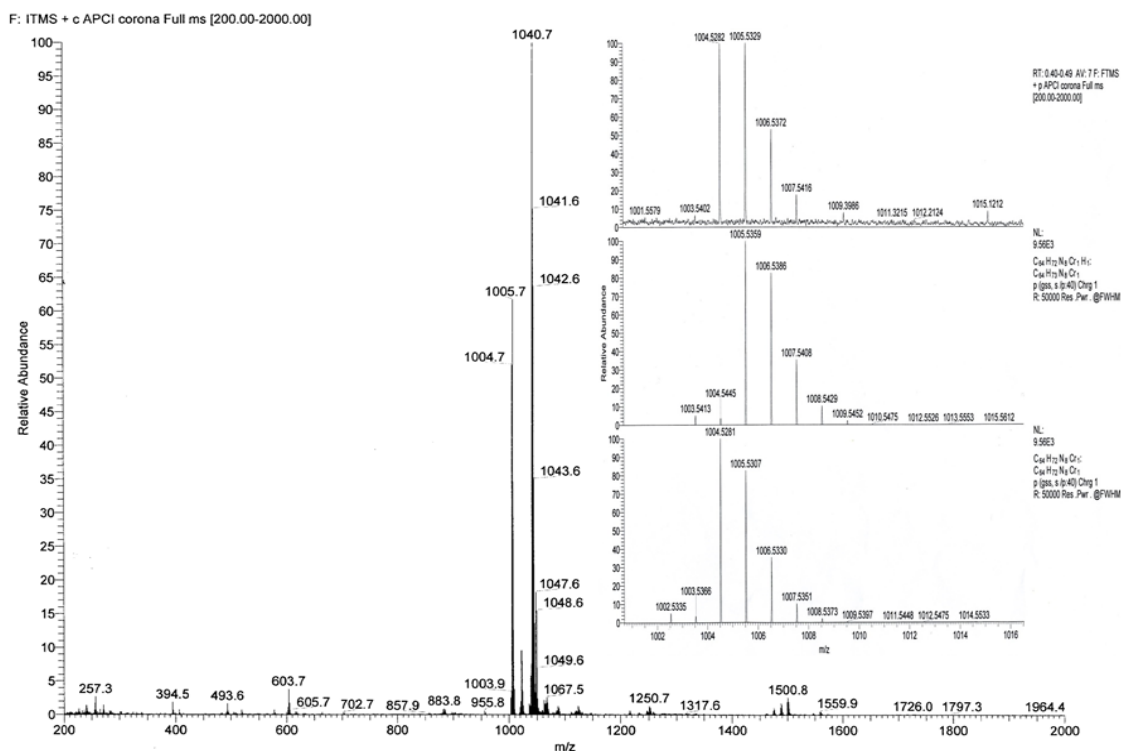
Figure 57: APCI+ Mass Spectrum of [Pc*Cr]. On the right, a high resolution of the molecular ion peak position is shown compared with its theoretically calculated isotopic pattern.

The UV-Vis. spectra of the complexes were measured in chloroform. [Pc*CrCl] and [Ppz*CrCl] showed, respectively, intense Q-bands at 708 and 646 nm, in addition to clear B bands around 340-360 nm (Figure 58).
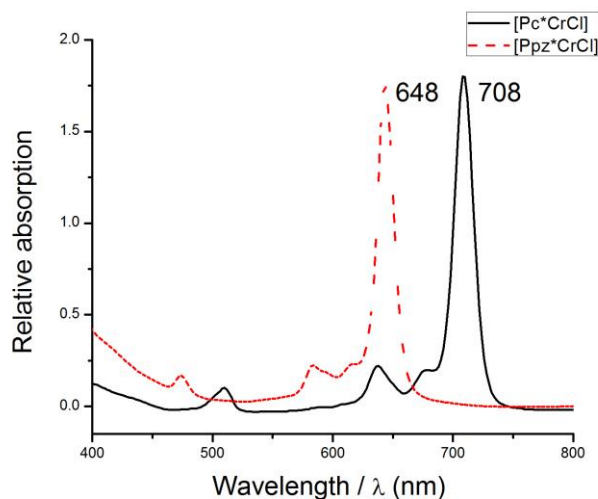
Figure 58: UV/Vis. spectra of [Pc*CrCl] and [Ppz*CrCl] in CHCl$_3$.

Mainly, the spectrum of [Pc*CrCl] is red shifted compared to that of [Ppz*CrCl]. Other bands in the range of 470-550 nm could be attributed to the MLCT. The UV-Vis. spectra

of [Pc*Cr] and [Ppz*Cr] are similar to those obtained for [Pc*CrCl] and [Ppz*CrCl]. This is because the HOMO and LUMO levels are mostly localized in the aromatic systems of the macrocycles and changing the axial ligand only has little influence on the position of these levels.[229-232] Another reason might be the transfer of a chlorine radical from the chloroform to the Cr(II) complexes during the measurement. In CNP, the Q-band of [Pc*Cr] was reported to absorb at 710 nm. [198]

2.3.7 Manganese(III) Complexes [Pc*MnCl] and [Ppz*MnCl]

Heating PDN* or PzDN* with $MnCl_2$ and urea in neat under an argon atmosphere led to the formation of a solid residue (Figure 59). After purification by column chromatography ($CHCl_3$, Al_2O_3), an orange [Pc*MnCl] or a green [Ppz*MnCl] was obtained. These complexes are highly soluble in a variety of organic solvents, such as $CHCl_3$, DCM, toluene and THF. [Pc*MnCl] and [Ppz*MnCl] formed in 29 % and 15 %, respectively. It is worthwhile to mention that the reaction is accompanied with oxidation of Mn(II) to Mn(III). Oxidation of Mn(II) during the MnPcs formation has been reported previously.[233, 234] Generally, the neutral Mn(II)Pc, i.e. [PcMn], is unusual[241] in two ways: firstly, it provides an almost unique example of the intermediate-spin state for Mn(II), S = 3/2; secondly, it is a rare example of a ferromagnetic molecular crystal.[242, 243]
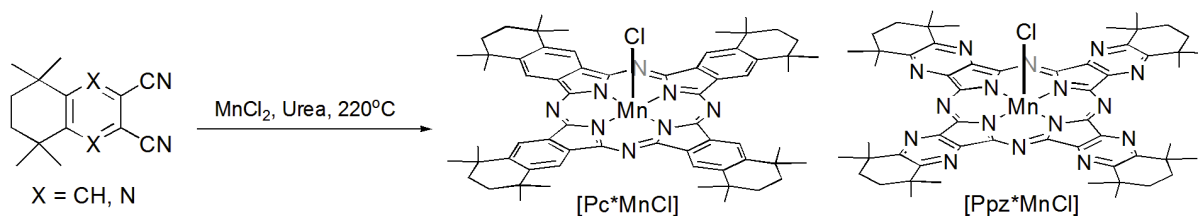
Figure 59: Synthesis of [Pc*MnCl] and [Ppz*MnCl].

An APCI+ MS experiment was performed for each complex. While the [Ppz*MnCl] spectrum displayed a protonated molecular ion peak at 1051.6, the [Pc*MnCl] spectrum (Figure 60) showed an ion peak at m/z = 1007.6, corresponding to [Pc*Mn + H]+. These values led to some doubt about the actual oxidation state of the central manganese ion, as both the interaction of the divalent manganese complexes with chlorine and the cleavage of the axial chlorine bonded to a trivalent manganese ion during the MS experiment are possible. Therefore, to properly identify the obtained complexes, performing other analyses was necessary.

Figure 60: APCI+ Mass Spectrum of [Pc*MnCl]. On the right, a high resolution of the ion peak [MH-Cl]+ position is shown compared with its theoretically calculated isotopic pattern.

A method to distinguish between [Pc*MnCl] and [Pc*Mn] is the analysis of the chlorine content. While the first complex theoretically contains 3.40 % of chlorine, it is obvious that no chlorine should be detected when analyzing the latter. Elemental analysis of the complex indicated 3.14 % of chlorine, confirming its structure as [Pc*MnCl].

Unlike the other macrocycles, which are usually blue or green, Mn(III)Pcs in particular show a highly red shifted Q band.[202] In detail, the intense Q band of any other MPc usually lies at the red end of the visible spectrum and absorbs the red light, so that the transmitted light appears blue or green. In Mn(III)Pcs, the Q-band is shifted out of the visible region so that the color of the complex is now determined by the absorption at the blue end of the spectrum between 400–500 nm, and the red shift of the Q band is typical of the Mn(III)Pc complexes[207-210]; hence these complexes appear reddish.[209] The UV-Vis. spectra of [Pc*MnCl] and [Ppz*MnCl] measured in $CHCl_3$ are shown in Figure 61. The [Pc*MnCl] spectrum showed a typical B-band at 374 nm while the Q-band is highly red-shifted to 749 nm. The spectrum of [Ppz*MnCl] seems similar to that of [Pc*MnCl], however all the bands are blue shifted, due to its higher HOMO-LUMO gap compared to that of [Pc*MnCl]. Thus the complex Q and B bands appeared at 674 and 366 nm. Both [Pc*MnCl] and [Ppz*MnCl] displayed an additional band typical of Mn(III)Pcs[213, 214] at 545 and 489 nm, respectively. This band is due to charge transfer between the metal and the ligand.[202]

51
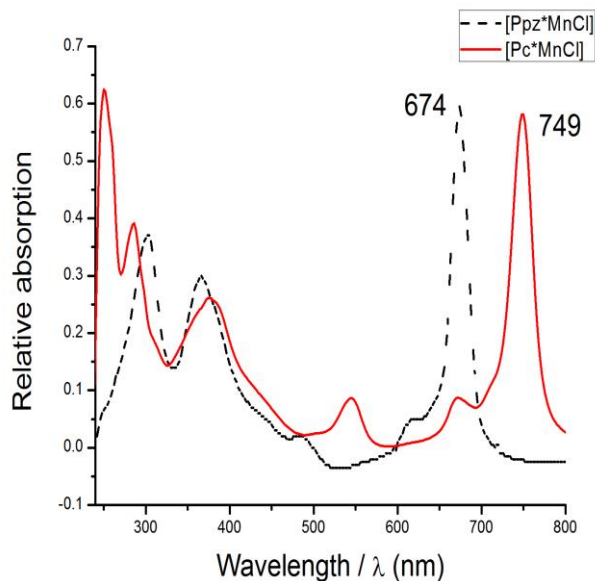
Figure 61: UV/Vis. spectra of [Pc*MnCl] and [Ppz*MnCl] in CHCl$_3$.

By controlled diffusion of pentane into a chloroform solution of [Ppz*MnCl], metallic dark blue plates of [Ppz*MnCl].5CHCl$_3$ were obtained. The complex (Figure 62) crystallized in the tetragonal space group P4$_2$/n, with four formula units per unit cell. Selected bond lengths (Å) and angles (°) for [Ppz*MnCl].5CHCl$_3$ are shown in Table 6.
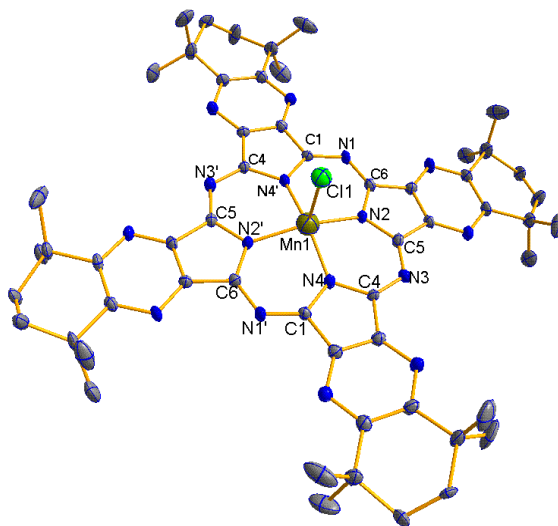
Figure 62: Molecular structure of [Ppz*MnCl].5CHCl$_3$ crystallized from chloroform. All the CHCl$_3$ molecules and H atoms are omitted for clarity. Ellipsoids are shown at 50% probability.

The molecular structures of other Mn(III)Pc complexes have been rarely reported, and no crystal structure of the unsubstituted [PcMnCl] has been reported yet. Thus, we compared the obtained complex to [Mn(TPP)Cl] (TPP = meso-tetraphenylporphyrinate)[239] (Figure 63) and to [PcMnI].0.5I$_2$.[240] In all cases, the Mn

52

center is coordinated to the four pyrrole nitrogen atoms of the ring and one terminal halogen, forming a slightly distorted square pyramid. In [Ppz*MnCl].5CHCl$_3$, the Mn atom is displaced 0.2928 Å above the N4 plane towards the apical chlorido ligand. The displacement is longer than that in both [Mn(TPP)Cl] and [PcMnI].0.5I$_2$. Additionally, the average Mn-N(isoindole) distance is shorter than that of [Mn(TPP)Cl] (2.02 Å), but agrees well with that of [PcMnI].0.5I$_2$ (1.966(4) Å). This might be attributed to the larger central cavity of the TPP ring compared to that of the Pc one. The Mn-Cl distance (2.3439(18) Å) is slightly shorter than that in [Mn(TPP)Cl] (2.37 Å). Furthermore, It is shorter compared to the Mn-I distance of [PcMnI].0.5I$_2$, as the lower electronegativity of iodine compared to that of chlorine results in longer and weaker bonds.
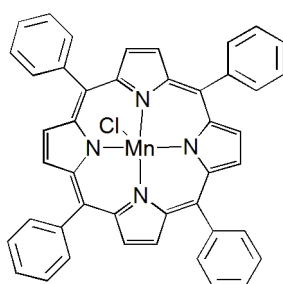
Figure 63: Structure of [Mn(TPP)Cl].

Table 6: Selected Bond Lengths (Å) and Angles (°) for [Ppz*MnCl].5CHCl$_3$.

Bond lengths/ Å		Angles/ °		Angles/ °
Mn1-N2	1.974(3)	N4-Mn1-N2	87.98(15)	
Mn1-N4	1.970(4)	Cl1-Mn1-N2	98.78(11)	
Mn1-N2'	1.974(3)	Cl1-Mn1-N4	98.53(11)	
Mn1-N4'	1.970(4)	Cl1-Mn1-N2'	98.79(11)	
Mn1-Cl1	2.3439(18)	Cl1-Mn1-N4'	98.54(11)	
dMn(out of plane)	0.2928	N4-Mn1-N2'	89.43(15)	
d(P$_1$-P$_2$)	4.289	N4-Mn1-N4'	162.9(2)	
d(Mn$_1$-Mn$_2$)	12.920	N2-Mn1-N2'	162.4(2)	

d(P$_1$-P$_2$) the distance between two neighboring N$_4$ planes

The crystal packing of [Ppz*MnCl].5CHCl$_3$ is columnar, forming face to back dimers (Figure 64) with very little interaction between the π-systems of neighboring molecules. The intermolecular distance is 4.289 Å with manganese –manganese distance of 12.920 Å , these values sugesst weak electrical conductivity of the crystal.
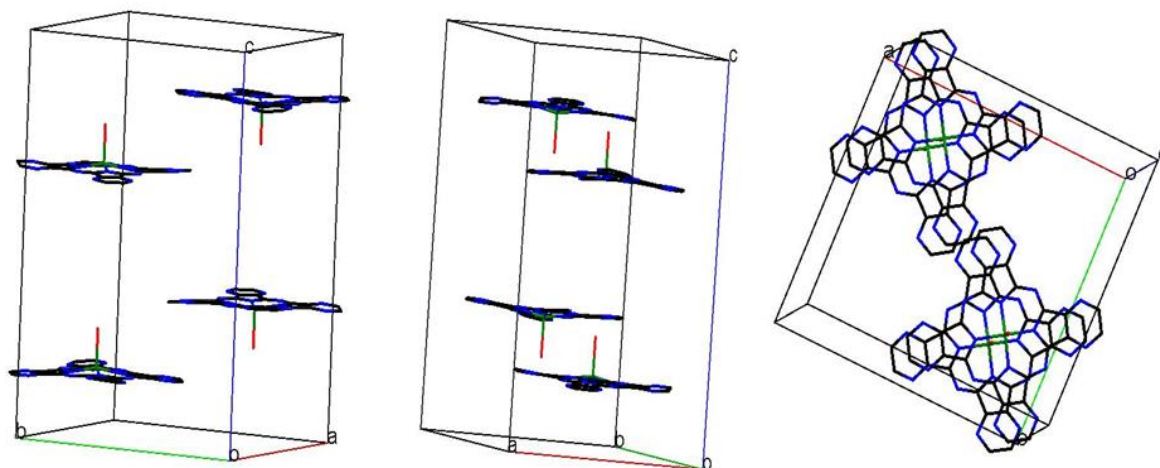
Figure 64: Unit cell packing of [Ppz*MnCl].5CHCl$_3$ molecules in the solid state. All the solvent molecules, aliphatic substituents and H atoms are removed for clarity.

2.3.8 Iron Complexes ([Pc*Fe], [Ppz*Fe], [Pc*FeCl] and [Ppz*FeCl])

Using PDN* or PzDN*, four different iron macrocycles, *viz.* [Pc*Fe], [Ppz*Fe], [Pc*FeCl] and [Ppz*FeCl] (Figure 65), were prepared. The synthetic strategy depends on melting Fe(II) or Fe(III) chloride with the dinitrile in the presence of urea and then purifying the obtained residue using column chromatography (CHCl$_3$, Al$_2$O$_3$). Generally, the Fe(II) complexes formed in higher yield compared to the Fe(III) ones, i.e. 38 % for [Pc*Fe], 33 % for [Ppz*Fe], 7 % for [Pc*FeCl] and 19 % for [Ppz*FeCl]. The complexes are all green and highly soluble in common organic solvents such as CHCl$_3$, toluene, DCM and THF. However, in solution, unlike the stable [Ppz*Fe] and [Ppz*FeCl] complexes, green solutions of [Pc*Fe] and [Pc*FeCl] are highly light and air sensitive as they decompose fast to unidentified products forming brown solutions.
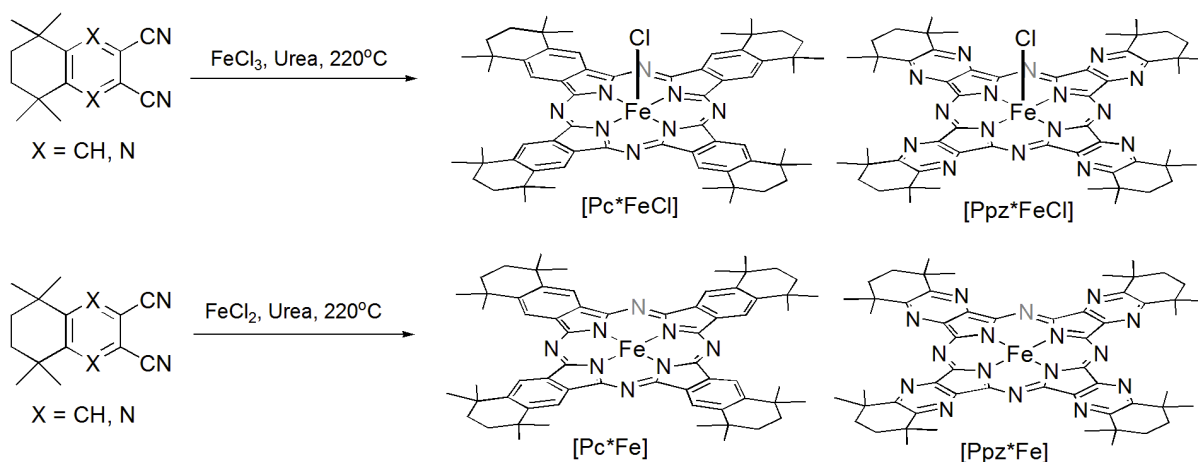
Figure 65: Synthesis of [Pc*Fe], [Pc*FeCl], [Ppz*Fe] and [Ppz*FeCl].

54

Mass spectra of [Pc*Fe], [Pc*FeCl], [Ppz*Fe] and [Ppz*FeCl], measured by the APCI⁺ technique, showed intense protonated molecular ion peaks of the complexes at 1009.7, 1044.5, 1017.6 and 1052.6, respectively. The spectrum of [Ppz*FeCl] is shown in Figure 66. Bsides the molecular ion peak (m/z = 1052.6), an ion peak was observed at 1017.6, which resulted from cleavage of the axial chlorine moiety during the measurement.
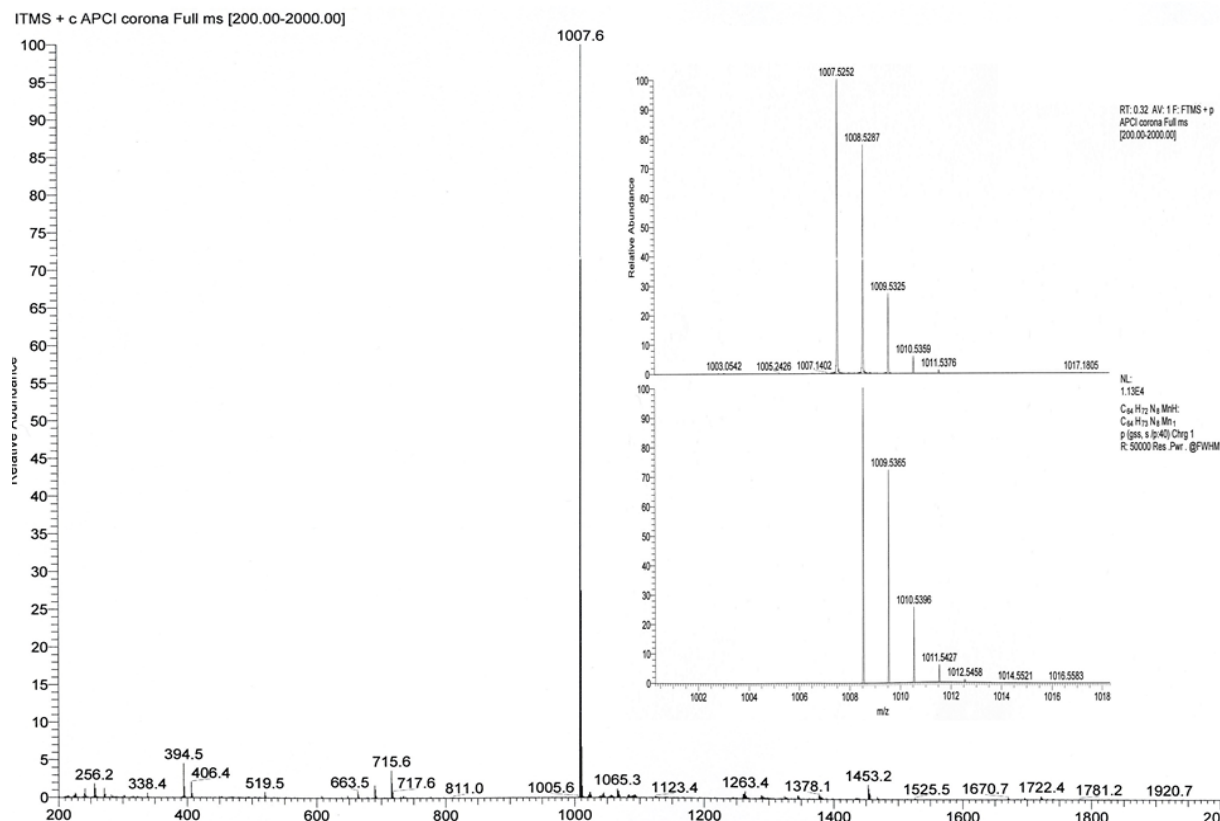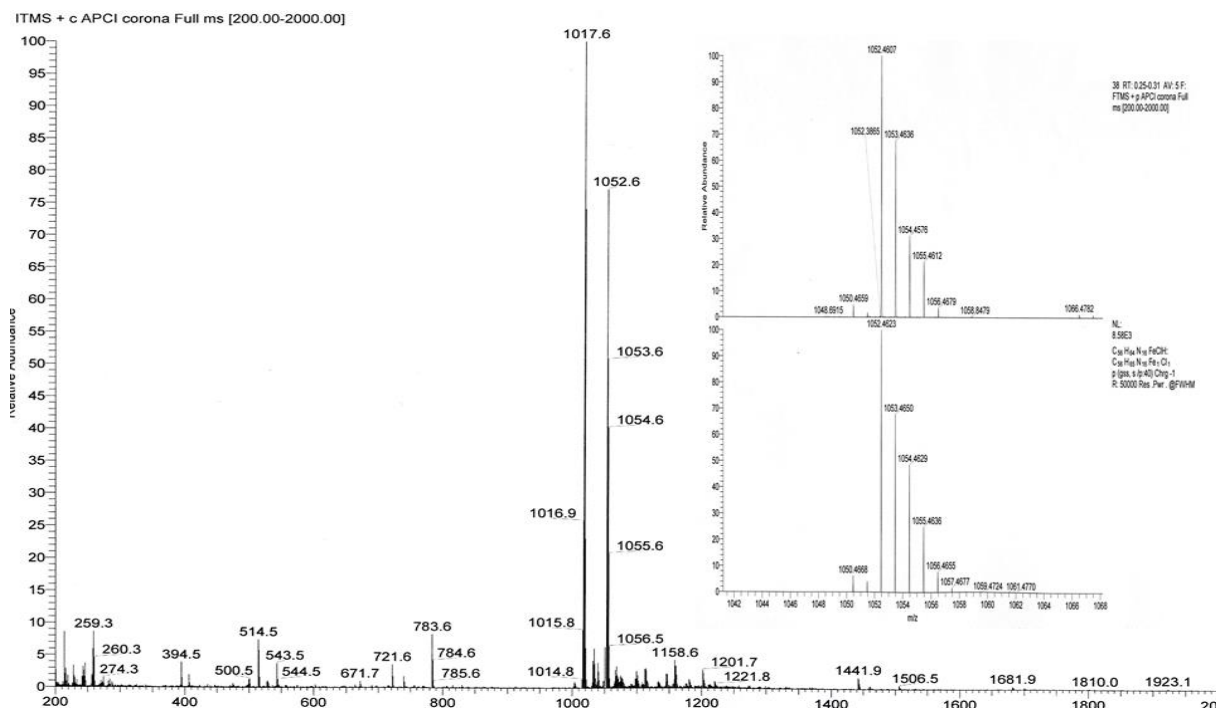

Figure 66: APCI⁺ Mass Spectrum of [Ppz*FeCl]. On the right, a high resolution of the molecular ion peak position is shown compared with its theoretically calculated isotopic pattern.

UV-Vis. spectra of [Pc*FeCl] and [Ppz*FeCl] (Figure 67) in $CHCl_3$ showed two strong absorption regions, namely, 300–350 nm (Soret or B band) and Q-band at 678 and 636 nm, respectively. The spectra of the analogous Fe(II) complexes are similar as the axial ligand does not have a large impact on the position of the Q-band.
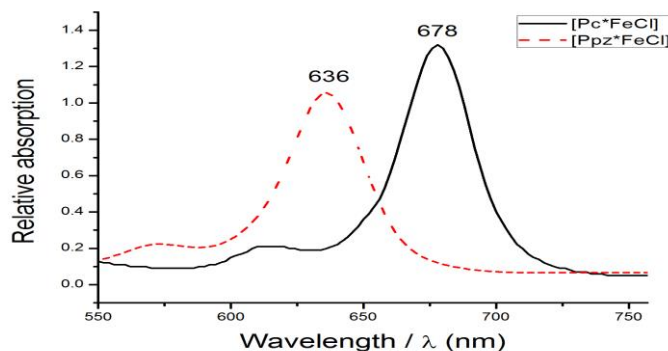
Figure 67: UV/Vis. spectra of [Ppz*Fe] and [Ppz*FeCl] in $CHCl_3$.

55

Additionally, a broad weak band was observed in the spectra of [Pc*FeCl] and [Ppz*FeCl] at 878 nm (Figure 68). Comparing with literature [215-219], this peak is assigned to $a_{1u}(\pi)$ or $a_{2u}(\pi)$ to $e_g(d_{\pi*})$ charge transfer transitions in high spin iron (III) porphyrins and phthalocyanines. In [Pc*Fe] and [Ppz*Fe], this peak is completely absent, confirming the proposed structures for the complexes.
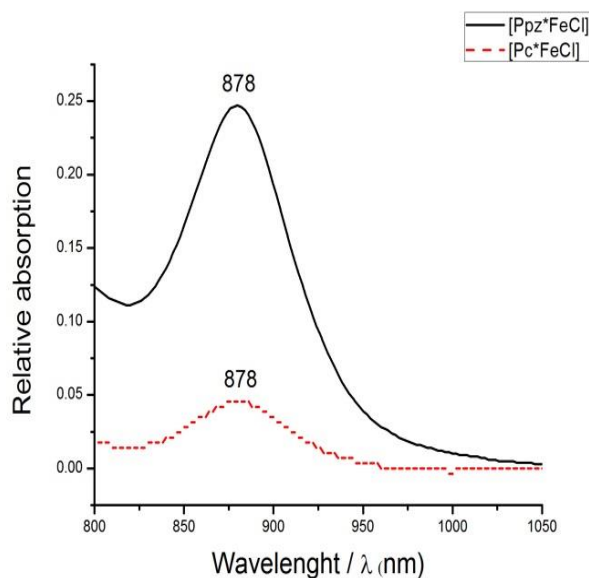
Figure 68: The $a_{1u}(\pi)/a_{2u}(\pi)$ to $e_g(d\pi*)$ transition for high spin iron(III)Pcs.

2.3.9   Attempted Synthesis of [(Ppz*Fe)$_2$N]

Once the iron complexes were prepared, we attempted to obtain complexes of the type (PcFe)$_2$N. The reason was to find a green catalyst for the selective, low temperature oxidation of methane. It has been reported that the binuclear MPc complexes exhibited better catalytic properties than the monomers.[297] The μ-Nitrido iron phthalocyanine complex (FePc)$_2$N contains two equivalent iron centres, with a formal +3.5 oxidation state, bridged *via* nitrogen, was synthesized.[298] However, the insolubility of (FePc)$_2$N in organic solvents makes its purification and use in catalysis difficult.

Thus, the soluble complex [(FePct-Bu$_4$)$_2$N][299] was obtained. [(FePct-Bu$_4$)$_2$N] was found to interact with H$_2$O$_2$. In detail, (FePct-Bu$_4$)$_2$N coordinates H$_2$O$_2$ to form the hydroperoxo complex, Fe^{IV}NFe^{III}OOH, which is probably in equilibrium with the deprotonated form Fe^{IV}NFe^{III}OO$^-$. Furthermore, (FePct-Bu$_4$)$_2$N oxo-complex could be formed from Fe^{IV}NFe^{III}OOH *via* heterolytic cleavage of the O–O bond.

Remarkably, the catalytic system ((FePct-Bu$_4$)$_2$N + H$_2$O$_2$) showed high stability with a possibility of recycling. It also exhibited a very high performance; more than 150 moles CH$_4$ per mole of catalyst were oxidized to useful C$_1$-products (formic acid and methanol).

This catalytic system showed several attractive features; the ecologically friendly oxidant (H_2O_2), the reaction medium (H_2O) and the fact that the solid catalyst can easily be separated by filtration. Moreover, in contrast to the much more expensive porphyrin and non-heme complexes, phthalocyanines can be accessible in bulk quantities.[300]

Unfortunately, owing to its instability in solution, it is not possible to use [Pc*Fe] as a starting material to prepare the nitrido complex. Moreover, the Ppz analog [Ppz*Fe] was destroyed when heated with sodium azide in 1-CNP (Figure 69).
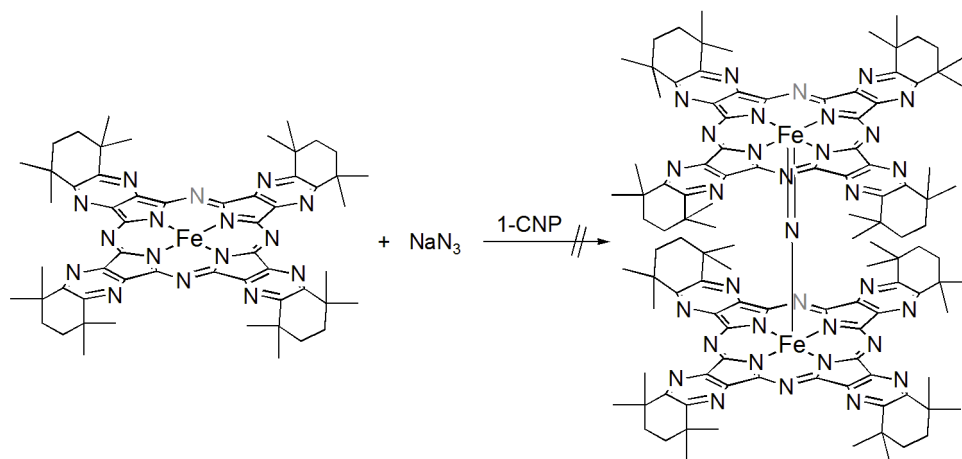
Figure 69: Attempted synthesis of [(Ppz*Fe)$_2$N].

2.3.10 Cobalt(II) Complexes [Pc*Co] and [Ppz*Co]

The highly soluble cobalt complexes were also prepared by melting $CoCl_2$ with PDN* or PzDN* at 220°C in an inert atmosphere (Figure 70), then purifying the products by column chromatography ($CHCl_3$, Al_2O_3). In the case of [Ppz*Co], no urea is required, but its prescence is always desirable to enhance the reaction yield, i.e. 62 % for [Pc*Co] and 33 % for [Ppz*Co]. The obtained complexes dissolve well in DCM, $CHCl_3$, THF and toluene.
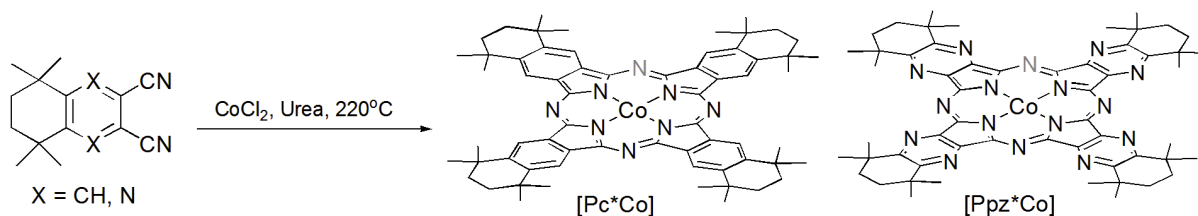
Figure 70: Synthesis of [Pc*Co] and [Ppz*Co].

The expected mass values measured using the APCI$^+$ MS technique corresponded with the theoretical values for the complexes. The protonated molecular ion peaks of [Pc*Co] and [Ppz*Co] were observed at 1012.7 and 1020.7 (Figure 71), respectively.

Figure 71: APCI⁺ Mass Spectrum of [Ppz*Co]. On the right, a high resolution of the molecular ion peak position is shown compared with its theoretically calculated isotopic pattern.

The electronic spectral differences between the two cobalt complexes could be attributed to the difference in their HOMO-LUMO gaps, which resulted from the stronger electron donating ability of the [Pc*Co] benzene rings compared to the [Ppz*Co] pyrazine ones (Figure 72). In CHCl₃, [Pc*Co] and [Ppz*Co] showed the characteristic single Q absorption band for the π- π* transition at 684 and 630 nm, respectively, with a weak vibrational band (shoulder) observed at around 616 and 572 nm. The B-bands were observed in the range of 295-333 nm.
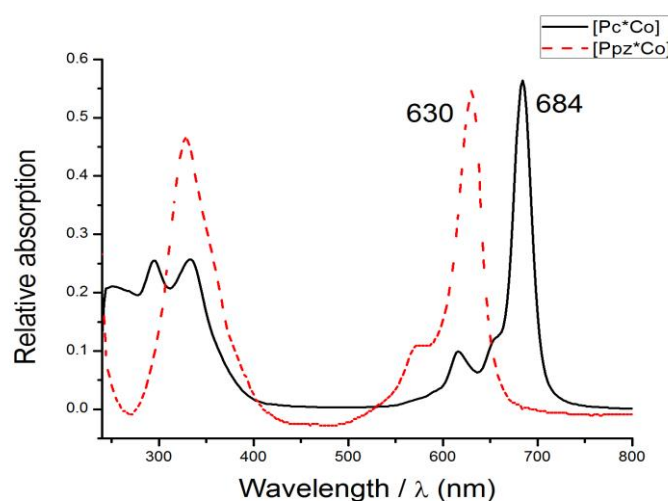
Figure 72: UV/Vis. spectra of [Pc*Co] and [Ppz*Co] in CHCl₃.

Blue needles of [Pc*Co](Figure 73) formed by controlled diffusion of pentane into a chloroform solution of the complex. The complex crystallized in the triclinic space group P$\bar{1}$ with an unidentified number of distorted solvent molecules. Thus, all the solvent molecules were not included into refinment to enable the crystal structure to be solved.

The bond lengths and angles of [Pc*Co](Table 7) fit well with the data reported for the unsbstituted [PcCo].[241] Generally, [PcCo] was reported to be of the monoclinic, β-polymorph type. The molecule is planar, and the Co atom occupies the Pc cavity with N3-Co and N4-Co distances of 1.906(2) Å and 1.902(2) Å, respectively. The average distance between the Co and the N4 nitrogen atoms is 1.907(2) Å. Additionally, the two angles N3-Co-N4 and N4-Co-N3' of the complex are 90.7(1) and 89.3(1); very close to the determined values of [Pc*Co], i.e. 90.06(6) and 89.94(6).
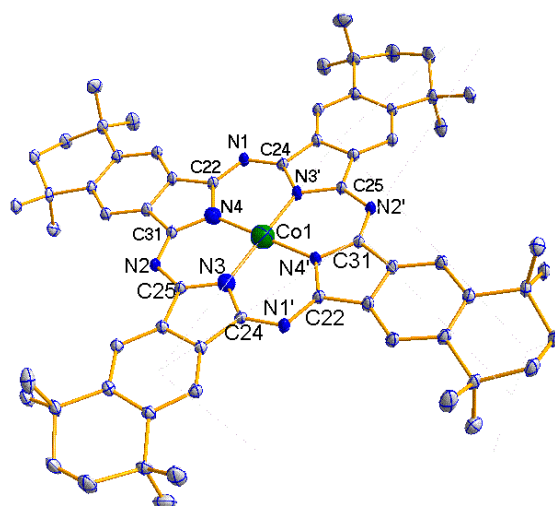
Figure 73: Molecular structure of [Pc*Co] crystallized from CHCl$_3$. H atoms are omitted for clarity. Ellipsoids are shown at 50% probability.

Table 7: Selected Bond Lengths (Å) and Angles (°) for [Pc*Co].

Bond lengths/ Å		Angles/ °	
Co1-N3	1.9162(15)	N3-Co1-N4	89.94(6)
Co1-N4	1.9218(15)	N3'-Co1-N4'	89.94(6)
Co1-N4'	1.9217(15)	N3-Co1-N4'	90.06(6)
Co1-N3'	1.9163(15)	N4-Co1-N3'	90.06(6)
d(P$_1$-P$_2$)	3.984		
d(Co$_1$-Co$_2$)	13.714		

d(P$_1$-P$_2$) the distance between two neighboring N$_4$ planes

The crystal packing of the complex (Figure 74) includes four molecules per unit cell. A columnar structure of co-planar Pc rings is observed. The closest intermolecular distance between two N4 Planes is 3.984 Å with a centroid-centroid distance of 13.714 Å. These values are indicative for the low level of π- π interaction in the crystal. The

reason for that is probably the prescence of aliphatic substituents which hinder the interaction between the molecules. Generally, low electrical conductivity between the macrocycles is presumed.
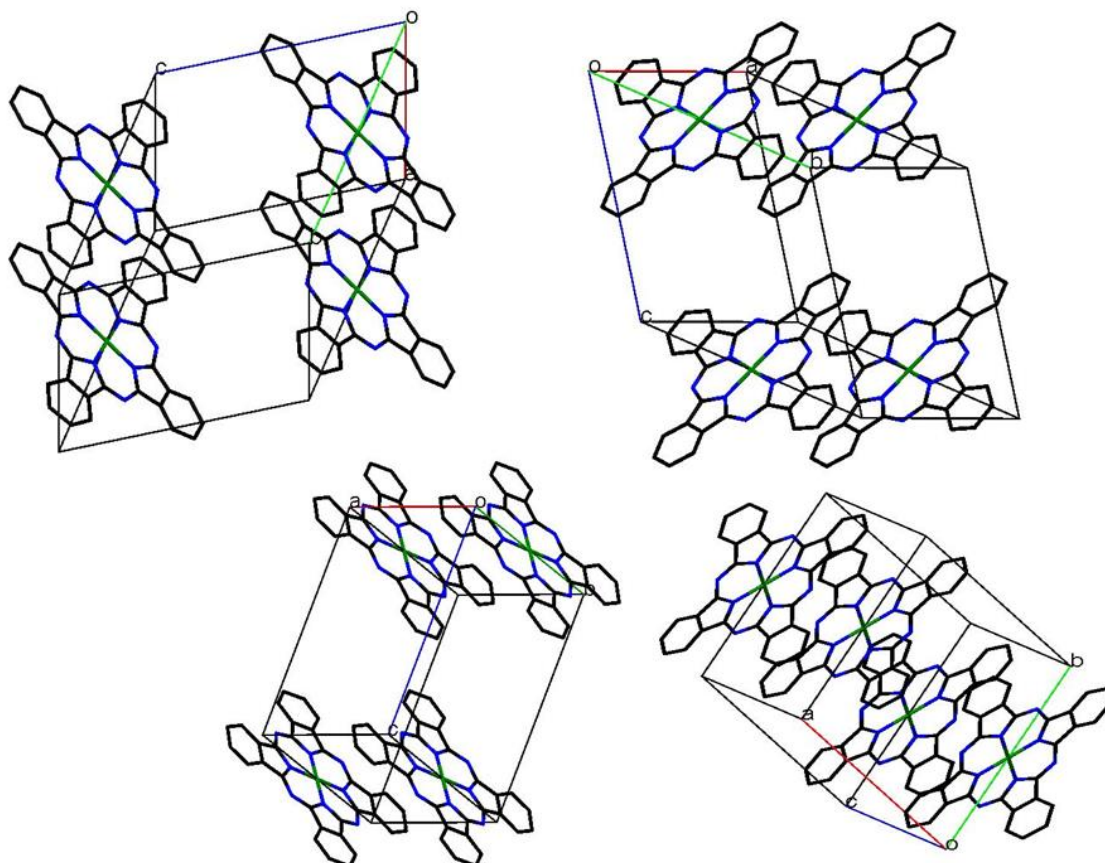
Figure 74: Unit cell packing of [Pc*Co] molecules in the solid state. Aliphatic substituents and H atoms are removed for clarity.

2.3.11 Attempted conversion of [Ppz*Co] to [Ppz*CoI]

Cobalt(III) salen co-catalysts are reported[305, 306] for coupling of CO_2 and epoxides to produce polycarbonates and cyclic carbonates. For this reason, it was desirable to obtain the Co(III) macrocycle [Ppz*CoI]. Unfortunately, the Co(II) complex remained stable against oxidation with iodine in a potassium iodide solution (Figure 75).
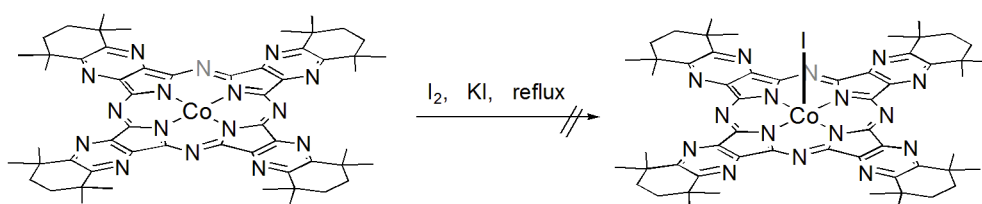
Figure 75: Attempted synthesis of [Ppz*CoI].

2.3.12 Nickel(II) Complexes [Pc*Ni] and [Ppz*Ni]

The nickel macrocycles formed upon heating the substituted dinitrile with $NiCl_2$ and urea at 220°C under an argon atmosphere (Figure 76). To purify them, the reaction products were chromatographed using ($CHCl_3$, Al_2O_3). The products formed in high yield, i.e. 57 % for [Pc*Ni] and 84 % for [Ppz*Ni]. They also showed high solubility in a variety of solvents, such as $CHCl_3$, DCM, THF and toluene.
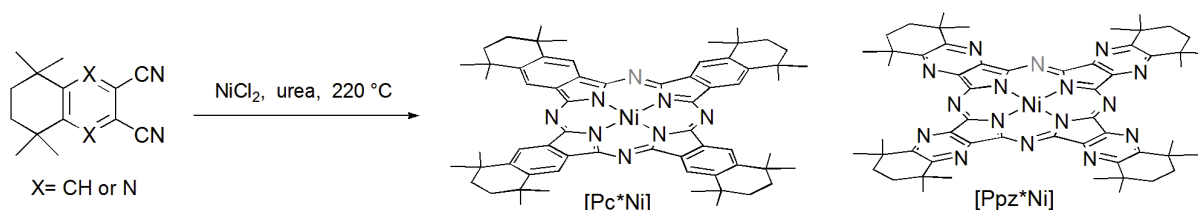
Figure 76: Synthesis of [Pc*Ni] and [Ppz*Ni].

The APCI+ mass spectra of [Pc*Ni] (Figure 77) and [Ppz*Ni] clearly showed intense signals for their protonated molecular ions at 1011.6 and 1019.8, respectively.
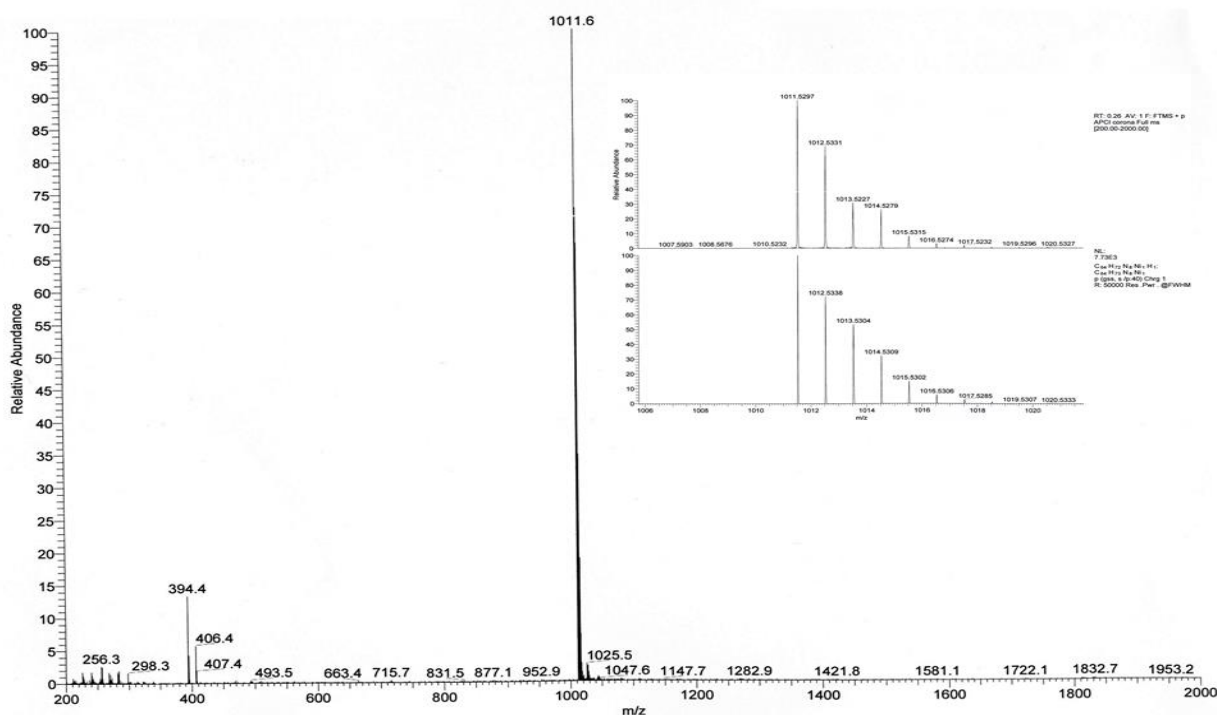
Figure 77: APCI+ Mass Spectrum of [Pc*Ni]. On the right, high resolution of the molecular ion peak position is shown compared with its theoretical calculated isotopic pattern.

The typical UV–Vis. spectra of the complexes in $CHCl_3$ exhibit characteristic Q and B bands (Figure 78). The first is in the visible region at 686 and 630 nm for [Pc*Ni] and [Ppz*Ni], respectively (The Q band appears with a shoulder at the slightly higher energy side for the Pc[218]) attributed to the π- π* transition from the highest occupied

61

molecular orbital (HOMO) to the lowest unoccupied molecular orbital (LUMO) of the ring. The other B bands appeared in the UV region at 300–380 nm, arising from deeper π – levels to LUMO transition.
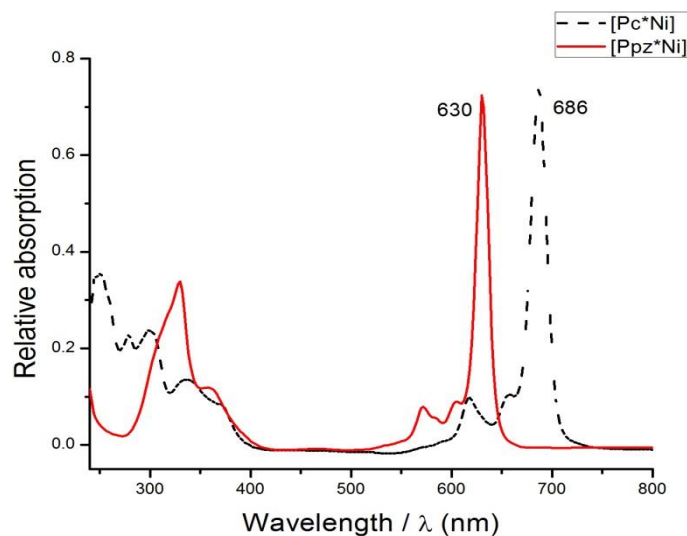
Figure 78: UV/Vis. spectra of [Pc*Ni] and [Ppz*Ni] in CHCl$_3$.

When pentane vapor was allowed to diffuse into a saturated chloroform solution of [Pc*Ni], the complex (Figure 79) crystallized as green needles suitable for XRD measurements.
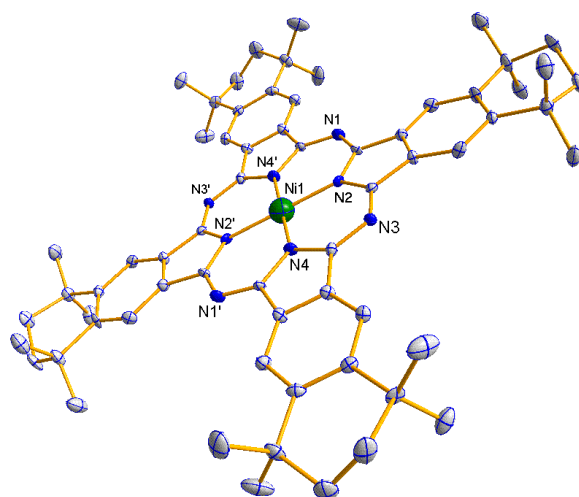
Figure 79: Molecular structure of [Pc*Ni].4CHCl$_3$ crystallized from chloroform. All the CHCl$_3$ molecules and H atoms are omitted for clarity. Ellipsoids are shown at 50% probability.

Selected bond-distances and angles for [Pc*Ni] are shown in Table 8. The obtained crystals grew in the monoclinic space group P2$_1$/c as [Pc*Ni].4CHCl$_3$. The reports counted on the XRD measurements of the unsubstituted [PcNi][244, 245] did not fully

describe its crystal structure. However, it could be concluded that the unsubstituted complex crystallized nearly tetragonally but a small deformation still exists, with an average Ni-N distance ≈ 1.83 Å, which is a little shorter than that of [Pc*Ni].4CHCl$_3$ (1.889(4) Å) . Also, in agreement with our results for [Pc*Ni].4CHCl$_3$, the nickel atom of [PcNi] is coplanar with the four surrounding isoindole nitrogen atoms.

Table 8: Selected Bond Lengths (Å) and Angles (°) for [Pc*Ni].4CHCl$_3$.

Bond lengths/ Å		Angles/ °	
Ni1-N3	1.889(4)	N2-Ni1-N4	89.50(17)
Ni1-N4	1.889(4)	N2'-Ni1-N4'	89.50(17)
Ni1-N4'	1.889(4)	N4-Ni1-N2'	89.50(17)
Ni1-N3'	1.889(4)	N2-Ni1-N4'	89.50(17)
d(P$_1$-P$_2$)	4.027		
d(Ni$_1$-Ni$_2$)	11.727		

d(P$_1$-P$_2$) the distance between two neighboring N$_4$ planes
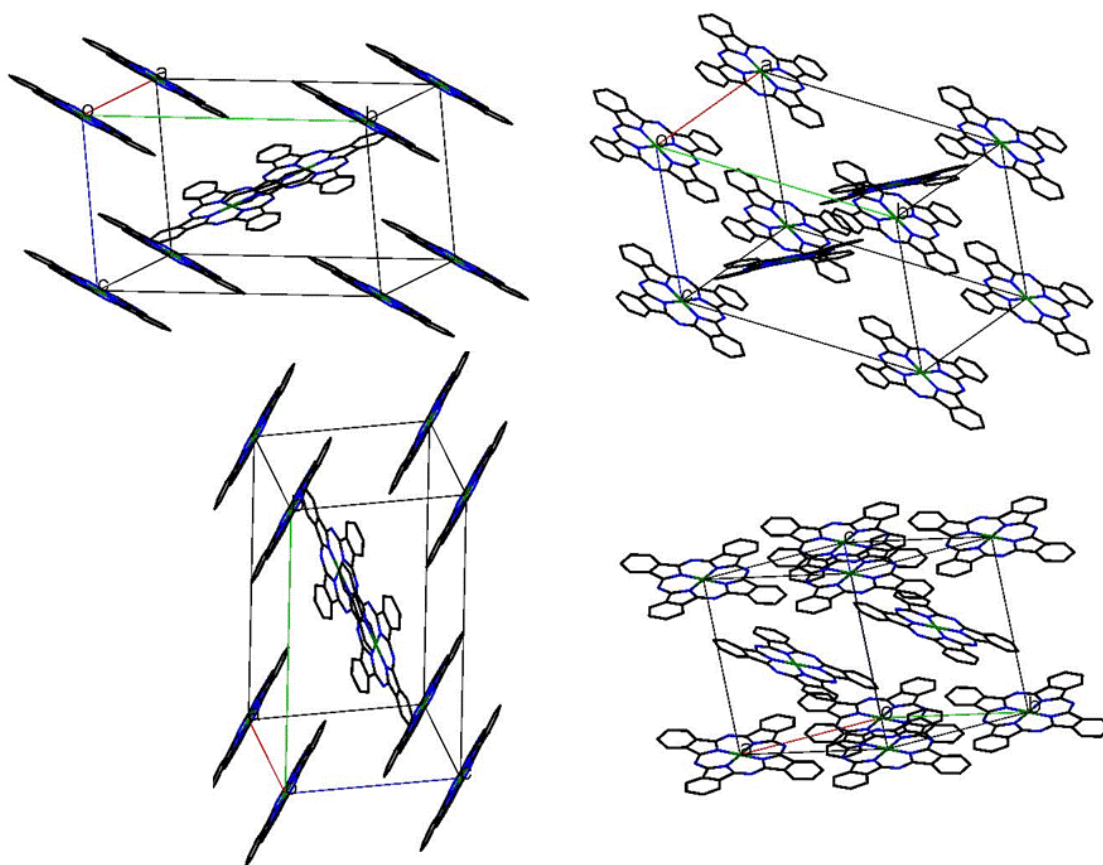
Figure 80: Unit cell packing of [Pc*Ni] molecules in the solid state. All the solvent molecules, aliphatic substituents and H atoms are removed for clarity.

The molecular packing of a unit cell is shown in Figure 80; the complex is packed in a layered structure with independent two stacks of parallel but only slightly overlapping molecules, thus very little coupling between the aromatic systems of the adjacent

molecules. The closest distance between two N4 planes is 4.027 Å with a distance of 11.727 Å between the two neighboring nickel atoms.

2.3.13 Copper(II) Complexes [Pc*Cu] and [Ppz*Cu]

When the organic precursors were heated with $CuCl_2$ in an inert atmosphere at 220°C, [Pc*Cu] and [Ppz*Cu] (Figure 81) were formed. The reaction proceeds in the absence of any base catalyst, but the addition of urea improves the reaction yield. To purify them, the chromophores were subjected to column chromatography ($CHCl_3$, Al_2O_3). The macrocycles are sublimable and also highly soluble in common organic solvents, such as THF, $CHCl_3$, DCM and toluene. The products, in absence of urea, were obtained in 33 % for [Pc*Cu] and 39 % for [Ppz*Cu].
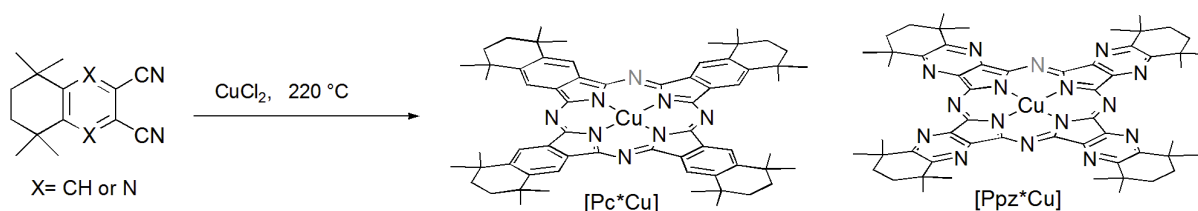
Figure 81: Synthesis of [Pc*Cu] and [Ppz*Cu].

The APCI[+] MS of the macrocycles confirmed the proposed structures. The protonated molecular ion peaks of the complexes appeared at 1016.8 and 1024.8 for [Pc*Cu] (Figure 82) and [Ppz*Cu], respectively.
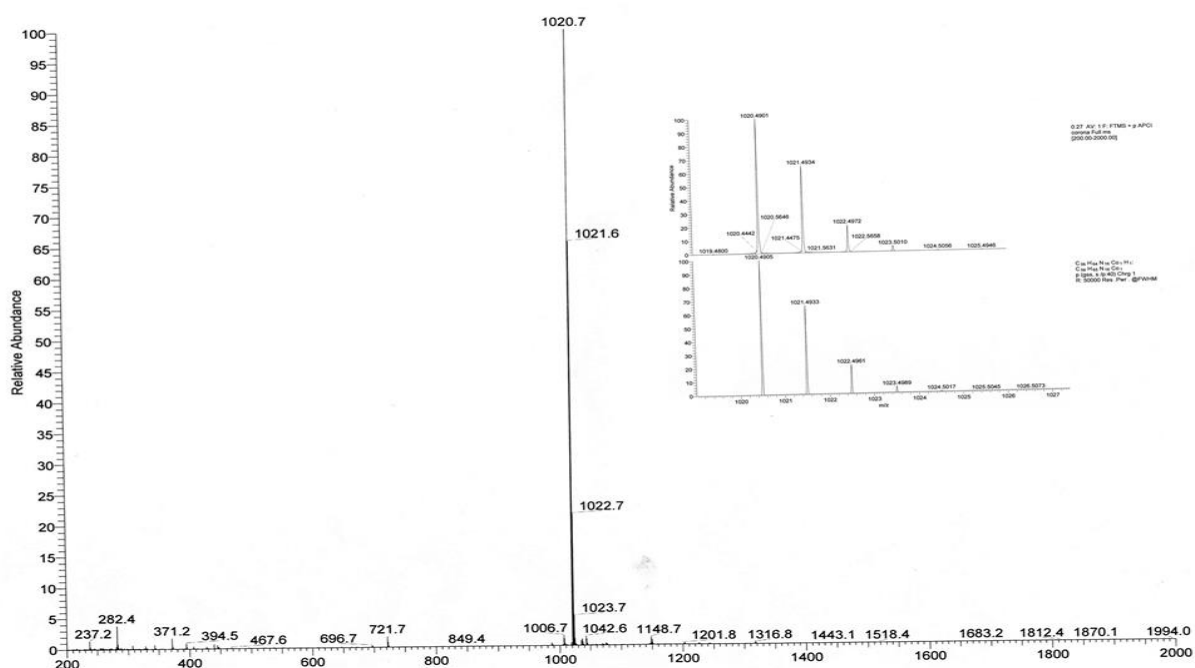

Figure 82: APCI[+] Mass Spectrum of [Pc*Cu]. On the right, a high resolution of the molecular ion peak position is shown compared with its theoretically calculated isotopic pattern.
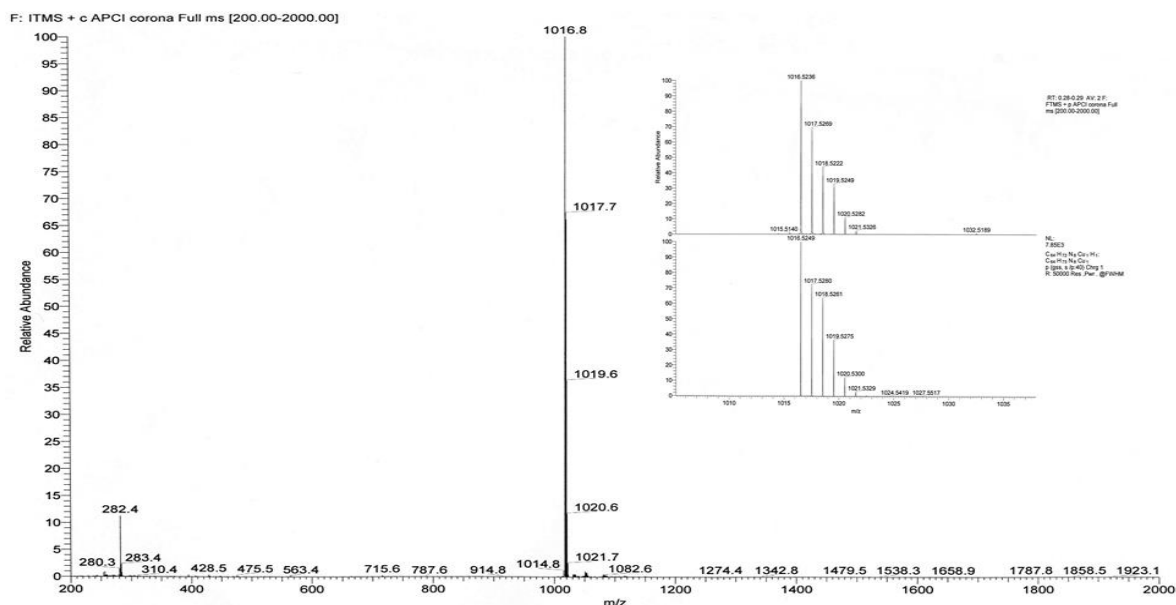
The CuPcs show typical electronic spectra, with two strong absorption regions; a Soret band at 300–400 nm, arising from deeper π- π* transition, and a Q-band in the range of 600–700 nm attributed to the π- π* transition from the HOMO to LUMO levels of the Pc core.[202] The electronic spectra of [Pc*Cu] and [Ppz*Cu] were measured in CHCl₃ (Figure 83). The Q-band of [Ppz*Cu] appeared at 638 nm, while, owing to the electron density enhancement of the ring by the akyl substituents, which resulted in lowering the HOMO-LUMO gap, the Q-band of [Pc*Cu] was shifted to 694 nm. Additionally, weak vibronic bands at 624 and 580 nm could be observed for the [Pc*Cu] and [Ppz*Cu], respectively.[221] In [Ppz*Cu], a red-shifted shoulder was observed compared to the main Q-band; this might be attributed to the formation of J aggregates in solution. Aggregation effects of several Pc dyes have been documented.[310, 311] Two main aggregate species have been identified as J- and H- aggregates, with J-aggregates marked by a red shift in the monomer peak due to face-to-tail aggregation, while H-aggregates correspond to face-to-face dimerization marked by a blue shift.[142, 312]
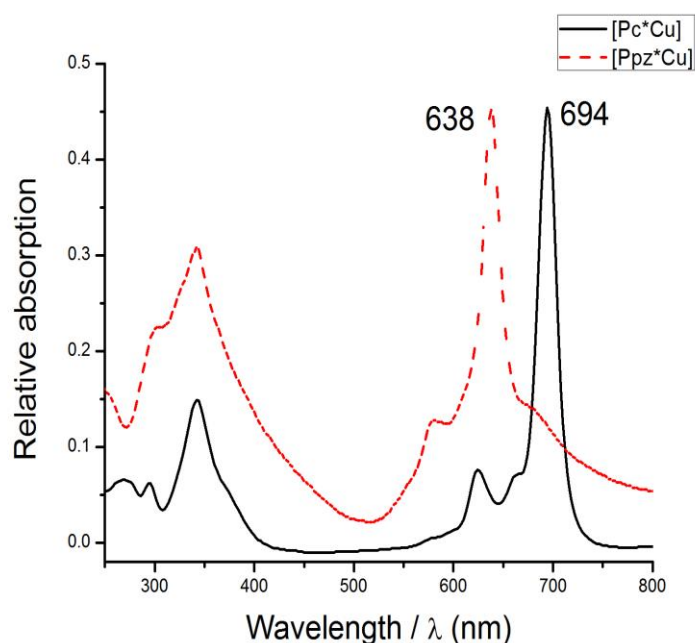
Figure 83: UV/Vis. spectra of [Pc*Cu] and [Ppz*Cu] in CHCl₃.

Slipped π-π -stacking arrangements with bathochromically shifted J-bands are of crucial importance for the applications of Pcs in the solid state as functional pigments.[329] CuPcs, depending on their packing arrangements in the solid state, different polymorphs are formed. The polymorph "β modification" is the thermodynamically most stable one, and is able to provide the cleanest shades of turquoise blue, as required for the cyan ink in three- and four-color printing. While CuPc are promising for achieving a pure cyan hue, its broadening and the bathochromic shift of the absorption band in the aggregate make this pigment an outstanding cyan colorant. Both effects can be related to the

excitonic coupling of the monomeric dyes in the crystal, where a major effect (bathochromic shift) arises from the coupling between adjacent dyes within the one-dimensional π stacks and minor effects (band broadening) arise from the coupling to more distant dyes that are located in the neighboring π stacks. Different coloristic properties are accessible from the same dye molecule as a consequence of the different packing of the CuPc monomers in other polymorphs. Thus, the α and the ε modifications exhibit a more reddish blue hue, which is desirable for automotive finishes in both solid and metallic shades (α-CuPc) and for blue color filters of liquid-crystal displays (ε-CuPc).

Blue-green prisms-like crystals of [Pc*Cu].4CHCl$_3$ (Figure 84), suitable for XRD measurements, were obtained by controlled diffusion of pentane into a chloroform solution of the complex. The bond lengths and angles are listed in Table 9. It crystallized in the monoclinic space group P 2$_1$/c.

The molecular structure of [PcCu] (β-polymorph) was previously solved.[246] The unsubstituted complex was found to have Cu-N mean distance of 1.934 Å in a square planar coordination system. This value lies in the range of the Cu-N distances obtained for [Pc*Cu].
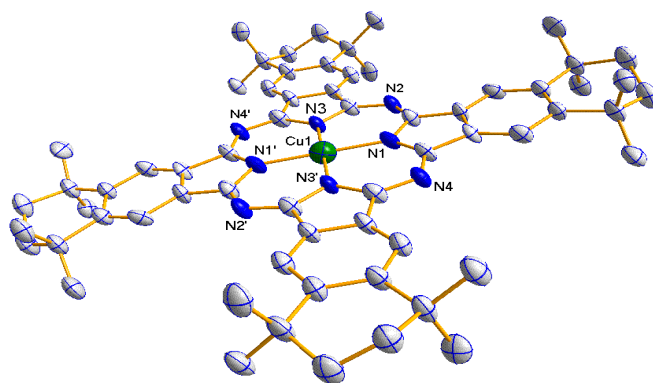
Figure 84: Molecular structure of [Pc*Cu].4CHCl$_3$ crystallized from chloroform. All the CHCl$_3$ molecules and H atoms are omitted for clarity. Ellipsoids are shown at 50% probability**.**

Table 9: Selected Bond Lengths (Å) and Angles (°) for [Pc*Cu].4CHCl$_3$.

Bond lengths/ Å		Angles/ °	
Cu1-N3	1.918(6)	N1-Cu1-N3	90.4(2)
Cu1-N1	1.949(5)	N1'-Cu1-N3'	89.6(2)
Cu1-N3'	1.918(6)	N3-Cu1-N1'	90.4(2)
Cu1-N1'	1.949(5)	N1-Cu1-N3'	89.6(2)
d(P$_1$-P$_2$)	3.885		
d(Cu$_1$-Cu$_2$)	11.776		

d(P$_1$-P$_2$) the distance between two neighboring N$_4$ planes

[Pc*Cu], with the solvent molecules omitted, is packed similarly to [Pc*Ni] with ten molecules per unit cell in two stacks of parallel molecules of different orientation (Figure 85). Owing to the steric hindrance caused by the bulky substituents, the closest intermolecular distance between two N4 planes is 3.885 Å with a centroid – centroid distance of 11.776 Å, that reveals almost no overlap between the π- electrons of adjacent molecules.
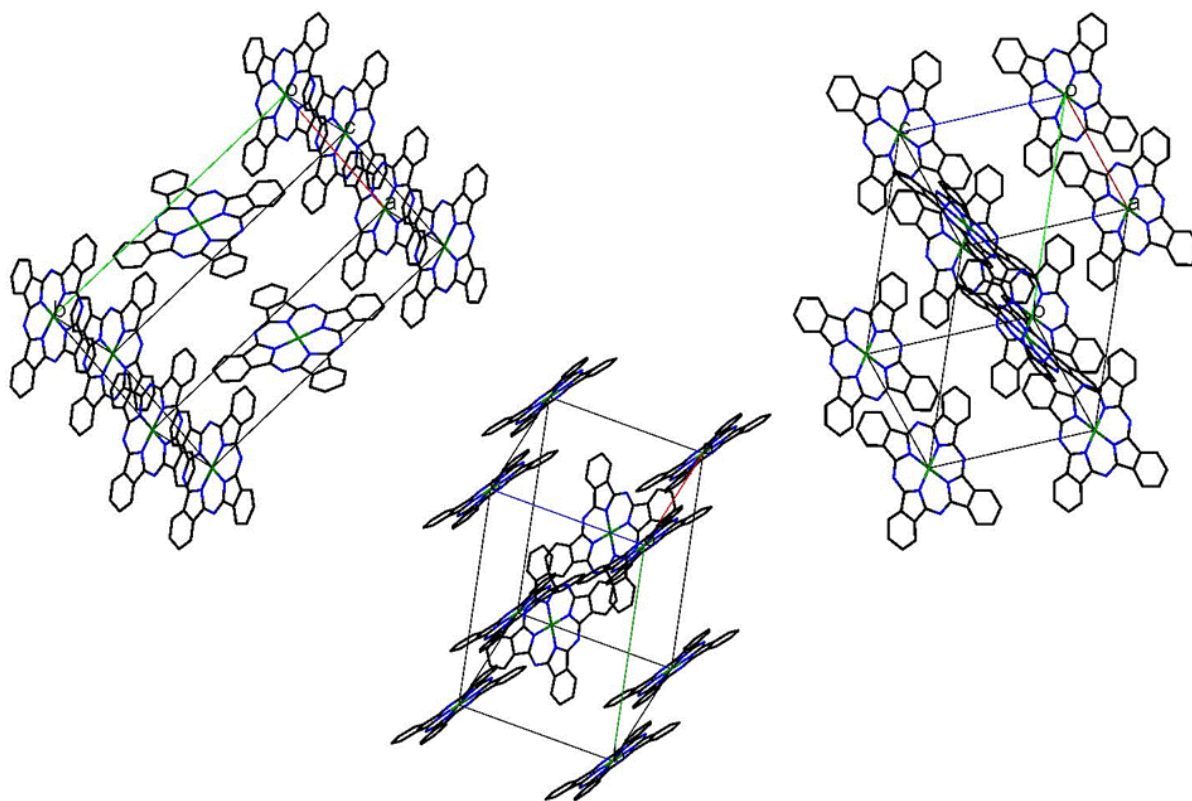
Figure 85: Unit cell packing of [Pc*Cu] molecules in the solid state. All the solvent molecules, aliphatic substituents and H atoms are removed for clarity.

2.3.14 Zinc(II) Complexes [Pc*Zn] and [Ppz*Zn]

Heating PzDN* with zinc template in neat resulted in the formation of a solid residue. After purification using (CHCl$_3$ / Al$_2$O$_3$), the blue complex [Ppz*Zn] was obtained in 30 % yield. The Pc* analog was synthesized using similar procedures but in the prescence of urea (Figure 86). However, the desired product appeared only upon elution with ethylacetae. In spite of the exhausting efforts to purify this complex, [Pc*Zn] which formed in 22 % yield, was not obtained in high purity. The macrocycles [Pc*Zn] and [Ppz*Zn] dissolved well in a variety of solvents, including DCM, CHCl$_3$, THF and toluene.
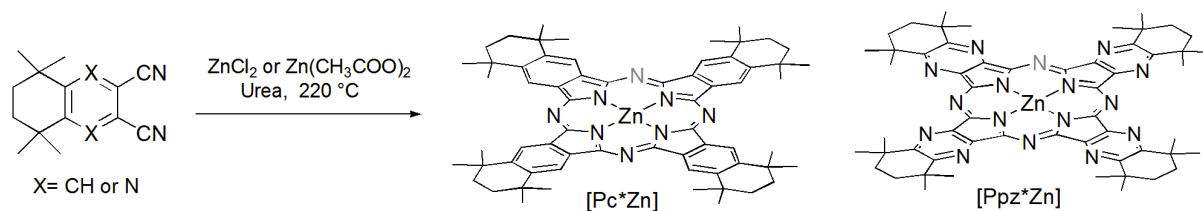
Figure 86: Synthesis of [Pc*Zn] and [Ppz*Zn].

The protonated molecular ion peaks of [Pc*Zn] and [Ppz*Zn] (Figure 87), measured using APCI⁺ MS, were observed at 1017.6 and 1025.6, respectively. The values overlapped exactly with the theoretically calculated isotopic pattern of the elemental composition of the complex.
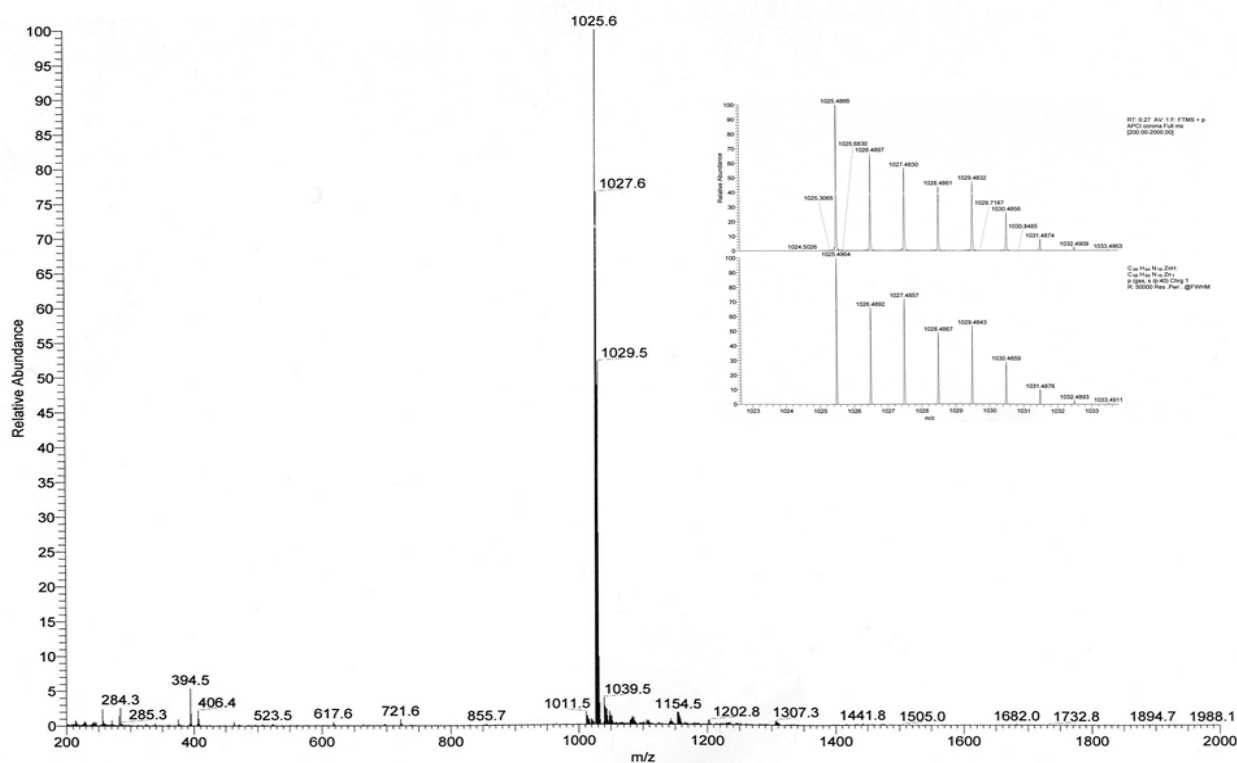
Figure 87: APCI⁺ Mass Spectrum of [Ppz*Zn]. On the right, a high resolution of the molecular ion peak position is shown compared with its theoretically calculated isotopic pattern.

The UV-Vis. spectrum of the [Ppz*Zn] in CHCl$_3$ (Figure 88) includes an intense Q-absorption band at 642 nm indicative for the complex HOMO-LUMO gap and a B-band at 349 nm resulting from deeper π- π* transition . On the other hand, although the [Pc*Zn] spectrum does not look really clean, its Q-band could be clearly seen at 692 nm.
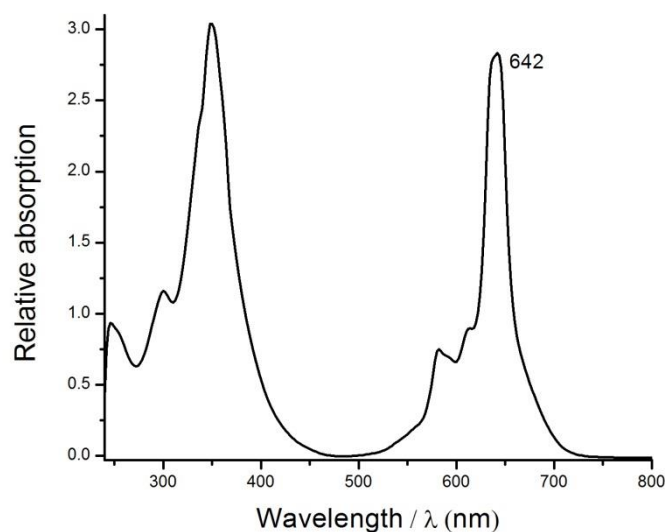
Figure 88: UV/Vis. spectrum of [Ppz*Zn] in CHCl$_3$.

The ^{1}H NMR spectrum of [Ppz*Zn] in CDCl$_3$ (Figure 89) displayed two singlet peaks. While the fourty-eight methyl protons appeared at 1.64 ppm, the CH$_2$ protons could be seen at 1.90 ppm. On the other hand, the ^{1}H NMR spectrum of [Pc*Zn] is not well resolved. The characteristic three singlets displayed at 9.36, 2.04 and 1.78 ppm, corresponded to the aromatic, the methylene and the methyl protons, respectively. Other unidentified signals in the spectrum were also present.
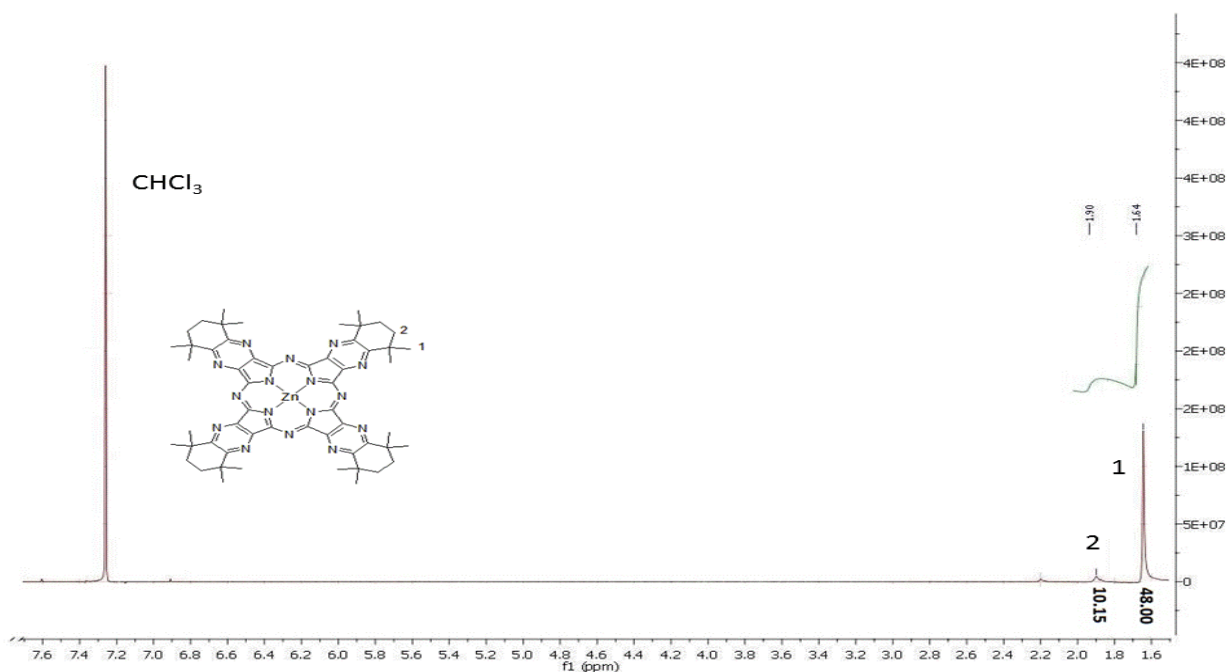
Figure 89: ^{1}H-NMR spectra of [Ppz*Zn] in CDCl$_3$ (300 MHz).

69

2.3.15 Aluminium(III) Complexes [Pc*AlCl] and [Ppz*AlCl]

The aluminium complexes were prepared in neat by reacting the dinitriles with $AlCl_3$ and urea at 220°C under an inert atmosphere (Figure 90). The synthesis of [Pc*AlCl] does not proceed in absence of urea; however, in the case of [Ppz*AlCl], addition of urea just enhances the reaction yield. Both [Ppz*AlCl] and [Pc*AlCl] were purified by column chromatography on alumina using THF and $CHCl_3$, respectively. The synthesized complexes are highly soluble in common organic solvents, such as THF, DCM, $CHCl_3$ and toluene. The macrocycles [Pc*AlCl] and [Ppz*AlCl] were obtained in yield of 26 % and 71 %, respectively.
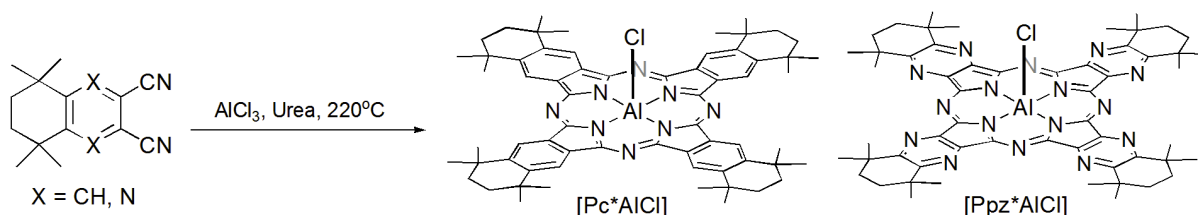
Figure 90: Synthesis of [Pc*AlCl] and [Ppz*AlCl].

Usually, the Pc*/Ppz* complexes are better purified by column chromatography using nonpolar solvents. That is because the product becomes more contaminated, when a more polar solvent is used. Therefore, $CHCl_3$ is considered the perfect eluent. However, usually complexes having an axial dipole moment such as [Pc*AlCl] and [Ppz*AlCl], prefer to stick in the Al_2O_3 column, with no chance of obtaining the desired products when $CHCl_3$ is used as an eluent. Therefore, a solvent of a slightly higher polarity (THF) was used instead of $CHCl_3$. In this case, highly pure [Ppz*AlCl] was obtained, however, [Pc*AlCl] of lower purity was obtained. Furthermore, unlike [Ppz*AlCl], the molecular ion peak of [Pc*AlCl] can not be detected by APCI[+] MS in the prescence of trace amount of THF. THF gets protonated under APCI-MS conditions and the protonated solvent then reacts with [Pc*AlCl] with elimination of HCl. Thus, in this case, a parent peak assignable for [Pc*Al(thf)][+] was detected (Figure 91). That was not observed in the case of [Ppz*AlCl], probably due to its lower Ppz* donor character, thus the chlorido ligand is more efficiently bound to the Al metal in [Ppz*AlCl] and does not react with the protonated THF solvent. To isolate pure [Pc*AlCl], the product obtained by elution using THF must be well dried under vacuum at 200°C. However, an easier and more effective approach for highly pure [Pc*AlCl] is eluting the product using $CHCl_3$ through a very short Al_2O_3 column ($\approx$ 5 cm).
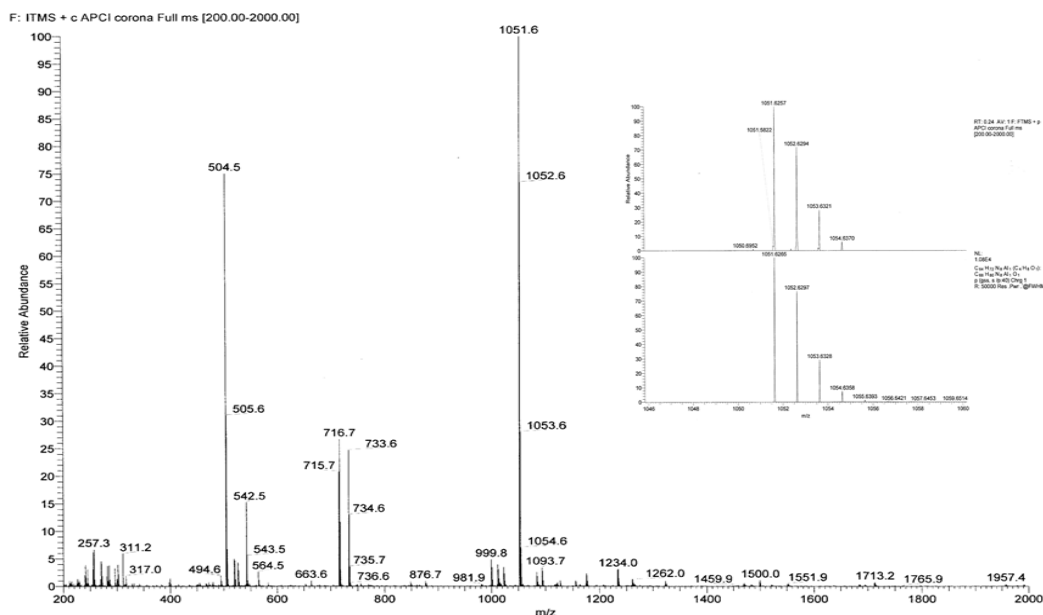
Figure 91: APCI+ Mass Spectrum of [Pc*AlCl] obtained in prescence of THF. On the right, a high resolution of the ion peak [Pc*Al(thf)]+ position is shown compared with its theoretically calculated isotopic pattern.

The APCI+ MS of [Pc*AlCl] and [Ppz*AlCl] showed molecular ion peaks at m/z= 1015.7 and 1023.6, respectively; supporting the proposed formula for the complexes. The spectrum of [Ppz*AlCl] is shown in Figure 92. In addition to the molecular ion peak, two other peaks appeared at 1019.5 and 1059.3 corresponding to [Ppz*AlOMe+H]+ and [Ppz*AlCl$_2$+H]+, respectively, as the measurements were taken from solutions containing NaCl and methanol. Hence, substitution of the axial chlorido ligand with a methoxy group or addition of another chlorine atom to the chromophore is possible.
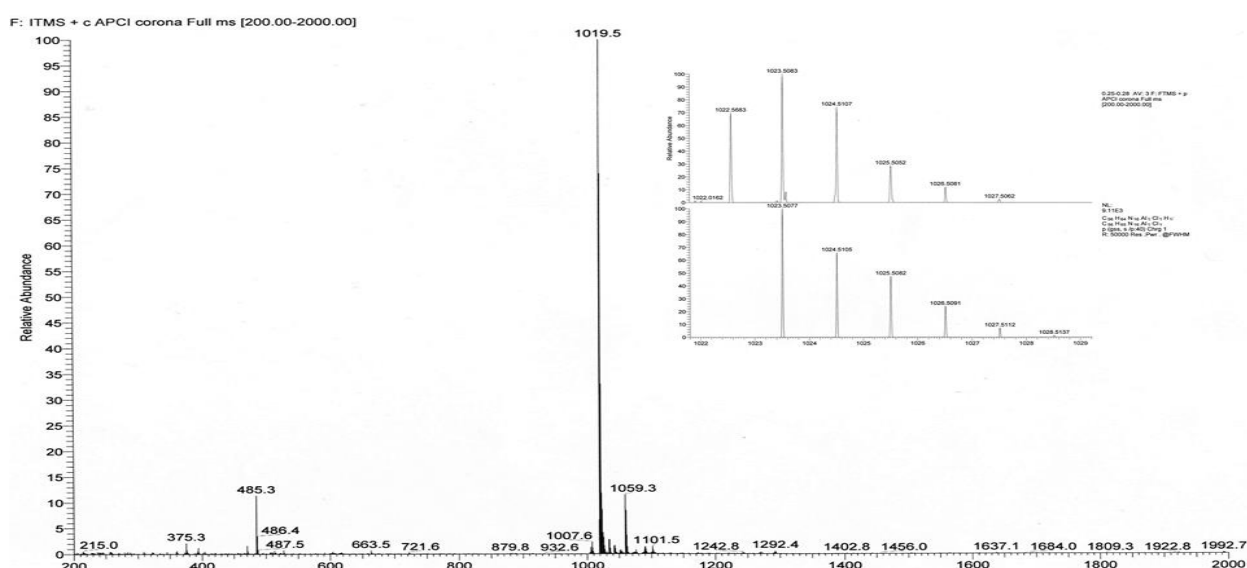
Figure 92: APCI+ Mass Spectrum of [Ppz*AlCl]. On the right, a high resolution of the molecular ion peak position is shown compared with its theoretically calculated isotopic pattern.

71

The UV/Vis. spectra of [Pc*AlCl] and [Ppz*AlCl] show sharp Q-bands at 706 and 642 nm, respectively, in addition to B-bands appear around 290-360 nm (Figure 93). In general, the Q-band of [Pc*AlCl] is red-shifted compared to that of [Ppz*AlCl] as a result of the complex lower π-π* HOMO-LUMO gap, but the B-band of [Pc*AlCl] (346 nm) is blue-shifted compared to that of [Ppz*AlCl] (352 nm).
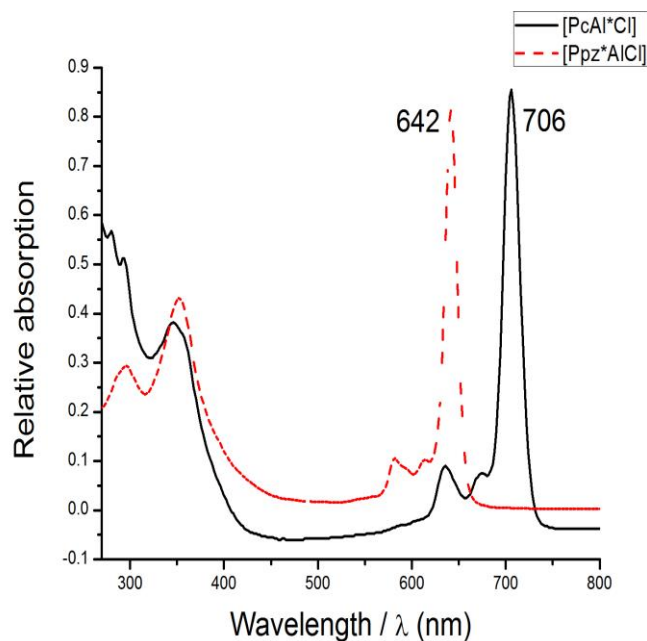
Figure 93: UV/Vis. spectra of [Pc*AlCl] and [Ppz*AlCl] in CHCl$_3$.

^{1}H-NMR spectra for [Pc*AlCl] and [Ppz*AlCl], measured in CDCl$_3$, showed the expected pattern. The deshielded, aromatic protons of [Pc*AlCl] appear at 9.61 ppm, while the two singlet peaks at 1.83 and 1.43 ppm are assigned to the methylene and the methyl protons, respectively. Figure 94 shows the ^{1}H NMR spectrum of [Ppz*AlCl], it displays two singlets at 1.44 and 2.28 ppm assigned to the methyl and methylene protons, respectively. It should be mentioned, although an axial ligand is present, the methyl protons appear to be chemically equivalent. This may be regarded as an indication that, due to the Lewis acidic nature of the cation in [Ppz*AlCl], a soluble coordination polymer or oligomer with [-Al-Cl-Al-Cl-Al-] backbone is present in non coordinating solvents. Such structural motif has been confirmed for some aluminium and gallium complexes, e.g. [(PcAl)]$_2$O and [PcGaF].[326]
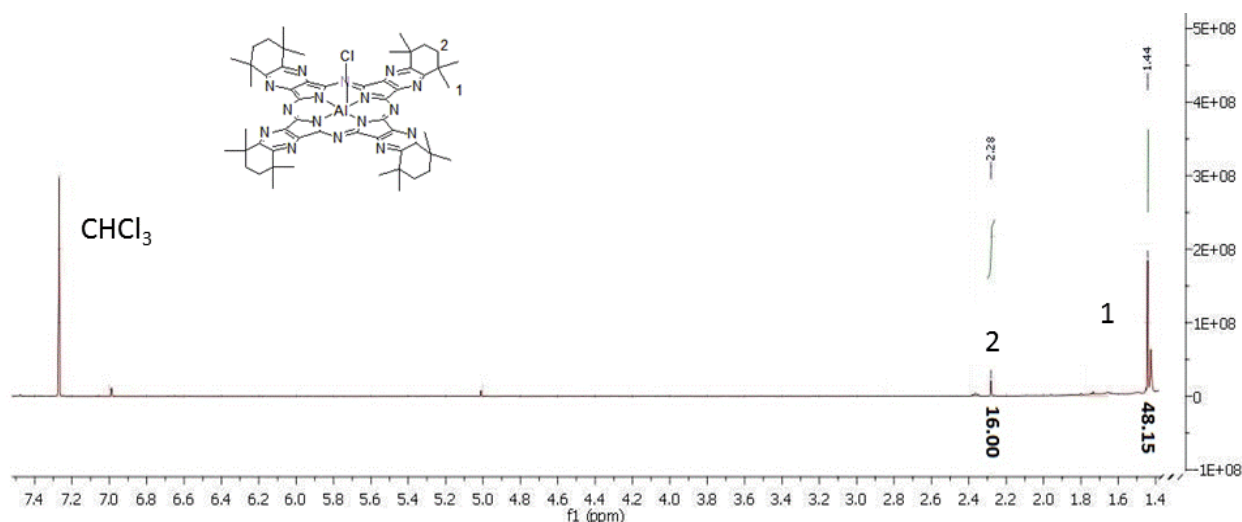
Figure 94: ^{1}H-NMR spectra of [Ppz*AlCl] in CDCl$_3$ (300 MHz).

2.3.16 Attempted Synthesis of [Pc*AlOP(O)(OH)$_2$] or [(Pc*AlO)$_2$P(O)(OH)]

Unlike the other Pc complexes (e.g. TiPcs), few examples for axial functionalization of Group 13 Pcs are known.[326-328] Thus, we tried to substitute the axial chlorido-ligand with other functionalities. The start was to try having an axial acidic anchor directly linked to the Al atom to allow connecting the macrocyles to an oxide semiconductor. Here the sensitivity of the Pc* and Ppz* complexes towards phosphoric acid was studied (Figure 95, the testing conditions are listed in Table 10).
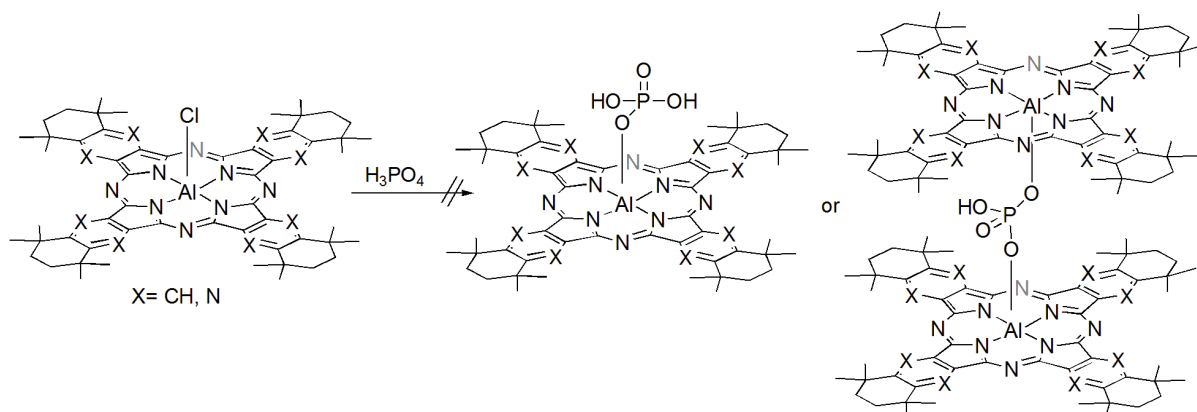
Figure 95: Attempted synthesis of [LAlOP(O)(OH)$_2$] or [(LAlO)$_2$P(O)(OH)], L=Pc* or Ppz*.

Unfortunately, the axial ligand of [Pc*AlCl] showed high stability against substitution with a phosphoric acid moiety. While the analogous complex [Ppz*AlCl] showed no reaction at room temperature, the chromophore decomposed to unidentified products under refluxing conditions.

Table 10: Unsuccessful synthestic strategies of [LAlOP(O)(OH)$_2$] or [(LAlO)$_2$P(O)(OH)], L=Pc* or Ppz*.

Target compound	Reactants	Testing conditions	Product
[Pc*AlOP(O)(OH)$_2$] or [(Pc*AlO)$_2$P(O)(OH)]	[Pc*AlCl] + H$_3$PO$_4$ (85 %)	Reflux/ overnight	No reaction
[Ppz*AlOP(O)(OH)$_2$] or [(Ppz*AlO)$_2$P(O)(OH)]	[Ppz*AlCl] + H$_3$PO$_4$ (85 %)	Stirring/ 24 hours / 110°C	No reaction
		Reflux/overnight	Decomposition products

2.3.17 Gallium(III) Complexes [Pc*GaCl] and [Ppz*GaCl]

[Pc*GaCl] and [Ppz*GaCl] were prepared using the similar strategy that applied for synthesis of the aluminium macrocycles (Figure 96), except that GaCl$_3$ was used as a metal template and no urea was required for the reaction to proceed, but only to enhance the reaction yield. The products were purified by column chromatography: [Pc*GaCl] was purified by elution with CHCl$_3$ through a short column ($\approx$ 5 cm) of Al$_2$O$_3$, while [Ppz*GaCl] was purified using THF and Al$_2$O$_3$.
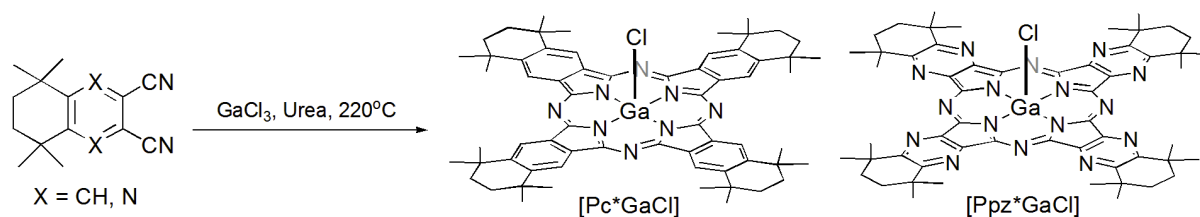
Figure 96: Synthesis of [Pc*GaCl] and [Ppz*GaCl].

Usually chloroform is used to purify the products *via* column chromatography. In this case, due to the axial dipole moment imposed by the Ga-Cl bond, CHCl$_3$ is not a sufficiently polar solvent to elute the product, and a mobile phase of higher polarity is required. Hence, we used THF to obtain the pure [Ppz*GaCl] complex. In the case of [Pc*GaCl], when THF was used, the desired product was eluted with lower purity. Additionally, owing to the higher basicity of [Pc*GaCl] compared to the basicity of [Ppz*GaCl], the molecular ion peak of [Pc*GaCl] was not detected in the prescence of trace amount of THF. THF becomes protonated under the APCI-MS conditions then reacts with the complex. With elimination of HCl, a parent peak corresponding to [Pc*Ga(thf)]$^+$ was detected (Figure 97). The pure [Pc*GaCl] complex is accessible by two ways. Firstly, after elution with THF, the complex must be then dried at 200°C for 2 hours to remove any solvent molecules or organic matter. Secondly, the pure [Pc*GaCl] could be obtained directly by column chromatography (CHCl$_3$, Al$_2$O$_3$), however, in this case, only a short aluminium oxide column was used. The reaction yield is high relative to the other soluble Pc complexes, *viz.* 46 % for [Pc*GaCl] and 42 % for [Ppz*GaCl] in the

absence of any catalyst. The complexes dissolve well in a variety of organic solvents including DCM, CHCl₃, THF and toluene.
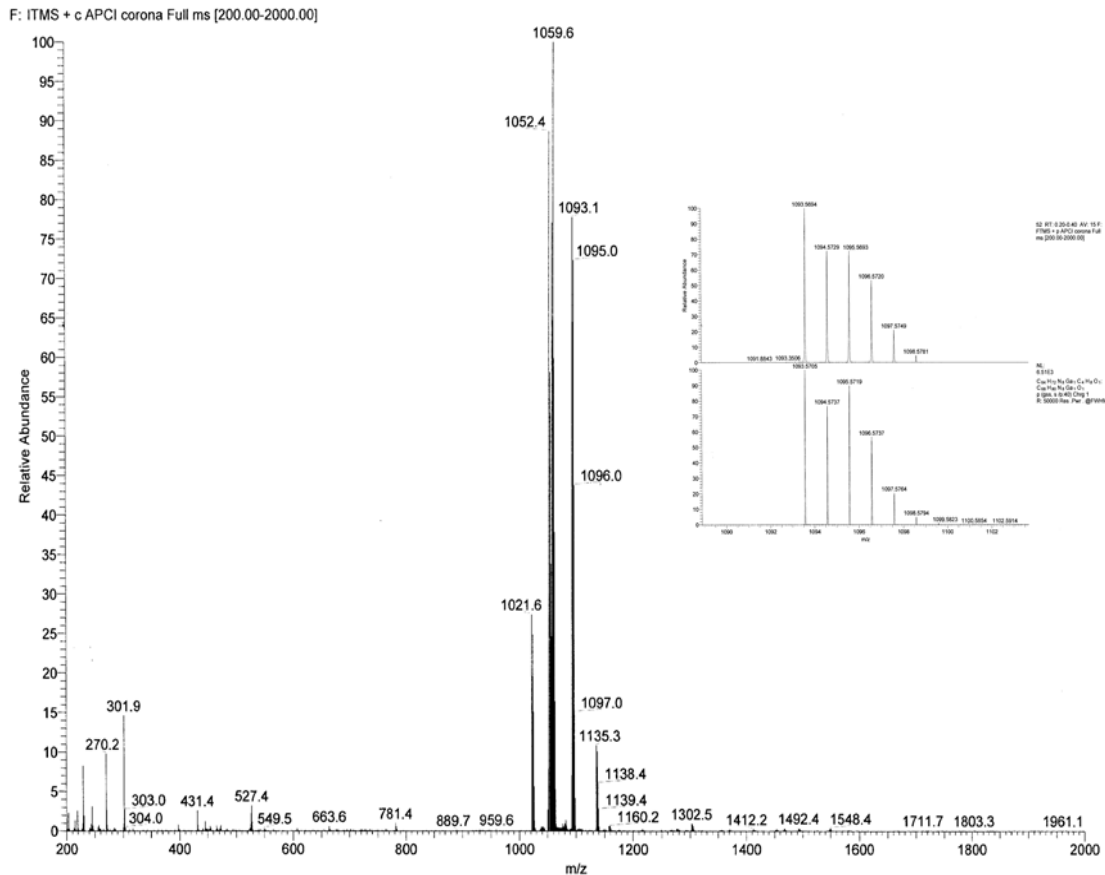
Figure 97: APCI⁺ Mass Spectrum of [Pc*GaCl] in prescence of THF. On the right, a high resolution of the ion peak [Pc*Ga(thf)]⁺ position is shown compared with its theoretically calculated isotopic pattern.

The APCI⁺ MS results of [Pc*GaCl] and [Ppz*GaCl] confirmed the proposed structures. The protonated molecular ion peaks were identified at m/z: 1059.80 [M+H]⁺ for [Pc*GaCl] and m/z: 1067.5 [M+H]⁺ for [Ppz*GaCl]. The spectrum of [Pc*GaCl] is shown in Figure 98; besides the protonated molecular ion peak of the complex, additional peaks were observed at 1052.6 and 1021.8, representing [Pc*GaOMe + H]⁺ and [Pc*Ga +H]⁺, respectively. The methoxy group originates from the co-solvent methanol.

Figure 98: APCI⁺ Mass Spectrum of [Pc*GaCl]. On the right, a high resolution of the molecular ion peak position is shown compared with its theoretically calculated isotopic pattern.

UV-Vis. spectra of [Pc*GaCl] and [Ppz*GaCl] (Figure 99) in CHCl₃ showed two strong absorption regions: B-bands appeared in the range of 300-360 nm and Q-bands appeared at 712 and 648 nm for [Pc*GaCl] and [Ppz*GaCl], respectively. The red-shift of the Q-band of [Pc*GaCl] compared to that of [Ppz*GaCl] is attributed to its lower π-π* HOMO-LUMO gap, which resulted from the enhanced electron donating ability of the benzene rings relative to the pyrazine ones. However, the main B-band of [Pc*GaCl] is 2 nm blue-shifted compared to the B-band of [Ppz*GaCl].
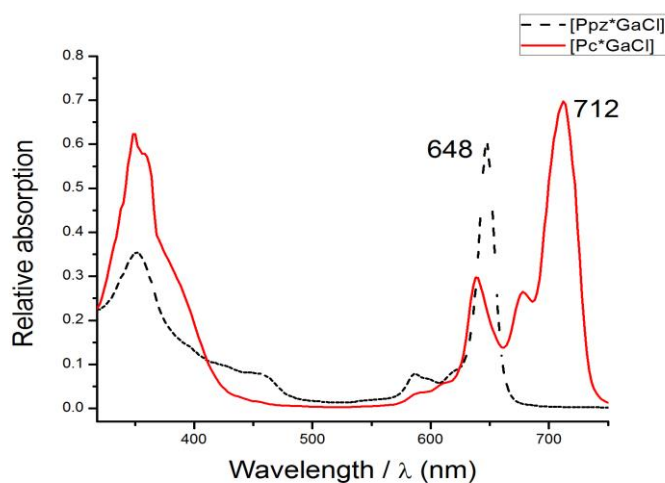
Figure 99: UV/Vis. spectra of [Pc*GaCl] and [Ppz*GaCl] in CHCl₃.

Comparing the Ga complexes with the Al containing ones revealed a 6 nm red-shifted Q-band in the case of Ga complexes. This might be attributed to the lower electron density of Pc*/Ppz* core in the case of aluminium relative to that when gallium is present, i.e., the weaker Lewis acidity character of gallium compared to that of aluminium; therefore, gallium withdraws little electron density from the Pc*/Ppz* core than aluminium does. The absorbance of the vibronic peak present at the higher energy side of the Q-band of [Pc*GaCl] is unusually higher than the expected pattern, but that might arise from the prescence of face to tail aggregates of the complex in the chloroform solution.

Fiigure 100 shows the ¹H NMR spectrum of [Ppz*GaCl] in CDCl₃. In the figure, the two characteristic singlets of the complex could be clearly observed at 1.84 and 2.08 ppm, corresponding to the complex methyl and methylene protons, respectively. [Pc*GaCl] showed a very similar ¹H NMR spectrum, but, in this case, three singlets are present at 1.82, 2.07 and 9.60 ppm; the singlet peaks observed for the complex are assigned to its methyl, methylene and aromatic protons, respectively. In both cases, although of their molecular C_{4v} symmetry, the peaks are not split. This might indicate an oligomeric or polymeric nature of the complex with [-Ga-Cl-Ga-Cl-Ga-] backbone in the solid state and even in a solution of non-coordinating solvent.
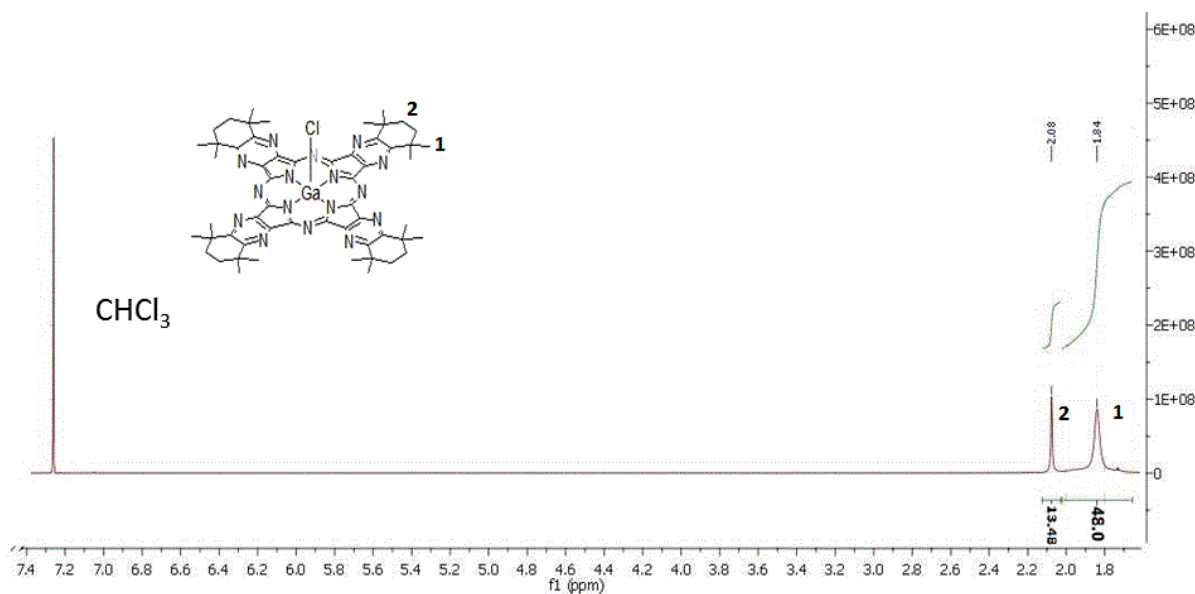
Figure 100: ¹H-NMR spectra of [Ppz*GaCl] in CDCl₃ (300 MHz).

2.3.18 Attempted Synthesis of Al(III) or Ga(III) Complexes Bearing Axial -OH or -SH Functionality

Here, we tried to substitute the axial chlorido-ligand of four complexes, the Al- and Ga-complexes of Pc* and Ppz*, with either an –OH or an –SH moiety. Generally, insoluble complexes of the type [PcAlOH] and [PcGaOH] are known, while the Ppz counterparts

are not yet reported. Group 13 metal complexes with an axial -SH moiety are not known. Figure 101 and Table 11 display the preparative strategies followed to prepare the substituted complexes, with much focus on the Ppz* ones. Substitution of the axial Cl of the complexes with an SH moiety was attempted using NaSH in a variety of solvents under refluxing conditions (i.e. toluene and acetone). Unfortunately, no reaction occurred in toluene, and the Ppz complex [Ppz*AlCl] decomposed to unidentified products when allowed to react in refluxing acetone. The C=N bonds of the chromophore were probably attacked by the highly nucleophilic SH- anion. Attempted synthesis of axial hydroxido complexes using a variety of different methods was also usuccessful. The tetramerization reaction of the nitriles in the presence of Al(OH)$_3$ and DBU occured only at 220°C leading to formation of the metal free ligands Pc*H$_2$ and Ppz*H$_2$. Furthermore, [Ppz*AlCl] did not react with NH$_4$OH in either water or triethylammine; however, when [Pc*GaCl] was refluxed in NH$_4$OH/pyridine mixture, [Pc*Ga(pyridine)Cl] was obtained (Figure 102) and confirmed only by APCI$^+$ MS and elemental analysis. The APCI$^+$ MS of [Pc*Ga(pyridine)Cl] is shown in Figure 103: the parent ion peak of the complex was observed at 1100.4, corresponding to [Pc*Ga(pyridine)]$^+$. Besides this peak, two other fragments were detected corresponding to [Pc*GaCl+H]$^+$ and [Pc*Ga]$^+$. If the complex [Pc*Ga(pyridine)Cl] is heated at 200°C, it loses the coordinating pyridine ligand. Hence, analysis of the resulting compound confirms its structure as [Pc*GaCl].
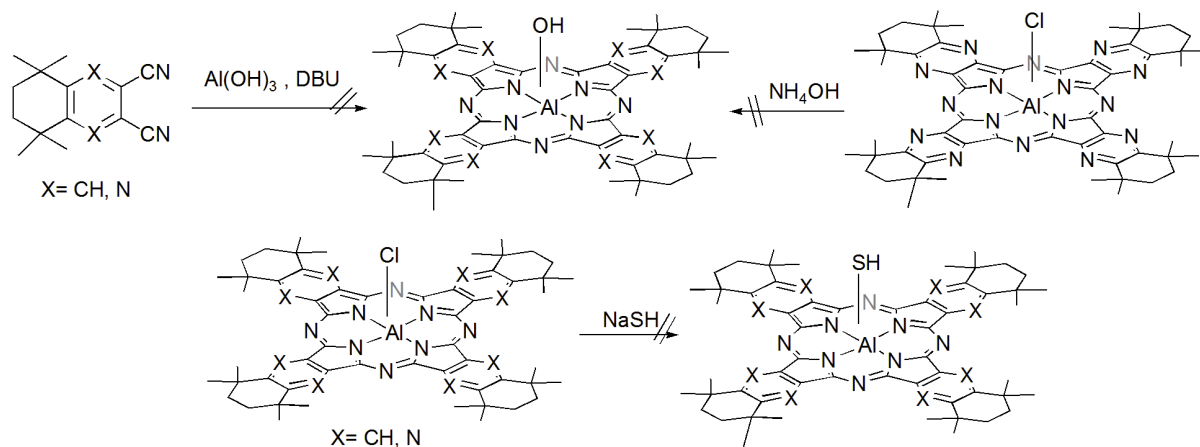
Figure 101: Attempted synthesis of [LAlOH], L=Pc* or Ppz and [LMSH], M= Al or Ga.
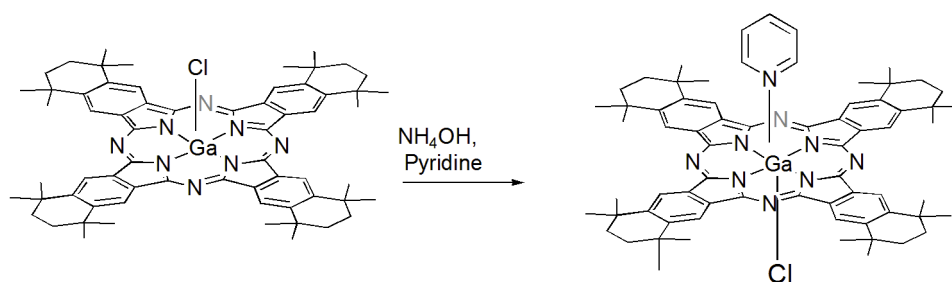
Figure 102: Synthesis of [Pc*Ga(pyridine)Cl].

78

Table 11: Attempted synthesis of [Pc*AlOH], [Pc*AlSH], [Ppz*AlOH] and [Pc*GaSH].

Target compound	reactants	Base	Coditions Solvent/temperature/duration	Result
[Pc*AlOH]	PDN* + Al(OH)$_3$	DBU	1-pentanol/220°C/1hour	Pc*H$_2$
			1-pentanol/160°C/overnight	No reaction
[Ppz*AlOH]	PzDN* + Al(OH)$_3$	DBU	1-pentanol/220°C/1 hour	Ppz*H$_2$
			1-pentanol/160°C/1 hour	No reaction
	[Ppz*AlCl] + NH$_4$OH		Water/reflux/overnight	No reaction
			Triethylamine/25°C/48 hours	No reaction
[Pc*GaOH]	[Pc*GaCl] + NH$_4$OH		Pyridine/reflux/5 hours	[Pc*Ga(pyridine)Cl]
			Water /reflux/4 hours	No reaction
[Pc*AlSH]	[Pc*AlSH] + NaSH		Toluene /reflux/overnight	No reaction
[Ppz*AlSH]	[Ppz*AlCl] + NaSH		Toluene/reflux/overnight	No reaction
			Acetone/reflux/3 hours	Decomposition, chromophore destroyed
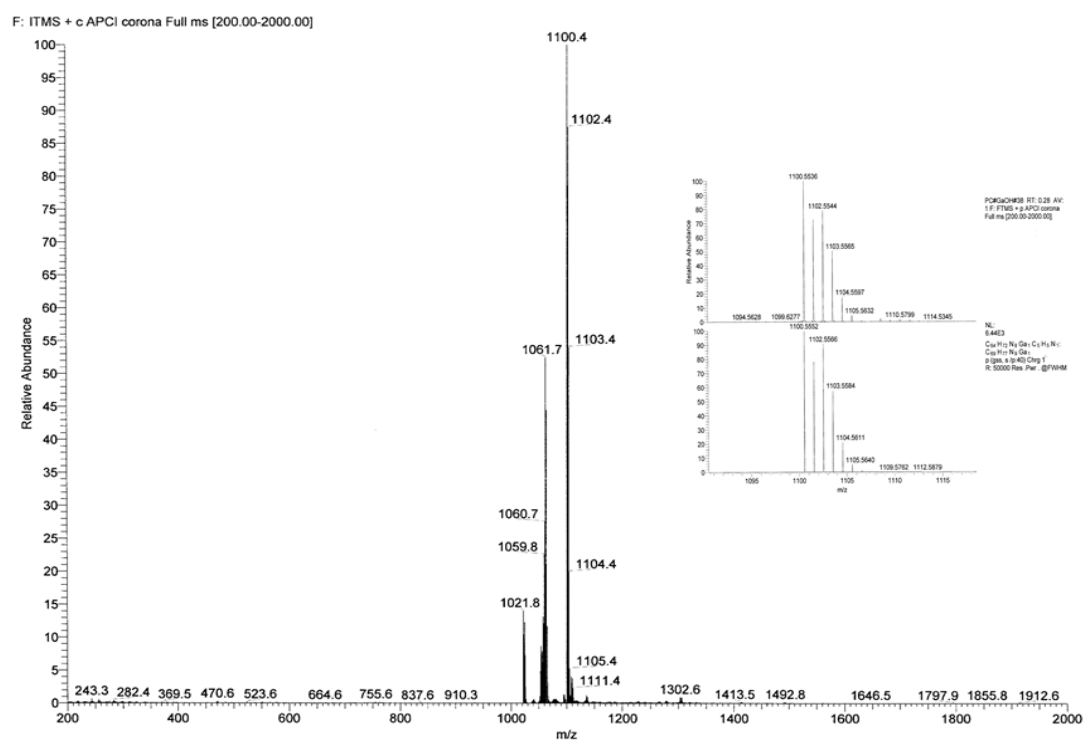
Figure 103: APCI[+] Mass Spectrum of [Pc*Ga(pyridine)Cl]. On the right, a high resolution of the ion peak [Pc*Ga(pyridine)][+] position is shown compared with its theoretically calculated isotopic pattern.

2.3.19 Synthesis of [Pc*GaX] (X=CH$_3$, C$_4$H$_9$, C$_6$H$_{13}$ and C$_6$H$_5$)

When the [Pc*GaCl] was allowed to react with methyl-, n-butyl-, n-hexyl or phenyl-lithium overnight in dry THF, the axialy substituted alkyl- and phenyl- gallium phthalocyanines ([Pc*GaCH$_3$], [Pc*GaC$_4$H$_9$], [Pc*GaC$_6$H$_{13}$], [Pc*GaC$_6$H$_5$]) were

successfully obtained (Figure 104) in high yield of 82 %, 71 %, 44 % and 71 %, respectively. The complexes are very soluble in a variety of solvents, including THF, DCM, CHCl₃ and toluene. Additionally, compared to the chlorido-ligand, the alkyl- and aryl- substituents introduce steric crowding and should reduce the tendency to form aggregates.
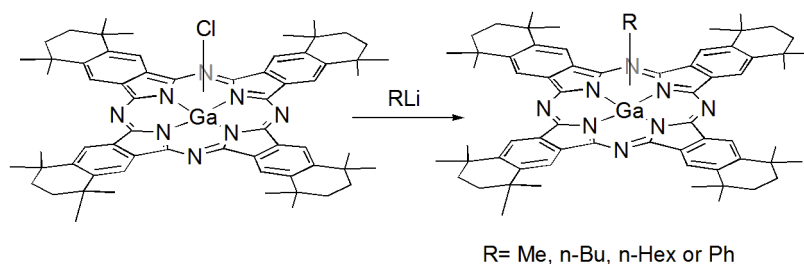
Figure 104: Synthesis of [Pc*GaMe], [Pc*Ga(n-Bu)], [Pc*Ga(n-Hex)] and [Pc*Ga(Ph)].

The APCI⁺ MS results of [Pc*GaMe], [Pc*Ga*(n-Bu)], [Pc*Ga(n-Hex)] and [Pc*GaPh] confirmed the proposed structures. The protonated molecular ion peak for each complex was identified at 1037.6, 1079.6, 1107.7 and 1099.6, respectively. In all cases, other peaks appear at higher m/z values. Representative examples are shown in Figures 105 & 106. The spectrum of [Pc*GaC₄H₉] is shown in Figure 105, besides the protonated molecular ion peak of the complex, additional peaks were observed at 1195.7 and 1253.7 representing [Pc*Ga(C₄H₉)₃ + H]⁺ and [Pc*Ga(C₄H₉)₄ + H]⁺. Furthermore, the spectrum of [Pc*GaPh] is shown in Figure 106, it also shows two ion peaks at 1099.5 and 1178.6. These peaks correspond to [Pc*GaPh + H]⁺ and [Pc*Ga(Ph)₂ + H]⁺.
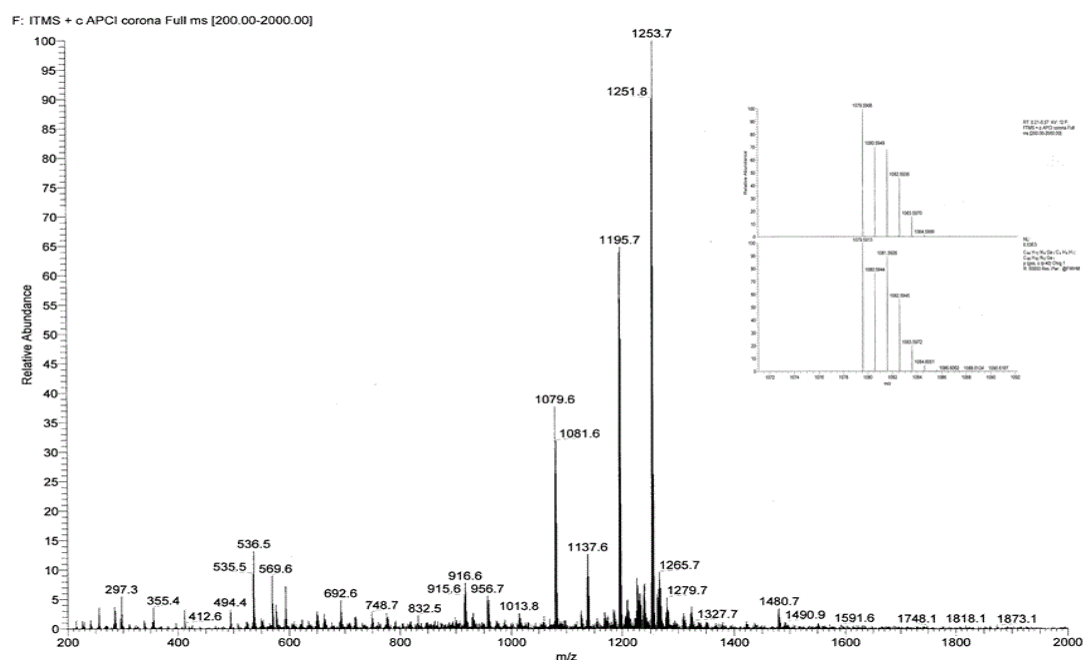
Figure 105: APCI⁺ Mass Spectrum of [Pc*Ga(n-Bu)]. On the right, a high resolution of the molecular ion peak position is shown compared with its theoretically calculated isotopic pattern.
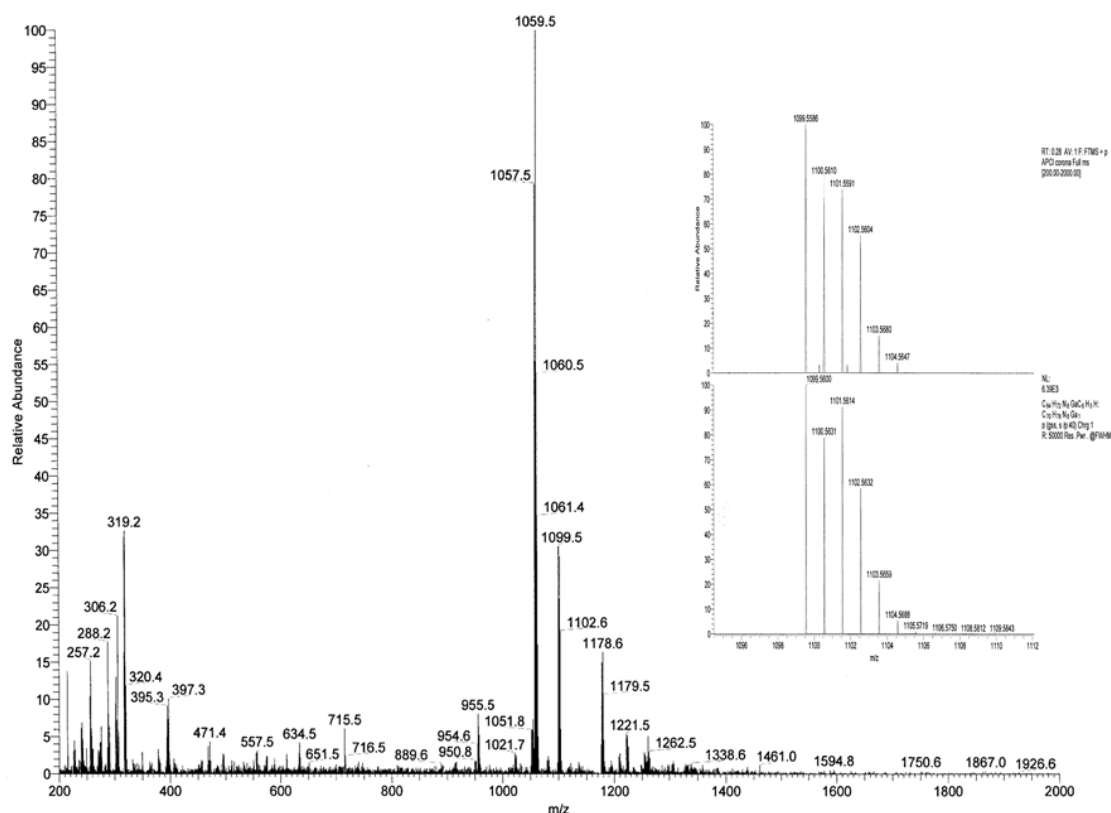
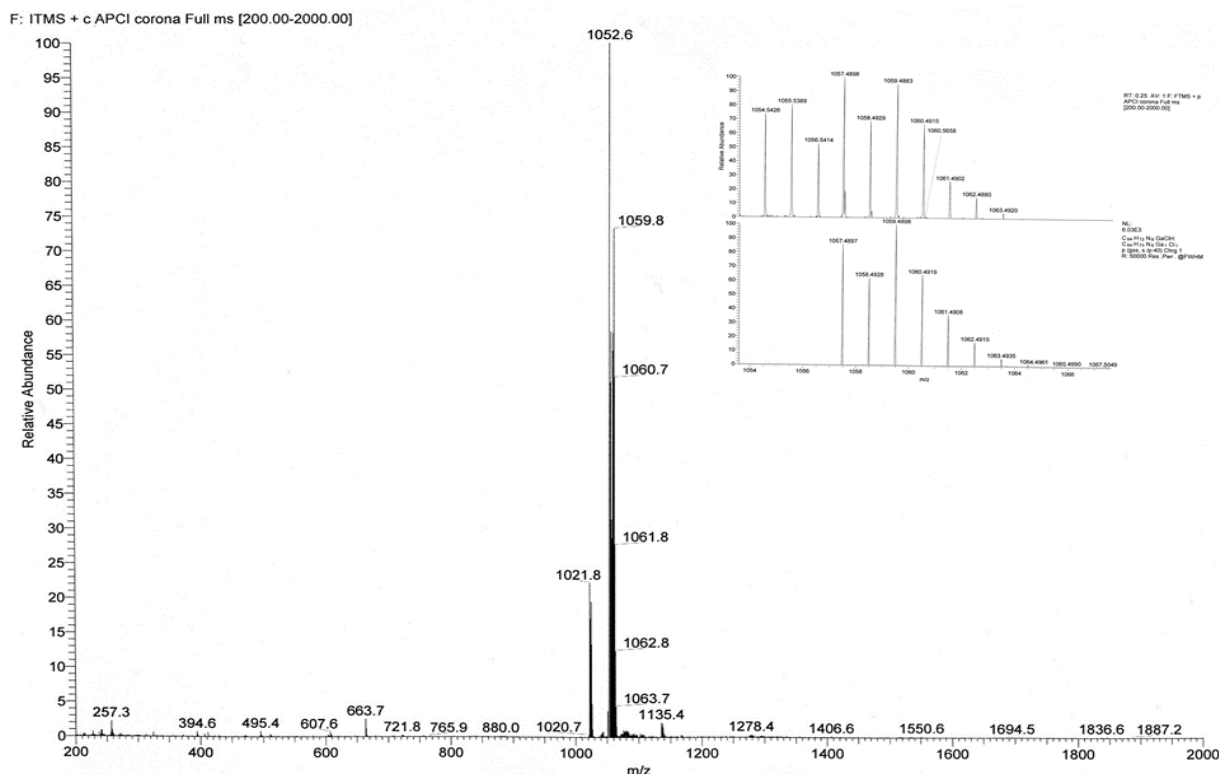**Figure 106**: APCI+ Mass Spectrum of [Pc*GaPh]. On the right, a high resolution of the molecular ion peak position is shown compared with its theoretically calculated isotopic pattern.

The ^{1}H-NMR spectra for the complexes are not completely understood with multiple peaks appearing, due to some splitting of the singlet peaks which probably resulted from some decomposition or prescence of the starting complex [Pc*GaCl]; also the mono-lithio reactants, RLi, were found to be reactive at room temperature, so that by-products like dilithio phthalocyanine, formed almost exclusively.[307] However, the respective protons appeared at the expected chemical shifts. The ^{1}H-NMR spectra of [Pc*GaCH$_3$], and [Pc*GaC$_6$H$_5$] (Figure 107) measured in CDCl$_3$ displayed better resolved results. [Pc*GaCH$_3$] showed four peaks at 9.55, 2.07, 1.85 and 0.88 ppm, correponding to the aromatic, methylene, methyl protons of Pc* and the axial CH$_3$ moiey, respectively. On the other hand, the protons of the axial phenyl group of [Pc*GaC$_6$H$_5$] appeared at 7.61 ppm, while the ring protons appear in the same regions as for [Pc*GaCH$_3$], except that the methyl protons appear in two sets at 1.82 and 1.79 ppm. Additionally, in [Pc*GaC$_6$H$_5$], the methylene and aromatic protons appear at 2.08 and 9.60 ppm, respectively.

81
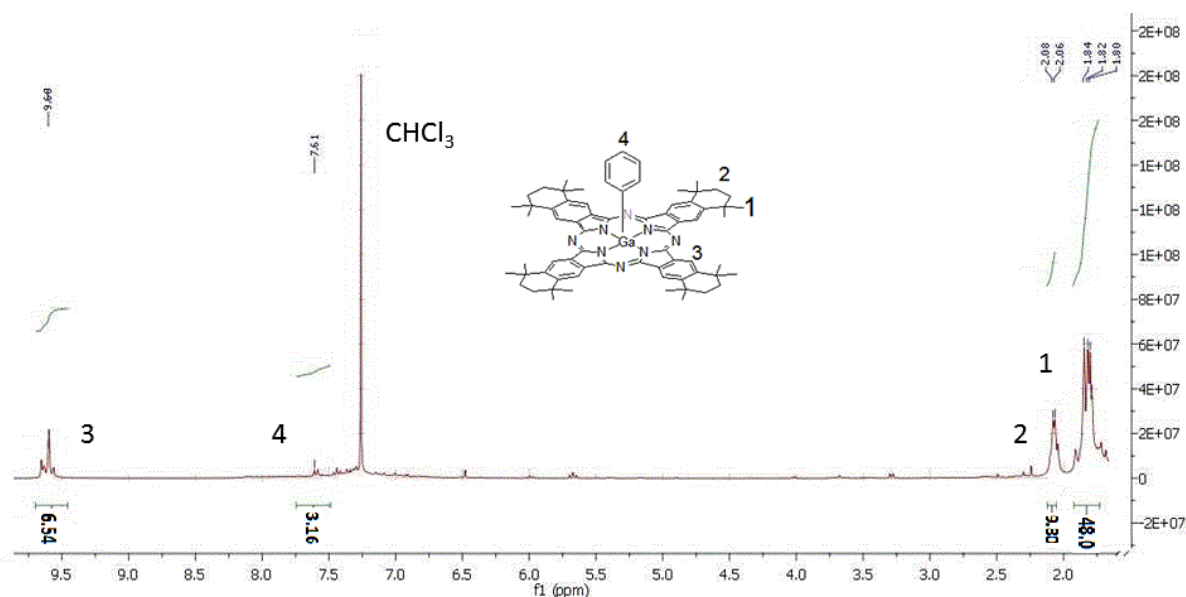
Figure 107: ^{1}H-NMR spectra of [Ppz*GaPh] in CDCl$_3$ (300 MHz).

The exact nature of the side products could not be fully identified. Owing to the prescence of molecular ions with three and four alkyl groups, e.g. n-butyl, per gallium atom, and the relatively higher carbon content found in the elemental analysis of these complexes, the side products might arise from the nucleophilic attack of the highly reactive R groups of LiR reagents at one, two, or three C=N bonds of the chromophore. This should be associated with the destruction of the π-system. The UV/Vis. spectra (Figure 109) shows relatively broad Q-bands accompanied by unusually strong bands in the higher energy region. This is probably indicative for the prescence of impurities of chromophore fragments of smaller π-system. A representative example of RLi addition to the chromophore followed by hydrolysis is shown in Figure 108.
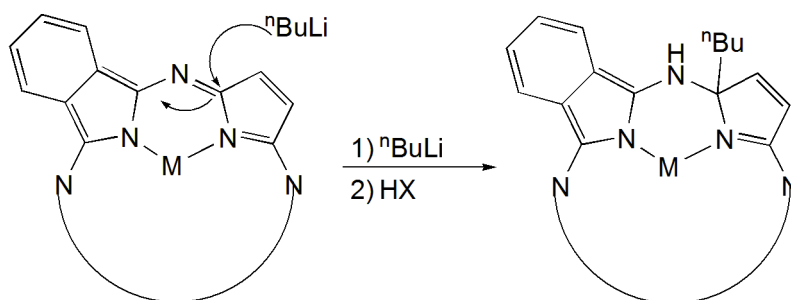
Figure 108: Proposed mechanism for attacking the Pc* ring with organolithium reagents.

The axially substituted gallium complexes (Figure 109) showed UV-Vis. spectra (in CHCl$_3$) very similar to the spectrum of [Pc*GaCl], except that a short blue shift (2 nm) was observed. This blue shift was previously reported for axially substituted aryloxy gallium Pcs., as the substitution of the Cl atom results in a weak (2–3 nm) blue shift of

the *Q*-band.[307] Furthermore, the B-bands of the axially substituted Ga complexes are not sharp and not really clear, as a result of the impurities.
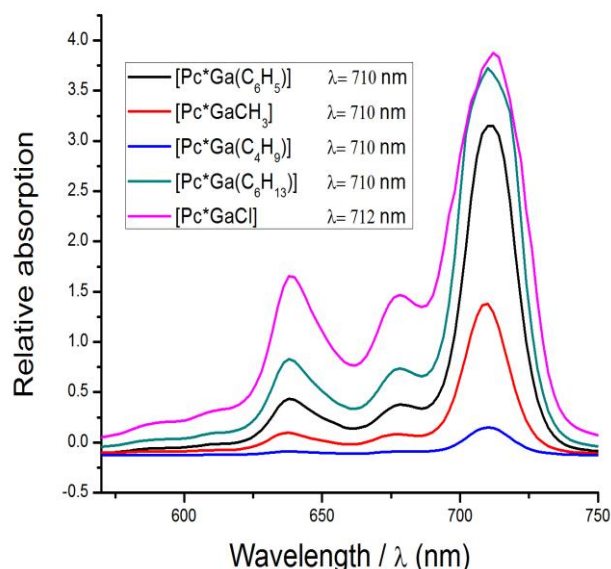
Figure 109: UV/Vis. spectra of [Pc*GaCl], [Pc*GaMe], [Pc*Ga(n-Bu)], [Pc*(n-hex)] and [Pc*Ph] in CHCl$_3$.

[Pc*GaCl] was the only starting material to react selectively in some cases. All the Ppz* complexes and the aluminium complex [Pc*AlCl] did not react at all or did react unselectively with the alkylating reagents. The testing conditions are summarized in Figure 110 and Table 12.

It is worthwhile to mention, after synthesizing the axially substituted alkyl- and phenyl-gallium complexes, we aimed to hydrolize them to obtain [Pc*GaOH]. However, the Ga complexes showed unexpected stability against hydrolysis with some amount of other decomposition products.
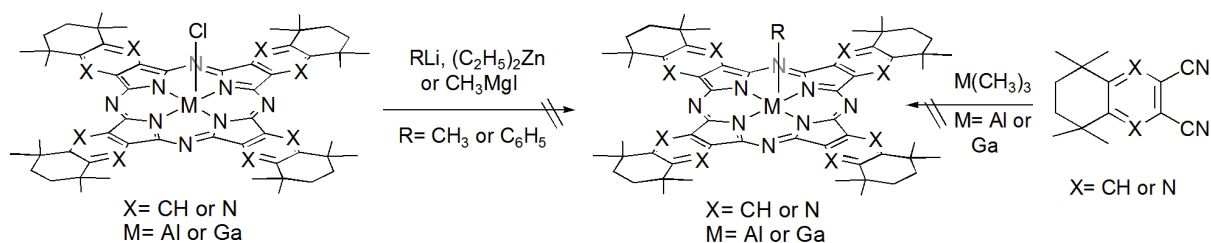
Figure 110 : Attempted synthesis of [LMR], L=Pc* or Ppz*, R=CH$_3$, C$_2$H$_5$ or C$_6$H$_5$ and M= Al or Ga.

Table 12 : Successful/unsuccessful synthetic strategies of [LMR], L=Pc* or Ppz*, M= Al or Ga, R= alkyl or phenyl.

Target compound	Reactants	Conditions Solvent/temperature/duration	Result
[Pc*AlCH$_3$]	[Pc*AlCl] +CH$_3$Li	THF/room temperature/overnight	No reaction
	[Pc*AlCl] +CH$_3$MgI	THF/room temperature/overnight	No reaction
[Pc*AlC$_6$H$_5$]	[Pc*AlCl] +C$_6$H$_5$Li	THF/room temperature/overnight	No reaction
[Ppz*AlCH$_3$]	[Ppz*AlCl] +CH$_3$Li	Toluene/room temperature/3 hours	Unidentified decomposition products
		Diethyl ether/room temperature/3 hours	Unidentified decomposition products
	[Ppz*AlCl] +CH$_3$MgI	THF/room temperature/3 hours	Unidentified decomposition products
		Toluene /120°C /3 hours	No reaction
	PzDN* + Al(CH$_3$)$_3$	--------/220°C/30 minutes	Unidentified green product
[Ppz*AlC$_2$H$_5$]	[Ppz*AlCl] + (C$_2$H$_5$)$_2$Zn	Diethyl ether / room temperature / 3 hours	Unidentified decomposition products
[Ppz*AlC$_6$H$_5$]	[Ppz*AlCl] + C$_6$H$_5$Li	Toluene / 120°C/ 3 hours	Unidentified decomposition products
[Pc*GaCH$_3$]	[Pc*GaCl] + CH$_3$Li	THF / room temperature/ overnight	[Pc*GaCH$_3$]
[Pc*GaC$_4$H$_9$]	[Pc*GaCl] + C$_4$H$_9$Li	THF / room temperature/ overnight	[Pc*GaC$_4$H$_9$]
[Pc*GaC$_6$H1$_3$]	[Pc*GaCl] + C$_6$H$_{13}$Li	THF / room temperature/ overnight	[Pc*GaC$_6$H$_{13}$]
[Pc*GaC$_6$H$_5$]	[Pc*GaCl] + C$_6$H$_5$Li	THF / room temperature/ overnight	[Pc*GaC$_6$H$_5$]
[Ppz*GaCH$_3$]	[Ppz*GaCl] + CH$_3$MgI	Toluene/ 100°C/ overnight	No reaction
		THF/ room temperature/ overnight	Unidentified decomposition products
[Ppz*GaCH$_3$]	[Ppz*GaCl] + CH$_3$Li	Toluene / room temperature/ overnight	Unidentified decomposition products
	PzDN* + Ga(CH$_3$)$_3$	----- / 220°C/ 30 minutes	Unidentified green product

2.3.20 Attempted Synthesis of Axially Substituted Amido Aluminium and Gallium Complexes

After synthesis of [Pc*GaCH$_3$], [Pc*GaC$_4$H$_9$], [Pc*GaC$_6$H$_{13}$] and [Pc*GaC$_6$H$_5$], we aimed to synthesize the axially substituted amido complexes by reacting the chlorido complexes with lithiated amides. Furthermore, titanium tetrakis(dimethylamide) was also allowed to react with [Ppz*AlCl]. Unfortunately, all attempts (Figure 111, Table 13) were unsuccessful.
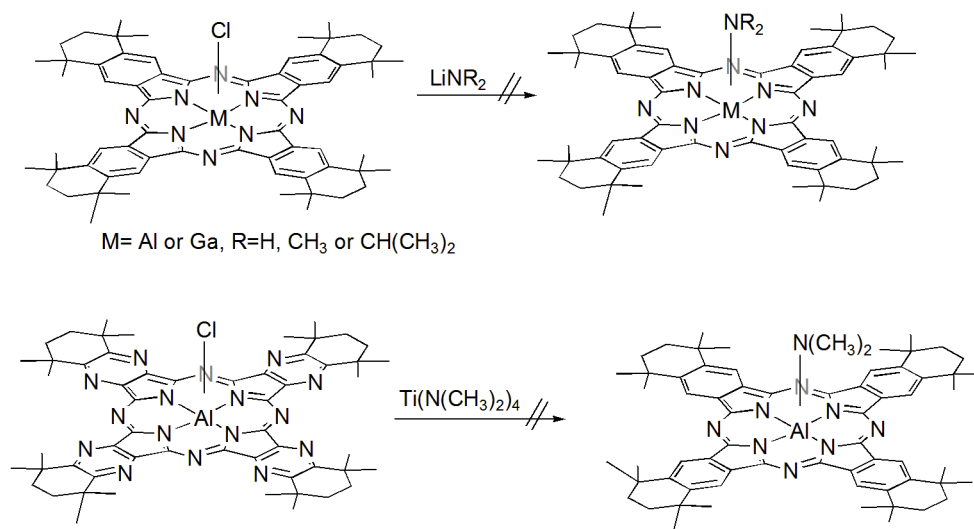
Figure 111: Attempted synthsis of [LMR], L=Pc* or Ppz*, M= Al or Ga and R= H, CH₃ or CH(CH₃)₂.

Table 13 : Attempted synthesis of [LMR], L=Pc* or Ppz*, M= Al or Ga and R= H, Me or i-Pr.

Target compound	Reactants	Conditions Solven/temperature/duration	Result
[Pc*AlNH₂]	[Pc*AlCl] + LiNH₂	THF/room temperature/overnight	No reaction
[Pc*Al(NMe₂)]	[Pc*AlCl] + LiN(Me)₂	THF/room temperature/overnight	No reaction
[Pc*Al(NⁱPr₂)]	[Pc*AlCl] + LiN(ⁱPr)₂	THF/room temperature/overnight	No reaction
[Pc*GaNH₂]	[Pc*GaCl] + LiNH₂	THF/room temperature/overnight	No reaction
[Pc*Ga(NMe₂)]	[Pc*GaCl] + LiN(Me)₂	THF/room temperature/overnight	No reaction
[Pc*GaN(NⁱPr₂)]	[Pc*GaCl] + LiN(ⁱPr)₂	THF/room temperature/overnight	No reaction
[Ppz*Al(NMe₂)]	[Ppz*AlCl] +Ti(NMe₂)₄	Diethyl ether/ room temperature / 3 hours	No reaction
		Toluene/ 100ºC / 3 hours	No reaction

2.3.21 Indium(III) Complexes [Pc*InCl] and [Ppz*InCl]

When PDN* and PzDN* were allowed to melt with InCl₃ and urea under an argon atmosphere at 220ºC, the desired complexes were obtained (Figure 112). However, in this case, purification of the products by column chromatography was not possible. Usually, the indium complexes are completely adsorbed on the top of the Al₂O₃ column when less polar eluents, such as DCM, THF and CHCl₃, were used. Also, polar solvents such as CH₃CN and methanol tend more to elute the reaction by-products. Thus, to purify the products, the reaction products were washed with methanol until the filtrate became colorless. Afterwards, the solid was collected and dissolved in DCM. After filtration, removing the DCM under vacuum resulted in obtaining the desired products in

low yield; 12 % for [Pc*InCl] and 13 % for [Ppz*InCl]. The products showed high solubility in DCM, THF, CHCl$_3$ and toluene.
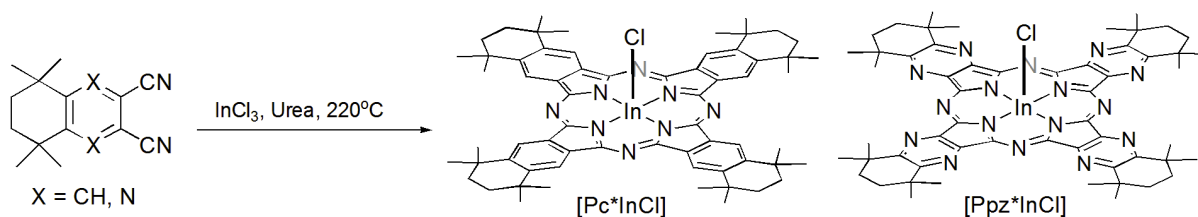
Figure 112: Synthesis of [Pc*InCl] and [Ppz*InCl].

The presence of [Pc*InCl] and [Ppz*InCl] were confirmed by mass spectra (APCI$^+$) showing protonated molecular ion peaks at 1103.6 and 1111.4, respectively. The spectrum of [Pc*InCl] is shown in Figure 113; the ion peak observed at 1165.5 is attributed to the complex adduct with two methoxy groups.
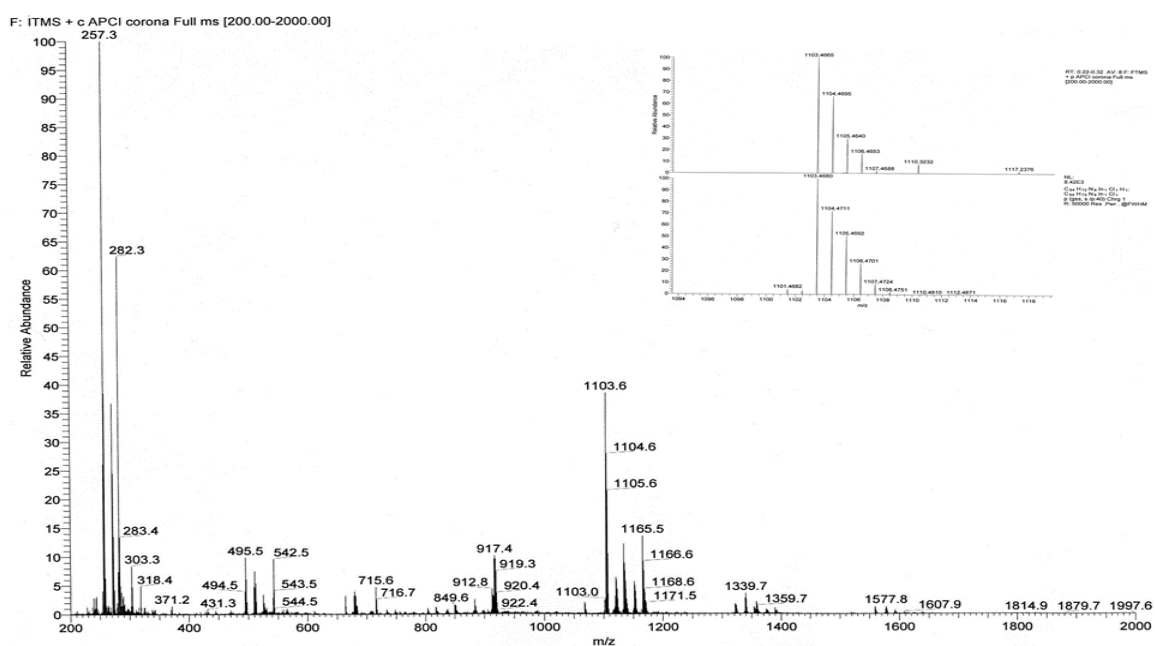
Figure 113: APCI$^+$ Mass Spectrum of [Pc*InCl]. On the right, a high resolution of the molecular ion peak position is shown compared with its theoretically calculated isotopic pattern.

The UV-Visible spectra of [Pc*InCl] and [Ppz*InCl] in CHCl$_3$ showed the expected Q- and B-bands of the complexes (Figure 114). Generally, the main B-band of [Ppz*InCl] (356 nm) is red-shifted compared to that of [Pc*InCl] (354 nm). The Q-band of [Pc*InCl] lies at 714 nm. However, owing to its higher HOMO-LUMO gap compared to that of [Pc*InCl], the Q-band of [Ppz*InCl] lies at 648 nm. In comparison with the gallium complexes, substitution of Ga with In resulted in a small redshift of 2 nm for the Pc* complexes. This shift is not observed in the case of the Ppz* complexes as the Q-band of [Ppz*InCl] and [Ppz*GaCl] lies almost at the same wavelength.
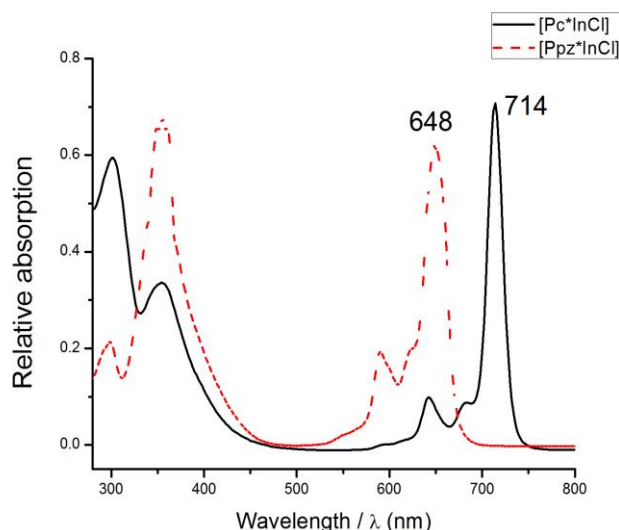
Figure 114: UV/Vis. spectra of [Pc*InCl] and [Ppz*InCl] in CHCl$_3$.

Figure 115 shows the ^{1}H NMR spectrum of [Ppz*InCl]. As a result of the molecule's C$_{4v}$ symmetry, the ^{1}H-NMR spectrum in CDCl$_3$ displayed only three singlets. The methyl protons appear as a set of two equivalent singlets at 1.83 and 1.93 ppm, integrating for twenty-four protons each. This effect can be explained by lowering of the molecular symmetry imposed by the axial In-Cl group. The upper and lower hemisphere of the macrocycle become inequivalent, and the methyl groups pointing towards the In-Cl moiety (endo) and those pointing away (exo) are located in different chemical environments. The other sixteen aliphatic CH$_2$ protons are observed at 2.29 ppm. On the other hand, the ^{1}H-NMR spectrum of [Pc*InCl] in CDCl$_3$ showed its characteristic three singlets. However, here, the fourty-eight protons of the methyl groups appeared as one singlet at 1.86 ppm; also the sixteen CH$_2$ protons appeared at 2.26 ppm, and the signal observed at 9.52 ppm corresponds to the eight aromatic protons.

A monomeric or dimeric structure (Figure 116, A or B) is in accordance with chemically non equivalent methyl protons, while a chain structure / oligomer (Figure 116, C) would be in accordance with chemically equivalent methyl protons.

87
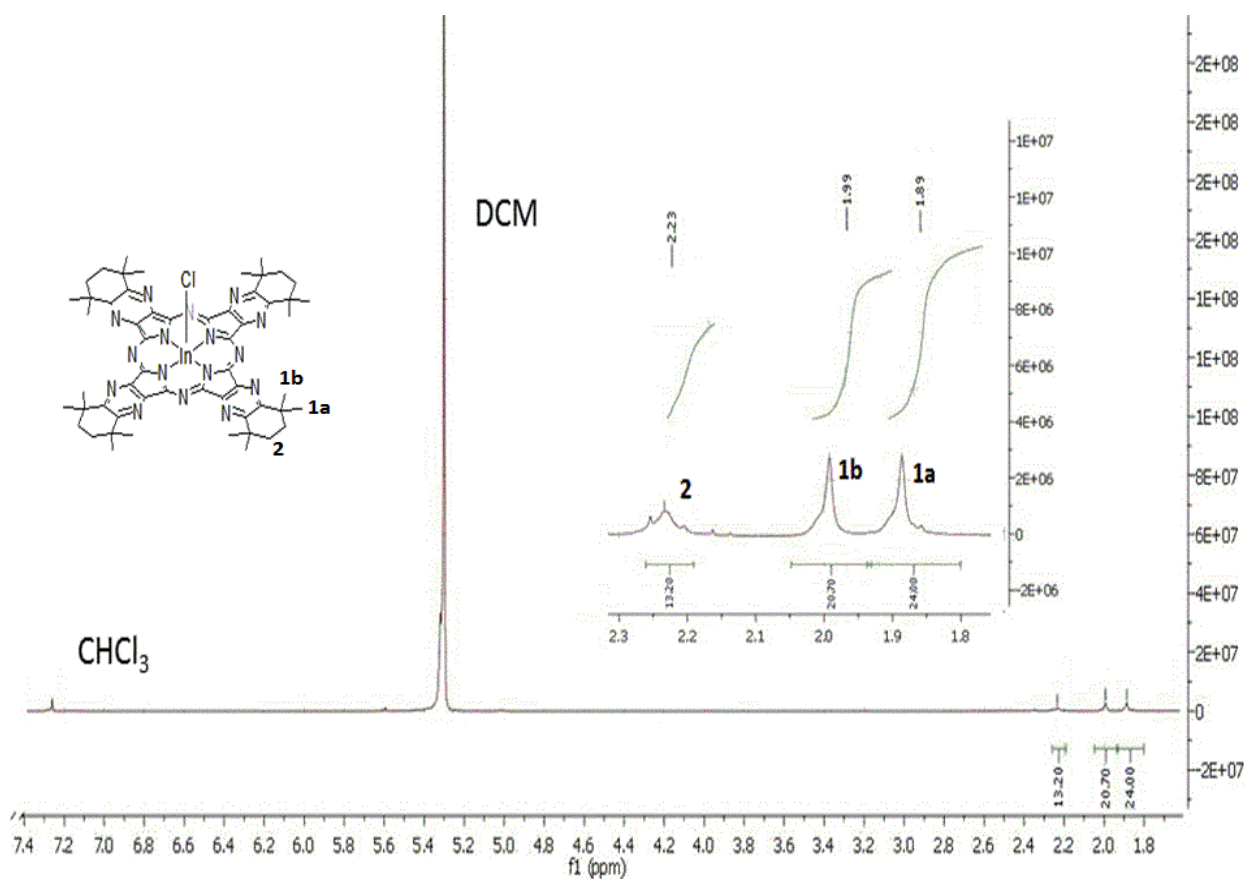
Figure 115: ^{1}H-NMR spectra of [Ppz*InCl] in CDCl$_3$ (300 MHz).
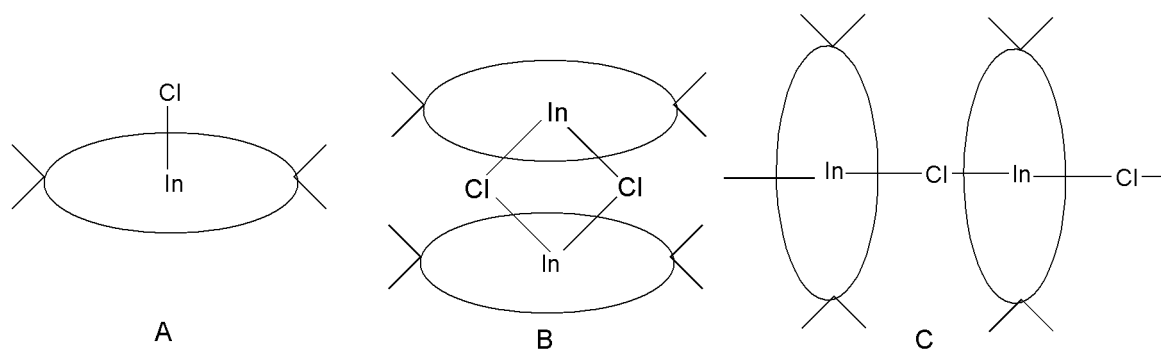
Figure 116: Proposed structure for the indium complexes.

2.3.22 Reactions of [Pc*MCl] and [Ppz*MCl]; M=Al, Ga, In with KF

Refluxing [Pc*AlCl] or [Ppz*AlCl] with KF in water resulted in the formatiom of the fluoro analogs [Pc*AlF] or [Ppz*AlF] (Figure 117). The products formed in high yield, i.e 89 % for [Pc*AlF] and 96 % for [Ppz*AlF], and showed high solubility in a variety of organic solvents such as THF, toluene, DCM and CHCl$_3$. Although the fluoro aluminium complexes were obtained this way, similar strategies, when applied for the gallium and indium complexes, were unsuccessful.

88
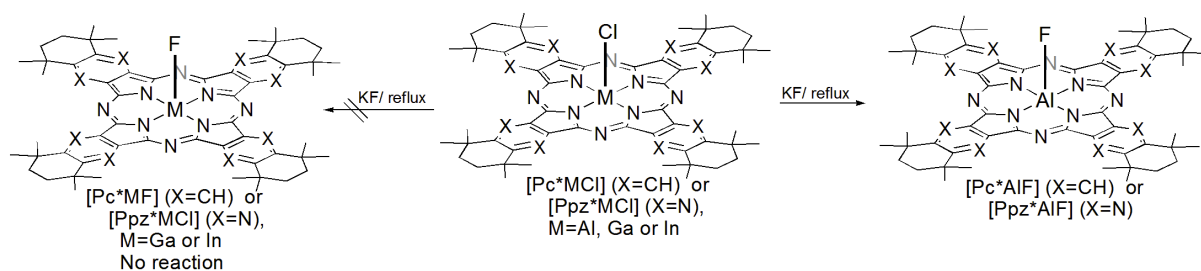
Figure 117: Reactions of [Pc*MCl] and [Ppz*MCl], M= Al, Ga or In with KF.

The expected mass values measured using the APCI+ MS technique corresponded with the theoretical values for the complexes. The protonated molecular ion peaks of [Pc*AlF] and [Ppz*AlF] were observed at 999.6 and 1007.6 (Figure 118), respectively.

Figure 118: APCI+ Mass Spectrum of [Ppz*AlF]. On the right, a high resolution of the molecular ion peak position is shown compared with its theoretically calculated isotopic pattern.

The UV/Vis. spectra of [Pc*AlF] and [Ppz*AlF] (Figure 119) show similar results compared to those of the chloro-analogs as the axial ligand does not influence the electronic spectra of the complexes. In detail, sharp Q-bands at 706 and 642 are observed for [Pc*AlF] and [Ppz*AlF], respectively. Generally, the Q-band of [Pc*AlF] is red-shifted compared to that of [Ppz*AlF] as a result of the lower HOMO-LUMO gap of the Pc* core compared to that of the Ppz* one. Additionally, substituting the benzene rings of the Pc* core with pyrazine ones led to a small redshift of the B-band of 4 nm, i.e, the B bands of [Pc*AlF] and [Ppz*AlF] lie at 344 and 348 nm, respectively.
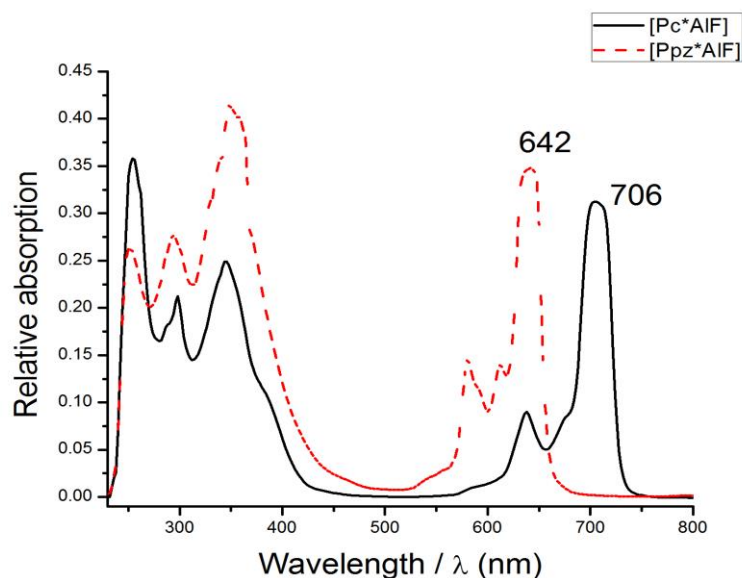
Figure 119: UV/Vis. spectra of [Pc*AlF] and [Ppz*AlF] in CHCl$_3$.

Figure 120 shows the ^{1}H-NMR spectrum of [Ppz*AlF] measured in CDCl$_3$. The spectrum agrees well with the expected pattern. The two singlets displayed at 1.43 and 2.27 ppm are assigned and integrated well for the complex methyl and methylene proton. As no splitting is observed in the characterstic NMR signals of [Ppz*AlF], this might indicate an oligomeric or polymeric nature of the complex with [-Al-F-Al-F-Al-] backbone in the solid state or in a solution of nonpolar solvents. On the other hand, [Pc*AlF] showed its aromatic protons at 9.59 ppm. Additionally, the peak observed at 2.08 ppm integrated well for the sixteen methylene protons of the Pc* ring. However, in this case, the methyl protons appear as a set of two equivalent singlets at 1.82 and 1.85 ppm integrating for twenty-four protons each. This can be attributed to the lowering of the molecular symmetry of the molecule imposed by the axial Al-F moiety. Hence, two sets of protons pointing towards the Al-F moiety (endo) and away (exo) are located in different chemical environments.
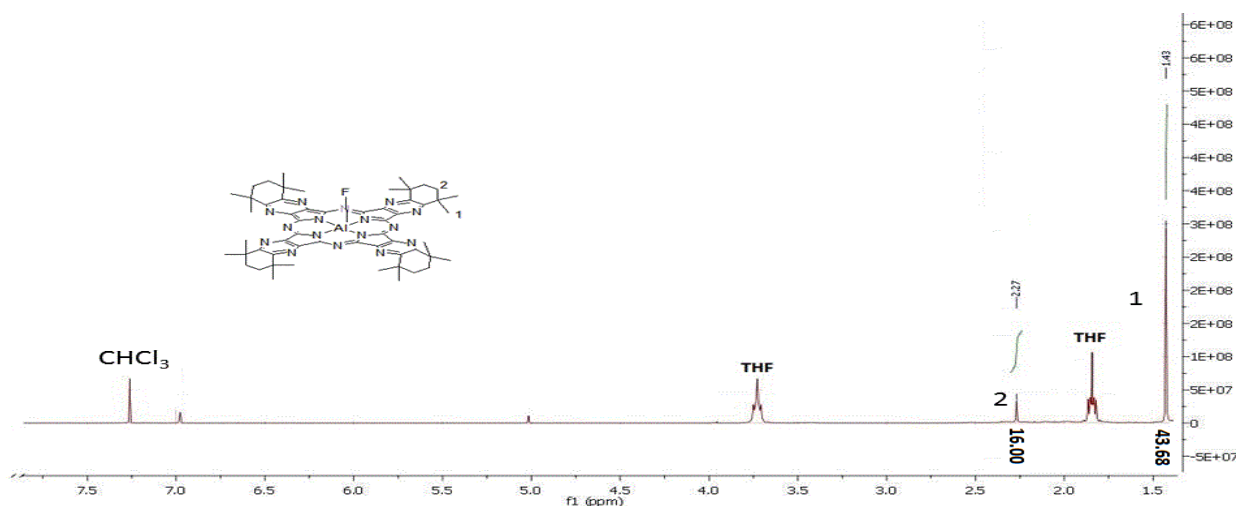
Figure 120: ^{1}H-NMR spectra of [Ppz*AlF] in CDCl$_3$ (300 MHz).

Crystals of [Ppz*AlF] suitable for X-ray diffraction were obtained by slow diffusion of pentane vapor into a chloroform solution of the complex. The complex crystallizes in the monoclinic space group P2$_1$/c as four molecules per unit cell. The structure of the crystals is not fully resolved, due to the low quality of the crystals obtained. Thus, an unidentified number of disorded solvent molecules are present, but an octahedral aluminium species, [Ppz*AlF(OH$_2$)], was identifiable (Figure 121). In general, few reports counted on the octahedral arrangement of aluminium phthalocyanines, rather than the bridged fluor- or chloro- aluminium phthalocyanine, AlPcs having *trans* thf radicals[328], or nitrito ligands[327] were also reported.

As no coordinated water molecules were detected using FT-IR and the abscence of any molecular peak corresponds to [Ppz*AlF(OH$_2$)] species in the APCI-MS measurement, we believe that the water molecule just coordinated to the metal during the crystallization process.
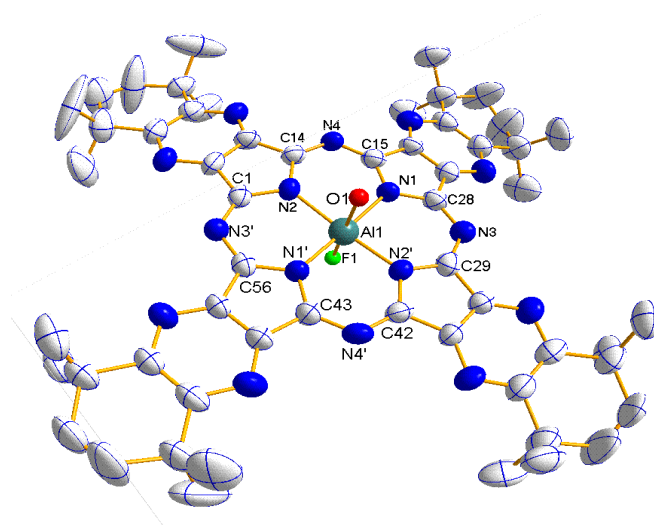
Figure 121: Structure of [Ppz*AlF(OH$_2$)] crystallized from chloroform. All solvent molecules and H atoms are omitted for clarity, Ellipsoids are shown at 50% probability.

91

The aluminum atom sits 'atop' or 'out-of the N4 plane' towards the fluorido ligand and is present in a centre of an octahedron. Both the fluorine and oxygen atoms are *trans*-to each other. The four isoindole rings in the molecule are equivalent, and the fused cyclohexene rings adopt a half-chair conformation. Selected structural parameters of the obtained species [Ppz*AlF(OH$_2$)] are summarized in Table 14.

Table 14: Selected Bond Lengths (Å) and Angles (°) for [Ppz*AlF(OH$_2$)].

Bond lengths/ Å		Angles/ °		Angles/ °	
Al1-N2	1.952(6)	N1-Al1-N2	89.7(2)	N1-Al1-N1'	173.7(3)
Al1-N1	1.987(6)	F1-Al1-N2	91.4(2)	O1-Al-N2	89.2(2)
Al1-N2'	1.969(6)	F1-Al1-N1	92.9(2)	O1-Al1-N1	88.2(2)
Al1-N1'	1.949(6)	F1-Al1-N2'	93.3(2)	O1-Al1-N2'	86.1(2)
Al1-F1	1.732(5)	F1-Al1-N1'	91.4(2)	O1-Al1-N1'	85.5(2)
Al1-O1	2.006(6)	N2-Al1-N1'	85.4(2)	F1-Al1-O1	178.8(3)
d(P$_1$-P$_2$)	2. 900	N2-Al1-N2'	175.3(3)	N2-Al1-N1'	89.4(2)
d(Al$_1$-Al$_2$)	6.601	N1-Al1-N2'	89.9(2)		

d(P$_1$-P$_2$) the distance between two neighboring N$_4$ planes

The polymeric nature along Al-F axis was proposed for the unsubstituted [PcAlF]$_n$ crystals[308], due to the complex's low solubility and low volatility, as well as the absence of an AlPcF$^+$ peak in the mass spectrum of the complex and the prescence of an array for this ion in the spectrum of the pyridine washed precursor of the fluoride. Similar to our case, the structure of [PcAlCl] was determined[309]. The chlorido complex crystallized in the triclinic space group P$\bar{1}$. The four Al-N distances were elucidated as 1.961(12) Å, 1.962(13) Å, 1.966(12) Å and 2.018(12) Å. Thus, the mean distance is 1.977(12) Å; slightly longer than that of [Ppz*AlF(OH$_2$)] (1.964(6) Å). The four N-Al-Cl angles [102.7(4)° , 100.7(4)° , 102.4(4)° and 102.1(4)°] are also longer than the four N-Al-F angles of [Ppz*AlF(OH$_2$)] . The reported four vicinal N-Al-N angles of [PcAlCl] are 86.8(5)°, 90.4(5)°, 84.9(5)° and 88.0(5)°, while the two N-Al-N angles of the opposite nitrogen atoms are 157.2(5)° and 154.2(6)°. In [Ppz*AlF(OH$_2$)], the last two angles are 175.3(3)° and 178.8(3)°, indicating that the Al atom deviates less form the N4 plane in the case of [PpzAlF(OH$_2$)]. It is obvious that the Al-F bond 1.732(5) Å is shorter than the Al-Cl (2.179(6) Å).[309]

Literature[313] reported on aluminium phthalocyanines bearing axial water molecule. It was suggested, in the presence of water, due to the Lewis acidity of the complex, a water molecule coordinates to the Al atom.

The relative arrangement of [Ppz*AlF(OH$_2$)] species is shown in Figure 122. The unit cell packing is composed of four formular units of [Ppz*AlF(OH$_2$)]. Each two complex molecules are almost parallel but both overlap to the other two molecules. Face to back arrangement of each two parallel molecules is observed. Generally, the Pcs could be considered electrically conductive if the π-systems of the adjacent molecules are able to

overlap to promote the transfer of electrons or holes. In [Ppz*AlF(OH$_2$)], although the closest intermolecular distance between two N4 neighboring planes is in the range of the effective π-π interactions for the planar phthalocyanines,[237] the closest centroid – centroid distance is 6.601 Å indicating weak ovelaping between the complex molecules.
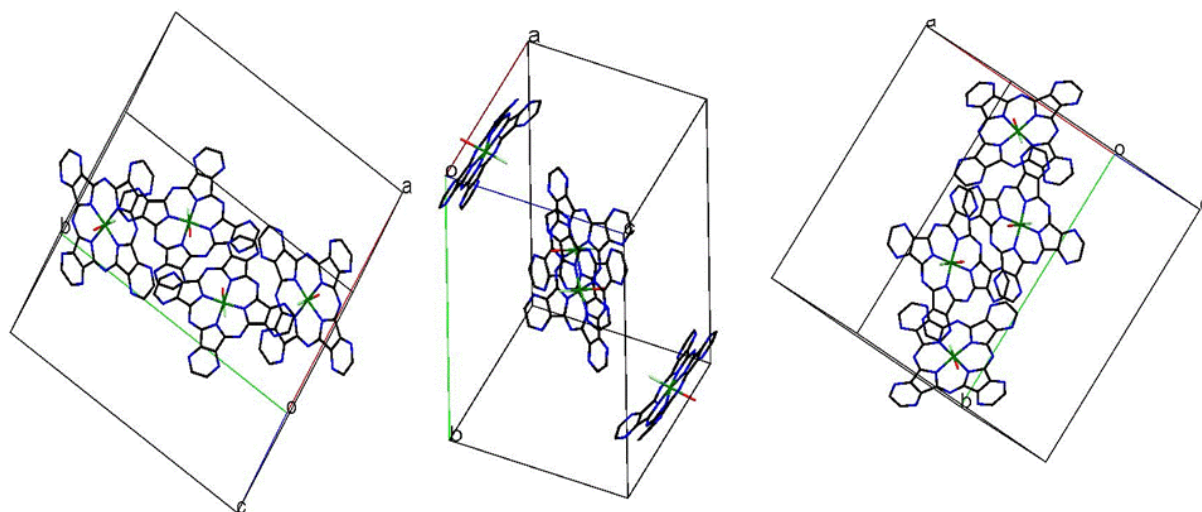
Figure 122: Unit cell packing of [Ppz*AlF(OH$_2$)] molecules in the solid state. All solvent molecules, aliphatic substituents and H atoms are omitted for clarity.

2.3.23 Silicon Si(IV) and Ge(IV) Complexes [Ppz*SiCl$_2$] and [Ppz*Ge(OH)$_2$]

Melting a mixture of PzDN*, urea and SiCl$_4$ or GeCl$_4$ at 220°C under an argon atmosphere resulted in the formation of a solid residue. The residues were chromatographed using (CHCl$_3$, Al$_2$O$_3$) to yield [Ppz*SiCl$_2$] and [Ppz*Ge(OH)$_2$] in 27 % and 28 % yield, respectively. The addition of urea is mandatory, as no reaction occurs in its absence. The formation of [Ppz*Ge(OH)$_2$] might be explained by the larger size of Ge atom compared to the Si one. In the case of Ge, the atom is too large to occupy the central cavity. Hence, once the precursor is allowed to react with GeCl$_4$, the complex [Ppz*GeCl$_2$] with a *cis* arrangement of its two chlorido axial ligands is formed first. However, hydrolysis of this product to [Ppz*Ge(OH)$_2$] during its chromatographic purification is more readily occurring than in case of the corresponding silicon complex. The complexes are very soluble in common organic solvents. However, using the same preparative procedures, the analogous Pc* complexes could not be obtained (Figure 123, Table 15).
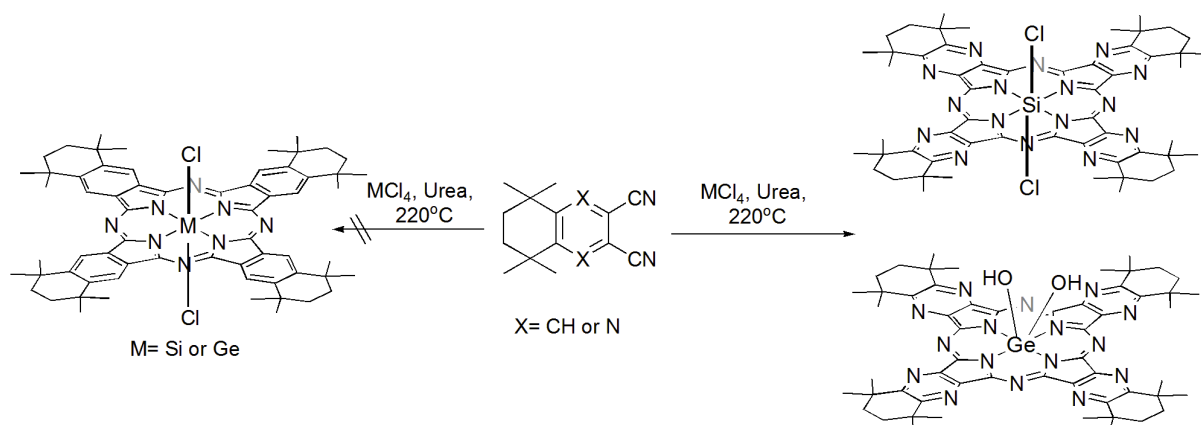
Figure 123: Reactions of PDN* and PzDN* with SiCl$_4$ and GeCl$_4$.

Table 15 : Successful/unsuccessful synthetic strategies of [LMCl$_2$] or [LMO], L=Pc* or Ppz*, M= Si or Ge.

Target compound	Reactant	Base	Conditions Duration/temperature	Result
[Ppz*SiCl$_2$]	PzDN* + SiCl$_4$	Urea	30 minutes /220°C	[Ppz*SiCl$_2$]
[Ppz*Ge(OH)$_2$]	PzDN* + GeCl$_4$	Urea	30 minutes /220°C	[Ppz*Ge(OH)$_2$]
[Pc*SiCl$_2$]	PDN* + SiCl$_4$	Urea	30 minutes /220°C	Unidentified uncolorful product
[Pc*Ge(OH)$_2$]	PDN* + GeCl$_4$	Urea	30 minutes /220°C	Unidentified uncolorful product

An APCI$^+$ MS experiment was performed for each complex. The [Ppz*Ge(OH)$_2$] spectrum displayed only one peak at 1065.6 corresponding to [PpzGeOMe+ H]$^+$, the Me moiety resulted from the methanol added during the measurement. To distinguish between [Ppz*Ge(OH)$_2$] and [Ppz*GeCl$_2$], as cleavage of the chlorido ligands is possible during the APCI$^+$ MS measurement, analysis of chlorine content was performed. Since no chlorine was detected in the sample, the formula [Ppz*Ge(OH)$_2$] is best suited for the complex. The molecular ion peak at 1059.6 of [Ppz*SiCl$_2$] is attributed to [M+H]$^+$ (Figure 124), in addition to [M+H]$^+$, an intense peak at 1051.7 is present. This peak is attributed to [Ppz*Si(OMe)$_2$]$^+$ as the MS measurement was conducted in the presence of methanol.

94

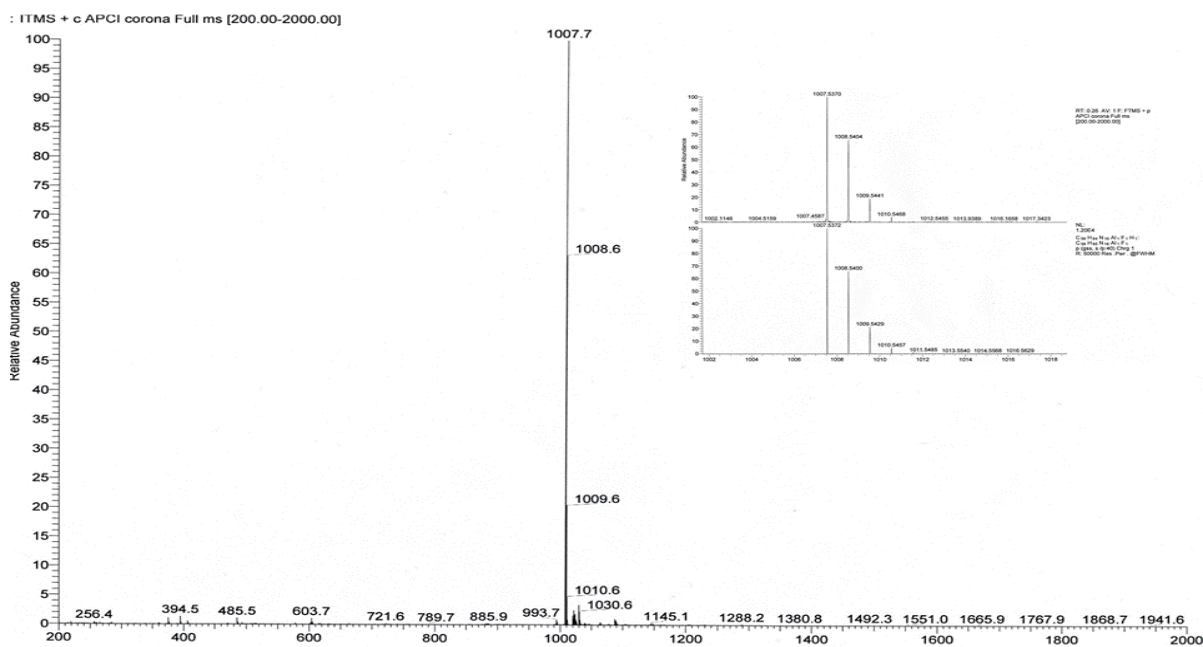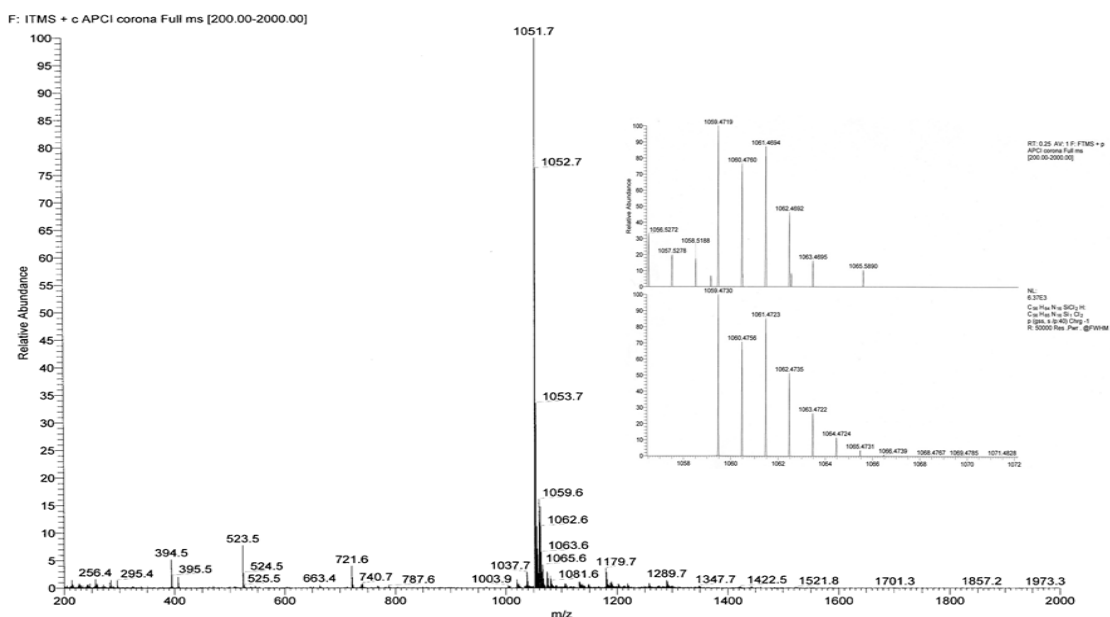**Figure 124:** APCI⁺ Mass Spectrum of [Ppz*SiCl₂]. On the right, a high resolution of the molecular ion peak position is shown compared with its theoretically calculated isotopic pattern.

The electronic absorption spectra of the complexes measured in CHCl₃ are shown in Figure 125. The two main absorption regions for the complexes appear as follows; the B-band of [Ppz*SiCl₂] and [Ppz*Ge(OH)₂] lies at 357 and 354 nm, respectively, and the complexes show their charcterstic Q-bands at 652 and 636 nm, respectively. In this case, the electronic spectral differences between the two complexes might be explained by the electronegativity of the axial ligands, the central element and the configuration of the complex. Taking into account the higher electronegativity of oxygen compared to chlorine, the hydroxido ligands probably withdraw more electrons from the ring compared to the chloroido ligands. Furthermore, the *trans* arrangement of the chlorido ligands in the case of [Ppz*SiCl₂] probably hinders their ability for withdrawing electrons from the ring, hence the electrons are probably centered close to the cental element. Finally the Ge atom is larger than Si, that means at least the Si-N bonding electrons are of higher covalent character compared to the Ge-N bonding electrons.

95
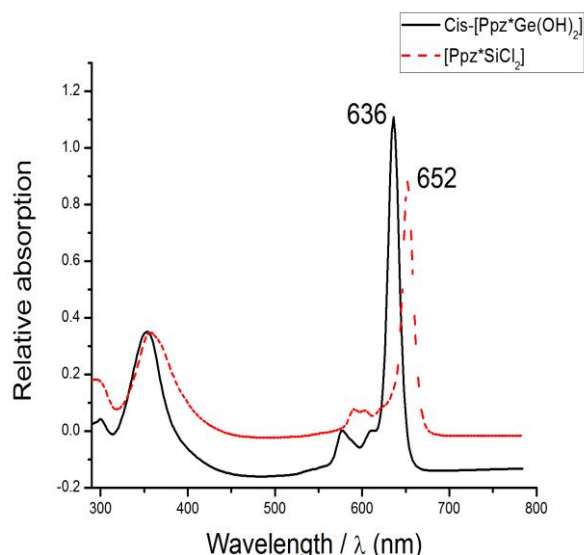
Figure 125: UV/Vis. spectra of [Pc*Ge(OH)$_2$] and [Ppz*SiCl$_2$] in CHCl$_3$.

The distinction between the different geometrical configurations of the complexes is indicated in their ^{1}H-NMR spectra. In the case of [Pc*SiCl$_2$] (Figure 126), the small Si atom occupies the Ppz* cavity perfectly. Hence, the axial ligands prefer the *trans* arrangement, leading to a D$_{4h}$ symmetry. In this case, the methyl protons pointing towards the two chlorido-ligands are chemically equivalent and appear as one singlet at 1.97 ppm. Additionally, the methylene protons of [Pc*SiCl$_2$] appear as one singlet at 2.25 ppm. On the other hand, in [Ppz*Ge(OH)$_2$] (Figure 127), the comparatively larger Ge atom does not fit well in the Ppz* cavity and is probably located above the N4 plane. Hence, a C$_{4V}$ pyramidal symmetry is obtained. That makes the hydrogen atoms chemically inequivalent (pointing towards different chemical environments). Hence, they appear as a set of two singlets at 1.95 and 1.96 ppm in close proximity. The methylene protons of [Ppz*Ge(OH)$_2$] appear at 2.24 ppm as two singlets in close proximity. Additionally, a broad signal integrated for two protons is observed at 3.33 ppm. This signal could be attributed to the two protons of the Ge(OH)$_2$ moiety.
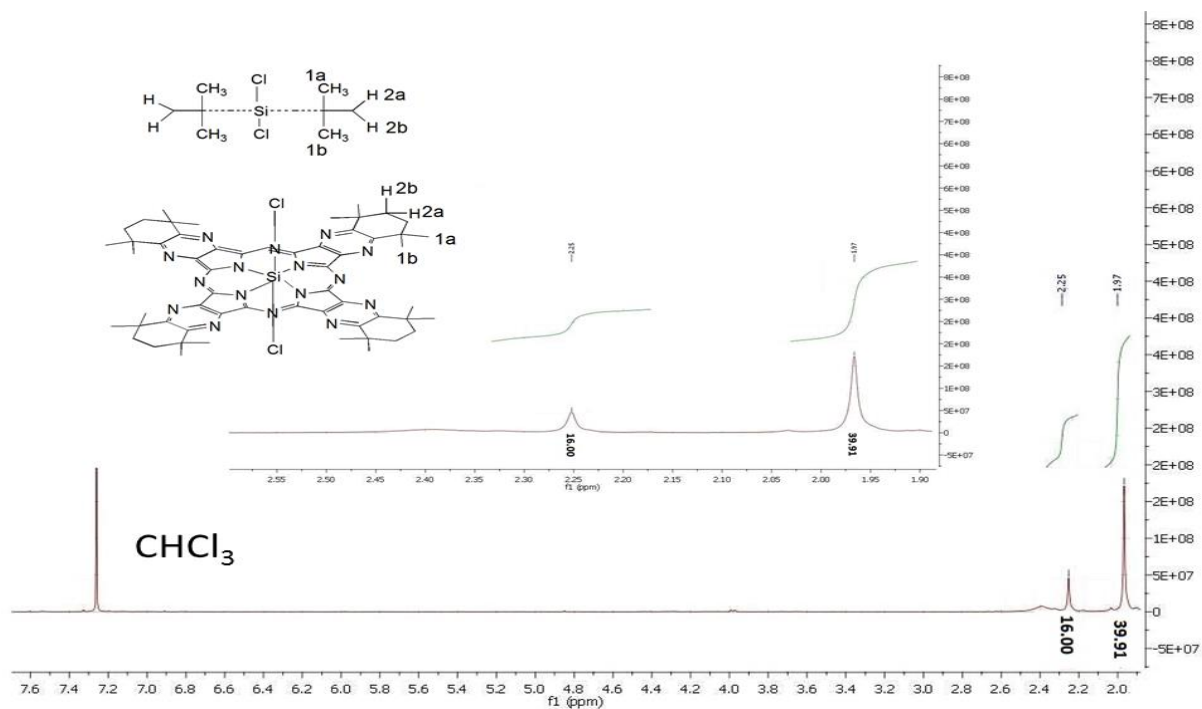
Figure 126: ^{1}H-NMR spectra of [Ppz*SiCl$_2$] in CDCl$_3$ (300 MHz).
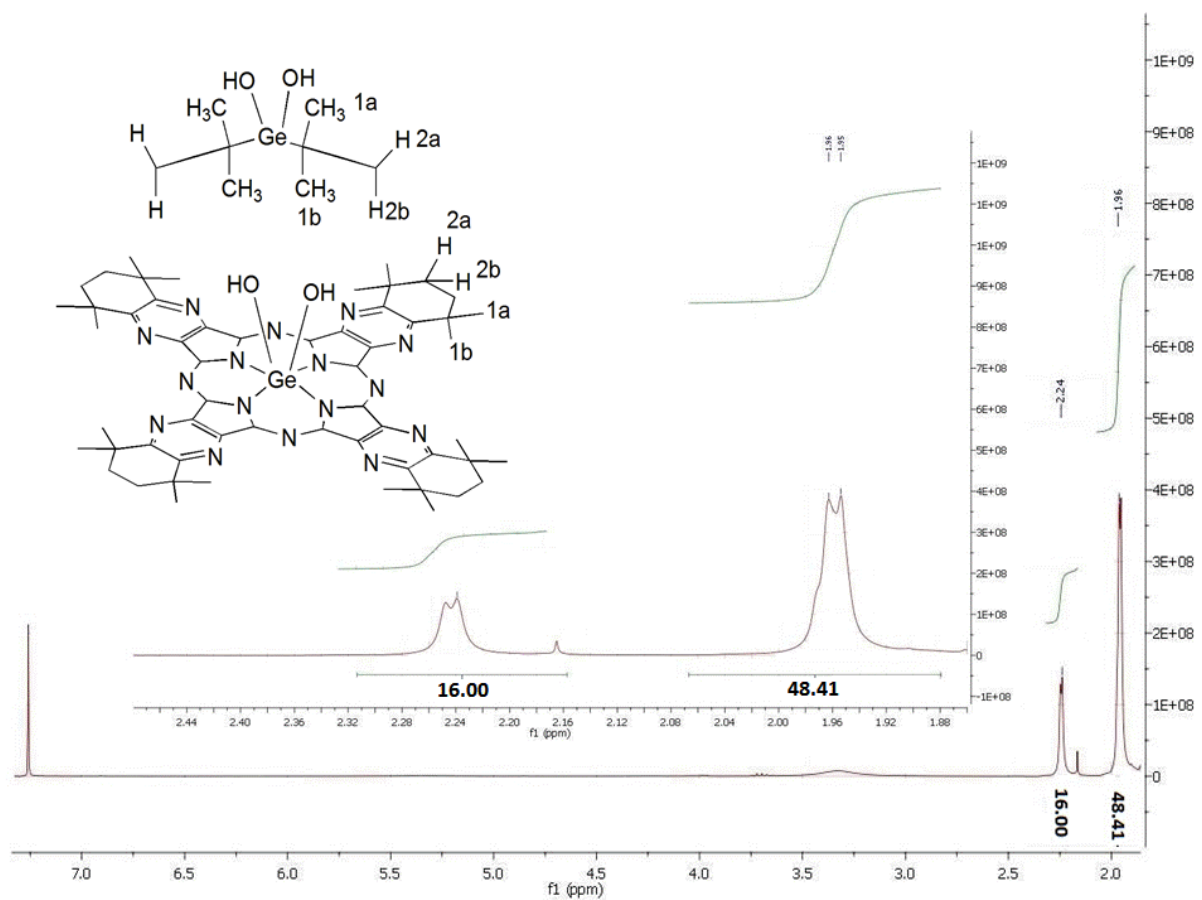
Figure 127: ^{1}H-NMR spectra of [Ppz*Ge(OH)$_2$] in CDCl$_3$ (300 MHz).

2.3.24 Attempted Synthesis of Axially Substituted Silicon Pyrazinoporphyrazines

To obtain other axially substituted silicon complexes, several procedures were followed including tetramerization of PzDN* in the presence of dimethyl or diphenyl silicon dichloride, addition of lithiated or Grignard reagents to [Ppz*SiCl₂] and refluxing the latter complex with KF solution or isopropanol (Figure 128). All conditions used are listed in Table 16. Except for a small signal corresponding to [Ppz*Si(OC$_3$H$_7$)$_2$+ H]$^+$ in the APCI$^+$ MS was observed indicating a successful reaction of [Ppz*SiCl₂] with refluxing isopropanol, none of the other desired products could be isolated.
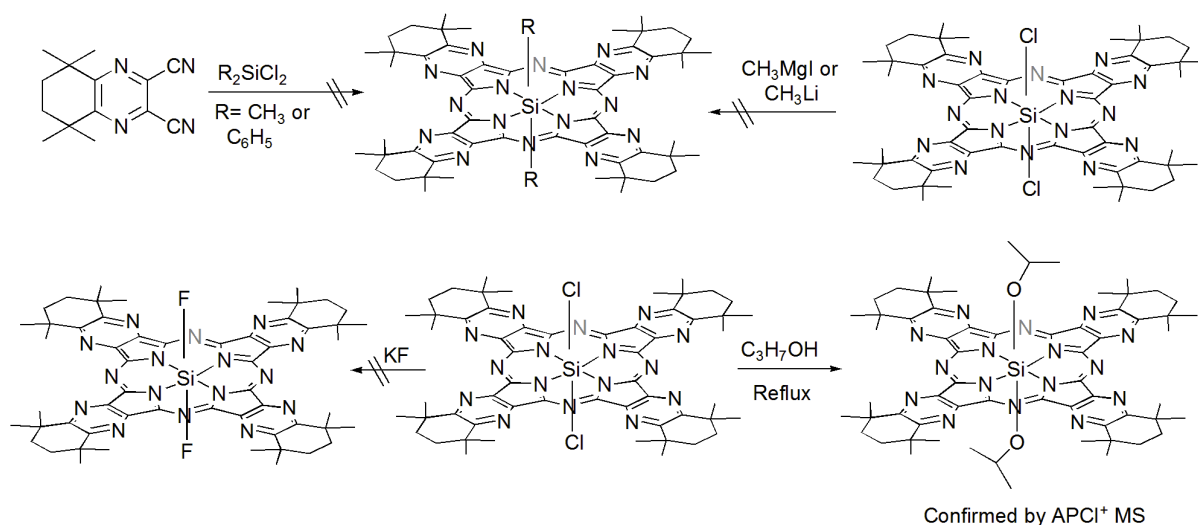
Figure 128: Successeful/unsuccessful synthesis of axially substituted silicon pyazinoporphyrazine.

Table 16 : Testing conditions for synthesis of [Ppz*SiL₂], L=OC$_3$H$_7$, F, CH$_3$ and C$_6$H$_5$.

Target compound	Reactant	Base	Conditions Solvent/ temperature /duration	Result
[Ppz*Si(OC$_3$H$_7$)$_2$]	[Ppz*SiCl₂] + C$_3$H$_7$OH		Iso-propanol/reflux/overnight	[Ppz*Si(OC$_3$H$_7$)$_2$]
[Ppz*SiF₂]	[Ppz*SiCl₂] + KF		Water/ reflux/overnight	No reaction
[Ppz*Si(CH$_3$)$_2$]	[Ppz*SiCl₂] + CH₃MgI		THF/ room temperature/overnight	Unidentified decomposition products
			Toluene/ room temperature/overnight	Unidentified decomposition products
	[Ppz*SiCl₂] + CH₃Li		Toluene/ room temperature/overnight	Unidentified decomposition products
	PzDN* + (CH₃)₂SiCl₂	Urea	----------/220°C /30 minutes	Unidentified green product
[Ppz*Si(C$_6$H$_5$)$_2$]	PzDN* + (C₆H₅)₂SiCl₂	Urea	----------/220°C /30 minutes	Unidentified green product

2.3.25 Attempted Synthesis of Other Pc*/Ppz* Complexes

In addition to the previousely reported results, Table 17 lists several unsuccessful attempts to obtain other Pc*/Ppz* complexes.

Table 17: Attempted synthesis of other Pc*/Ppz* Complexes.

Target compound	Reactant	Base	Conditions Solvent/temperature /duration	Result
[Pc*Mg]	PDN* + $MgCl_2.6H_2O$	DBU	1-pentanol/160°C/overnight	Unidentified product
[Pc*ScCl]	PDN* + $ScCl_3$	Urea	1-CNP/160°C/overnight	Unidentified product
[Pc*Cd]	PDN* + $CdCl_2.H_2O$	DBU	1-pentanol/160°C/overnight	Unidentified product
		Urea	------------ /220°C/30 minutes	Unidentified product
[Ppz*Mg]	PDN* + $MgCl_2.6H_2O$	DBU	1-pentanol/220°C/20 minutes	Unidentified product
[Ppz*ScCl]	PzDN* + $ScCl_3$	Urea	1-CNP/160°C/overnight	Unidentified product
		Urea	------/220°C/30 minutes	Unidentified product
		DBU	1-Pentanol/220°C(60 minutes)/ 160°C(overnight)	Unidentified product
[Ppz*ZrCl_2]	PzDN* + $ZrCl_4$	Urea	-------/220°C / 30 minutes	Unidentified product
			1-CNP/220°C/90 minutes	Unidentified product
[Ppz*ZrBr_2]	PzDN* + $ZrBr_4$	Urea	-------/220°C / 30 minutes	Unidentified product
[Ppz*Mo]	PzDN* + $Mo(CO)_6$	Urea	-------/220°C / 30 minutes	Unidentified product
[Ppz*MoO]	PzDN* + $(NH_4)_6Mo_7O_{24}.4H_2O$	$(NH_4)_6Mo_7O_{24}.4H_2O$	-------/220°C / 30 minutes	Unidentified product
[Ppz*MoN]	PzDN* + $[MoN(Ot-Bu)_3]$	Urea	-------/220°C / 30 minutes	Unidentified product
[Ppz*W]	PzDN* + $W(CO)_6$	Urea	-------/220°C / 30 minutes	Unidentified product
[Ppz*WN]	PzDN* + $WNCl_3$	Urea	-------/220°C / 30 minutes	Unidentified product
[Ppz*W(Nt-Bu)Cl]	PzDN* + $[W(Nt-Bu)_2Cl_2(Pyridine)_2]$	Urea	-------/220°C / 30 minutes	Unidentified product
[Ppz*WW Ppz*]	PzDN* + $[(Me_2N)_3WW(NMe_2)_3]$	Urea	-------/220°C / 30 minutes	Unidentified product

Table 17: Continued.

Target compound	Reactant	Base	Conditions Solvent/temperature /duration	Result
[Ppz*Re(Nt-Bu)Cl]	PzDN* + [Re(Nt-Bu)$_2$Cl$_3$]	Urea	-------/220°C / 30 minutes	Unidentified product
[Ppz*Cd]	PzDN* + CdCl$_2$.H$_2$O	Urea	-------/220°C / 30 minutes	Unidentified product
		DBU	1-pentanol/220°C(20 minutes) /160°C (overnight)	Unidentified product
[Ppz*SnCl$_2$]	PzDN* + SnCl$_4$.5H$_2$O	Urea	-------/220°C / 30 minutes	Unidentified product
[Ppz*Pb]	PzDN* + PbO	Urea	-------/220°C / 30 minutes	Unidentified product
	PzDN* + Pb(CH$_3$COO)$_2$	Urea	-------/220°C / 30 minutes	Unidentified product

2.4 Complexes of PzDN#

PzDN# was heated at 220°C with a metal chloride (CoCl$_2$ or CuCl$_2$) and urea in neat under an argon atmosphere (Figure 129). The residues obtained were throughly washed with CHCl$_3$, ethanol and water, and then eluted from a short Al$_2$O$_3$ column using pyridine. Although the formation of [Ppz#Co] and [Ppz#Cu] was confirmed by the APCI$^+$ MS (the protonated molecular ion peaks appear at 796.3 and 800.3, respectively), we did not proceed with further reactions using this precursor due to some disadvantages including the very poor solubility of the products and the necessity of purifying the chromophores using (Pyridine, Al$_2$O$_3$), as washing the insoluble products with the common solvents was insufficient to properly purify them.
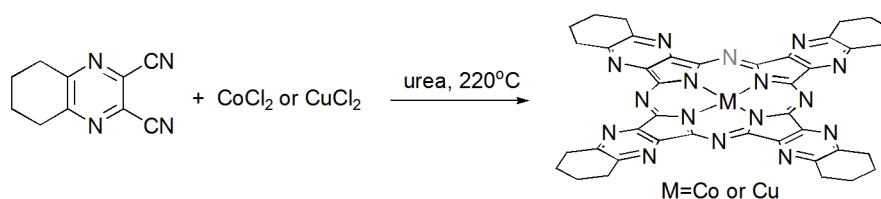
Figure 129: Synthesis of [Pz#Co] and [Pz#Cu].

2.5 Fluorescence Study

Owing to the strong fluorescent character of MPpz complexes, which could often be observed with the eye, it was important to study the fluorescence spectra of some of these complexes, e.g. [Ppz*TiO], [Ppz*VO], [Ppz*CrCl], [Ppz*AlCl], [Ppz*GaCl] and [Ppz*InCl].

To measure the fluorescence spectra, all compounds were excited by UV light with an excitation wavelength λ_{Ex} of 350 nm, since this lies in the absorption range of the B

bands. The absorption and emission spectra of [Ppz*TiO], [Ppz*VO], [Ppz*CrCl], [Ppz*AlCl], [Ppz*GaCl] and [Ppz*InCl] are shown in Figure 130. Table 18 lists the peak absorbance and peak emission as well as the Stokes shift, the difference between the two maxima. In all cases, the shift observed is only a few nanometers; showing that there is very little reorganization between the ground and excited states.[322] Therefore, the absorption and emission bands overlap in this area. The largest shift of 13 nm, is shown by the vanadium complex [Ppz*VO].
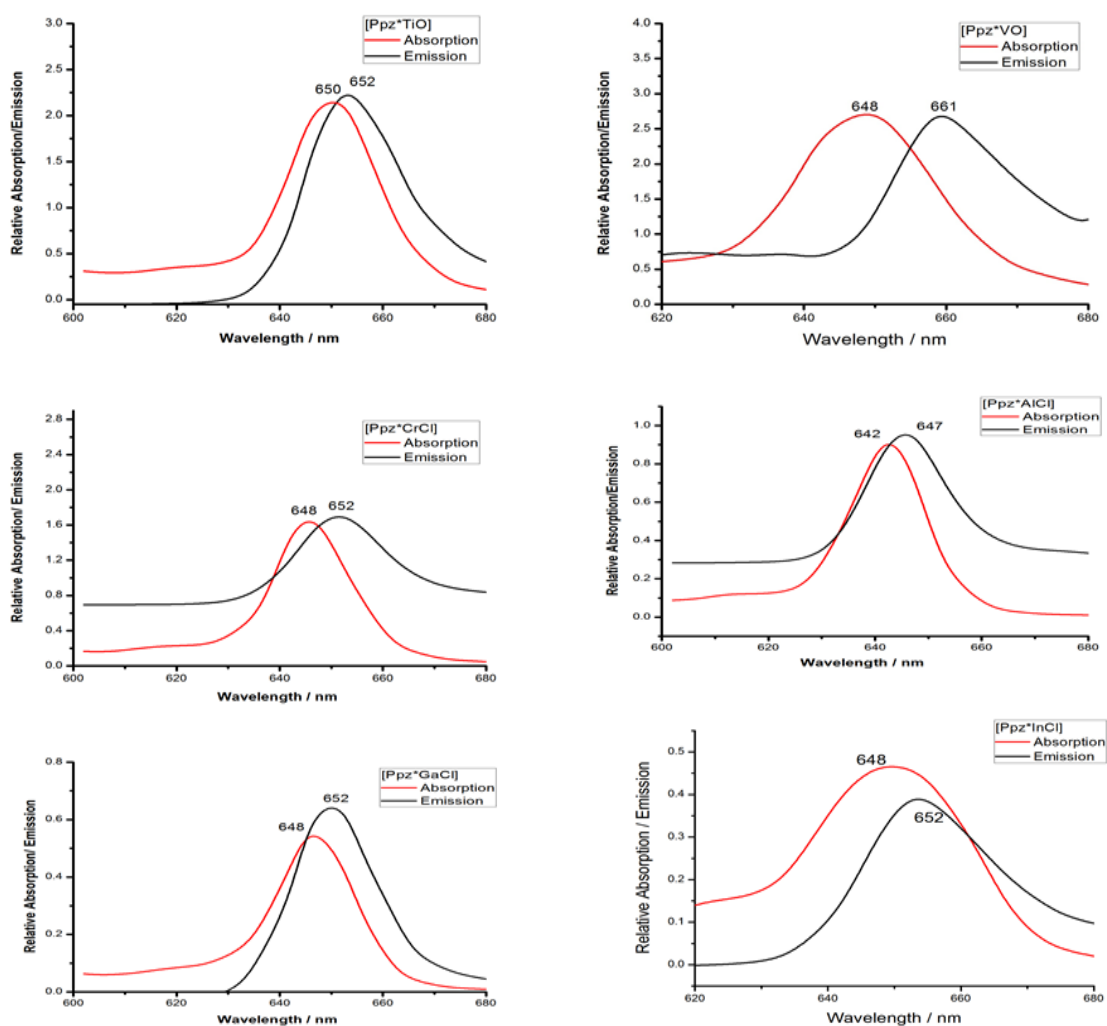
Figure 130: Absorption / Emission spectra of [Ppz*TiO], [Ppz*VO], [Ppz*CrCl], [Ppz*AlCl], [Ppz*GaCl] and [Ppz*InCl] in CHCl$_3$. λ_{Ex} = 350 nm.

Table 18: Absorption and Emission maxima of selected [Ppz*M]

complexes in CHCl$_3$, λ_{Ex} = 350 nm.

Complex	λ_{Abs}/nm	λ_{Em}/ nm	$\Delta(\lambda_{Em}$-$\lambda_{Abs})$
[Ppz*TiO]	650	652	2
[Ppz*VO]	648	661	13
[Ppz*CrCl]	646	652	6
[Ppz*AlCl]	642	647	5
[Ppz*GaCl]	448	652	4
[Ppz*InCl]	648	652	5

2.6 Cyclic Voltammetry Study

Cyclic voltammetry (CV) is a very versatile and modern electroanalytical technique for the characterization of electroactive species. It has been used to evaluate the diffusion of redox active reagents in different systems.[280] It provides valuable information regarding the stability of the analyte oxidation states and the electron transfer rate between the electrode and the analyte. Applications of CV have been extended to almost every aspect of chemistry.[281-285] Usually, the standard reduction potentials of the first oxidation and first reduction of a complex can be correlated to the energies of its highest occupied molecular orbital (HOMO) and lowest unoccupied molecular orbital (LUMO), respectively.

Cyclic voltammograms are obtained from measuring the Faradaic current as a function of the applied potential. Starting at an initial potential and varying it in a linear manner up to a limiting value. At this value, the scan direction is reversed and the same potential range is scanned in the opposite direction. Consequently, the species formed by oxidation on the forward scan might be reduced on the reverse scan.

Generally, the anodic peak current ($i_{p,a}$) denotes the current observed when scanning positively and when the scan is reversed; it is called the cathodic peak current ($i_{p,c}$). The peak potentials corresponding to the Faradic currents are called the anodic peak potential ($E_{p,a}$) and the cathodic peak potential ($E_{p,c}$).

The half-wave potential ($E_{½}$) is given by:

$$E_{1/2} = \frac{E_{p,a} + E_{p,c}}{2}$$

The difference between the two peak potentials (ΔE_p) allows for determination of the number of electrons involved in the redox process.

$$\Delta E_p = \frac{RT}{nF}$$

Where R is the gas constant (8.314 J.K^{-1}mol^{-1}), T is the temperature in Kelvin, n is the number of electrons and F is Faraday's constant. If T=298 K, $\frac{RT}{nF} = \frac{0.059}{n}$ $Volts$. Thus, in a reversible, one electron redox process, ΔE_p = 0.059 V.

A reversible system is one wherein the starting material is regenerated after oxidation or reduction with a rapid exchange rate of electrons between the working electrode and the analyte. Also, for a reversible reaction, $\frac{i_{p,a}}{i_{c,a}} = 1$, and the current is defined by the Ilkovic equation:

$$i_p = 2.69 \; x \; 10^5 n^{3/2} A C D^{1/2} V^{1/2}$$

Where i$_p$ is the peak current, n (the mol equivalent), A (the electrode area), D (the diffusion coefficient), C (the analyte concentration) and V (the scan rate).

When only a single oxidation or reduction wave is observed, this indicates an irreversible system. Slow electron exchange or chemical reactions at the electrode are common reasons for irreversibility. Quasi-reversibility is suggested when the return peak current is smaller than its couple or when ΔE is larger than what was expected for a reversible system. The current may be controlled by mass transport of any of the reaction components.[293] The peak current of an irreversible system is given by;

$$i_p = 2.69 \; x \; 10^5 \alpha^{1/2} A C D^{1/2} V^{1/2}$$

where α is the transfer coefficient.

The electrochemistry of MPcs is very rich with many redox processes. Incorporation of different metals into the Pc core and variations in the substituents on the periphery of the ring result in complexes of varied properties.[294]

Redox processes occurring in MPc complexes may be centered at the Pc core or at the metal. It is possible to observe two, successive one-electron oxidations of the Pc ring by removal of electrons from the a$_{1u}$ orbital and four, successive one-electron reductions into the e$_g$ orbital. If metal orbitals lie at energies within the HOMO and LUMO of the ring, oxidation or reduction may occur at the central metal.[294] Redox processes occurring in MPcs are influenced by several factors, including the nature of the substituents on the Pc ring, the nature and oxidation state of the central metal, the nature of the axial ligands and the solvent.

The CV technique is accomplished with a three-electrode arrangement: the potential is applied to the working electrode with respect to a reference electrode, while an auxiliary (counter) electrode is used to complete the electrical circuit. The potential at which a reversible redox couple takes place is recorded. However, the zero point potential is arbitrary. Conventionally, potentials are referenced to the Normal Hydrogen Electrode (NHE), but, experimentally, it is usually difficult to assemble a hydrogen

electrode for comparison. Other references commonly used are the Saturated Calomel Electrode (SCE), with the reduction potential at 0.241 V vs NHE, and the Ag/AgCl electrode at 0.197 V vs NHE. All of these are cumbersome to assemble, and the Fc/Fc$^+$ couple of ferrocene has become a standard for calibration[286-290], since both ferrocene and ferrocenium are chemically rather inert. The oxidation of ferrocene Fe(C$_5$H$_5$)$_2$ to the Fe(C_2H_5)$_2^+$ is a standard, one-electron process, and the electron transfer rate is fast.[291, 292] Furthermore, this couple is reversible and Nernstian in the majority of organic solutions, and its redox potential is only weakly influenced by such solvents.[295, 296] In practice, when the CV of a compound of interest is recorded, ferrocene is added to the solution, and the redox potentials of the compound are referenced to the Fc/Fc$^+$ couple as zero or the experimental couple can be referenced to any of the other standard reference electrodes by noting that the Fc/Fc$^+$ couple appears at 0.400 V vs NHE.[206]

2.6.1 Cyclic voltammetry of Pc*/Ppz* Complexes

The CV measurements were performed in about 5 mM DCM solutions, while the concentration of TBAPF$_6$ (to insure that the mass transfer of the analyte is only diffusion controlled) in the same solution is 0.1 M. Tables (19-30) list the assignments of the redox couples and the electrochemical parameters, including the half-wave peak potentials (E$_{1/2}$), anodic to cathodic peak potential separation (ΔE$_p$), ratio of anodic to cathodic peak currents (I$_{p,a}$/I$_{p,c}$) and the difference between the first oxidation and reduction potentials (ΔE$_{1/2}$).

Redox processes in MPcs can be located at the ligand and at the metal center.[211, 269, 270] Reduction of the ligand is associated to the position of LUMO ([M(II)Pc(−2)] + e ⇔ [M(II)Pc(−3)]$^−$) whereas oxidation of the ligand (M(II)Pc(−2) ⇔[(M(II)Pc(−1)]$^−$ +e) is associated to the position of the HOMO. MPcs having a metal that possesses energy levels lying between the HOMO and the LUMO of the Pc ligand, will exhibit redox processes centered on the metal. This is the case for the Pcs of Cr, Mn, Co and Fe [259, 269, 270], which have open d-shell structures.[269–271]

2.6.1.1 Cyclic voltammetry of Pcs/Ppzs having a redox inactive metal center

2.6.1.1.1 Metal free (aza)phthalocyanines Pc*H$_2$ and Ppz*H$_2$

Figure 131 shows the CV of Pc*H$_2$ in DCM containing TBAPF$_6$. The free ligand gives two, one-electron reduction processes, labelled R1 at −1.553 V and R2 at -1.92V, and two, one-electron oxidation processes, labeled O1 at 0.073 V and O2 at 0.778 V, versus Fc/Fc$^+$ couple at 0.100 Vs^{-1} scan rate. As no metal is present, all couples in the figure are assigned to the Pc ring. The values of the anodic to the cathodic peak separation (ΔE$_p$= 136-151 mV) and I$_{p,a}$/I$_{p,c}$ (for the reduction processes) are close to unity, suggesting reversible to quasi-reversible redox processes.[211] While the anodic component of the

second oxidation process, O2, is split into two peaks, the cathodic one is very broad, both splitting and broadness indicate the presence of aggregation-disaggregation equilibrium between the complex species.[254, 263] This process is reversible to quasi-reversible; however, the peak broadness led to difficulty in determining the cathodic peak potential and the $I_{p,c}/I_{p,a}$ for the O2 process.

The separation between the first and second ring reductions was found to be approximately 0.367 V. This peak separation is in agreement with the reported values for redox processes in metal-free Pcs.[212]
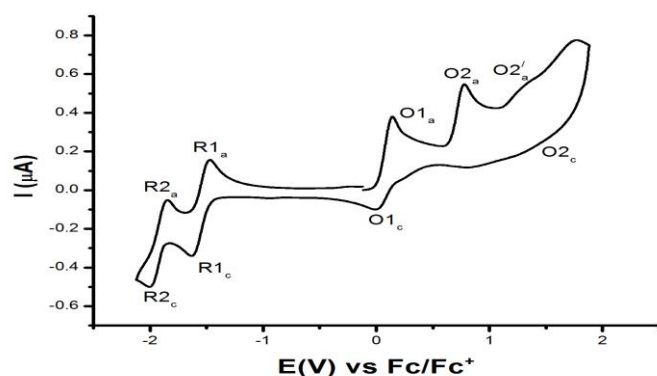
Figure 131: Cyclic voltammogram of 5 mM Pc*H_2 in TBAPF$_6$/DCM.

A comparison between the voltammograms of Pc*H_2 and Ppz*H_2 (Figure 132) obtained under the same conditions clearly reveals that the reduction potentials of the former, probably owing to its higher electron density, shift to relatively more negative values, and its oxidation potentials shift to less positive values. This suggests that, the redox potentials, and thus the efficiency of the Pc compounds in various applications, can be remarkably changed by altering the electron density of the ring. Ppz*H_2 also gives two reductions, but only one oxidation couple (Table 19); however, the anodic component of the reduction couple (R2) is split, which implies the presence of aggregated species in solution.[212] The ΔE_p values indicate reversible to quasireversible behavior for the reduction processes, and irreversibility of the oxidation process was suggested due to the absence of any corresponding cathodic current in the reverse scan.

Figure 132: Cyclic voltammogram of 5 mM Ppz*H_2 in TBAPF$_6$/DCM.

Table 19: The electrochemical data for the metal free (aza)phthalocyanines

Complex	Ring oxidation	O1 [L(-1)H₂]⁺ /[L(-2)H₂]	O2 [L(0)H₂]²⁺ /[L(-1)H₂]⁺	Ring Reduction	R1 [L(-2)H₂] /[L(-3)H₂]⁻	R2 [L(-3)H₂]⁻ /[L(-4)H₂]²⁻	ΔE₁/₂
Pc*H₂	E₁/₂	0.073	0.778ᵃ	E₁/₂	-1.553	-1.92	1.626
	ΔEₚ	0.136		ΔEₚ	0.151	0.142	
	Iₚ,c/Iₚ,a			Iₚ,a/Iₚ,c	0.93	0.85	
Ppz*H₂	E₁/₂	1.220ᵃ		E₁/₂	-0.737	-1.089	1.957
	ΔEₚ			ΔEₚ	0.055	0.117	

$E_{1/2} = (E_{p,a} + E_{p,c})/2$ at 100mVs⁻¹, $\Delta E_p = E_{p,a} - E_{p,c}$ at 100mVs⁻¹, $\Delta E_{1/2} = E_{1/2}$ (first oxidation)$-E_{1/2}$ (first reduction)
=HOMO–LUMO gap, a anodic current

Reduction of the Pc ligand is associated with the position of the lowest unoccupied molecular orbital (LUMO), whereas oxidation of the ligand is related to the position of the highest occupied molecular orbital (HOMO). Thus, the difference between the half-peak potentials of the first oxidation and the first reduction processes ($\Delta E_{1/2}$) reflects the HOMO-LUMO gap for metal-free Pcs. This gap decreases by increasing the electron density of the ring[220], thus it is 1.626 V for Pc*H₂ and 1.957 V for Ppz*H₂ (Table 19).

2.6.1.1.2 Nickel (aza)phthalocyanines [Pc*Ni] and [Ppz*Ni]

According to literature [250], all the redox processes for NiPcs are attributed to the Pc ring system. The complex [Pc*Ni] (Figure 133) displays two reduction (R1 and R2) and two oxidation (O1 and O2) couples. The values of $I_{p,a}/I_{p,c}$ and ΔE_p suggest a purely diffusion controlled, reversible, electron-transfer processes for at least three couples (R1, R2 and O1).[211] For O2, the cathodic to anodic peak current and the anodic to cathodic potential separation could not be accurately defined, due to broadness of the cathodic component of the process; this broadness could be attributed to an aggregation- disaggregation equilibrium of the complex species.[263]
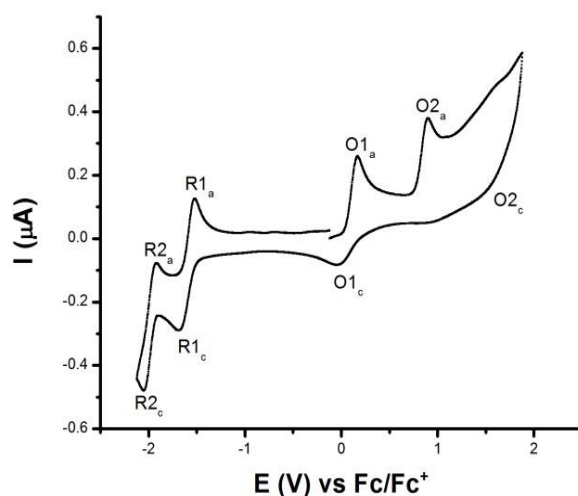
Figure 133: Cyclic voltammogram of 5 mM [Pc*Ni] in TBAPF₆/DCM.
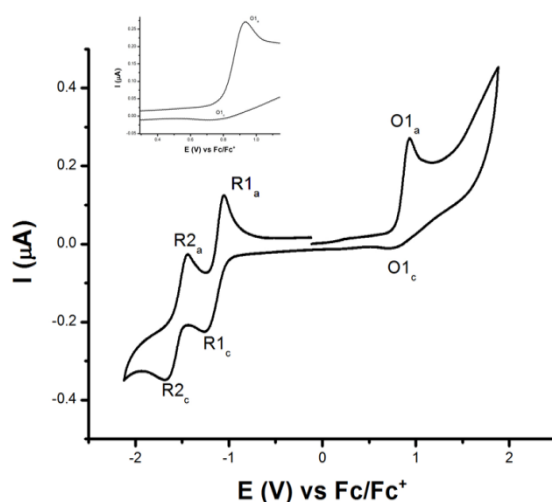
Figure 134: Cyclic voltammogram of 5 mM [Ppz*Ni] in TBAPF$_6$/DCM.

The analogous complex [Ppz*Ni] (Figure 134) shows similar behavior; however, it displays only one oxidation process (O1). As shown in Table 20, as a result of the lower electron density of the Ppz* ring compared to the Pc* one, oxidation of this complex is more difficult (at higher positive potential) but it is easier to be reduced (less negative potential). Reversibility of the redox processes was confirmed by the ΔE_p and $I_{p,c}/I_{p,a}$ values.

Table 20: The electrochemical data for the nickel (aza)phthalocyanines.

Complex	Ring oxidation	O1 [L(-1)Ni]$^+$ /[L(-2)Ni]	O2 [L(0)Ni]$^{2+}$ /[L(-1)Ni]$^+$	Ring Reduction	R1 [L(-2)Ni] /[L(-3)Ni]$^-$	R2 [L(-3)Ni]$^-$ /[L(-4)Ni]$^{2-}$	$\Delta E_{1/2}$
[Pc*Ni]	$E_{1/2}$	0.068	0.900a	$E_{1/2}$	-1.6	-1.987	1.668
	ΔE_p	0.204		ΔE_p	0.154	0.13	
	$I_{p,c}/I_{p,a}$			$I_{p,a}/I_{p,c}$	0.98		
[Ppz*Ni]	$E_{1/2}$	0.857		$E_{1/2}$	-1.15	-1.555	2.007
	ΔE_p	0.147		ΔE_p	0.20	0.23	
	$I_{p,c}/I_{p,a}$			$I_{p,a}/I_{p,c}$	0.92	0.88	

$E_{1/2}$ = ($E_{p,a}$ + $E_{p,c}$)/2 at 100mVs^{-1}, ΔEp = $E_{p,a}$ – $E_{p,c}$ at 100mVs^{-1}, $\Delta E_{1/2}$ = $E_{1/2}$ (first oxidation)–$E_{1/2}$ (first reduction) =HOMO–LUMO gap, a anodic current

In comparison with the metal free complexes, the displacement of two protons with the nickel(II) ion shifts the first reduction potential of the ring to more negative values; this may be attributed to the increase in the negative charge on the ligand as a result of the strong coordination of nitrogen atoms to the metal ion.[267] The π-back-donation of the dπ of the metal ion into the empty Pc*(Ppz*)-π* orbitals, and the polarization of the ligand due to the e$_g$ symmetry with the displacement of protons by the metal ion, were previously reported[139] providing an additional support for the negative shift in the reduction potential of the macrocyclic ring.

2.6.1.1.3 Zinc (aza)phthalocyanines [Pc*Zn] and [Ppz*Zn]
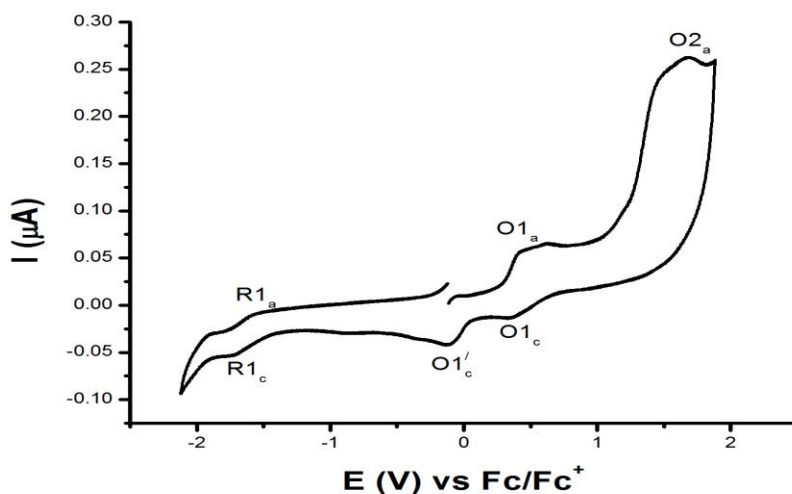
Figure 135: Cyclic voltammogram of 5 mM [Pc*Zn] in TBAPF$_6$/DCM.

Oxidation and reduction reactions of zinc phthalocyanines in solution are expected to occur at the Pc ring only, since Zn metal is electro-inactive.[251, 252] Figures 135 and 136 show typical cyclic voltammograms of [Pc*Zn] and [Ppz*Zn], respectively. The voltammograms of both show very broad oxidation peaks indicating a high degree of aggregation-disaggregation equilibrium between the complex species.[263] Depending on the cathodic-to-anodic potential peak separations (Table 21), both [Pc*Zn] and [Ppz*Zn] display one reversible to quasi-reversible reduction process.[252] While the complex [Pc*Zn] gives two oxidation processes (O1 and O2), [Ppz*Zn] diplays only an irreversible O1 process within the same potential window. The first oxidation process O1 of [Pc*Zn] is reversible to quasireversible, depending on its ΔE_p value.[252] The voltammogram of the complex [Pc*Zn] shows an irreversible oxidation process, O2, just at the end of the potential window. Although a very broad peak in the voltammogram of [Ppz*Zn] was detected, this peak could not be considered as a second oxidation process O2. This might be attributed to aggregation of molecules in solution. The reason, why it does not represent a second oxidation process, is its potential value, as a second oxidation of [Ppz*Zn], due to its lower electron density, must occur at a more positive potential relative to the potential of the O2 process of the corresponding complex [Pc*Zn].
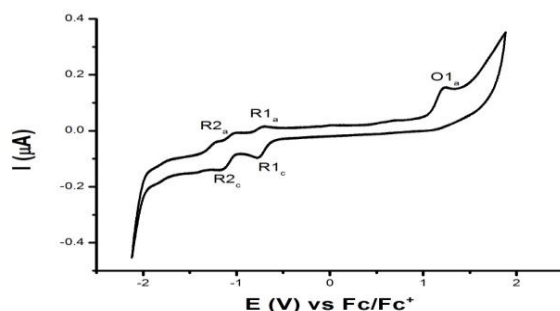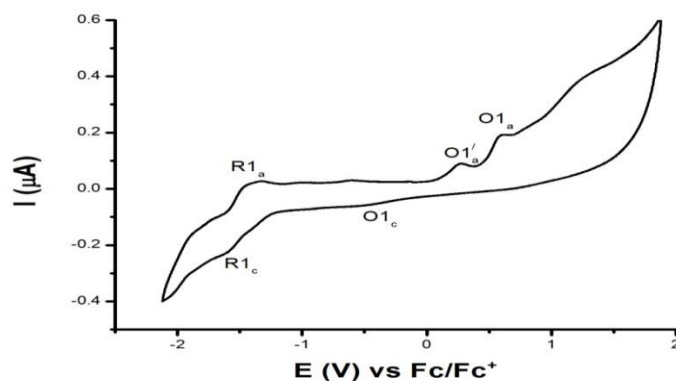
Figure 136: Cyclic voltammogram of 5 mM [Ppz*Zn] in TBAPF$_6$/DCM.

Table 21: The electrochemical data for the nickel (aza)phthalocyanines.

Complex	Ring oxidation	O1 [L(-1)Zn]$^+$ /[L(-2)Zn]	O2 [L(0)Zn]$^{2+}$ /[L(-1)Zn]$^+$	Ring Reduction	R1 [L(-2)Zn] /[L(-3)Zn]$^-$	$\Delta E_{1/2}$
[Pc*Zn]	E$_{1/2}$	0.439	1.69^a	E$_{1/2}$	-1.645	2.084
	ΔE_p	0.142		ΔE_p	0.154	
[Ppz*Zn]	E$_{1/2}$	0.583^a		E$_{1/2}$	-1.509	2.092
	ΔE_p			ΔE_p	0.168	

$E_{1/2}$ = ($E_{p,a}$ + $E_{p,c}$)/2 at 100mVs^{-1}, ΔE_p = $E_{p,a}$ – $E_{p,c}$ at 100mVs^{-1}, $\Delta E_{1/2}$ = $E_{1/2}$ (first oxidation)–$E_{1/2}$ (first reduction) =HOMO–LUMO gap, a anodic current

2.6.1.1.4 Copper (aza)phthalocyanines [Pc*Cu] and [Ppz*Cu]

Figure 137 shows a typical cyclic voltammogram of [Pc*Cu], at 0.1 Vs^{-1} scan rate in DCM/TBAPF$_6$. It displays one reduction (R1) and two oxidation couples. It is well known that Cu(II) in the cavity of Pc core is redox inactive. Therefore, these redox couples are ligand-based.[253, 254]
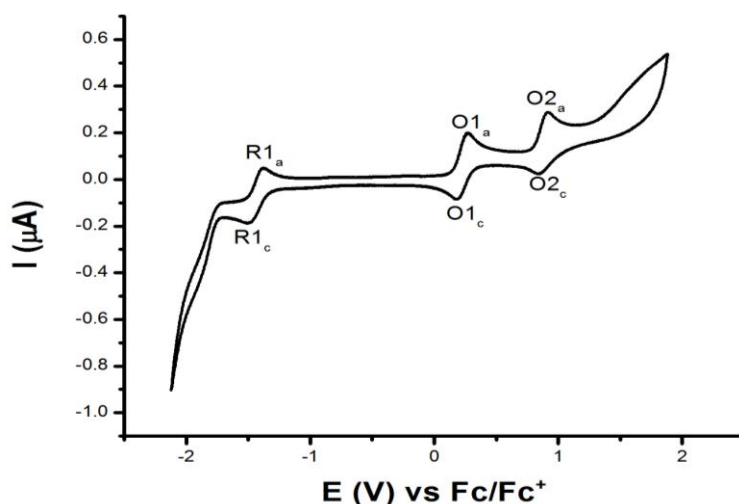
Figure 137: Cyclic voltammogram of 5 mM [Pc*Cu] in TBAPF$_6$/DCM.

Owing to the lower electron density of [Ppz*Cu] (Figure 138) compared to [Pc*Cu], reduction of this complex is much easier than for [Pc*Cu], however, it is more difficult to be reduced. On the contrary of [Pc*Cu], the redox behavior of [Ppz*Cu] (Table 22) shows two reduction (R1, R2) and one oxidation O1 couple within the same potential window. The peak current of the oxidation process O1 is much higher than those of the other reduction processes. This observation provides strong support for a high adsorption tendency of the complex on the platinum working electrode. High adsorption tendency of CuPcs on platinum electrodes has also been reported previously.[255-257]
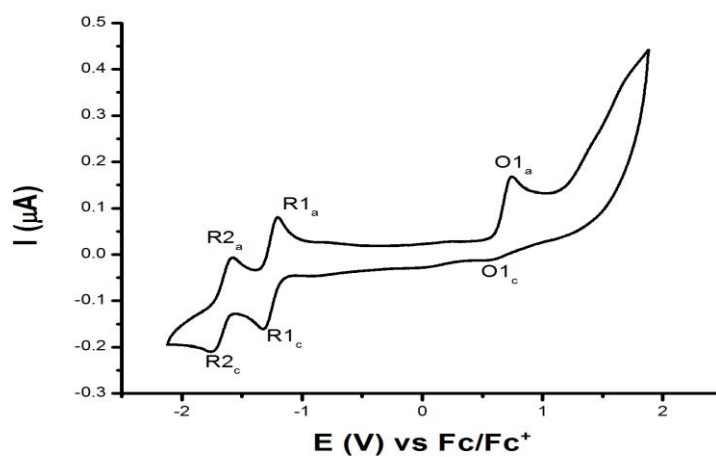
Figure 138: Cyclic voltammogram of 5 mM [Ppz*Cu] in TBAPF$_6$/DCM.

Table 22: The electrochemical data for the copper (aza)phthalocyanines.

Complex	Ring oxidation	O1 [L(-1)Cu]$^+$ /[L(-2)Cu]	O2 [L(0)Cu]$^{2+}$ /[L(-1)Cu]$^+$	Ring Reduction	R1 [L(-2)Cu] /[L(-3)Cu]$^-$	R2 [L(-3)Cu]$^-$ /[L(-4)Cu]$^{2-}$	$\Delta E_{1/2}$
[Pc*Cu]	$E_{1/2}$	0.226	0.881	$E_{1/2}$	-1.438		1.664
	ΔE_p	0.074	0.075	ΔE_p	0.105		
	$I_{p,c}/I_{p,a}$			$I_{p,a}/I_{p,c}$	0.985		
[Ppz*Cu]	$E_{1/2}$	0.664		$E_{1/2}$	-1.26	-1.661	1.924
	ΔE_p	0.155		ΔE_p	0.112	0.158	
	$I_{p,c}/I_{p,a}$			$I_{p,a}/I_{p,c}$	0.875	0.98	

$E_{1/2}$ = ($E_{p,a}$ + $E_{p,c}$)/2 at 100mVs^{-1}, ΔE_p = $E_{p,a}$ – $E_{p,c}$ at 100mVs^{-1}, $\Delta E_{1/2}$ = $E_{1/2}$ (first oxidation)–$E_{1/2}$ (first reduction) =HOMO–LUMO gap, a anodic current

Generally, the values of $I_{p,a}/I_{p,c}$ and anodic to cathodic peak separation of the [Pc*Cu] and [Ppz*Cu] redox processes suggest reversible redox processes.[211] The HOMO – LUMO gap was calculated as the difference between the first oxidation and the first reduction potentials for the complexes. $\Delta E_{1/2}$ for complex [Pc*Cu] is 1.664 V (comparable with other studies 1.3 -1.7 V[268]), and the analogous [Ppz*Cu], due to its lower electron density, shows a higher HOMO – LUMO gap of 1.924 V.

2.6.1.1.5 Oxovanadium (aza)phthalocyanines [Pc*VO] and [Ppz*VO]

The cyclic voltammogram of [Pc*VO] (Figure 139) displays two reduction (R1-R2) and three oxidation (O1-O3) couples. In comparison with literature,[264] the processes R1, R2 and O1 could be easily assigned to $[V(IV)OPc*(-2)]/[V(IV)OPc*(-3)]^-$, $[V(IV)OPc*(-3)]^-/[V(IV)OPc*(-4)]^{2-}$ and $[V(IV)OPc*(-1)]^+/[V(IV)OPc*(-2)]$. A second oxidation process of oxovanadium Pcs is rarely mentioned[264], and it implies a second, ring-based oxidation of $[V(IV)OPc*(0)]^{2+}/[V(IV)OPc*(-1)]^+$. The third oxidation process cannot be firmly assigned, usually, a maximum of two, successive one-electron oxidation processes of the Pc core is allowed. Additionally, oxidation of the VO group in the cavity of a Pc has never been reported; however, there is no reports on the electrochemistry of the VPcs at this high positive potential. Hence, we propose that the third oxidation process O3 is metal based $V(IV) \rightarrow V(V)$. The V(V) species might be stabilized by the electron donating ability of the Pc* ligand.
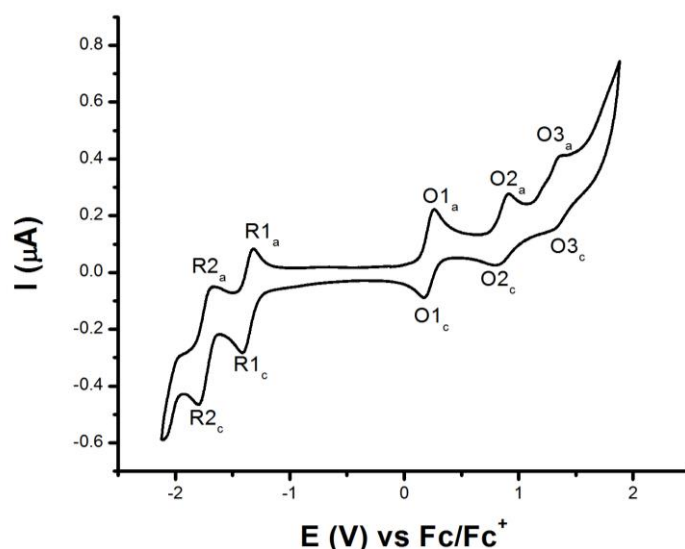
Figure 139: Cyclic voltammogram of 5 mM [Pc*VO] in $TBAPF_6$/DCM.

The analogous complex [Ppz*VO] (Figure 140), is more prone for reduction and more difficult to be oxidized (Table 23). Thus, it displays two reduction and only one ligand-based oxidation processes. Except for the oxidation process of [Ppz*VO], the other two redox processes are reversible to quasirversible. ΔE_p suggests slow, electron-transfer redox processes for [Ppz*VO] compared to [Pc*VO]. Although ΔE_p value of the R2 of the complex [Ppz*VO] is somewhat high, reversibility is illustrated by the similarity in the forward and reverse scan.[78]
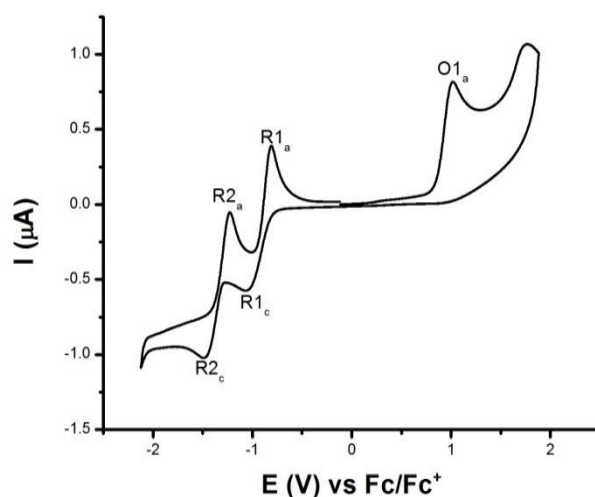
Figure 140: Cyclic voltammogram of 5 mM [Ppz*VO] in TBAPF$_6$/DCM.

Table 23: The electrochemical data for the oxovanadium (aza)phthalocyanines

Complex	Ring oxidation	O1 [L(-1)VO]$^+$ /[L(-2)VO]	O2 [L(0)VO]$^{2+}$ /[L(-1)VO]$^+$	O3 [L(0)V^{IV}O]$^{3+}$ /[L(-1)V^{V}O]$^{2+}$	Ring Reduction	R1 [L(-2)VO] /[L(-3)VO]$^-$	R2 [L(-3)VO]$^-$ /[L(-4)VO]$^{2-}$	ΔE$_{1/2}$
[Pc*VO]	E$_{1/2}$	0.218	0.868	1.338	E$_{1/2}$	-1.36	-1.73	1.578
	ΔE$_p$	0.082	0.088	0.03	ΔE$_p$	0.08	0.10	
	I$_{p,c}$/I$_{p,a}$				I$_{p,a}$/I$_{p,c}$	0.94	0.89	
[Ppz*VO]	E$_{1/2}$	1.017[a]			E$_{1/2}$	-0.929	-1.525	1.946
	ΔE$_p$				ΔE$_p$	0.141	0.241	

E$_{1/2}$ = (E$_{p,a}$ + E$_{p,c}$)/2 at 100mVs^{-1}, ΔEp = E$_{p,a}$ – E$_{p,c}$ at 100mVs^{-1}, ΔE$_{1/2}$ = E$_{1/2}$ (first oxidation)−E$_{1/2}$ (first reduction) =HOMO–LUMO gap, a anodic current

2.6.1.1.6 Fluoroaluminium (aza)phthalocyanines [Pc*AlF] and [Ppz*AlF]

As shown in Figures 141 and 142, both [Pc*AlF] and [Ppz*AlF] complexes, with electroinactive metal centers[279], give two, irreversible, ligand-based oxidation processes (Table 24), while no clear reduction peaks could be seen within the potential window (- 2V vs Fc/Fc$^+$ couple).

Figure 141: Fraction of the cyclic voltammogram of 5 mM [Pc*AlF] in TBAPF$_6$/DCM.
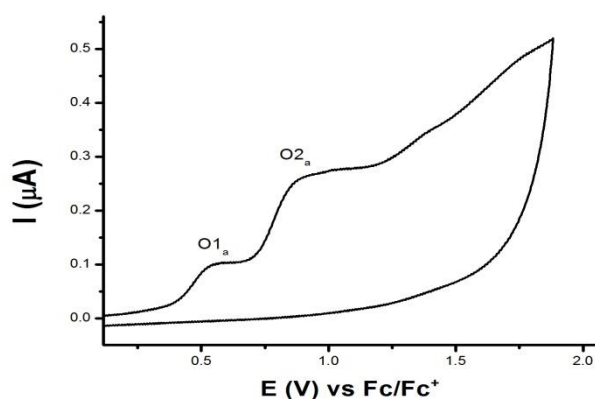
Figure 142: Fraction of the cyclic voltammogram of 5mM [Ppz*AlF] in TBAPF$_6$/DCM.

Table 24: The electrochemical data for the fluoro aluminium (aza)phthalocyanines.

Complex	Ring oxidation	O1 [L(-1)AlF]$^+$ /[L(-2)AlF]	O2 [L(0)AlF]$^{2+}$ /[L(-1)AlF]$^+$
[Pc*AlF]	E$_a$ (anodic wave potential)	0.218 [a]	0.405 [a]
[Ppz*AlF]	E$_a$ (anodic wave potential)	0.533 [a]	1.058 [a]

2.6.1.2 Cyclic voltammetry of complexes with a redox active metal center

2.6.1.2.1 Manganese(III) (aza)phthalocyanines [Pc*MnCl] and [Ppz*MnCl]

MnPcs have very interesting electrochemistry due to the fact that Mn exhibits variable oxidation states ranging from Mn(I) to Mn(IV) in such MnPc complexes.[207, 208, 213, 265, 266] This makes MnPcs potential catalysts for many reactions. Substituted MnPcs are still relatively rare, and their electrochemistry is not fully understood, compared to the other first-row transition metal MPc complexes. For example, the first reduction in [Pc(-2) Mn(II)] has been a subject of some controversy, with some reports proposing ring reduction to the [Mn(II)Pc(-3)]$^-$ species and others suggesting metal reduction to [Mn(I)Pc(-2)]$^-$.[202]

The voltammogram of the complex [Pc*MnCl] (Figure 143) clearly displays two reversible to quasi-reversible reduction R1 and R2 and two irreversible oxidation O1 and O2 processes. In comparison with literature values,[208, 210, 265, 266] we assign R1 to metal reduction process [Pc*(-2)Mn(III)]/[Pc*(-2)Mn(II)]$^-$. Process R2 is then assigned to ring reduction, [Pc*(-2)Mn(II)]$^-$/[Pc*(-3)Mn(II)]$^{2-}$. Furthermore, the oxidation processes O1 and O2 are assigned to two successive metal and ligand oxidation processes [Pc*(-2)Mn(IV)]$^+$/[Pc*(-2)Mn(III)] and [Pc*(-1)Mn(IV)]$^{2+}$/ [Pc*(-2)Mn(IV)]$^+$.

113
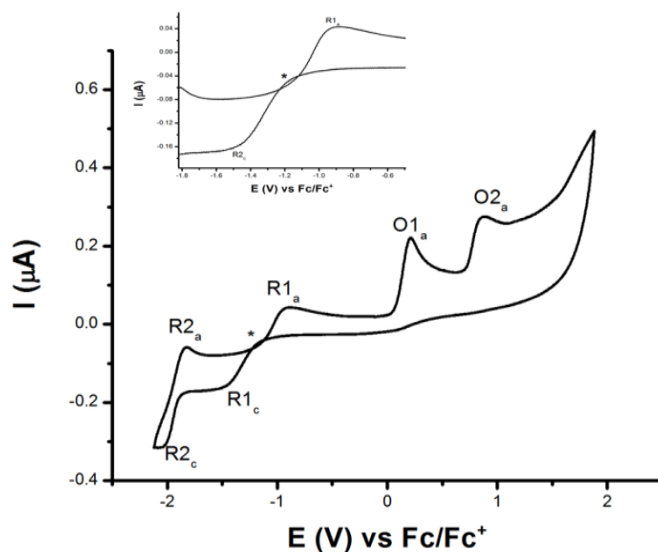
Figure 143: Cyclic voltammogram of 5 mM [Pc*MnCl] in TBAPF$_6$/DCM.

[Ppz*MnCl] (Figure 144) also undergoes two oxidation processes (the first oxidation is usually hard to be detected[210] and can be assigned to [Ppz*(-2)Mn(IV)]$^+$/[Ppz*(-2)Mn(III)]), but, as a result of its lower electron density, three reduction processes for the complex can occur, and the third reduction is attributed to a second ring-based reduction [Ppz*(-3)Mn(II)]$^{2-}$/[Ppz*(-4)Mn(II)]$^{3-}$. ΔE_p values of all the reduction processes suggest a slow electron transfer mechanism (Table 25).
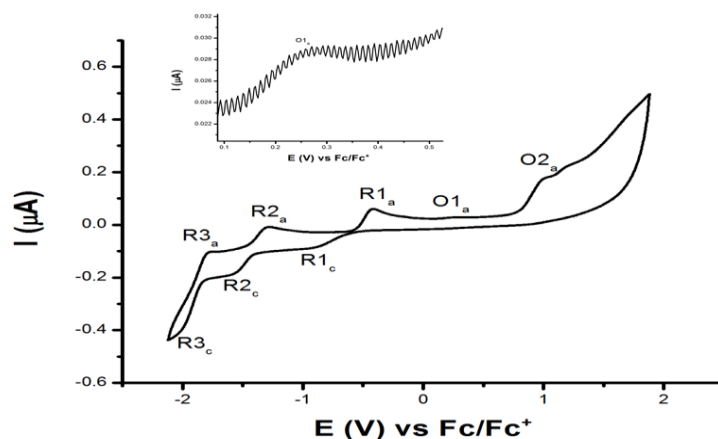
Figure 144: Cyclic voltammogram of 5 mM [Ppz*MnCl] in TBAPF$_6$/DCM.

It can be observed that the anodic and cathodic scans cross (Figures 143), or become very close (Figure 144) to, each other and this current shift occurs at a midpoint between the cathodic and the anodic components of the first reduction process. This suggests a system change such as a chemical reaction at this point. It has been documented that decreasing the oxidation state of a metal ion favors lower coordination, especially for CoPc and MnPc complexes.[251, 264] Actually, two chemical reactions could occur for the manganese (III) complexes during the voltammetric measurements, but

formation of the oxo-MnPc complex [PcMn^{III}–O–Mn^{III}Pc] is diminished as the analyte solution was prepared in a glove box under an inert atmosphere just prior to measurement; hence, the only proposed mechanism is removal of the axial chlorine[264] and formation of the new complexes [Pc*Mn(II)] and [Ppz*Mn(II)].

Table 25: The electrochemical data for the manganese (aza)phthalocyanines.

Complex	Ox.	O1 [L(-2)M^{IV}]$^+$ /[L(-2)M^{III}]	O2 [L(-1)M^{IV}]$^{2+}$ /[L(-2)M^{IV}]$^+$	Red.	R1 [L(-2)M^{III}] /[L(-2)M^{II}]$^-$	R2 [L(-2)M^{II}]$^-$ /[L(-3)M^{II}]$^{2-}$	R3 [L(-3)M^{II}]$^{2-}$ /[L(-4)M^{II}]$^{3-}$
[Pc*MnCl]	E$_{1/2}$	0.210[a]	0.862[a]	E$_{1/2}$	-1.206	-1.915	
	ΔE$_p$			ΔE$_p$	0.565	0.19	
[Ppz*MnCl]	E$_{1/2}$	0.268[a]	1.006[a]	E$_{1/2}$	-0.660	-1.441	-1.889
	ΔE$_p$			ΔE$_p$	0.500	0.288	0.192

E$_{1/2}$ = (E$_{p,a}$ + E$_{p,c}$)/2 at 100mVs^{-1}.   ΔE$_p$ = E$_{p,a}$ – E$_{p,c}$ at 100mVs^{-1}, a anodic current,

** A reaction, e.g. removal of the axial chlorine is expected and hence M= Mn or MnCl

2.6.1.2.2 Iron azaphthalocyanines [Ppz*Fe] and [Ppz*FeCl]

Owing to the air and light sensitivity of [Pc*Fe] and [Pc*FeCl], no clean voltammograms could be obtained for these complexes. However, herein we can explain the main CV behavior of the analogous [Ppz*Fe] or [Ppz*FeCl] complexes.

Already reported,[260] iron(II) Pcs exhibit metal-based and ligand-based redox processes, regardless of the solvent used, the first oxidation and first reduction are metal-based processes[261]. However, usually when reduced, the reduction products get easily adsorbed onto the electrode, and the complexes degrade rapidly upon oxidation. Hence, in this work, we were only able to observe an irreversible reduction process R2. The irreversible behavior of this peak (Figure 145) suggests its assignment to the metal based reduction [Ppz*(-2)FeII] /[Ppz*(-2)FeI]$^{-}$[261] (Table 26).

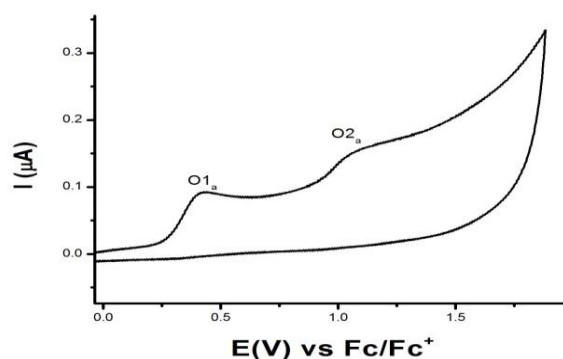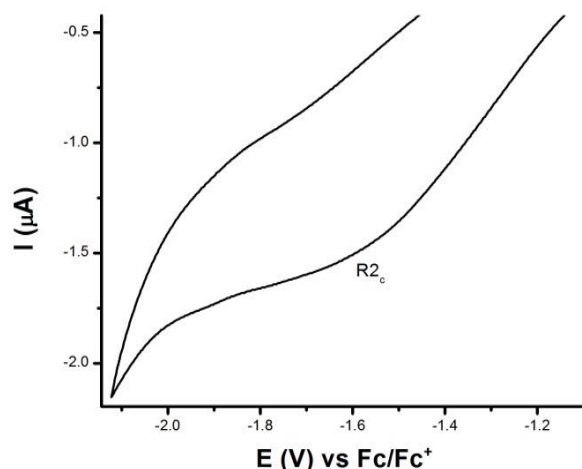**Figure 145:** Fraction of the cyclic voltammogram of 5 mM [Ppz*Fe] in TBAPF$_6$/DCM.
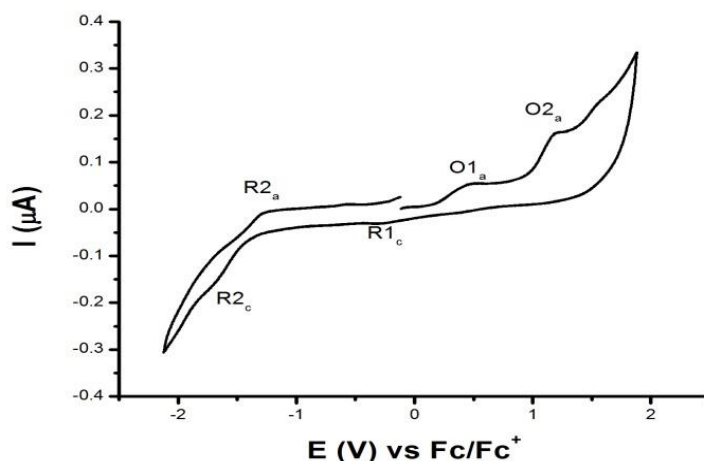
Figure 146: Cyclic voltammogram of 5 mM [Ppz*FeCl] in TBAPF$_6$/DCM.

Table 26: The electrochemical data for the Iron azaphthalocyanines

Complex	Ox.	O1 [Ppz*(-1)M^{III}]$^+$ /[Ppz*(-2)M^{III}]	O2 [Ppz*(0)M^{III}]$^{2+}$ /[Ppz*(-1)M^{III}]$^+$	Red.	R1 [Ppz*(-2)M^{III}] /[Ppz*(-2)M^{II}]$^-$	R2 [Ppz*(-2)M^{II}]$^-$ /[Ppz*(-2)M^{I}]$^{2-}$
[Ppz*Fe]	E$_{1/2}$			E$_{1/2}$		-1.573[c**]
[Ppz*FeCl]	E$_{1/2}$	0.465[a]	1.155[a]	E$_{1/2}$	-0.271	-1.464[a]
	ΔE$_p$			ΔE$_p$		0.404

E1/2 = (Epa + Epc)/2 at 100mVs^{-1}, ΔEp = Epa – Epc at 100mVs^{-1}, a anodic current, c cathodic current, M=Fe or FeCl

** Also it denotes R2, this is the first reduction process in case of [Ppz*Fe], also, in this case, the formal charge of the complex oxidized and reduced forms are 0 and -1 respectively.

[FePpz*Cl] (Figure 146) shows two reduction and two oxidation couples. Usually, iron (III) Pcs are highly aggregated at the concentrations used for cyclic voltammetry, and the observed peaks are mainly due to the aggregated species, with some contribution from the monomeric components.[213] As a result, only the cathodic or anodic component of the redox processes could be precisely determined. According to literature,[262] the two reduction processes are assigned to the metal reduction Fe^{III}/Fe^{II} and Fe^{II}/Fe^{I}, while the oxidation processes are ligand based (Table 26).

2.6.1.2.3 Cobalt (aza)phthalocyanines [Pc*Co] and [Ppz*Co]

For CoPc complexes, it is known that the first reduction reaction of CoPc in solution or film states is expected to be a cobalt-based process because of the electroactive nature of cobalt metal coordinated to the macrocycle unit.[258, 272, 273] On the other hand, a second reduction of CoPc is based on the Pc ring. This behavior does not depend on solvent or electrolyte systems used in experiment. However, the first oxidation process usually occurs on the Pc ring in nonpolar solvents, such as DCM[254], as donor solvents strongly favour [Co(III)Pc(-2)] by coordinating along the axis to form a six coordinate species. If

such solvents are absent, then oxidation to Co(III) is inhibited and ring oxidation occurs first.[212]

Therefore, as shown in Figure 147, the voltammogram of [Pc*Co] shows one reduction and three oxidation couples. The first reduction process of the complex is assigned to the [Pc(-2)Co(II)] / [Pc(-2)Co(I)]⁻, while the first oxidation, O1, is ligand-based due to [Pc*(-1)Co(II)]⁺ / [Pc*(-2)Co(II)] (Table 27). The second and third oxidation couples are assigned to the [Pc*(-1)Co(III)]²⁺ / [Pc*(-1)Co(II)]⁺ and [Pc*(0)Co(III)]³⁺ / [Pc*(-1)Co(III)]²⁺ respectively.

On the contrary of [Pc*Co], the voltammogram of [Ppz*Co] (Figure 148) shows two reduction and two oxidation couples. All the couples could be easily assigned as; R1 is [Ppz*(-2)Co(II)] / [Ppz*(-2)Co(I)]⁻, R2 is [Ppz*(-2)Co(I)]⁻ / [Ppz*(-3)Co(I)]²⁻, O1 is [Ppz*(-1)Co(II)]⁺ / [Ppz*(-2)Co(II)] and O2 is [Ppz*(-1)Co(III)]²⁺ / [Ppz*(-1)Co(II)]⁺.
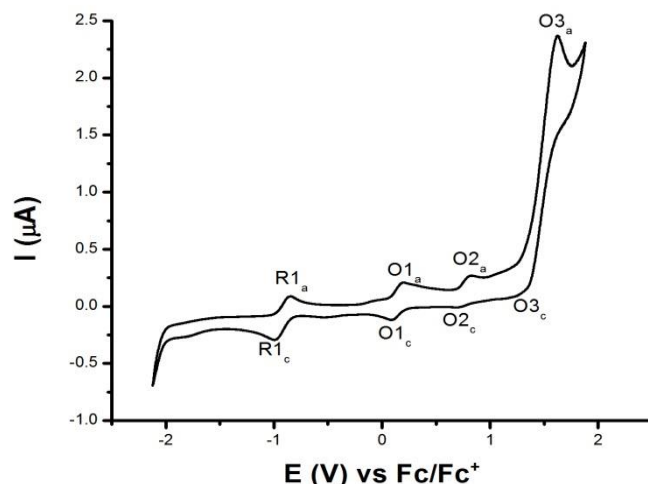
Figure 147: Cyclic voltammogram of 5 mM [P*Co] in TBAPF$_6$/DCM.

The oxidation process O2 of [Ppz*Co] shows irreversible behavior. For the other couples, except for O3 for [Pc*Co], the redox processes exhibit anodic to cathodic peak separation (ΔE_p) from 61 to 147 mV (Table 27), suggesting reversible electron transfer.[211] Although, of the higher ΔE_p value of O3, some reversibility was shown in the reverse scan; suggesting the slow, electron-transfer mechanism for this process.
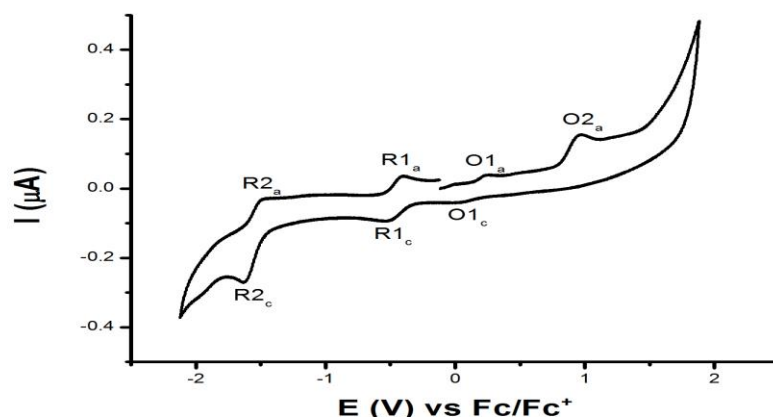
Figure 148: Cyclic voltammogram of 5 mM [Ppz*Co] in TBAPF$_6$/DCM.

Table 27: The electrochemical data for the manganese (aza)phthalocyanines.

Complex	Ox.	O1 [L(-1)Co^{II}]$^+$ /[L(-2)Co^{II}]	O2 [L(-1)Co^{III}]$^{2+}$ /[L(-1)Co^{II}]$^+$	O3 [L(0)Co^{III}]$^{3+}$ /[L(-1)Co^{III}]$^{2+}$	Red.	R1 [L(-2)Co^{II}] /[L(-2)Co^{I}]$^-$	R2 [L(-2)Co^{I}]$^-$ /[L(-3)Co^{I}]$^{2-}$
[Pc*Co]	E$_{1/2}$	0.1405	0.7705	1.424	E$_{1/2}$	-0.924	
	ΔE$_p$	0.093	0.119	0.391	ΔE$_p$	0.147	
	I$_{p,c}$/I$_{p,a}$	0.92			I$_{p,c}$/I$_{p,a}$	0.89	
[Ppz*Co]	E$_{1/2}$	0.153	0.968^a		E$_{1/2}$	-0.459	-1.551
	ΔE$_p$	0.201			ΔE$_p$	0.109	0.139

E$_{1/2}$ = (E$_{p,a}$ + E$_{p,c}$)/2 at 100mVs^{-1}, ΔE$_p$ = E$_{p,a}$ – E$_{p,c}$ at 100mVs^{-1}, a anodic current

2.6.1.2.4 Oxotitanium (aza)phthalocyanines [Pc*TiO] and [Ppz*TiO]

Detailed electrochemical studies of TiPcs are not reported, as many as other reports on the electrochemistry of MPcs, such as ZnPc, CuPc and CoPc are given. Silver et al.[274] studied the thin film voltammetric behavior of [PcTiO] complex. They showed that [PcTiO] complex coated on ITO electrode displayed two ring reduction processes and decompose during the oxidation process. Nyokong and co-workers[199] studied the solution electrochemistry of TiPc derivatives, and reported that these complexes might give three reduction processes assignable to a two-electron metal centered reduction from Pc(2–)Ti^{IV}O to Pc(2–)Ti^{II}O for first reduction couple, a combination of a one-electron ligand reduction from Pc(2–)Ti^{II}O to Pc(3–)Ti^{II}O and a metal-centered one-electron reduction from Pc(3–)Ti^{II}O to Pc(3–)Ti^{I}O for the second reduction and finally, a one electron ligand reduction from Pc(3–)Ti^{I}O to Pc(4–)Ti^{I}O. However, according to literature,[275] the titanium complex showed clearly the one electron metal center reductions from [Pc(2–)Ti^{IV}O] to [Pc(2–)Ti^{III}O]$^-$ and from [Pc(2–)Ti^{III}O]$^-$ to [Pc(2–)Ti^{II}O]$^{2-}$ for the first two reduction couples and finally a one electron ligand reduction from [Pc(2–)Ti^{II}O]$^{2-}$ to [Pc(3–)Ti^{II}O]$^{3-}$.

In this study, the cyclic voltammogram of [Pc*TiO] (Figure149) displays two quasi-reversible reduction couples at -1.03 and -1.46 V, and, in comparison with literature,[275]

these half wave potentials are close to the second and third reduction processes of the complex. However, an overlap of the voltammograms for another substituted TiPc, whereby two 1-electron reductions resulted in one couple, was reported.[199, 276] Owing to the presence of three oxidation components for the two redox processes and the position of the first oxidation component at – 0.26 V (0.677 V far from the $E_{1/2}$ for the first reduction couple) and the deviation of the anodic to the cathodic current from unity, where ($I_{p,a}(R1_a)$ / $I_{p,c}(R1_c)$ = 0.83 but $I_{p,a}$ ($R1_a$+$R1_{a*}$) / $I_{p,c}$ ($R1_c$) = 0.94), we believe that the first reduction of the complex is a two electron process, however when the potential scan is reversed the molecule was re-oxidized clearly in two steps to the original molecule.
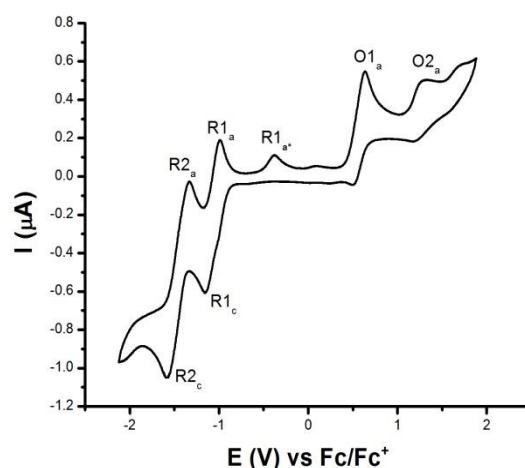
Figure 149: Cyclic voltammogram of 5 mM [Pc*TiO] in TBAPF$_6$/DCM.

While reduction is expected to occur at both the central metal, as well as, on the ring, oxidation of TiPcs is expected to occur only at the ring[276], and hence, the two, irreversible oxidation processes shown in Figure 149 are assigned to the ring-based oxidations, Pc*(-1)/Pc*(-2) and Pc*(-0)/Pc*(-1).
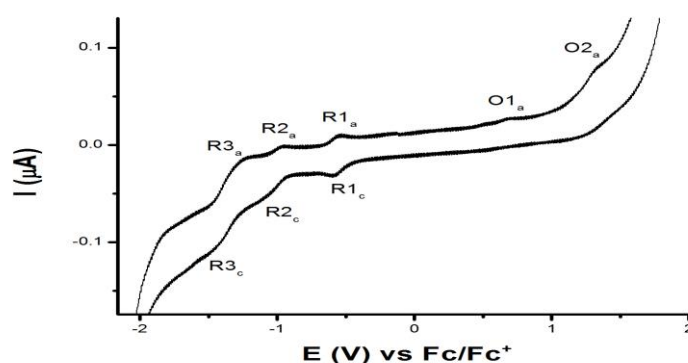
Figure 150: Fraction of the cyclic voltammogram of 5 mM [Ppz*TiO] in TBAPF$_6$/DCM.

119

Although the voltammogram of the analogous complex [Ppz*TiO] looks very broad (Figure 150), probably due to the presence of aggregated species,[254, 263] three quasireversible reduction couples and two irreversible oxidation processes could be detected. The first two reduction couples are metal based while the third one is ligand based; however, in this case no overlap is expected. The ligand based oxidation couples O1 and O2 are shifted to a higher positive potential (Table 28) due to the relative difficulty in oxidizing the Ppz* core compared to the Pc* one.

Table 28: The electrochemical data for the oxotitanium (aza)phthalocyanines.

Complex	Ox.	O1 $[L(-1)Ti^{IV}O]^+$ $/[L(-2)Ti^{IV}O]$	O2 $[L(0)Ti^{IV}O]^{2+}$ $/[L(-1)Ti^{IV}O]^+$	Red.	R1 $[L(-2)Ti^{IV}O]$ $/[L(-2)Ti^{III}O]^-$	R2 $[L(-2)Ti^{III}O]^-$ $/[L(-2)Ti^{II}O]^{2-}$	R3 $[L(-2)Ti^{II}O]^{2-}$ $/[L(-3)Ti^{II}O]^{3-}$
[Pc*TiO]	$E_{1/2}$	0.642 [a]	1.271 [a]	$E_{1/2}$	-1.068 [a]		-1.458**
	ΔE_p			ΔE_p	0.168		0.249
	$I_{p,c}/I_{p,a}$			$I_{p,a}/I_{p,c}$	0.94		0.95
[Ppz*TiO]	$E_{1/2}$	0.688 [a]	1.320 [a]	$E_{1/2}$	-0.573	-1.061	-1.440
	ΔE_p			ΔE_p	0.028	0.129	0.167

$E_{1/2} = (E_{p,a} + E_{p,c})/2$ at 100mVs^{-1}, $\Delta E_p = E_{p,a} - E_{p,c}$ at 100mVs^{-1}, a anodic current, ** shown as R2 in the literature and the voltammogram

2.6.1.2.5 Chromium (aza)phthalocyanines [Pc*CrCl] and [Ppz*CrCl]

The electrochemical data for the Cr(III) Pcs are very sparse. In the voltammogram of [Pc*CrCl], five redox processes were observed (Figure 151). The first reduction is known to occur at the central metal to give Cr(II)Pcs;[251, 278] thus, it is assigned to [Pc*(-2)Cr(III)Cl]/[Pc*(-2)Cr(II)Cl]$^-$. The cathodic component of this process is split, probably due to the presence of aggregated species. The second reduction could be attributed to the ligand-based reduction, [Pc*(-2)Cr(II)Cl]$^-$/[Pc*(-3)Cr(II)Cl]$^{2-}$.[278] In comparison with reported data,[278] the three oxidation processes of the complex are assigned to the metal oxidation [Pc*(-2)Cr(IV)Cl]$^+$/[Pc*(-2)Cr(III)Cl] followed by two ligand-based oxidations [Pc*(-1)Cr(IV)Cl]$^{2+}$/[Pc*(-2)Cr(IV)Cl]$^+$ and [Pc*(0)Cr(IV)Cl]$^{3+}$/[Pc*(-1)Cr(IV)Cl]$^{2+}$ (Table 29).
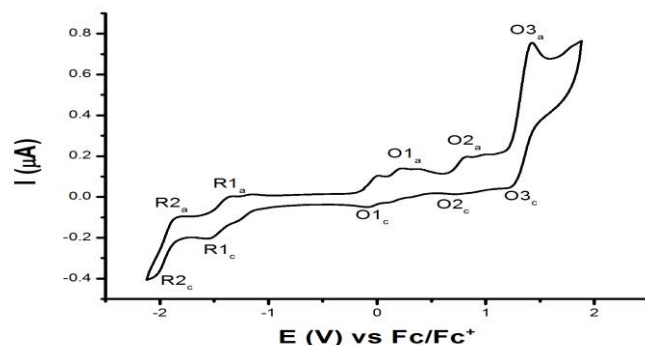
Figure 151: Cyclic voltammogram of 5 mM [Pc*CrCl] in TBAPF$_6$/DCM.

The complex [Ppz*CrCl] shows similar behavior (Figure 152); however, in this case, only two oxidation processes could be observed within the same potential window. This is attributed to the lower electron density of the Ppz* ring compared to the electron density of the Pc* one. Owing to the same reason, the reduction couples shift to less negative potentials. Moreover, while all the redox processes of [Pc*CrCl] show some reversibility, except for R1, no reversibility could be observed in the [Ppz*CrCl] voltammogram.
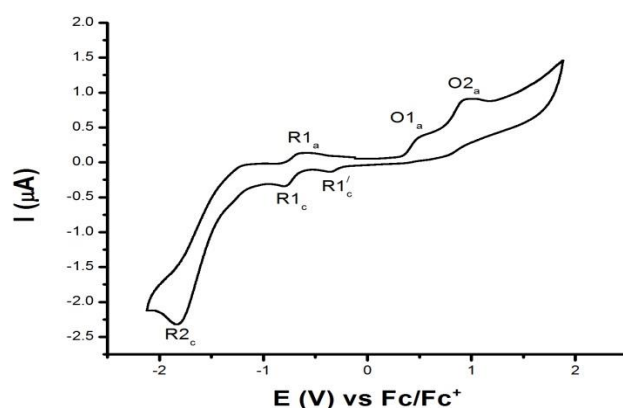
Figure 152: Cyclic voltammogram of 5 mM [Ppz*CrCl] in TBAPF$_6$/DCM.

Table 29: The electrochemical data for the chlorochromium(III) (aza)phthalocyanines.

Complex	Ox.	O1 $[L(-2)Cr^{IV}Cl]^+$ $/[L(-2)Cr^{III}Cl]$	O2 $[L(-1)Cr^{IV}Cl]^{2+}$ $/[L(-2)Cr^{IV}Cl]^+$	O3 $[L(0)Cr^{IV}Cl]^{3+}$ $/[L(-1)Cr^{IV}Cl]^{2+}$	Red.	R1 $[L(-2)Cr^{III}Cl]$ $/[L(-2)Cr^{II}Cl]^-$	R2 $[L(-2)Cr^{II}Cl]^-$ $/[L(-3)Cr^{II}Cl]^{2-}$
[Pc*CrCl]	$E_{1/2}$	0.064	0.772	1.319	$E_{1/2}$	-1.445	-1.935
	ΔE_p	0.281	0.072	0.207	ΔE_p	0.163	0.180
[Ppz*CrCl]	$E_{1/2}$	0.499a	0.945a		$E_{1/2}$	-0.709	-1.842a
	ΔE_p				ΔE_p	0.168	

$E_{1/2} = (E_{p,a} + E_{p,c})/2$ at 100mVs^{-1}. $\Delta E_p = E_{p,a} - E_{p,c}$ at 100mVs^{-1}.   a anodic current

2.6.1.2.6 Germanium azaphthalocyanine [Ppz*Ge(OH)$_2$]

Unlike the SiPcs which experience only ligand based redox processes, as electrochemical reduction to Ge(II) Pcs is known,[277] both metal and ligand based redox processes for GePcs is expected.

The complex displays four redox processes (Figure 153), in comparison with literature,[277] oxidation of the ring, O1, and two successive ring reductions, R1 and R2, (Table 30) are possible. Although the available voltammograms of the GePcs do not show more than two reduction couples, in our study, a third reduction process, R3, followed by a crossing point, *, was observed. This crossing might indicate an associated

121

chemical reaction (removal of the axial ligand and formation of [Ppz*Ge(II)] complex. Hence, we assume the third reduction is a two-electron transfer process corresponding to the metal based process Ge(IV) to Ge(II). Unfortunately, the R3 components are split and rounded; thus, the anodic and/or cathodic current could not be accurately determined.
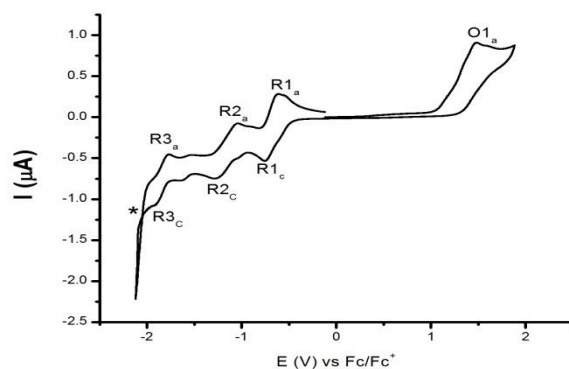
Figure 153: Cyclic voltammogram of 5 mM [Ppz*Ge(OH)$_2$] in TBAPF$_6$/DCM.

Table 30: The electrochemical data for [Ppz*Ge(OH)$_2$].

Complex	Ox.	O1 [Ppz(-1)Ge^{IV}(OH)$_2$]$^+$ /[Ppz(-2)Ge^{IV}(OH)$_2$]	Red.	R1 [Ppz*(-2)Ge^{IV}(OH)$_2$] /[Ppz*(-3)Ge^{IV}(OH)$_2$]$^-$	R2 [Ppz(-3)Ge^{IV}(OH)$_2$]$^-$ /[Ppz(-4)Ge^{IV}(OH)$_2$]$^{2-}$	R3 [Ppz(-4)Ge^{IV}(OH)$_2$]$^{2-}$ /[Ppz(-4)Ge^{II}]$^{4-}$
[Ppz*GeO]	E$_{1/2}$	0.642 [a]	E$_{1/2}$	-1.068[a]		-1.458**
	ΔE$_p$		ΔE$_p$	0.168		0.249

E$_{1/2}$ = (E$_{p,a}$ + E$_{p,c}$)/2 at 100mVs^{-1}.   ΔEp = E$_{p,a}$ – E$_{p,c}$ at 100mVs^{-1}, a anodic current

3 Summary

The aim of this work was to synthesize novel phthalocyanines and pyrazinoporphyrazines with the main group elements and transition metals. The conformational rigidity and the steric bulk of their peripherally annelated cyclohexene rings tend to reduce the degree of aggregation, thus enhancing the solubility of these 42 π- Hückel aromatic system without inhibiting their tendencies to form crystalline phases. For central metals having an oxidation state > II, the possibility of introducing anionic axial ligands L_{ax}, at the metal center was investigated and the optical properties of these chromophores were determined. In addition to their high solubility, some of the synthesized chromophores were found to be sublimable. Phthalocyanines and related compounds are interesting materials for optoelectronic applications; thus, a study of the electronic HOMO and LUMO alignment and coupling of these new chromophores at different heterojunction interfaces is outlined.

[Pc*ML_ax]   [Ppz*ML_ax]
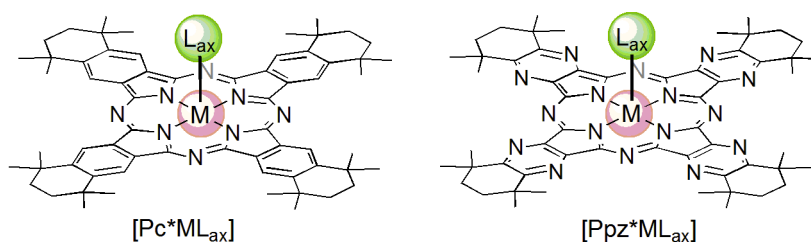
The synthesis of four substituted phthalonitriles and pyrazine dinitriles as chromophore building blocks is discussed.

PDN*   PzDN*   PzDN#   CatPzDN*
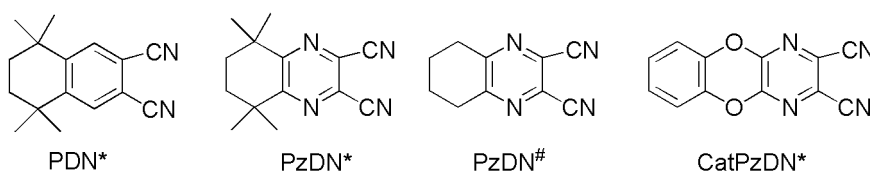
While CatPzDN* does not tetramerize, the usefulness of PzDN# is greatly limited by the poor yield and solubility of its complexes. The use of PDN* and PzDN* as precursors led to the formation of highly soluble macrocycles, which could be analysed by ^{1}H NMR and sometimes by ^{13}C NMR spectroscopy. Moreover, the isomerical purity of the chromophores facilitates their crystallization and analyzing their crystal structures.

3d metal complexes

Except for scandium, Pc*/Ppz* complexes with all 3d elements were prepared:
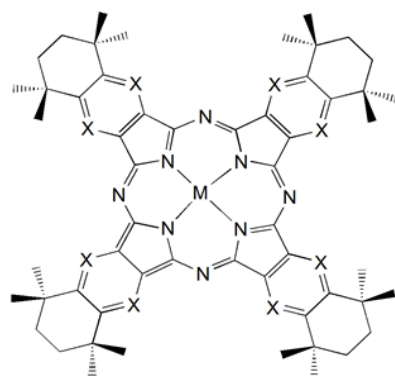
X=CH	X=N
[Pc*TiO]	[Ppz*TiO]
[Pc*VO]	[Ppz*VO]
[Pc*Cr]	[Ppz*Cr]
[Pc*CrCl]	[Ppz*CrCl]
[Pc*MnCl]	[Ppz*MnCl]
[Pc*Fe]	[Ppz*Fe]
[Pc*FeCl]	[Ppz*FeCl]
[Pc*Co]	[Ppz*Co]
[Pc*Ni]	[Ppz*Ni]
[Pc*Cu]	[Ppz*Cu]
[Pc*Zn]	[Ppz*Zn]

In Pc* and Ppz* complexes with chromium and iron, the metal center could be inserted in either oxidation state II or III. Except for [Pc*Fe] and [Pc*FeCl], all the other 3d metal complexes are highly air and light stable. The metal free ligands (Pc*H$_2$ and Ppz*H$_2$) as well as the copper complexes ([Pc*Cu] and [Ppz*Cu]) were found to be sublimable without decomposition. The metal complexes were fully characterized, and, among the 3d metal complexes, the molecular and lattice structure of six chromophores was determined. Representative molecular and lattice structures are shown below:
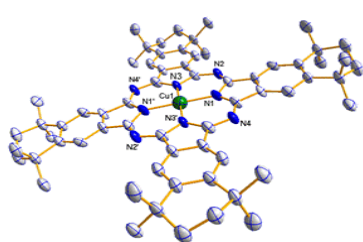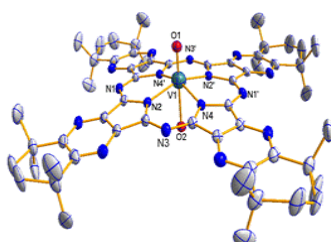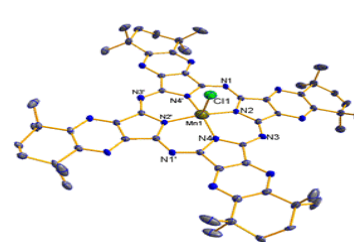
[Pc*Cu]   [Ppz*VO(OH$_2$)]   [Ppz*MnCl]
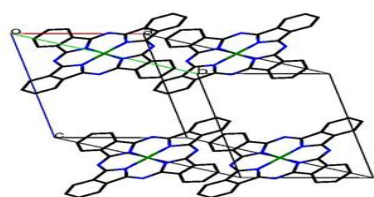
Lattice Structures   [Pc*Co]   [Ppz*VO(OH$_2$)]

124
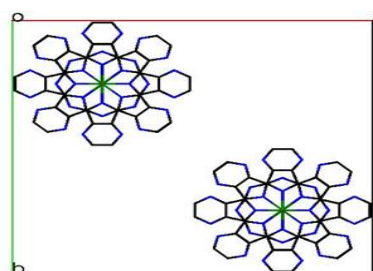
While [Pc*VO] does not coordinate water, it was found that the corresponding [Ppz*VO] coordinates an aqua ligand in an octahedrally configured complex. This is a result of the weaker Lewis acidity of Pc* complex compared to that of the Ppz* counterpart. To distinguish between the d^1 complex [Ppz*VO(OH$_2$)] and the d^0 [Ppz*VO(OH)], the paramagnetic nature of the complex was confirmed by SQUID and the magnetic susceptibility of the complex was found to be temperature dependent.
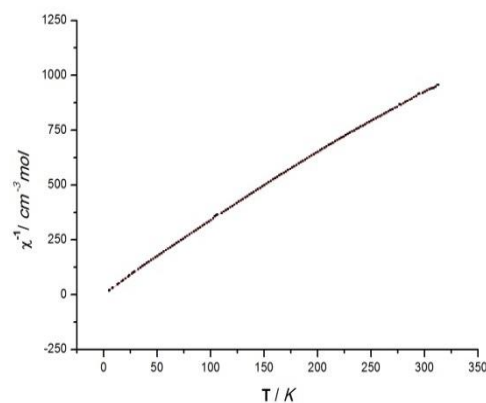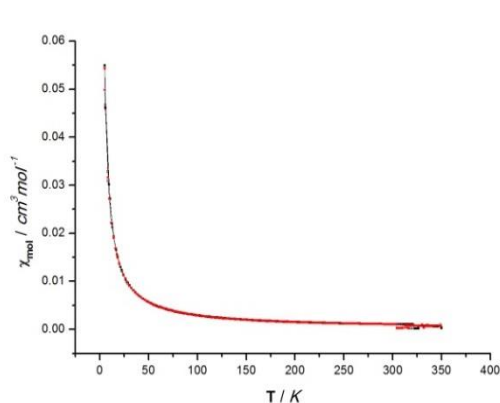
Due to the larger HOMO-LUMO gap of Ppz* complexes compared to Pc* counterparts, the Pc* complexes showed red-shifted Q-bands. The Q-band energy of the 3d complexes almost follows the trend Mn > Ti ≈ V > Cr > Zn ≈ Cu > Co ≈ Ni ≈ Fe. The position of the Q-absorption band in Pc*/Ppz* with Cr and Fe is not affected by the metal oxidation state; however, a broad, weak band, observed in the spectra of [Pc*FeCl] and [Ppz*FeCl] at 878 nm assigned to $a_{1u}(\pi)$ or $a_{2u}(\pi)$ to $e_g(d_{\pi*})$ charge transfer transitions in high spin iron(III) complexes, is used to distinguish between the Fe(II) and Fe(III) complexes.
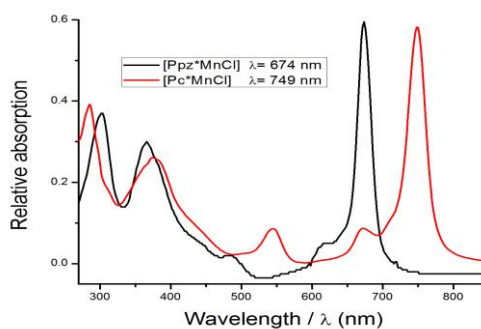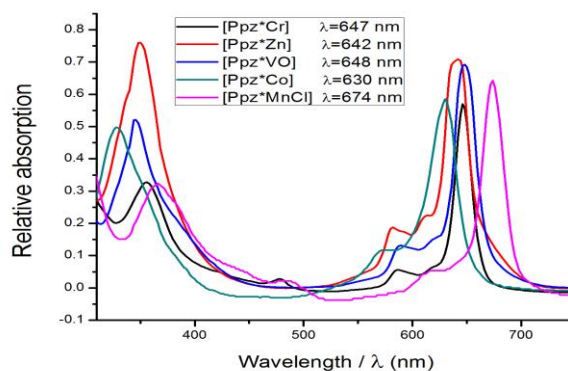
Complexes of main group elements (Groups 13 & 14)

The Pc*/Ppz* complexes of Group 13 (Al, Ga and In) and Group 14 elements (Si and Ge) were also prepared and fully characterized. Solutions of [Pc*InCl] are photosensitive and degrade rapidy in light, while the other complexes show high stability.

X=CH	X=N
[Pc*AlCl]	[Ppz*AlCl]
[Pc*AlF]	[Ppz*AlF]
[Pc*GaCl]	[Ppz*GaCl]
[Pc*GaMe]	[Ppz*InCl]
[Pc*Ga(n-butyl)]	[Ppz*SiCl$_2$]
[Pc*Ga(n-hexyl)]	[Ppz*Ge(OH)$_2$]
[Pc*GaPh]	
[Pc*InCl]	
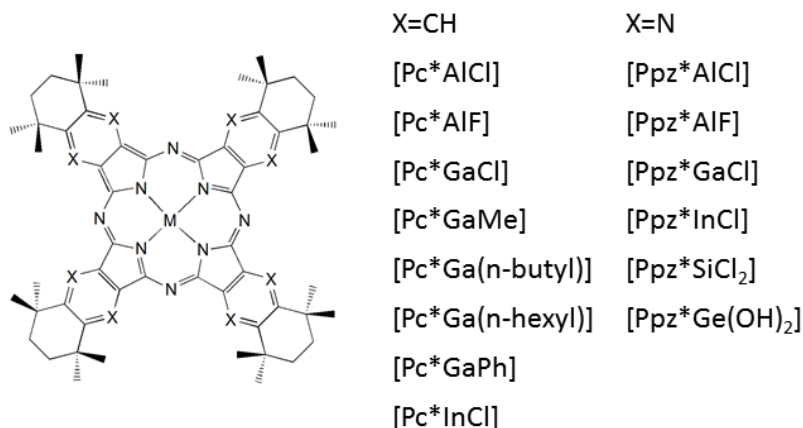
Regarding Group 13, and moving towards heavier atoms (Al→Ga→In), a red-shift of the Q- band was observed; this might be attributed to the reduced Lewis acidity of Group 13 elements in this sequence. However, in the case of Si and Ge complexes, an opposite trend is observed, i.e. the Q-band of [Ppz*Ge(OH)$_2$] is blue-shifted compared to that of [Ppz*SiCl$_2$]. It is believed that different structural configurations of both complexes are responsilble for this inverted trend: Chemically non-equivalent methyl and methylene protons are observed in the ^{1}H NMR spectrum of *cis*-[Ppz*Ge(OH)$_2$] indicative for a complex with a more distorted π-system, whereas [Ppz*SiCl$_2$] is displaying equivalent protons (1a/b and 2a/b) in accord with a trans complex with a perfectly planar aromatic system.
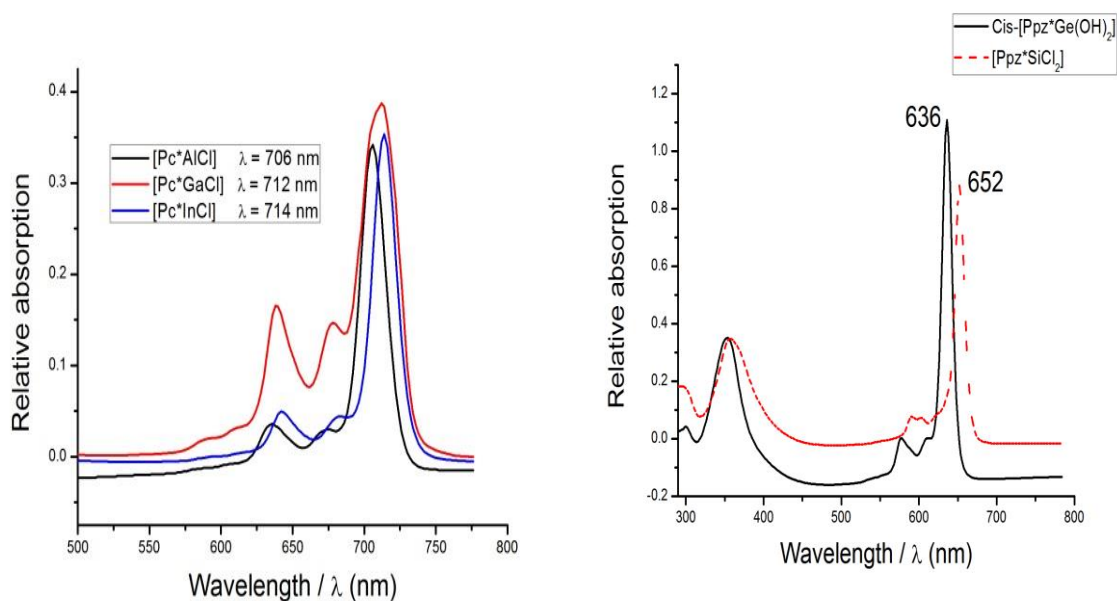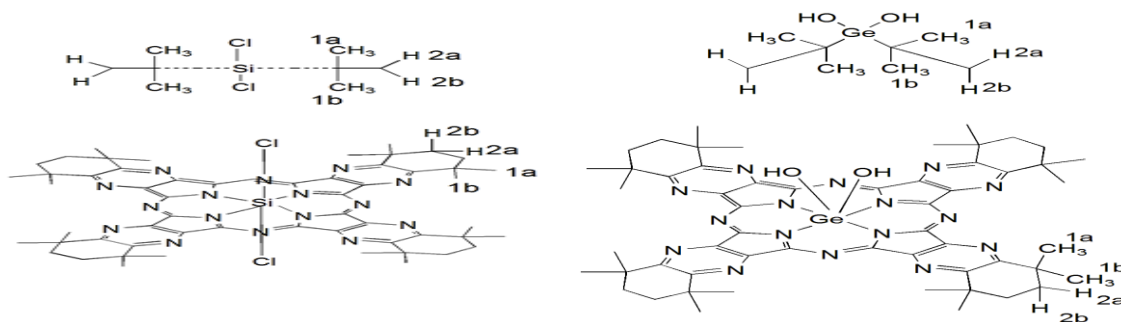
The M-Cl bonds in the case of [Pc*AlCl] and [Pc*GaCl] complexes were found to be more reactive than those of the Ppz* counterparts. While APCI+ MS measurements of [Ppz*AlCl] and [Ppz*GaCl] from THF solutions showed the expected molecular ions [MH]+, the corresponding [Pc*AlCl] and [Pc*GaCl] compounds did show pseudo molecular ions [PcM(thf)]+. These species were probably formed during the ionization process.

Attempts to functionalize tetravalent and trivalent metal complexes were performed. Owing to the ease of reduction of the Ppz* core, reactions involving reducing agents, e.g. potassium graphite, destroyed the ring. Furthermore, the Ppz* chromophores decompose very rapidly in the presence of organolithium reagents or in refluxing polar aprotic solvents, e.g. acetone and THF. However, solutions of Ppz* are quite stable in nonpolar solvents, e.g. toluene and chloroform, even in prescence of light and elevated temperatures. On the other hand, Pc* complexes are more stable with respect to nucleophilic or reducing reagents.

The interesting chromophores [Pc*AlF] and [Ppz*AlF] were obtained when the analogous chloro complexes were refluxed in aqueous KF solutions. Owing to the strong metal-fluorine bond, we anticipate that these chromophores, if orderly attached to a metal semiconductor interface, could promote the exciton dissociation, and hence allow to study the charge transfer dynamics at the semiconductors' heterojunction.
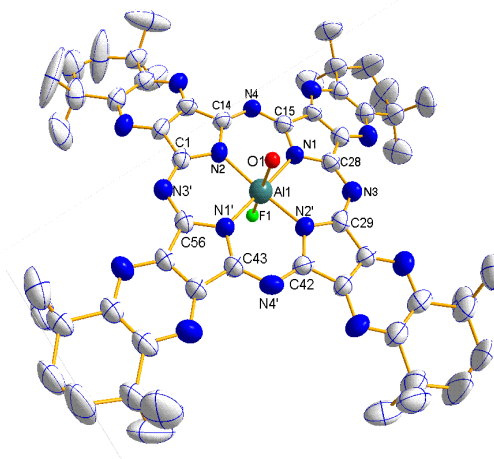
Attempts at synthesizing axial amido, alkyl and phenyl Al/Ga complexes of Pc* and Ppz* were also performed using either lithium or Grignard reagents. In general, the axial n-alkyl (methyl, butyl and hexyl) and phenyl gallium phthalocyanines, [Pc*GaR], were successfully obtained. The electronic spectra of these complexes showed only a very small blue shift of 2 nm of the Q-band relative to [Pc*GaCl].

127
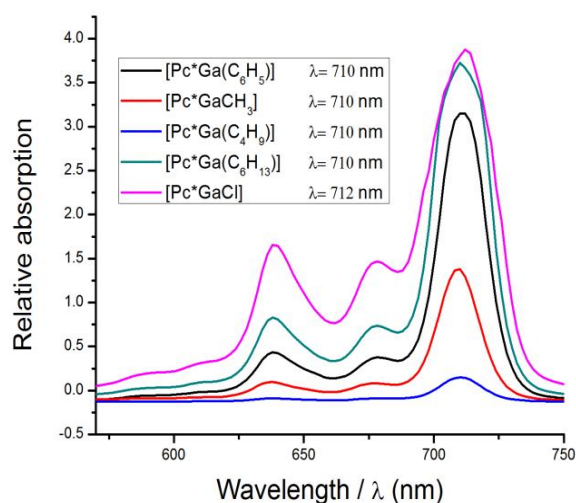
Fluorecence Spectra

The Ppz* complexes show strong fluorescence, which is even observable with the eye. The fluorescence spectra of some Ppz* complexes ([Ppz*TiO], [Ppz*VO], [Ppz*CrCl], [Ppz*AlCl], [Ppz*GaCl] and [Ppz*InCl]) were measured. The Stokes shift for each complex was determined. While the smallest shift was found for [Ppz*TiO] ≈ 2 nm, the largest shift was observed for the [Ppz*VO] ≈ 13 nm.
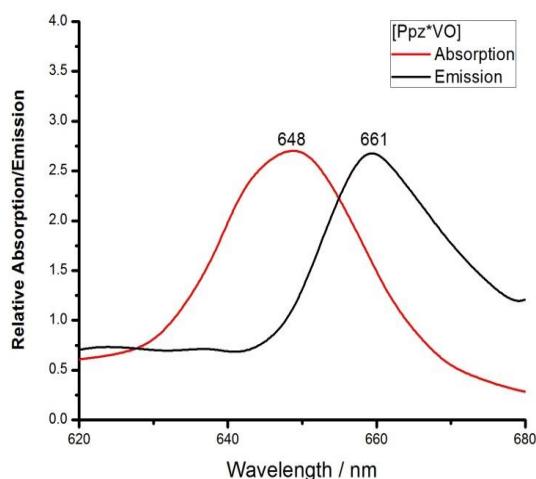
Cyclic Voltammetry

Cyclic voltammograms of the Pc*/Ppz* complexes were measured. The redox processes can be located at the ligand and at the metal center. Reduction of the ligand ([M(II)Pc(−2)] + e ⇔ [M(II)Pc(−3)]$^-$) is associated to the position of LUMO whereas oxidation of the ligand (M(II)Pc(−2) ⇔ [(M(II)Pc(−1)]$^-$ +e) is associated with the position of the HOMO. It is possible to observe two successive one-electron oxidations of the Pc ring tentatively assigned to removal of electrons from the a_{1u} orbital and four successive one-electron reductions into the two e_g orbitals. If metal orbitals lie at energies within the HOMO and LUMO of the macrocycle, oxidation or reduction may occur at the central metal. This is the case for Pc*/Ppz* complexes of Cr, Ti, Mn, Co and Fe.

Within the ligand potential window, some metals, e.g. Ni, Cu, and V, were found to be electronically inactive. In general, Ppz* is more easily reduced compared to the Pc* system, but it is more difficult to oxidize it. Hence, within the same potential window, the number of the reduction processes of Ppz* is equal to or greater than the corresponding number of Pc*. Also, the similar reduction processes of Ppz* must occur at less negative potential compared to the Pc*. Representative voltammograms of [Pc*Cu] and [Ppz*Cu] are shown below. The Pc* complex displayed two oxidation and one reduction process, while the Ppz* complex showed one oxidation and two reduction processes. Apart from the oxidation process of [Ppz*Cu], all the other processes are reversible. However, the anodic current of the oxidation processes of CuPcs is usually much greater than the cathodic current, due to the complexes' tendency to adsorb on the platinum electrodes. In that case, the HOMO-LUMO gap was measured by CV, the more electron rich the ligand is, the smaller the HOMO-LUMO gap: e.g. the gap is 1.664 V and 1.924 V for [Pc*Cu] and [Ppz*Cu], respectively.
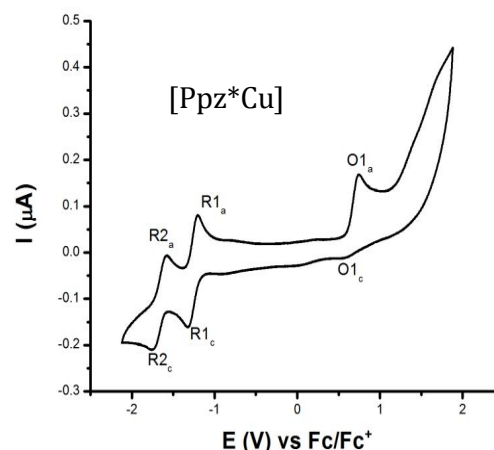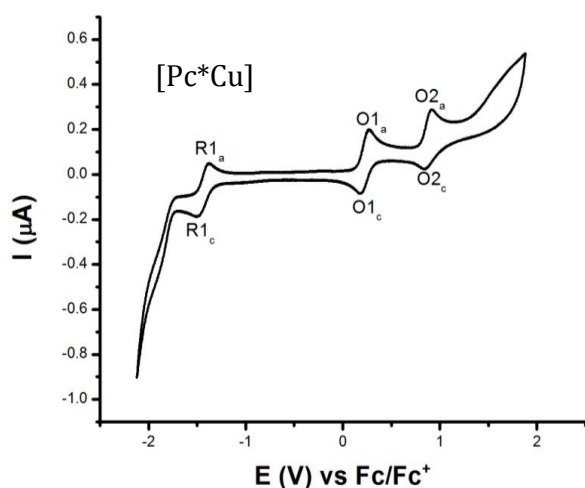
The electrochemical behavior of the Pc* / Ppz* complexes with electoactive metals is more complicated. For example, [Pc*Co], shows three oxidation and one reduction couples. Comparing with literature, the reduction process is metal-based. While the oxidation processes O1, O2 and O3 are assigned to the Pc^{2-}/Pc^{-}, Co^{2+}/Co^{3+} and Pc^{-}/Pc^{0} redox couples, respectively.
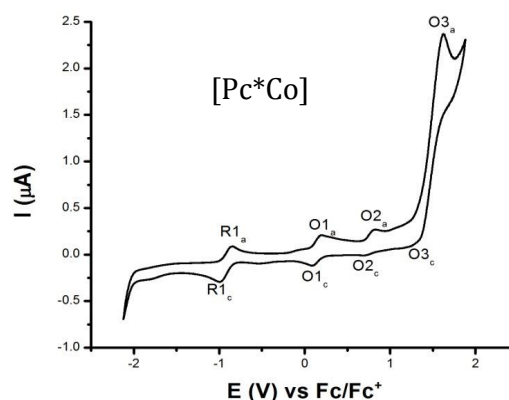
In summary, the formation of soluble and isomerically pure Pc* and Ppz* complexes of the 3d metals as well as Groups 13 & 14 elements was studied. The complexes were formed in

relatively high yields compared to the typical yields for ring substituted Pc complex syntheses. The structure of seven complexes was determined using XRD measurements. The optical and electrochemical characteristics of the complexes, which are important for their application in semiconductor heterojunctions, were systematically studied.

4 Experimental

4.1 General Techniques

All reactions of hydrolysis and / or oxidation sensitive substances were carried out either in neat or in the presence of dry solvents using Schlenk line techniques and under an inert gas atmosphere. A changeable tap line with a rotary vane pump (type Pfeiffer Company DMO 10 M, final pressure approx. 6×10^{-3} mbar) was used. The remaining water in the used nitrogen (purification degree 5.0, Air Liquide Company) was removed using a column filled with P_4O_{10}. Also, handling and storing of hydrolysis and oxidation sensitive compounds was carried out in glove boxes kept under an inert nitrogen atmosphere (Type MB 150 BG-1, manufactured by BRAUN, Lab Master 130, BRAUN Company). Reactions requiring temperatures over 200 °C were carried out in Wood's metal bath.[110]

4.1.1 Solvents, Reagents and Starting materials

All solvents were purified and rigorously dried according to the standard procedures.[178] The solvents were stored under dry argon over absorption columns filled with alumina/ 3Å molecular sieves/ R3-11G catalyst (BASF). Chlorine containing solvents were stored in dark bottles. Chloronaphthalene (CNP) was purchased from Acros as a mixture of 90% of 1-chloronaphthalene and 10% of 2-chloronaphthalene isomers. It was further dried by vacuum distillation over CaH_2.

The compounds/complexes PzDN,[179] PpzH2,[180] [PpzCu],[49] [PcTiO],[181] [PcTiS],[26] and [PcTiS2][26] were synthesized according to previously reported procedures.

All other chemicals were purchased and used directly without any further purification, unless otherwise stated.

4.1.2 Chromatography

The purification by column chromatography was performed at room temperature using silica gel 60 or neutral aluminum oxide 90. Both aluminum oxide and silica gel were purchased from Macherey-Nagel GmbH & Co. Aluminum TLC plates 60 F_{254} (MERCK) were used for thin layer chromatography. For detection, a UV-lamp (λ = (short wave) 254, (long wave) 366 nm) was used.

4.2 Analytical Methods

4.2.1 Elemental Analysis

CHNS analyses were carried out in the Department of Chemistry, Philipps-University Marburg using an ELEMNTAR Vario MICRO cube. Combustion of the samples was carried out at 950°C. Analysis of chlorine was carried out using 636 Titro-processor (Mit). All the values are given as weight percent.

4.2.2 NMR spectroscopy

^{1}H and ^{13}C-NMR spectra were measured in the Department of Chemistry, Philipps-University Marburg using an AV 300 BRUKER (^{1}H: 300.1 MHz, ^{13}C: 75.5 MHz) and deuterated solvents (CDCl$_3$, DMSO-d^6, C$_6$D$_6$ and C$_4$D$_8$O) were used. Measurements at a DRX 400-spectrometer BRUKER Company (^{1}H-NMR: 400.1 MHz, ^{13}C: 100.6 MHz) were carried out by the service for NMR spectroscopy at the Department of Chemistry, Philipps-Universität Marburg. All measurements were carried out at 300 K.

All the chemical shifts δ are reported in ppm, and the following abbreviations were used: s = singlet, d = doublet, t=triplet, m = multiplet and b = broad. Coupling between two nuclei X and Y with spin = ½ over n chemical bonds is indicated by the coupling constant in ^{n}J$_{xy}$ (Hertz). The signals were assigned according to the chemical shift, the integrals and the coupling pattern of the compound. The protons, to which the respective signal was assigned, are shown in italics (CH_2CH$_3$). Calibration of the ^{1}H-NMR and ^{13}C-NMR spectra was done using the residual proton signal of the solvent used[182] (^{1}H-NMR CDCl$_3$: 7.26 ppm, ^{1}H-NMR DMSO-d^6: 2.50 ppm, ^{1}H-NMR C$_6$D$_6$: 7.16 ppm, ^{1}H-NMR C$_4$D$_8$O: 1.73, 3.58 ppm, ^{13}C-NMR CDCl$_3$: 77.16 ppm, ^{13}C-NMR DMSO-d^6: 39.52 ppm, ^{13}C-NMR C$_6$D$_6$: 128.06 ppm, ^{13}C-NMR C$_4$D$_8$O: 25.5 ppm).

The assignment of the protons α, ε or δ of the metal complexes [Pc*M] and [Ppz*M] is shown in Figure 154.
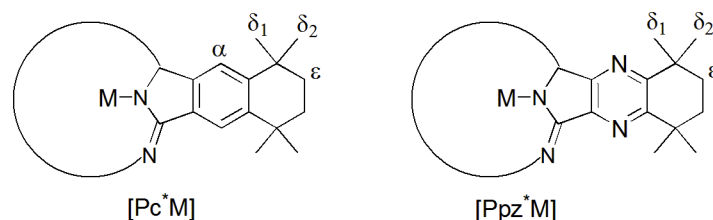
Figure 154: Assignment of the protons of [Pc*M] and [Ppz*M].

4.2.3 IR spectroscopy

The IR spectra were measured by a BRUKER Alpha FT-IR spectrometer including a diamond measuring cell in ATR mode (attenuated total reflection) with neat substances.

To describe the IR signals, some symbols are used, e.g. vs = very strong, s = strong, m = medium, w = weak, vw = very weak, ν = wave number, b = broadened.

4.2.4 UV / Vis. Spectroscopy

The UV/Vis. spectra were recorded in a quartz cuvette with 1 cm coat thickness using an UV-1601 PC spectrometer purchased from Shimadzu Company.

In analysis of the spectra, these abbreviations are used: λ = wavelength, s = strong, m = medium, sh = shoulder, w= weak, b = broadened.

4.2.5 Fluorescence Spectroscopy

Fluorescence spectral measurements were performed using a Varian Cary Eclipse-spectrometer in quartz fluorescence cuvettes of 1 cm pathlength. The excitation wavelength was in the range of 350-600 nm. Measurements were taken in the range of 400-1000 nm with a scan rate of 600 nm / min.

4.2.6 Mass Spectrometry

APCI mass spectra were performed in Department of Chemistry, Philipps-University Marburg using a Finnigan LTQ-FT spectrometer purchased from THERMO FISCHER SCIENTIFIC. Suitable solvents, usually DCM and $CHCl_3$, for sample preparation were used. EI mass spectra were measured with a Finnigan MAT95-Spectrometer of Thermo Fischer Scientific Company. MALDI measurements were performed using a Biflex III spectrometer purchased from Thermo Fischer Scientific Company.

Molecular masses are given as mass to charge ratio (m/z) in atomic mass units (amu). Only signals having the largest isotopic abundance are given. The abundance isotopic ratio was determined theoretically.

4.2.7 Magnetic susceptibility measurements

The magnetic susceptibilities were measured in the Department of Chemistry, Philipps-Universität Marburg using a Quantum Design SQUID magnetometer MPMS-XL. The magnetometer works between 1.8 and 400 K for dc applied fields ranging from -7 to 7 T.

4.2.8 Cyclic Voltammetry measurements

Cyclic voltammetry (CV) data were collected using the Autolab potentiostat PGSTAT 30 (Eco Chemie, Utretcht, The Netherlands) driven NOVA 1.10 software (Metrohm, Autolab B.V, Utrecht, The Netherlands) using the closed Microcell HC setup equipped with a temperature controller (rhd instruments) handled in a glove box (type 150 MB BG-1) manufactured by Braun Company. A three electrode setup consisting of a platinum working electrode (diameter 0.25 mm), a platinum wire psuedo reference electrode and a platinum crucible sample holder (counter electrode) was employed. Ferrocene was used as an internal reference. Electrochemical experiments were performed in dry DCM. The conducting electrolyte (tetrabutylammonium hexafluorophosphate (TBAPF$_6$) for electrochemical analysis (purity ≥ 99.0 %, Fluka)) was used. All measurements were using 5mM of the analyte and 0.1 M of TBAPF$_6$ at 25°C. Prior to scans, the platinum crucible and the working electrode were polished with polishing paste (xylene (0-0.5%) and fumed silica (99.8%), i.e pyrogenic silica, CAS number 112945-52-5) of 0.25 µm mean particle size, followed by washing with pentane and DCM.

4.3 Synthesis of the organic compounds

4.3.1 Synthesis of 6,7-dicyano-1,1,4,4-tetramethyltetraline

4.3.1.1 Synthesis of 2,5-dichloro-2,5-dimethylhexane[189]
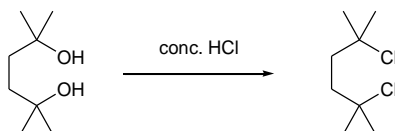
A mixture of 2,5-dimethyl-2,5-hexanediol (30.26 g, 206.9 mmol) and conc. HCl (300 mL) was stirred overnight at room temperature. To the mixture, DCM (300 mL) and water (300 mL) were added to dissolve the pink solid. Then, the aqueous layer was washed with DCM (2x50 mL) and the organics were collected. The combined organic layer was washed with water and 5% NaCl solution, dried using anhydrous MgSO$_4$ and filtered. Finally, the solvent was removed under reduced pressure.

Yield: 35.85 g, 235.5 mmol, 95 %.

^{1}H-NMR (CDCl$_3$, 300 MHz): δ/ ppm = 1.60 (s, 12H, CH_3), 1.95 (s, 4H, CH_2).

4.3.1.2 Synthesis of 1,1,4,4,6,7-hexamethyltetraline[189]
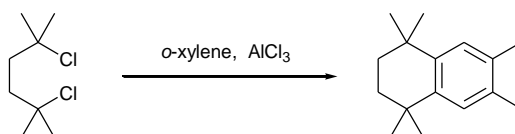
A solution of 2,5-dichloro-2,5-dimethylhexane (39.90 g, 217.9 mmol) in o-xylene (70 mL) was added dropwise to a solution of AlCl₃ (4.32 g , 30 mmol) in o-xylene (100 mL) at 0°C. After 1.5 h, the mixture was warmed up to room temperature and stirred for another 1 h. After filtration and washing with water, the organic phase was washed with 5% NaOH solution (2x50 mL) and distilled water (100 mL), dried over MgSO₄ and filtered before being concentrated under vacuum. The white product was recrystallized from pentane.

Yield: 37.64 g, 174.0 mmol, 80 %.

¹H-NMR (CDCl₃, 300 MHz): δ/ ppm = 1.26 (s, 12H, C(CH_3)₂), 1.66 (s, 4H, CH_2), 2.22 (s, 6H, Ar-CH_3), 7.10 (s, 2H, Ar-H).

4.3.1.3 Synthesis of 1,1,4,4-tetramethyltetraline-6,7-dicarboxylic acid[189]
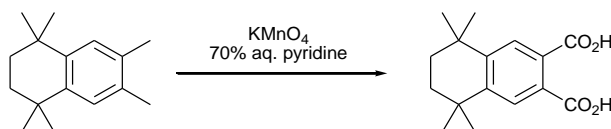
A solution of 1,1,4,4,6,7-hexamethyltetraline (15.06 g, 69.61 mmol) in 70% aqueous pyridine (250 mL) was heated up to 95°C, then KMnO₄ (56.64 g, 358.4 mmol) was added slowly. The mixture was refluxed for 2h, cooled to room temperature, filtered to remove MnO₂ and washed with 70% aqueous pyridine (2x100 mL). Stirring the filtrate was continued overnight until the disappearance of the violet color and formation of another amount of MnO₂. The MnO₂ was filtered and the water - pyridine mixture was concentrated under vacuum, then conc. HCl (200 mL) was added. Stirring the mixture was continued for 1h at 60°C. The resulting white solid was filtered and dried under vacuum.

Yield: 3.44 g, 12.45 mmol, 18 %.

¹H-NMR (DMSO-d⁶, 300 MHz): δ/ ppm = 1.26 (s, 12H, C(CH_3)₂), 1.67 (s, 4H, CH_2), 3.53 (bs, 2H, COOH), 7.58 (s, 2H, Ar-H).

4.3.1.4 Synthesis of 1,1,4,4-tetramethyltetraline-6,7-dicarboxylic acid anhydride[189]
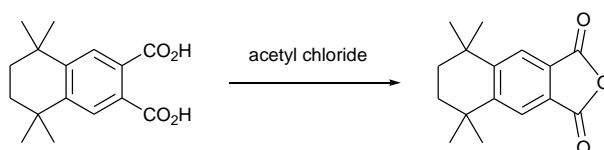
A mixture of 1,1,4,4-tetramethyltetraline-6,7-dicarboxylic acid (12.11 g, 43.82 mmol) and acetyl chloride (50 mL) was refluxed for 3h. Subsequently, the acetyl chloride was

removed under vacuum. The residue, 1,1,4,4-tetramethyltetraline-6,7-dicarboxylic acid anhydride, was obtained as a white precipitate.

Yield: 10.87 g, 42.08 mmol, 96 %.

¹H-NMR (CDCl₃, 300 MHz): δ/ ppm =1.36 (s, 12H, C(CH_3)₂), 1.75 (s, 4H, CH_2) 7.96 (s, 2H, Ar-*H*).

4.3.1.5 Synthesis of 1,1,4,4-tetramethyltetraline-6,7-dicarboxylic acid imide[189]
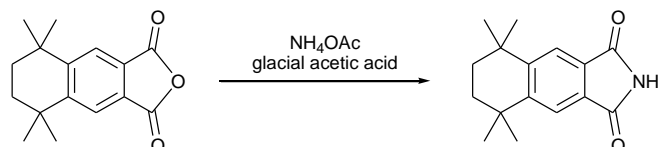
A mixture of 1,1,4,4-tetramethyltetraline-6,7-dicarboxylic acid anhydride (9.00 g, 34.84 mmol), ammonium acetate (9.06 g, 117.5 mmol) and glacial acetic acid (36 mL) was refluxed for 1 h. Subsequently, the unreacted glacial acetic acid was removed under vacuum and the residue was treated with 10% aqueous Na_2CO_3 solution (100 mL). The white solid was filtered, washed with water and dried under vacuum.

Yield: 8.52 g, 33.11 mmol 95 %.

¹H-NMR (CDCl₃, 300 MHz): δ / ppm = 1.33 (s, 12H, C(CH_3)₂), 1.73 (s, 4H, CH_2), 7.50 (bs, 1H, N*H*), 7.82 (s, 2H, Ar-*H*).

4.3.1.6 Synthesis of 1,1,4,4-tetramethyltetraline-6,7-dicarboxylic acid amide[189]
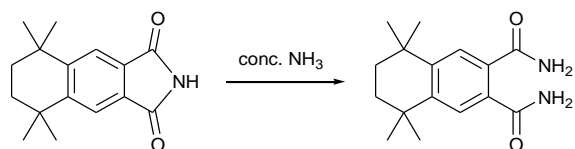
A mixture of 1,1,4,4-tetramethyltetraline-6,7-dicarboxylic acid imide (3.51 g, 13.64 mmol) and ammonia solution (25 %, 50 mL) was stirred for 24 h at room temperature. The resulting white solid was filtered, washed with dilute ammonia solution and dried under vacuum.

Yield: 2.74 g, 9.97 mmol, 73 %.

¹H-NMR (CDCl₃, 300 MHz): δ /ppm = 1.30 (s, 12H, C(CH_3)₂), 1.70 (s, 4H, CH_2), 5.77 (bs, 2H, NH_2), 6.66 (bs, 2H, NH_2), 7.63 (s, 2H, Ar-*H*).

4.3.1.7 Synthesis of 6,7-dicyano-1,1,4,4-tetramethyltetraline PDN*[189]
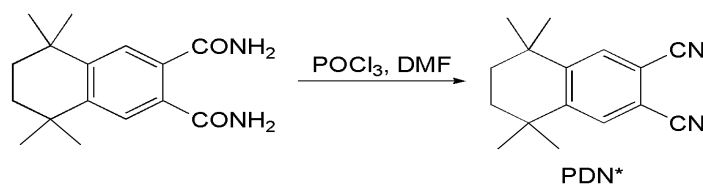
To a suspension of 1,1,4,4-tetramethyltetraline-6,7-dicarboxylic acid amide (1.8 g, 6.561 mmol) in DMF (19 mL) at about 0 °C, phosphoryl chloride (2.24 g, 14.61 mmol) was added slowly. The reaction mixture was stirred for 2.5 h at 5-10 °C before warming up to room temperature, then water (100 mL) was added. The white product was filtered, purified by column chromatography (CH_2Cl_2, silica gel) and dried under reduced pressure.

Yield: 1.07 g, 4.489 mmol, 68 %.

^{1}H-NMR (CDCl$_3$, 300 MHz): δ / ppm = 1.30 (s, 12H, C(C*H*$_3$)$_2$), 1.72 (s, 4H, C*H*$_2$), 7.71 (s, 2H, Ar-*H*).

4.3.2 Synthesis of 6,7-dicyano-1,1,4,4-tetramethyltetraline(other procedures)

4.3.2.1 Synthesis of 1,1,4,4-tetramethyltetraline[314]
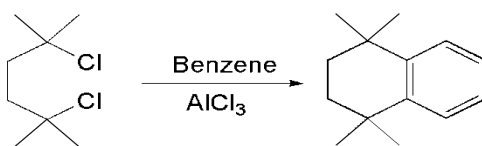
A solution of 2,5-dichloro-2,5-dimethylhexane (23.701 g, 129.4 mmol) in benzene (800 mL) was stirred for 10 minutes at 50 °C. Anhydrous AlCl$_3$ (6.873 g, 51.7 mmol) was added in small portions over 30 minutes. Afterwards, the solution was stirred at 55 °C for 24 hours. The resulting material was cooled to room temperature and the solvent was removed under vacuum. Dilute HCl solution was added, then the product was extracted using DCM. The organics were washed with water and dilute Na$_2$CO$_3$ solution, dried using MgSO$_4$ and filtered. The brown product was mixed with activated charcoal and filtered again. After removing the solvent under reduced pressure, the product was obtained as a yellow oil.

Yield: 22.37 g,118.8 mmol, 92 %.

^{1}H-NMR (300 MHz, CDCl$_3$): δ/ppm = 7.30 (d, 2H), 7.14 (d, 2H), 1.69 (s, 4H, C*H*$_2$), 1.29 (s, 12H, C(C*H*$_3$)$_2$).

4.3.2.2 Synthesis of 6,7-dibromo-1,1,4,4-tetramethyltetraline[314]
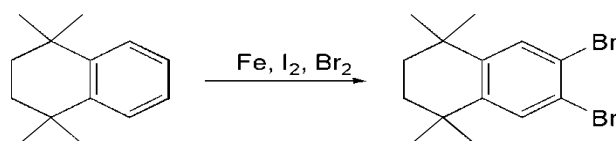
1,1,4,4-tetramethyltetraline (22.371 g, 118.8 mmol) was dissolved in DCM (350 mL), then iron powder (793 mg, 14.3 mmol) and iodine (302 mg, 1.2 mmol) were added. The mixture was cooled to 0°C and bromine (12.4 mL, 237.6 mmol) was added over 30 minutes. After completion of the addition, the reaction was allowed to warm up to room temperature and stirred for 24 hours. The mixture was washed with aqueous sodium thiosulfate and sodium bicarbonate to remove the unreacted bromine, then DCM and water were added. The organic layer was washed with water and NaCl solution, dried over $MgSO_4$ and filtered. The dark solution obtained was mixed with activated charcoal and filtered again, then dried under reduced pressure. The resulting solid was purified by column chromatography (PE:DCM (3:2), silica gel). After removing the solvent under reduced pressure, the product was obtained as a brownish-yellow solid.

Yield: 39.18 g, 113.2 mmol, 95 %.

^{1}H-NMR (300 MHz, CDCl$_3$): δ/ppm = 7.50 (s, 2H), 1.66 (s, 4H, CH_2), 1.25 (s, 12H, C(CH_3)$_2$).

4.3.2.3 Synthesis of 6,7-dicyano-1,1,4,4-tetramethyltetraline[314]
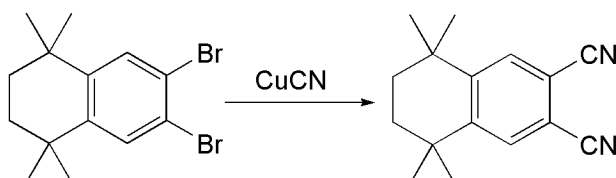
A mixture of 6,7-dibromo-1,1,4,4-tetramethyltetraline (1.52 g, 4.39 mmol) and CuCN (1.97 g, 21.99 mmol) was refluxed in dry DMF (15 mL) under argon for 16 h. The reaction mixture was then cooled to room temperature and poured into an ammonia solution (15 mL). Afterwards, the mixture was stirred for 24 h. The resulting material was extracted with diethyl ether, washed with water and Na_2CO_3, dried over $MgSO_4$ and filtered. The product was purified by column chromatography (PE:Et$_2$O (7:1), silica gel) and dried under vacuum.

Yield: 261 mg, 1.097 mmol, 25 %.

^{1}H-NMR (CDCl$_3$, 300 MHz): δ / ppm = 1.30 (s, 12H, C(CH_3)$_2$), 1.72 (s, 4H, CH_2), 7.71 (s, 2H, Ar-H).

Additional information

Attempted synthesis of the precursor using common procedures for cyanation of aryl bromides were unsuccessful.
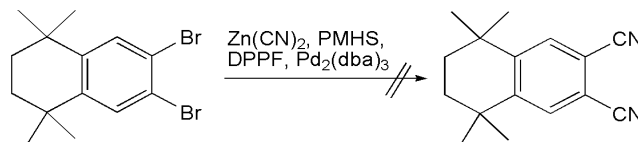
A mixture of 6,7-dibromo-1,1,4,4-tetramethyltetraline (7 g, 20.22 mmol), tris(dibenzylideneacetone)dipalladium (Pd$_2$(dba)$_3$, 370 mg, 0.4 mmol), 1,1′-bis(diphenylphosphino)ferrocene (DPPF, 303 mg, 0.5 mmol) and Zn(CN)$_2$ (2.375 g, 20.2 mmol) was dissolved in DMA (40 mL), then polymethylhydrosiloxane (PMHS, 0.4 mL) was added. The mixture was stirred overnight at 115 °C. As checked by TLC, no reaction took place.

4.3.3 2,3-Dicyano-5,5,8,8-tetramethyl-5,6,7,8-tetrahydroquinoxaline

4.3.3.1 Synthesis of 2,2,5,5-tetramethyladipic acid[191]
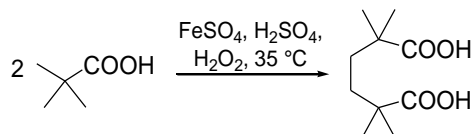
A 4 L reaction flask equipped with a KPG stirrer and two dropping funnels was charged with water (1200 mL), conc. sulfuric acid (15 mL) and pivalic acid (102.13 g, 1 mol). While the mixture was vigorously agitated, a hydrogen peroxide solution (150 mL, 6.67 M) and a ferrous sulfate solution (750 mL, 1.33 M, prepared from ferrous sulphate pentahydrate (278 g), sulfuric acid (55 mL) and water (575 mL)) were added simultaneously and equivalently. The temperature was held at 35°C by means of an ice bath during the 15 minutes required for the addition. Afterwards, a heater and a condenser were attached to the flask and about 500 mL of a mixture comprising water and pivalic acid was distilled. During distillation, a white crude product was formed. The product was purified by adding a conc. ammonia solution (100 mL, 35 %) and filtring to remove the iron compounds. The excess ammonia was boiled off, water (50 mL) was added, then a conc. HCl solution (50 mL) was added to precipitate the acid. The white resulting solid was separated and recrystallized from glacial acetic acid (1 mL / g).

Yield: 12.03 g, 59.48 mmol, 12 %.

^{1}H-NMR (300 MHz, DMSO-d^6): δ / ppm = 12.07 (s, 2H, COO*H*), 1.37 (s, 4H, C*H$_2$*), 1.06 (s, 12H, C*H$_3$*).

4.3.3.2 Synthesis of 2,2,5,5-tetramethyladipic acid diethyl ester[192]
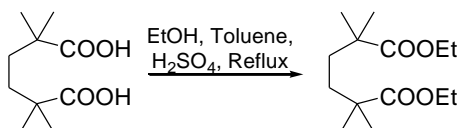
A mixture of 2,2,5,5-tetramethyladipic acid (15 g, 74.17 mmol), toluene (300 mL), ethanol (50 mL) and conc. sulfuric acid (4 mL) was refluxed for 20 h. Both the organic and aqueous layers were separated then the aqueous layer was washed with toluene (3x50 mL). The organics were collected and concentrated under vacuum, then diethyl ether (100 mL) was added. The combined organic layer was washed again using 10% Na_2CO_3 solution (3x50 mL), dried over $MgSO_4$, filtered and concentrated under vacuum. The product was obtained as a yellow liquid.

Yield: 15.38 g, 59.53 mmol, 80 %.

^{1}H-NMR (300 MHz, $CDCl_3$): δ / ppm = 4.11 (q, 4H, CH_2CH$_3$), 1.42 (s, 4H, CH_2), 1.23 (t, 6H, CH$_2$CH_3), 1.13 (s, 12H, C(CH_3)$_2$).

4.3.3.3 Synthesis of 3,3,6,6-tetramethyl-1,2-bis(trimethylsiloxy)cyclohexene[192]
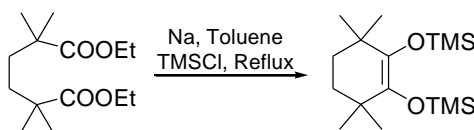
A mixture of sodium (5.50 g, 239.2 mmol) and toluene (700 mL) was refluxed until a suspension was obtained. After cooling to 90°C, trimethylsilyl chloride (26 mL, 205.3 mmol) and 2,2,5,5-tetramethyladipinic acid diethyl ester (10 g, 38.71 mmol) were added under argon. The mixture was refluxed for 20 h, cooled to room temperature and filtered over celite under an argon atmosphere. The residue was washed with THF (2x50 mL). After removing the solvent, the product was obtained as a yellow liquid.

Yield: 10.74 g, 34.14 mmol, 88 %.

^{1}H-NMR (CDCl$_3$, 300 MHz): δ = 0.19 (s, 18H, Si(CH_3)$_3$), 1.02 (s, 12H, C(CH_3)$_2$), 1.44 (s, 4H, CH_2) ppm.

4.3.3.4 Synthesis of 3,3,6,6-tetramethylcyclohexane-1,2-dione[192]
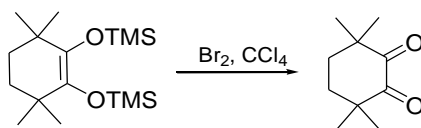
To a solution of 3,3,6,6-tetramethyl-1,2-bis(trimethylsiloxy)cyclohexene (6.15 g, 19.55 mmol) in CCl$_4$ (100 mL), Br$_2$ (1.1 mL, 21.36 mmol) was added dropwise. The solvent was

removed under reduced pressure. After drying under vacuum, the product was obtained as a yellow solid.

Yield: 3.26 g, 19.38 mmol, 99 %.

¹H-NMR (300 MHz, CDCl₃): δ / ppm = 1.86 (s, 4H, CH_2), 1.15 (s, 12H, CH_3).

4.3.3.5 Synthesis of 2,3-dicyano-5,5,8,8-tetramethyl-5,6,7,8-tetrahydroquinoxaline PzDN*[198]
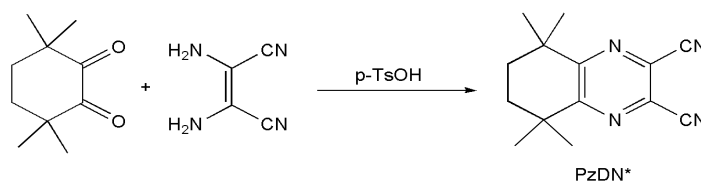
A mixture of 3,3,6,6-tetramethylcyclohexane-1,2-dione (5.00 g, 29.72 mmol) and DAMN (3.86 g, 35.71 mmol) was dissolved with a spatula tip of p-toluenesulfonic acid in dry ethanol (100 mL) and refluxed for 5 h. This resulted in a brown solution. After cooling, the solvent was removed under reduced pressure and the crude product was extracted with DCM. The DCM was removed and the product was purified by column chromatography ((DCM: PE) 1:1, silica gel). After drying under vacuum, the product was obtained as a pale yellow solid.

Yield: 5.17 g, 21.51 mmol, 72 %.

¹H-NMR (300 MHz, CDCl₃): δ / ppm = 1.85 (s, 4H, CH_2), 1.36 (s, 12H, CH_3).

4.3.4 Synthesis of 2,3-dicyanopyrazino[6,5-e]benzo[b][1,4]dioxane CatPzDN*

4.3.4.1 Synthesis of 2,3-dioxo-1,2,3,4-tetrahydropyrazine-5,6-dicarbonitrile[195]
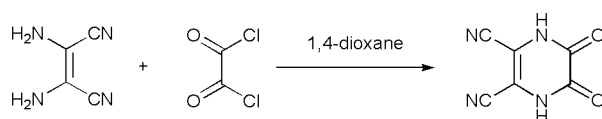
A solution of DAMN (9.6 8 g, 90.7 mmol) in dioxane (500 mL) was added dropwise to a vigorously stirred solution of oxalyl chloride (18.3 mL, 212 mmol) in dioxane (250 mL) over 3 h at 50°C. Stirring was continued at this temperature for another 3 hours. The precipitate was removed by filtration and the filtrate was concentrated under reduced pressure. The obtained product was purified by column chromatography (acetone, silica gel) and dried under vacuum.

Yield: 12.42 g, 76.6 mmol, 85 %.

¹³C-NMR (DMSO-d⁶), 75 MHz): δ/ppm = 105.9 (2C, C$_{Ar}$-CN), 111.1 (2C, CN), 155.0 (2C, C=O).

4.3.4.2 Synthesis of 5,6-dichloropyrazine-2,3-dicarbonitrile[195]
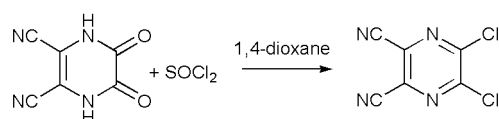
A mixture of 2,3-dioxo-1,2,3,4-tetrahydropyrazine-5,6-dinitrile (10.0 g, 61.7 mmol) and thionyl chloride (22 mL, 303 mmol) in dioxane (400 mL) was stirred at 60°C for 1 h. DMF (10 mL, 130 mmol) was added and the dark reaction mixture was stirred at this temperature for another 1.5 h. The solvent was removed under reduced pressure and the residue was extracted with hot toluene (3x 100 mL). After removong the solvent, a crude tan solid was obtained. The solid was chromatographed (acetone, silica gel). After removing the solvent under vacuum, the product was obtained as a yellow solid.

Yield: 7.69 g, 43.93 mmol, 71 %.

^{13}C-NMR (DMSO-d^6, 75 MHz): δ/ppm =125.5 (2C, C$_{Ar}$-CN), 110.7 (2C, CN), 153.9 (2C, C$_{Ar}$-Cl).

4.3.4.3 Synthesis of 2,3-dicyanopyrazino[6,5-e]benzo[b][1,4]dioxane CatPzDN*
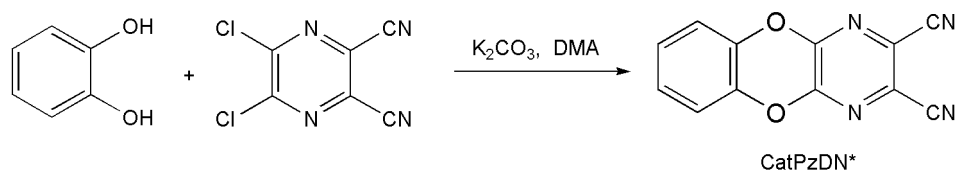
In a 250 mL round bottomed flask, 5,6-dichloropyrazine-2,3-dicarbonitrile (4.86 g, 24.4 mmol), dry K_2CO_3 (10.0 g, 72.4 mmol) and dry DMA (60 mL) were placed under an argon atmosphere. Then, catechol (2.68 g, 24.4 mmol) was added. The resulting mixture was stirred under argon at room temperature for 16h and at 50°C for 3h. Afterwards, it was poured into cold water (200 mL). The precipitate was collected by filtration and subjected to column chromatography (acetone, silica gel). After removing the solvent under vacuum, the desired product was isolated as a pale yellow solid.

Yield: 0.501 g, 2.12 mmol, 9 %.

Elemental analysis: ($C_{12}H_4N_4O_2$, 236.19 g/mol)

Found (Calculated): C: 58.70%(61.02 %), H: 1.83%(1.71 %), N: 22.48%(23.72 %).

^{1}H-NMR (DMSO-d^6, 300 MHz): δ/ppm =7.43 (d, 2 H), 7.52 (d, 2H).

4.3.5 Synthesis of 2,3-dicyano-5,6,7,8-tetrahydroquinoxaline PzDN#[222]
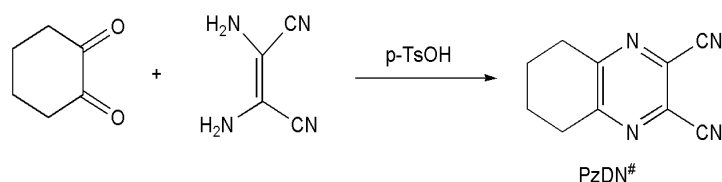
DAMN (2.64 g, 22.77 mmol), 1,2-cyclohexanedione (5.49 g, 48.96 mmol) and a spatula tip of p-toluenesulfonic acid were refluxed for 2 h in absolute ethanol (100 mL). After removing the solvent under reduced pressure, the product was extracted into the organic phase with diethyl ether (3x50 mL). After removing the solvent, the desired product was obtained as a yellow solid.

Yield: 3.12 g, 16.94 mmol, 69 %.

^{1}H-NMR (DMSO-d^6, 300 MHz): δ/ ppm = 1.92 (t, 4H), 3.05 (t, 4H).

4.3.6 Synthesis of 2,4-bis(4-phenoxyphenyl)-1,3,2,4-dithiadiphosphetan-2,4-disulphide.[315]
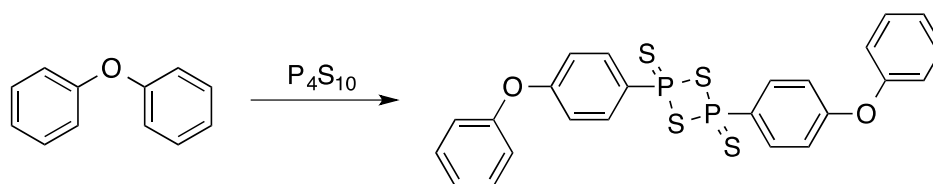
A mixture of P_4S_{10} (8.8 g, 19.798 mol) and diphenylether (35 mL, 217.7 mmol) was stirred under nitrogen at 160 °C for 9 hours, then at room temperature for 15 hours. The yellow product was filtered, washed with dry toluene and dried under vacuum.

Yield: 10.98 g, 20.8 mmol, 53 %.

^{1}H-NMR (300 MHz, C_4D_8O): δ/ppm = 8.50 (q, 2H), 7.44-6.96 (m, 16H).

^{13}C-NMR (300 MHz, C_4D_8O): δ/ppm = 193.6, 189.1, 188.6, 183.9, 182.0, 179.3, 177.7, 176.4.

MS(APCI-HRMS(+)):m/z=528.9929[MH]$^+$,calcd. for[$C_{24}H_{18}O_2P_2S_4H$]$^+$:528.9738.

MS (EI): m/z = 170 [$C_6H_4PS_2$]$^+$, 141 [C_6H_4PS]$^+$.

4.3.7 Synthesis of Woollin's Reagent

4.3.7.1 Synthesis of 1,2,3,4,5-pentaphenylpentaphospholane[317]
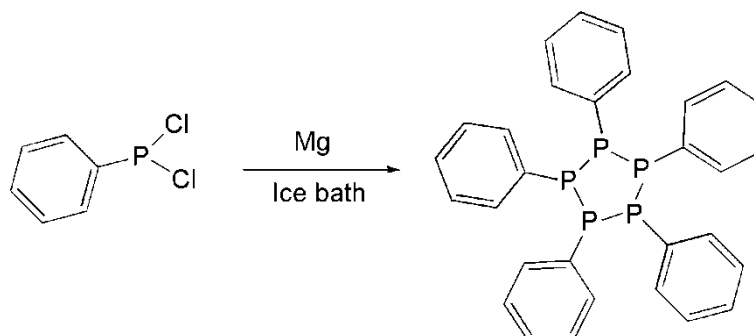
A mixture of PhPCl$_2$ (15.2 mL, 111.7 mmol) and Mg turnings (2.716 g, 111.7 mmol) was stirred in THF (100 mL) for 4 hours under nitrogen. Room temperature was maintained by means of an ice/water bath. Acetone (6 mL) was added and the excess Mg was filtered off. Water (100 mL) was added and the mixture was concentrated under reduced pressure until a precipitate was formed. The white product (PPh)$_5$ was collected by suction filtration and dried under vacuum.

Yield: 8.83 g, 81.7 mmol, 73 %.

^{1}**H-NMR** (300 MHz, C$_6$D$_6$): δ/ppm = 8.05-6.84 (m, 25H).

^{1}**H-NMR** (300 MHz, CDCl$_3$): δ/ppm = 7.93-7.76 (m, 10H), 7.63-7.57 (m, 5H), 7.54-7.47 (m, 10H).

4.3.7.2 Synthesis of 2,4-diphenyl-2,4-diselanylene-1,3,2,4-diselenadiphosphetane[317]
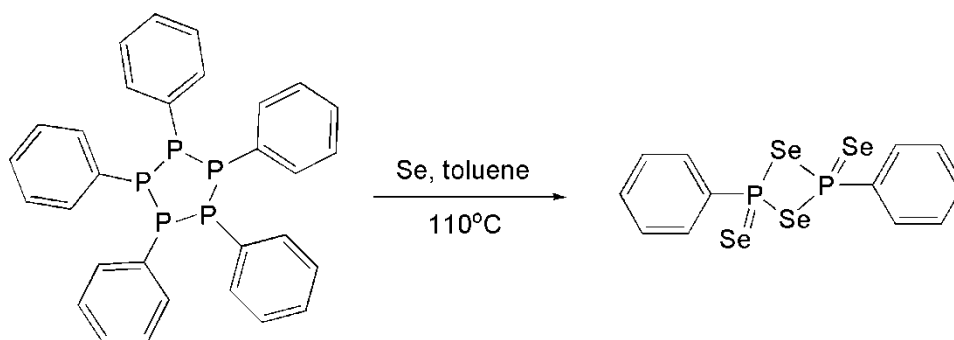
A mixture of (PPh)$_5$ (3.6 g, 6.7 mmol) and Se (3.6 g, 6.7 mmol) was refluxed in dry toluene (80 mL) for 5 h under nitrogen. After cooling to room temperature, the red product was collected by suction filtration, washed with toluene and dried under vacuum.

Yield: 8.00 g, 15.0 mmol, 90 %.

MS (EI): m/z = 266 [C$_6$H$_5$PSe$_2$]$^+$, 219 [P$_2$Se$_2$]$^+$.

4.3.8   Synthesis of [Ti(S-t-butyl)$_4$][318]

To a solution of Ti(NMe$_2$)$_4$ (1.323 g, 5.9 mmol) in pentane (5 mL) at 25 °C, tert-butylthiol (6.7 mL, 59.0 mmol) was added. Immediately after the addition, the solution became dark red. The pentane and excess tert-butylthiol were removed under vacuum and the dark residue was extracted with pentane (2x30 mL). The extracts were concentrated to 10 mL. Cooling the solution at -20 °C led to formation of the desired compound as red microcrystals.

Yield: 2.173 g, (5.4 mmol, 91.01%).

^{1}H-NMR (300 MHz, C$_6$D$_6$): δ/ppm = 1.76 (s, CMe$_3$).

^{13}C-NMR (300 MHz, C$_6$D$_6$): δ/ppm = 58.8 (s, CMe_3), 36.1 (s, CMe$_3$).

4.4   Synthesis of Pc* complexes

4.4.1   New synthetic method for [Pc*TiO]
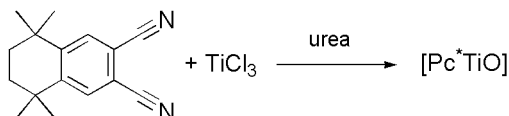
A mixture of PDN* (300 mg, 1.26 mmol), urea (149 mg, 2.49 mmol) and TiCl$_3$ (97 mg, 0.63 mmol) was heated at 220°C under an argon atmosphere for 30 minutes. The product was washed with diethyl ether (2x20 mL), and purified by column chromatography (CHCl$_3$, Al$_2$O$_3$). After removing the solvent, the product was obtained as a green solid.

Yield: 168 mg, 0.165 mmol, 52 %.

Elemental analysis: (C$_{64}$H$_{72}$N$_8$TiO, 1017.17 g/mol)

Found (Calculated): C: 77.61% (75.57%), H: 7.57% (7.13%), N: 9.33 % (11.02 %).

^{1}H-NMR (300 MHz, CDCl$_3$): δ/ppm = 9.63 (s, 8H, Ar-H), 2.09 (s, 16H, H$_\varepsilon$) , 1.89 (s, 24H, H$_{\delta 1}$), 1.81 (s, 24H, H$_{\delta 2}$).

^{13}C-NMR (75 MHz, CDCl$_3$): δ/ppm = 152.3, 149.3, 135.1, 121.9, 36.1, 35.6, 33.1, 29.6.

UV/Vis. (CHCl$_3$): λ/nm = 716 (s), 682 (sh), 645 (w), 390 (sh), 348 (m), 301 (m), 277 (m), 244 (m).

MS (APCI-HRMS(+)): m/z = 1017.5381[MH]$^+$, calcd. for C$_{64}$H$_{73}$N$_8$TiO$^+$: 1017.5389.

4.4.2 Attempted synthesis of [Pc*Ti(PO₄H)]
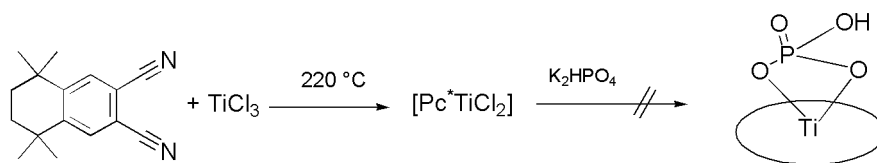
A mixture of PDN* (300 mg, 1.26 mmol), urea (149 mg, 2.49 mmol) and TiCl$_3$ (97 mg, 0.63 mmol) was heated at 220°C under an argon atmosphere for 30 minutes. To the purple product, K$_2$HPO$_4$ (242 mg, 1.389 mmol) and dry toluene (50 mL) were added, then the mixture was heated at 130°C for 4 hours. After cooling, the mixture was concentrated under reduced pressure, and purified by column chromatography (CHCl$_3$, Al$_2$O$_3$). The green product was isolated and characterized as [Pc*TiO].

4.4.3 Synthesis of [Pc*VO]
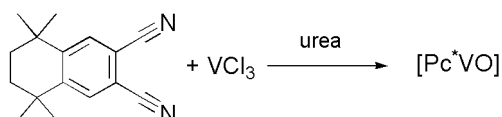
A mixture of PDN* (300 mg, 1.26 mmol), urea (149 mg, 2.49 mmol) and VCl$_3$ (99 mg, 0.63 mmol) was heated at 220°C under an argon atmosphere for 30 minutes. The product was washed with diethyl ether (2x20 mL) and purified by column chromatography (CHCl$_3$, Al$_2$O$_3$). After removing the solvent, the product was obtained as a green solid.

Yield: 162 mg, 0.158 mmol, 50 %.

Elemental analysis: (C$_{64}$H$_{72}$N$_8$VO, 1020.25 g/mol)

Found (Calculated): C: 72.35% (75.34%), H: 7.62% (7.11%), N: 8.66% (10.98%).

UV/Vis. (CHCl$_3$): λ/nm = 717 (s), 685 (sh), 646 (w), 348 (m), 298 (m), 278 (sh), 250 (m).

MS (APCI-HRMS(+)): m/z = 1020.5335 [MH]$^+$, calcd. for C$_{64}$H$_{73}$N$_8$VO$^+$: 1020.5342.

4.4.4 New synthetic method for [Pc*Cr]
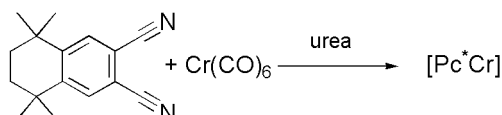
A mixture of PDN* (300 mg, 1.26 mmol), urea (149 mg, 2.49 mmol) and [Cr(CO)$_6$] (139 mg, 0.63 mmol) was heated at 220°C under an argon atmosphere for 30 minutes. The product was washed with diethyl ether (2x20 mL) and purified by column

chromatography (CHCl$_3$, Al$_2$O$_3$). After removing the solvent, the product was obtained as a green solid.

Yield: 93 mg, 0.0925 mmol, 29 %.

Elemental analysis: (C$_{64}$H$_{72}$N$_8$Cr, 1005.30 g/mol)

Found (Calculated): C: 73.87% (76.46%), H: 7.61% (7.22%), N: 10.17% (11.15%).

UV/Vis. (CHCl$_3$): λ/nm =708 (s), 675 (sh), 635 (w), 508 (w), 360 (m).

MS (APCI-HRMS(+)): m/z = 1005.5359 [MH]$^+$, calcd. for C$_{64}$H$_{73}$N$_8$Cr$^+$: 1005.5359.

4.4.5   Synthesis of [Pc*CrCl]
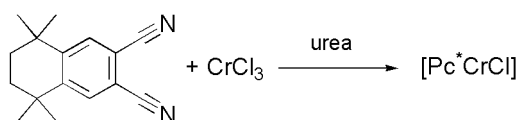
A mixture of PDN* (300 mg, 1.26 mmol), urea (149 mg, 2.49 mmol) and CrCl$_3$.6H$_2$O (168 mg, 0.63 mmol) was heated at 220°C under an argon atmosphere for 30 minutes. The product was washed with diethyl ether (2x20 mL) and purified by column chromatography (CHCl$_3$, Al$_2$O$_3$). After removing the solvent, the product was obtained as a green solid.

Yield: 123 mg, 0.118 mmol, 37 %.

Elemental analysis: (C$_{64}$H$_{72}$N$_8$CrCl, 1040.76 g/mol)

Found (Calculated): C: 72.12% (73.86%), H: 7.60% (6.97%), N: 8.60 % (10.77%).

UV/Vis. (CHCl$_3$): λ/nm = 708 (s), 673 (sh), 638 (w), 510 (w), 360 (m), 284 (m), 250 (m).

MS (APCI-HRMS(+)): m/z = 1040.5039[MH]$^+$, calcd. for C$_{64}$H$_{73}$N$_8$CrCl$^+$ 1040.5048.

4.4.6   Synthesis of [Pc*MnCl]
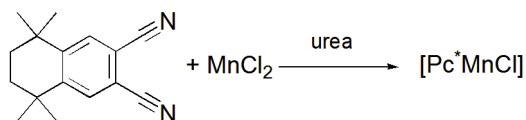
A mixture of PDN* (300 mg, 1.26 mmol), urea (149 mg, 2.49 mmol) and MnCl$_2$.4H$_2$O (125 mg, 0.63 mmol) was heated at 220°C under an argon atmosphere for 30 minutes. The product was washed with diethyl ether (2x20 mL) and purified by column chromatography (CHCl$_3$, Al$_2$O$_3$). After removing the solvent, the product was obtained as a red-orange solid.

Yield: 95 mg, 0.091 mmol, 29 %.

Elemental analysis: ($C_{64}H_{72}N_8MnCl$, 1043.70 g/mol)

Found (Calculated): C: 71.75 (73.65%), H: 7.62% (6.95%), N: 8.55% (10.74%), Cl: 3.19 % (3.40 %).

UV/Vis. ($CHCl_3$): λ/nm = 749 (s), 672 (w), 545 (w), 374 (m), 286 (m), 250 (s).

MS(APCI-HRMS(+)):m/z =1008.5287[MH-Cl]$^+$, calcd. for $C_{64}H_{73}N_8Mn^+$:1008.5209.

4.4.7 Synthesis of [Pc*Fe]
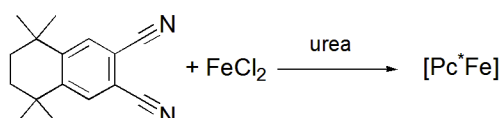
A mixture of PDN* (300 mg, 1.26 mmol), urea (149 mg, 2.49 mmol) and $FeCl_2.4H_2O$ (125 mg, 0.63 mmol) was heated at 220°C under an argon atmosphere for 30 minutes. The product was washed with pentane (2x20 mL), diethyl ether (20 mL) and purified by column chromatography ($CHCl_3$, Al_2O_3). After removing the solvent, the desired product was obtained as a green solid.

Yield: 120 mg, 0.119 mmol, 38 %.

Elemental analysis: ($C_{64}H_{72}N_8Fe$, 1009.15 g/mol)

Found (Calculated): C: 74.41% (76.17%), H: 7.73% (7.19%), N: 9.24 % (11.10 %).

UV/Vis. ($CHCl_3$): λ/nm = 678 (m), 610 (w), 317 (sh), 249 (s).

MS (APCI-HRMS(+)): m/z = 1009.5290 [MH]$^+$, calcd. for $C_{64}H_{73}N_8Fe^+$: 1009.5304.

4.4.8 Synthesis of [Pc*FeCl]
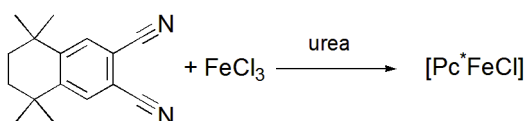
A mixture of PDN* (300 mg, 1.26 mmol), urea (149 mg, 2.49 mmol) and $FeCl_3.6H_2O$ (170 mg, 0.63 mmol) was heated at 220°C under an argon atmosphere for 30 minutes. The product was washed with diethyl ether (2x20 mL) and purified by column chromatography ($CHCl_3$, Al_2O_3). After removing the solvent, the desired product was obtained as a green solid.

Yield: 24 mg, 0.023 mmol, 7 %.

Elemental analysis: ($C_{64}H_{72}N_8FeCl$, 1044.61 g/mol)

Found (Calculated): C: 70.27% (73.59%), H: 6.87% (6.95%), N: 10.06% (10.73%).

UV/Vis. (CHCl$_3$): λ/nm = 878 (w), 678 (m), 615 (sh), 482 (sh), 343 (sh), 286 (sh), 248 (s).

MS (APCI-HRMS(+)): m/z = 1044.4991[MH]$^+$, calcd. for C$_{64}$H$_{73}$N$_8$FeCl$^+$:1044.4993.

4.4.9 New synthetic method for [Pc*Co]
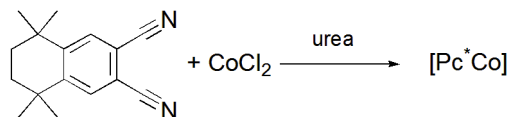
A mixture of PDN* (300 mg, 1.26 mmol), urea (149 mg, 2.49 mmol) and CoCl$_2$.6H$_2$O (150 mg, 0.63 mmol) was heated at 220°C under an argon atmosphere for 30 minutes. The product was washed with diethyl ether (2x20 mL) and purified by column chromatography (CHCl$_3$, Al$_2$O$_3$). After removing the solvent, the desired product was obtained as a blue solid.

Yield: 196 mg, 0.194 mmol, 62 %.

Elemental analysis: (C$_{64}$H$_{72}$N$_8$Co, 1012.24 g/mol)

Found (Calculated): C: 74.07% (75.94%), H: 7.56% (7.17%), N: 9.51 % (11.07 %).

UV/Vis. (CHCl$_3$): λ/nm = 684(s), 650 (sh), 616 (w), 333 (m), 295 (m), 251 (m).

MS (APCI-HRMS(+)): m/z = 1012.5277 [MH]$^+$, calcd. for C$_{64}$H$_{73}$N$_8$Co$^+$: 1012.5285.

4.4.10 Synthesis of [Pc*Ni]
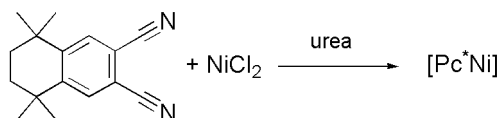
A mixture of PDN* (300 mg, 1.26 mmol), urea (149 mg, 2.49 mmol) and NiCl$_2$.6H$_2$O (150 mg, 0.63 mmol) was heated at 220°C under an argon atmosphere for 30 minutes. The product was washed with diethyl ether (2x20 mL) and purified by column chromatography (CHCl$_3$, Al$_2$O$_3$). After removing the solvent, the product was obtained as a green solid.

Yield: 182 mg, 0.180 mmol, 57 %.

Elemental analysis: (C$_{64}$H$_{72}$N$_8$Ni, 1012.00 g/mol)

Found (Calculated): C: 73.84% (75.96%), H: 7.52% (7.17%), N: 9.99 % (11.07 %).

UV/Vis. (CHCl$_3$): λ/nm = 686 (s), 662 (sh), 618 (w), 376 (sh), 336 (w), 298 (m), 278 (m), 246 (m).

MS (APCI-HRMS(+)): m/z = 1011.5297 [MH]$^+$, calcd. for C$_{64}$H$_{73}$N$_8$Ni$^+$: 1011.5304.

4.4.11 New synthetic method for [Pc*Cu]
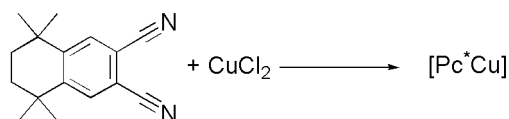
A mixture of PDN* (300 mg, 1.26 mmol) and $CuCl_2.2H_2O$ (107 mg, 0.63 mmol) was heated at 220°C under an argon atmosphere for 30 minutes. The product was washed with diethyl ether (2x20 mL) and purified by column chromatography ($CHCl_3$, Al_2O_3). After removing the solvent, the product was obtained as a blue solid.

Yield: 106 mg, 0.104 mmol, 33 %.

Elemental analysis: ($C_{64}H_{72}N_8Cu$, 1016.85 g/mol)

Found (Calculated): C: 73.80% (75.59%), H: 7.39% (7.14%), N: 9.47 % (11.02 %).

UV/Vis. ($CHCl_3$): λ/nm = 694 (s), 664 (sh), 624 (w), 342 (m), 295 (w), 269 (w).

MS (APCI-HRMS(+)): m/z = 1016.5236 [MH]$^+$, calcd. for $C_{64}H_{73}N_8Cu^+$: 1016.5249.

4.4.12 New synthetic method for [Pc*Zn]
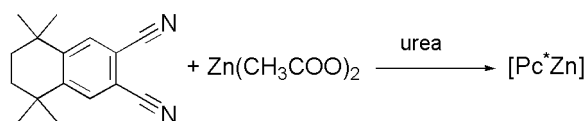
A mixture of PDN* (300 mg, 1.26 mmol), urea (149 mg, 2.49 mmol) and $Zn(CH_3COO)_2.2H_2O$ (138 mg, 0.63 mmol) was heated at 220°C under an argon atmosphere for 30 minutes. The product was washed with diethyl ether (2x20 mL) and purified by column chromatography (ethyl acetate, Al_2O_3). After removing the solvent, the desired product was obtained as a green solid.

Yield: 70 mg, 0.069 mmol, 22 %.

Elemental analysis: ($C_{64}H_{72}N_8Zn$, 1018.70 g/mol)

Found (Calculated): C: 71.90% (75.46%), H: 7.63 % (7.12%), N: 8.63% (11.00 %).

^{1}H-NMR (300 MHz, $CDCl_3$): δ/ppm = 9.36 (s, 8H, H$_\alpha$), 2.04 (s, 16H, H$_\varepsilon$), 1.78 (s, 48H, H$_{\delta 1+2}$).

UV/Vis. ($CHCl_3$): λ/nm = 692 (s), 630 (sh), 344 (s), 301(s), 254(m).

MS (APCI-HRMS(+)): m/z = 1017.5236 [MH]$^+$, calcd. for $C_{64}H_{73}N_8Zn^+$: 1017.5244.

150

4.4.13 New Synthetic method for Pc*H$_2$
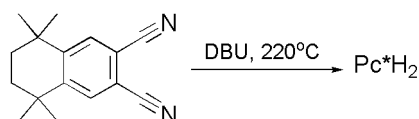
A mixture of PDN* (300 mg, 1.258 mmol) and DBU (0.5 mL) was heated at 220°C in 1-pentanol (1 mL) for 15 minutes. After cooling, pentane (100 mL) was added to precipitate a solid residue. The residue was purified using column chromatography (CHCl$_3$, Al$_2$O$_3$). After removing the solvent, the product was obtained as a green solid.

Yield: 44 mg, 0.046 mmol, 15 %.

MS (APCI-HRMS(+)): m/z = 955.6087 [MH]$^+$, calcd. for [C$_{64}$H$_{75}$N$_8$]$^+$: 955.6109.

4.4.14 Synthesis of [Pc*AlCl]
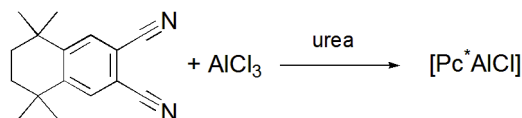
A mixture of PDN* (300 mg, 1.26 mmol), urea (149 mg, 2.49 mmol) and AlCl$_3$ (84 mg, 0.63 mmol) was heated at 220°C under an argon atmosphere for 30 minutes. The product was washed with diethyl ether (2x20 mL) and purified by column chromatography (CHCl$_3$, Al$_2$O$_3$). After removing the solvent, the desired product was obtained as a green solid.

Yield: 83 mg, 0.082 mmol, 26 %.

Elemental analysis: (C$_{64}$H$_{72}$N$_8$AlCl, 1015.74 g/mol)

Found (Calculated): C: 71.48% (75.68%), H: 7.13% (7.14%), N: 10.13% (11.03%).

^{1}H-NMR (300 MHz, CDCl$_3$): δ/ppm = 9.61 (s, 8H, Ar-H), 1.83 (s, 16H, H$_\varepsilon$), 1.43 (s, 48H, H$_{\delta1+\delta2}$).

^{13}C-NMR (75 MHz, CDCl3): δ/ppm = 132.6, 35.1, 34.1, 31.5.

UV/Vis. (CHCl$_3$): λ/nm = 706 (m), 675 (sh), 636 (w), 346 (w), 293 (w), 285 (sh), 246 (s).

MS(APCI-HRMS(+)):m/z = 1015.5448 [MH]$^+$, calcd. for C$_{64}$H$_{73}$N$_8$AlCl$^+$: 1015.5457.

4.4.15 Synthesis of [Pc*AlF]
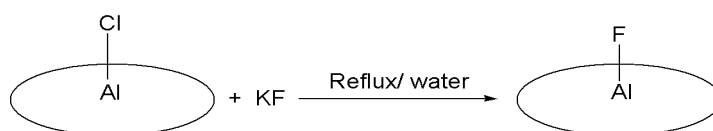
A mixture of [Pc*AlCl] (122 mg, 0.120 mmol), KF (1.46 g, 25.2 mmol) and H_2O (100 mL) was refluxed overnight. After cooling, the green solid was filtered, washed with water and dried under vacuum.

Yield: 107 mg, 0.107 mmol, 89 %.

Elemental analysis: ($C_{64}H_{72}N_8AlF$, 999.29 g/mol)

Found (Calculated): C: 78.18% (76.92%), H: 7.60% (7.26%), N: 11.30% (11.21%).

^{1}H-NMR (300 MHz, $CDCl_3$): δ/ppm = 9.59 (s, 8H, Ar-H) , 2.08 (s, 16H, H_ε), 1.85 (s, 24H, $H_{\delta1}$) 1.82 (s, 24H, $H_{\delta2}$).

^{13}C-NMR (75 MHz, $CDCl_3$): δ/ppm = 151.7, 132.7, 115.9, 112.6, 36.1, 34.1, 31.6.

IR: $\tilde{v}$/cm^{-1} = 431 (w), 699 (m), 797 (s), 1009 (s), 1080 (s), 1259 (s), 1456 (m), 2919 (m).

UV/Vis. ($CHCl_3$): λ/nm = 706 (s), 675 (sh), 637 (w), 346 (s), 298 (m), 254 (s).

MS (APCI-HRMS(+)): m/z = 999.5745 [MH]$^+$, calcd. for $C_{64}H_{73}N_8AlF^+$: 999.5752.

4.4.16 Attempted synthesis of [Pc*Al(OH)]
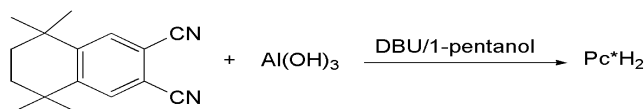
A mixture of PDN* (300 mg, 1.26 mmol), $Al(OH)_3$ (357 mg, 4.58 mmol), 0.5 mL DBU and 1-pentanol (2 mL) was heated at 220°C for 60 minutes. After cooling, pentane (20 mL) was added to precipitate a green solid. The solid was isolated and purified by column chromatography ($CHCl_3$, Al_2O_3). After removing the solvent, the green product was identified as Pc*H$_2$.

Additional information

When a similar mixture was heated overnight at 160°C, no reaction took place.

4.4.17 Attempted synthesis of [Pc*AlCH$_3$]

152
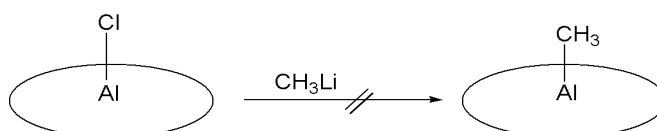
Attempt 1: A mixture of [Pc*AlCl] (132 mg, 0.130 mmol), CH$_3$Li (5.61 mg, 0.255 mmol contained in 0.16 mL of 1.595 M in diethyl ether) and dry THF (30 mL) was stirred overnight under an argon atmosphere, then the solvent was removed under reduced pressure. After washing with pentane, the resulting product was characterized as [Pc*AlCl].
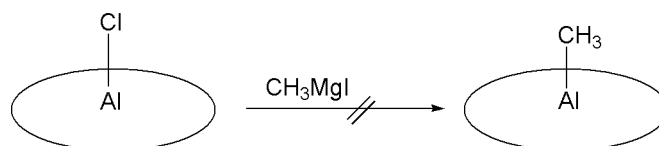
Attempt 2: A mixture of [Pc*AlCl] (113 mg, 0.111 mmol), CH$_3$MgI (55.31 mg, 0.333 mmol contained in 0.15 mL of 2.218 M in diethyl ether) and dry THF (30 mL) was stirred overnight under an argon atmosphere, then the solvent was removed under reduced pressure. After washing with pentane, the resulting compound was characterized as [Pc*AlCl].

4.4.18 Attempted synthesis of [Pc*AlPh]

A mixture of [Pc*AlCl] (110 mg, 0.108 mmol), PhLi (16.81 mg, 0.2 mmol contained in 0.1 mL of 2.0 M in dibuyl ether) and dry THF (30 mL) was stirred overnight under an argon atmosphere, then the solvent was removed under reduced pressure. After washing with pentane, the resulting compound was characterized as [Pc*AlCl].

4.4.19 Attempted synthesis of [Pc*AlNH$_2$]
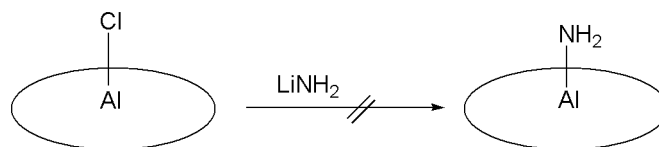
A mixture of [Pc*AlCl] (177 mg, 0.174 mmol), LiNH$_2$ (8 mg, 0.348 mmol) and dry THF (30 mL) was stirred overnight under argon. The solvent was removed under reduced pressure. After washing with pentane, the green solid was identified as [Pc*AlCl].

4.4.20 Attempted Synthesis of [Pc*AlNMe₂]
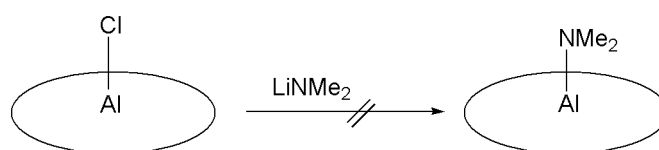
A mixture of [Pc*AlCl] (209 mg, 0.206 mmol), LiNMe₂ (21 mg, 0.412 mmol) and dry THF (30 mL) was stirred overnight under argon. The solvent was removed under reduced pressure. After washing with pentane, the green solid was identified as [Pc*AlCl].

4.4.21 Attempted Synthesis of [Pc*AlN(i-Pr)₂]
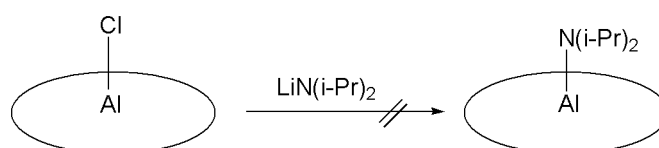
A mixture of [Pc*AlCl] (90 mg, 0.089 mmol), LiN(i-Pr)₂ (19 mg, 0.177 mmol) and dry THF (30 mL) was stirred overnight under an argon atmosphere. The solvent was removed under reduced pressure. After washing with pentane, the green solid was identified as [Pc*AlCl].

4.4.22 Attempted synthesis of [Pc*AlOP(O)(OH)₂] or [(Pc*AlO)₂P(O)(OH)]
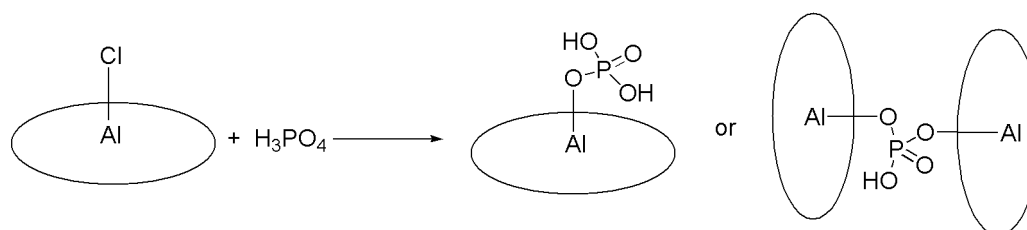
A mixture of [Pc*AlCl] (214 mg, 0.211 mmol) and H₃PO₄ (85 %, 100 mL) was refluxed overnight, then a precipitate was formed by adding water (300 mL). After filtration and washing with Na₂CO₃ solution. The product was characterized as [Pc*AlCl].

4.4.23 Synthesis of [Pc*GaCl]
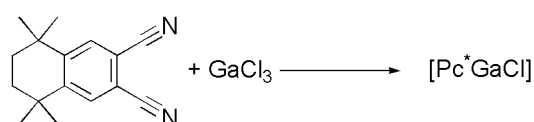
A mixture of PDN* (300 mg, 1.26 mmol) and GaCl₃ (111 mg, 0.63 mmol) was heated at 220°C under an argon atmosphere for 30 minutes. The product was washed with diethyl

ether (2x20 mL) and purified by column chromatography (CHCl$_3$, Al$_2$O$_3$). After removing the solvent, the product was obtained as a green solid.

Yield: 153 mg, 0.145 mmol, 46 %.

Elemental analysis: (C$_{64}$H$_{72}$N$_8$GaCl, 1058.48 g/mol)

Found (Calculated): C: 73.66% (72.62%), H: 7.45% (6.86%), N: 9.45% (10.59%).

^{1}H-NMR (300 MHz, CDCl$_3$): δ/ppm = 9.60 (s, 8H, Ar-H), 2.07 (s, 16H, H$_\varepsilon$), 1.82 (s, 48H, H$_{\delta1+\delta2}$).

^{13}C-NMR (75 MHz, CDCl$_3$): δ/ppm = 153.3, 149.1, 134.9, 121.7, 36.1, 33.1, 29.9.

UV/Vis. (CHCl$_3$): λ/nm = 712 (s), 677 (m), 638 (m), 350 (s), 302 (m).

MS(APCI-HRMS(+)): m/z= 1059.4883[MH]$^+$, calcd. for C$_{64}$H$_{73}$N$_8$GaCl$^+$: 1059.4898.

4.4.24 Attempted synthesis of [Pc*Ga(OH)]

$$[Pc^*GaCl] \xrightarrow{\text{NH}_4\text{OH / pyridine}} [Pc^*Ga(pyridine)Cl] \xrightarrow{200^\circ C} [Pc^*GaCl]$$
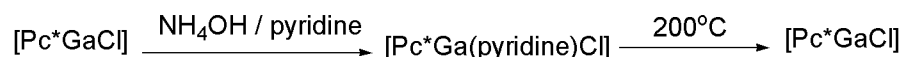
A mixture of [Pc*GaCl] (120 mg, 0.113 mmol), NH$_4$OH (20 mL) and pyridine (50 mL) was refluxed for 5 hours then the solvent was removed by filtration. After drying under vacuum, the resulting colorful green product was characterized as [Pc*Ga(pyridine)Cl].

Elemental analysis: [C$_{64}$H$_{72}$N$_8$Ga(C$_5$H$_5$N)Cl], 1137.58 g/mol)

Found (Calculated): C: 71.63% (72.85%), H: 7.11% (8.82%), N: 10.06% (11.08%).

MS (APCI-HRMS(+)): m/z = 1102.5544 [M-Cl]$^+$, calcd. for [C$_{64}$H$_{73}$N$_8$Ga(C$_5$H$_5$N)]$^+$: 1102.5566.

Additional information:

- Heating of [Pc*Ga(pyridine)Cl] at 200°C led to formation of [Pc*GaCl].
- When [Pc*GaCl] was refluxed in NH$_4$OH solution (30 %, 50 mL) for 4 hours, no reaction took place.

4.4.25 Attempted synthesis of [Pc*GaF]
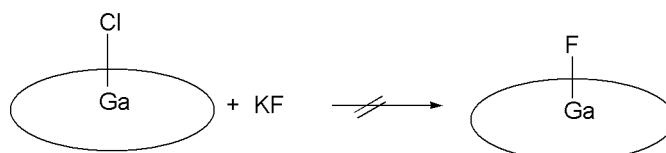
A mixture of [Pc*GaCl] (107 mg, 0.101 mmol), KF (1.27 g, 21.94 mmol) and H$_2$O (100 mL) was refluxed overnight. The green solid was filtered and characterized as [Pc*GaCl].

4.4.26 Synthesis of [Pc*GaCH₃]
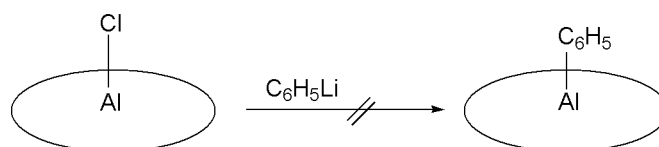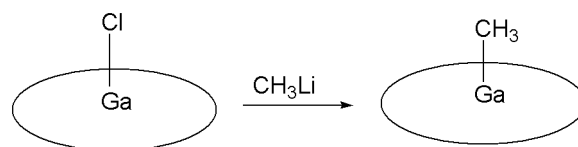

A mixture of [Pc*GaCl] (193 mg, 0.182 mmol), CH₃Li (7.71 mg, 0.351 mmol contained in 0.22 mL of 1.595 M in diethyl ether) and dry THF (30 mL) was stirred overnight under an argon atmosphere. The solvent was removed under reduced pressure. After washing with pentane, the green solid was identified as [Pc*GaCH₃].

Yield: 156 mg, 0.150 mmol, 82 %.

Elemental analysis: (C$_{64}$H$_{72}$N$_8$GaCH$_3$, 1038.06 g/mol)

Found (Calculated): C: 79.90% (75.20%), H: 10.14% (7.30%), N: 4.19% (10.80%).

¹H-NMR (300 MHz, CDCl₃): δ/ppm = 9.55 (s, 8H, Ar-H), 2.07 (s, 16H, H$_\varepsilon$), 1.85 (s, 48H, H$_{\delta 1+ \delta 2}$), 0.88 (CH₃-Ga).

¹³C-NMR (75 MHz, CDCl₃): δ/ppm = 168.9, 152.4, 122.5, 37.0, 34.8, 32.1, 29.9, 22.8, 14.2.

UV/Vis. (CHCl₃): λ/nm = 710 (s), 676 (sh), 635 (w), 477 (w), 346 (m).

MS(APCI-HRMS(+)):m/z=1037.5438[MH]⁺, calcd. for C$_{65}$H$_{76}$N$_8$Ga⁺:1037.5443.

4.4.27 Synthesis of [Pc*GaC₄H₉]
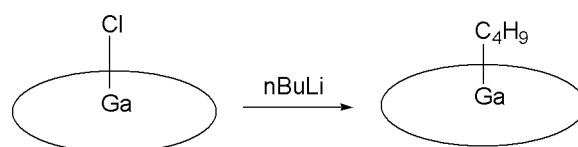
A mixture of [Pc*GaCl] (178 mg, 0.168 mmol), n-BuLi (21.62 mg, 0.338 mmol contained in 0.13 mL of 2.597 M in hexane) and dry THF (30 mL) was stirred overnight under an argon atmosphere. The solvent was removed under reduced pressure. After washing with pentane, the green solid was identified as [Pc*GaC₄H₉].

Yield: 120 mg, 0.129 mmol, 71 %.

Elemental analysis: (C$_{64}$H$_{72}$N$_8$GaC$_4$H$_9$, 1080.14 g/mol)

Found (Calculated): C: 80.00% (75.61%), H: 10.17% (7.57%), N: 4.18% (10.38%).

¹³C-NMR (75 MHz, CDCl₃): δ/ppm = 32.0, 29.9, 22.8, 14.2.

UV/Vis. (CHCl₃): λ/nm = 710 (m), 676 (sh), 637(w), 639 (w).

MS (APCI-HRMS(+)): m/z = 1079.5908 [MH]⁺, calcd. for C$_{68}$H$_{82}$N$_8$Ga⁺: 1079.5913.

4.4.28 Synthesis of [Pc*GaC$_6$H$_{13}$]
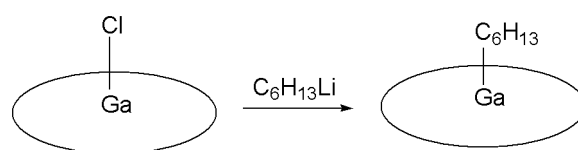
A mixture of [Pc*GaCl] (89 mg, 0.084 mmol), n-hexyllithium (14.81 mg, 0.161 mmol contained in 0.06 mL of 2.218 M in hexane) and dry THF (30 mL) was stirred overnight under an argon atmosphere. The solvent was removed under reduced pressure. After washing with pentane, the green solid was identified as [Pc*GaC$_6$H$_{13}$].

Yield: 41 mg, 0.0369 mmol, 44 %.

Elemental analysis: (C$_{64}$H$_{72}$N$_8$Ga C$_6$H$_{13}$, 1108.20 g/mol)

Found (Calculated): C: 80.05% (75.86%), H: 10.19% (7.75%), N: 4.22% (10.11%).

UV/Vis. (CHCl$_3$): λ/nm = 710 (s), 678 (sh), 638 (w), 350 (m).

MS (APCI-HRMS(+)) :m/z= 1107.6230[MH]$^+$, calcd. for C$_{70}$H$_{86}$N$_8$Ga$^+$: 1107.6226.

4.4.29 Synthesis of [Pc*GaC$_6$H$_5$]
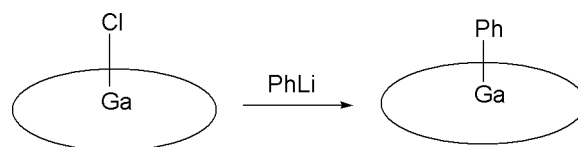
A mixture of [Pc*GaCl] (146 mg, 0.138 mmol), PhLi (23.94 mg, 0.26 mmol contained in 0.13 mL of 2.0 M in dibutyl ether) and dry THF (30 mL) was stirred overnight under an argon atmosphere. The solvent was removed under reduced pressure. After washing with pentane, the green solid was identified as [Pc*GaC$_6$H$_5$].

Yield: 107 mg, 0.097 mmol, 71 %.

Elemental analysis: (C$_{64}$H$_{72}$N$_8$GaC$_6$H$_5$, 1100.13 g/mol)

Found (Calculated): C: 80.11% (76.42%), H: 10.22% (7.07%), N: 4.21% (10.19%).

^{1}HNMR (300 MHz, CDCl$_3$): δ/ppm = 9.60 (s, 8H, Ar-H), 2.08 (s, 16H, H$_\varepsilon$), 1.82 (s, 24H, H$_{\delta 1}$), 1.79 (s, 24H, H$_{\delta 2}$), 7.61 (m, 5H, Ar-Ga).

^{13}CNMR (75 MHz, CDCl$_3$): δ/ppm = 153.2, 148.7, 135.1, 130.8, 128.8, 127.3, 125.7, 121.6, 35.9, 33.0, 29.8, 22.9, 14.2.

UV/Vis. (CHCl$_3$): λ/nm = 710 (s), 678 (sh), 638 (w), 380(sh), 351(m), 300(m).

MS (APCI-HRMS(+)): m/z = 1099.5586 [MH]$^+$, calcd. for C$_{70}$H$_{78}$N$_8$Ga$^+$: 1099.5600.

4.4.30 Attempted Synthesis of [Pc*GaNH₂]
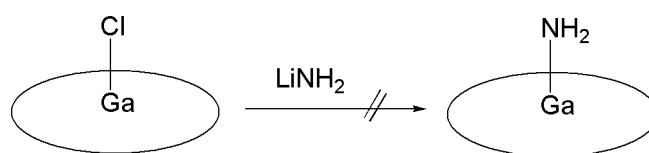
A mixture of [Pc*GaCl] (138 mg, 0.131 mmol), $LiNH_2$ (6 mg, 0.261 mmol) and dry THF (30 mL) was stirred overnight under argon. The solvent was removed under reduced pressure. After washing with pentane, the green solid was identified as [Pc*GaCl].

4.4.31 Attempted synthesis of [Pc*GaNMe₂]
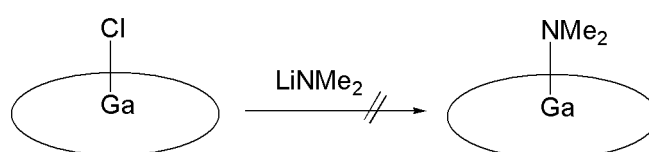
A mixture of [Pc*GaCl] (187 mg, 0.176 mmol), $LiNMe_2$ (18 mg, 0.351 mmol) and dry THF (30 mL) was stirred overnight under argon. The solvent was removed under reduced pressure. After washing with pentane, the product was identified as [Pc*GaCl].

4.4.32 Attempted synthesis of [Pc*GaN(i-Pr)₂]
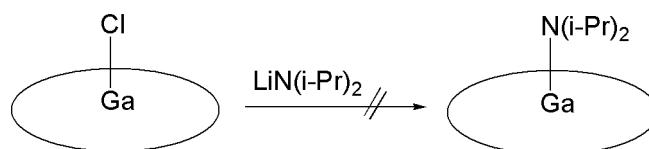
A mixture of [Pc*GaCl] (64 mg, 0.061 mmol), $LiN(i-Pr)_2$ (13 mg, 0.121 mmol) and dry THF (30 mL) was stirred overnight under argon. The solvent was removed under reduced pressure. After washing with pentane, the product was identified as [Pc*GaCl].

4.4.33 Synthesis of [Pc*InCl] complex
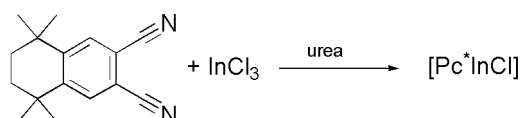
A mixture of PDN* (300 mg, 1.26 mmol) and $InCl_3$ (139 mg, 0.63 mmol) was heated at 220°C under an argon atmosphere for 30 minutes. After cooling, the product was added to CH_2Cl_2 (200 mL) and filtered to remove the solid residue. The solvent was removed under reduced pressure then the obtained solid was washed with methanol until the washing solution became colorless. The green product was dried under vacuum.

158

Yield: 42 mg, 0.038 mmol, 12 %.

Elemental analysis: ($C_{64}H_{72}N_8InCl$, 1103.58 g/mol)

Found (Calculated): C: 70.10% (69.65%), H: 6.80% (6.58%), N: 9.50% (10.15%).

^{1}H-NMR (300 MHz, $CDCl_3$): δ/ppm = 9.52 (s, 8H, Ar-H), 2.06 (s, 16H, H_ε), 1.86 (s, 48H, $H_{\delta1+\delta2}$).

UV/Vis. ($CHCl_3$): λ/nm = 714 (s), 683 (sh), 643 (w), 354 (m), 302 (s), 244 (s).

MS(APCI-HRMS(+)): m/z = 1103.4665[MH]$^+$, calcd. for $C_{64}H_{73}N_8InCl^+$: 1103.4680.

4.4.34 Attempted synthesis of [Pc*InF]
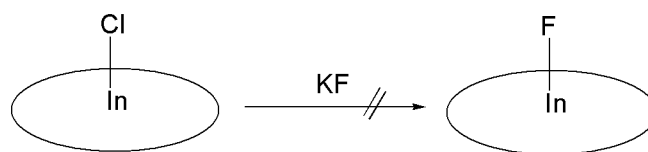
A mixture of [Pc*InCl] (72 mg, 0.0652 mmol), KF (0.635 g, 10.93 mmol) and H_2O (100 mL) was refluxed overnight, then the solid was filtered and characterized as [Pc*InCl].

4.4.35 Attempted synthesis of [Pc*Mg]
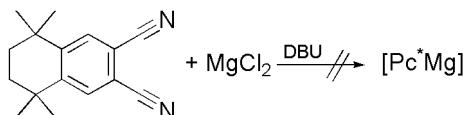
A mixture of PDN* (300 mg, 1.26 mmol), $MgCl_2.6H_2O$ (128 mg, 0.63 mmol), DBU (0.5 mL) and 1-pentanol (2 mL) was heated overnight at 160°C under an argon atmosphere. After cooling, pentane (20 mL) was added to precipitate a brown solid. The solid was isolated and purified by column chromatography ($CHCl_3$, Al_2O_3). The product could not be identified by either ^{1}H-NMR or MS (APCI-HRMS(+)) measurements.

4.4.36 Attempted synthesis of [Pc*ScCl]
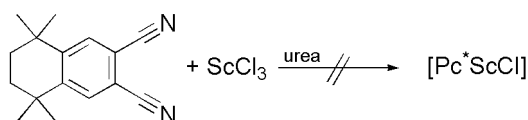
A mixture of PDN* (300 mg, 1.26 mmol), $ScCl_3$ (93 mg, 0.63 mmol), urea (149 mg, 2.49 mmol) and CNP (2 mL) was heated overnight at 160°C under an argon atmosphere. After cooling, pentane (20 mL) was added to precipitate a pale green solid. The solid was isolated and purified by column chromatography ($CHCl_3$, Al_2O_3). The obtained pale green product could not be identified by either ^{1}H-NMR or MS (APCI-HRMS(+)) measurements.

4.4.37 Attempted Synthesis of [Pc*Cd]
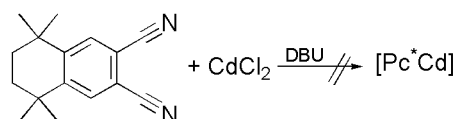
Attempt 1: A mixture of PDN* (300 mg, 1.26 mmol), $CdCl_2.H_2O$ (127 mg, 1.26 mmol), DBU (0.5 mL) and 1-pentanol (2 mL) was heated overnight at 160°C under an argon atmosphere. After cooling, pentane (20 mL) was added to precipitate a brown solid. The solid was isolated and purified by column chromatography ($CHCl_3$, Al_2O_3). The obtained product could not be identified by either ^{1}H-NMR or MS (APCI-HRMS(+)) measurements.
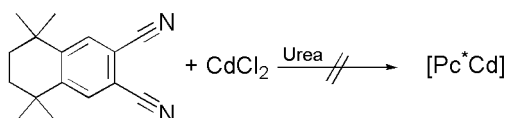
Attempt 2: A mixture of PDN* (300 mg, 1.26 mmol), $CdCl_2.H_2O$ (127 mg, 0.63 mmol) and urea (149 mg, 2.49 mmol) was heated for 30 minutes at 220°C under an argon atmosphere. The obtained residue was washed with diethyl ether (2x20 mL) and purified by column chromatography ($CHCl_3$, Al_2O_3). The resulting pale green product could not be identified by either ^{1}H-NMR or MS (APCI-HRMS(+)) measurements.

4.4.38 Attempted Synthesis of [Pc*SiCl₂]
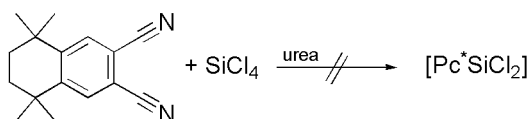
A mixture of PDN* (300 mg, 1.26 mmol), $SiCl_4$ (118.4 mg, 0.08 mL, 0.70 mmol) and urea (149 mg, 2.49 mmol) was heated for 30 minutes at 220°C under an argon atmosphere. The obtained solid residue was washed with diethyl ether (2x20 mL) and dissolved in $CHCl_3$, no chromophoric product was obtained.

4.4.39 Attempted synthesis of [Pc*GeCl₂]
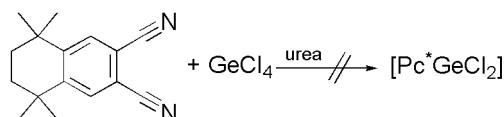
A mixture of PDN* (300 mg, 1.26 mmol), $GeCl_4$ (150.4 mg, 0.08 mL, 0.701 mmol) and urea (149 mg, 2.49 mmol) was heated for 30 minutes at 220°C under an argon atmosphere. The obtained solid residue was washed with diethyl ether (2x20 mL) and dissolved in $CHCl_3$, no chromophoric product was obtained.

4.5   Synthesis of Ppz* complexes

4.5.1   New synthetic method for [Ppz*TiO]
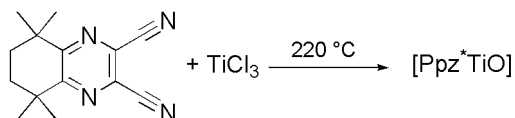
A mixture of PzDN* (300 mg, 1.248 mmol) and TiCl$_3$ (96 mg, 0.624 mmol) was heated at 220°C under an argon atmosphere for 30 minutes. The product was washed with diethyl ether (2x20 mL) and purified by column chromatography (CHCl$_3$, Al$_2$O$_3$). After removing the solvent, the product was obtained as a green solid.

Yield: 146 mg, 0.142 mmol, 46 %.

Elemental analysis: (C$_{56}$H$_{64}$N$_{16}$TiO, 1025.08 g/mol)

Found (Calculated): C: 63.12% (65.61%), H: 7.30% (6.29%), N: 19.54% (21.86%).

^{1}H-NMR (300 MHz, CDCl$_3$): δ/ppm = 2.26 (s, 16H, H_ε), 2.03 (s, 24H, $H_{\delta1}$), 1.93 (s, 24H, $H_{\delta2}$).

IR: $\tilde{v}$/cm^{-1} = 1998 (s), 1954 (s), 1561 (b), 852 (w), 736 (w), 613 (w), 531 (w), 489 (m), 461 (m), 432 (vs), 419 (s).

UV/Vis. (CHCl$_3$): λ/nm = 650 (s), 622 (sh), 590 (w), 348 (m), 302 (m), 246 (m).

Fluorescence (CHCl$_3$): λ = 652 nm.

MS(APCI-HRMS(+)):m/z=1025.5001[MH]$^+$, calcd. for [C$_{56}$H$_{65}$N$_{16}$TiO]$^+$:1025. 5008.

4.5.2   Attempted synthesis of [Ppz*TiS$_2$]
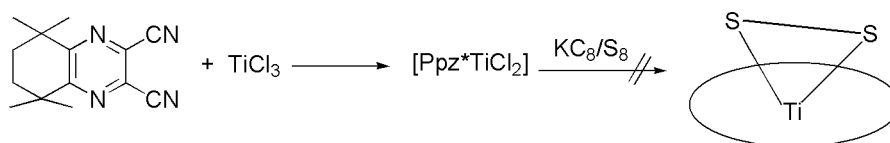
Attempt 1: A mixture of PzDN* (300 mg, 1.248 mmol) and TiCl$_3$ (96 mg, 0.624 mmol) was heated at 220°C under an argon atmosphere for 30 minutes. To the purple product, S$_8$ (320 mg, 1.24 mmol), KC$_8$ (422 mg, 3.12 mmol) and dry toluene (50 mL) were added. The mixture was heated overnight at 70°C then the insoluble residue was removed by filtration. The filtrate was concentrated under reduced pressure and purified by column chromatography (CHCl$_3$, Al$_2$O$_3$). The green product was characterized as [Ppz*TiO].

<u>Additional information</u>

When the experiment was performed in dry THF, the chromophore was destroyed.

161
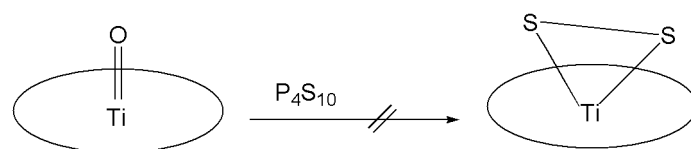
Attempt 2: A mixture of [Ppz*TiO] (238 mg, 0.232 mmol) and P_4S_{10} (206 mg, 0.463 mmol) in dry toluene was heated overnight at 100°C under an argon atmosphere then the solvent was removed under reduced pressure and the product was washed with diethyl ether. An unidentified colorful product was obtained.

4.5.3 Attempted synthesis of [Ppz*TiSe$_2$]
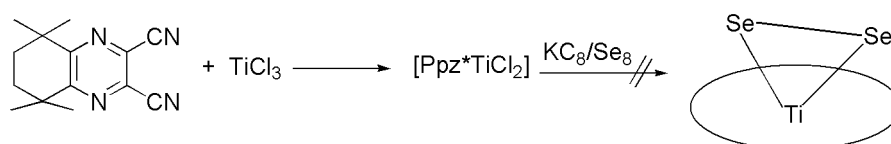
A mixture of PzDN* (300 mg, 1.248 mmol) and $TiCl_3$ (96 mg, 0.624 mmol) was heated at 220°C under an argon atmosphere for 30 minutes. To the purple product, Se_8 (789 mg, 1.249 mmol), KC_8 (422 mg, 3.122 mmol) and dry toluene (50 mL) were added. The mixture was heated overnight at 70°C then the insoluble residue was removed by filtration. The filtrate was concentrated under reduced pressure and purified by column chromatography (CHCl$_3$, Al$_2$O$_3$). The green product was characterized as [Ppz*TiO].

Additional information

When the experiment was performed in dry THF, the chromophore was destroyed.

4.5.4 Attempted synthesis of [Ppz*Ti(PO$_4$H)]
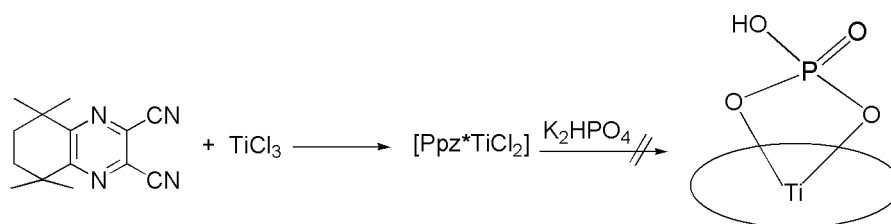
A mixture of PzDN* (300 mg, 1.248 mmol) and $TiCl_3$ (96 mg, 0.624 mmol) was heated at 220°C under an argon atmosphere for 30 minutes. To the product, K_2HPO_4 (231 mg, 1.326 mmol) and dry toluene (100 mL) were added, then the mixture was heated at 130°C for 4 hours. After cooling, the mixture was concentrated under reduced pressure and purified by column chromatography (CHCl$_3$, Al$_2$O$_3$). The blue – green product was characterized as [Ppz*TiO].

4.5.5 Synthesis of [Ppz*VO]
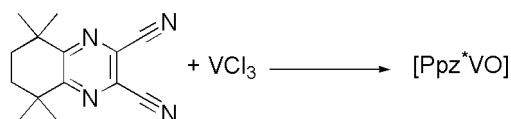
A mixture of PzDN* (300 mg, 1.248 mmol) and VCl$_3$ (98 mg, 0.624 mmol) was heated at 220°C under an argon atmosphere for 30 minutes. The product was washed with diethyl ether (100 mL) and purified by column chromatography (CHCl$_3$, Al$_2$O$_3$). After removing the solvent, the desired product was obtained as a blue - green solid.

Yield: 268 mg, 0.261 mmol, 84 %.

Elemental analysis: (C$_{56}$H$_{64}$N$_{16}$VO, 1028.15 g/mol)

Found (Calculated): C: 65.86% (65.42%), H: 7.64% (6.27%), N: 20.44% (21.80%).

IR: $\tilde{v}$/cm^{-1} = 3855 (w), 3710 (w), 2166 (m), 2037 (m), 1979 (m), 1941 (m), 463 (s), 442 (s), 417 (s).

UV/Vis. (CHCl$_3$): λ/nm = 648 (s), 618 (sh), 590 (w), 346 (s), 300 (m), 250 (m).

Fluorescence (CHCl$_3$): λ = 661 nm.

MS(APCI-HRMS(+)): m/z=1028.4961[MH]$^+$, calcd. for [C$_{56}$H$_{65}$N$_{16}$VO]$^+$: 1028.4962.

4.5.6 Attempted synthesis of [Ppz*V(NC$_8$H$_8$COOH)]
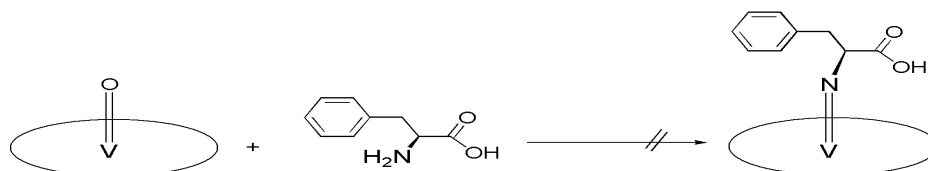
A mixture of [Ppz*VO] (173 mg, 0.168 mmol) and L-phenylalanine (32 mg, 0.194 mmol) was refluxed in acetone for 3 hours. The chromophore was destroyed.

4.5.7 Attempted synthesis of [Ppz*V(NSO$_3$H)]
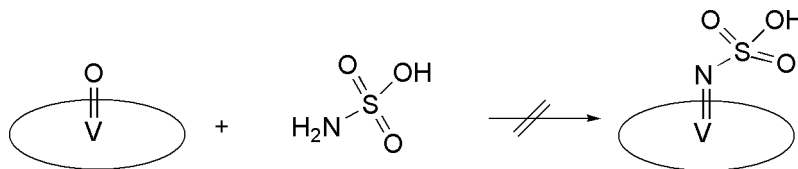
A mixture of [Ppz*VO] (310 mg, 0.302 mmol) and sulfamic acid (58 mg, 0.603 mmol) was refluxed in toluene for 3 hours. After removing the solvent under reduced pressure, the obtained solid was characterized as [Ppz*VO].

4.5.8 Attempted synthesis of [Ppz*V(NC$_6$H$_4$SO$_3$H)]
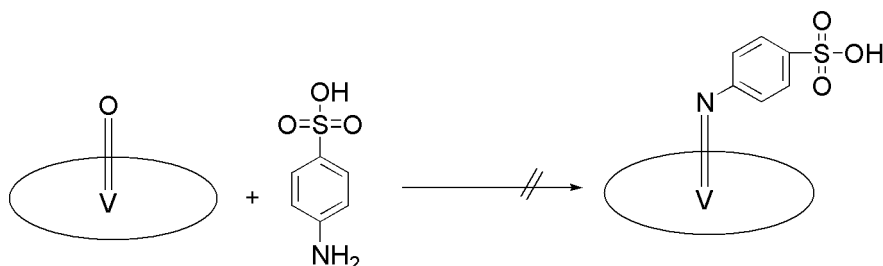
A mixture of [Ppz*VO] (278 mg, 0.270 mmol) and sulfanilic acid (93 mg, 0.542 mmol) was refluxed in toluene for 3 hours. After removing the solvent under reduced pressure, the obtained solid was characterized as [Ppz*VO].

4.5.9 Synthesis of [Ppz*Cr]
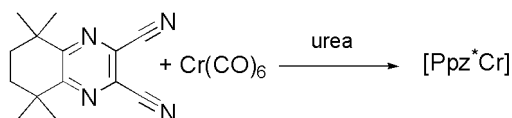
A mixture of PzDN* (300 mg, 1.248 mmol), [Cr(CO)$_6$] (137 mg, 0.624 mmol) and urea (149 mg, 2.49 mmol) was heated at 220°C under an argon atmosphere for 30 minutes. The product was washed with pentane and diethyl ether (20 mL) then purified by column chromatography (CHCl$_3$, Al$_2$O$_3$). After removing the solvent, the product was obtained as a green solid.

Yield: 158 mg, 0.156 mmol, 50 %.

Elemental analysis: (C$_{56}$H$_{64}$N$_{16}$Cr, 1013.21 g/mol)

Found (Calculated): C: 66.70% (66.38%), H: 8.16% (6.37%), N: 18.95% (22.12%).

IR: $\tilde{v}$/cm^{-1} = 2527 (m), 2359 (s), 2260 (s), 2147 (s), 2050 (s), 1958 (m), 1870 (m), 1540 (m), 727 (m), 672 (m), 589 (m), 558 (m), 471 (s), 444 (s), 405 (s).

UV/Vis. (CHCl$_3$): λ/nm = 647(s), 620(sh), 586(w), 478(w), 356(m), 300(m).

MS(APCI-HRMS(+)): m/z = 1013.4982[MH]$^+$, calcd. for [C$_{56}$H$_{65}$N$_{16}$Cr]$^+$: 1013.4979.

4.5.10 Synthesis of [Ppz*CrCl]
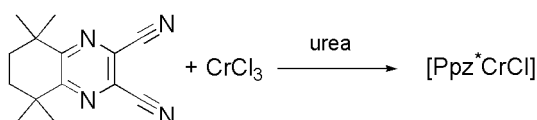
A mixture of PzDN* (300 mg, 1.248 mmol), CrCl$_3$.6H$_2$O (166 mg, 0.624 mmol) and urea (149 mg, 2.49 mmol) was heated at 220°C under an argon atmosphere for 30 minutes. The product was washed with diethyl ether (2x20 mL) and purified by column

chromatography (ethyl acetate, Al_2O_3). After removing the solvent, the product was obtained as a green solid.

Yield: 140 mg, 0.134 mmol, 43 %.

Elemental analysis: ($C_{56}H_{64}N_{16}CrCl$, 1048.66 g/mol)

Found (Calculated): C: 62.95% (64.14%), H: 7.49% (6.15%), N: 16.95% (21.37%).

IR: $\tilde{v}$/cm^{-1} = 1607 (w), 1489 (w), 1414 (w), 1330 (s), 1286 (m), 1162 (w), 1117 (s), 1066 (s), 960 (m), 892 (m), 726 (vs), 643 (m), 546 (w), 501 (w), 413 (w).

UV/Vis. (CHCl$_3$): λ/nm = 646 (s), 620 (sh), 568 (w), 474 (w), 344 (s), 318 (s), 292 (s), 252 (s).

Fluorescence (CHCl$_3$): λ = 652 nm.

MS(APCI-HRMS(+)):m/z=1048.4646[MH]$^+$,calcd. for $[C_{56}H_{65}N_{16}CrCl]^+$:1048.4668.

4.5.11 Synthesis of [Ppz*MnCl]
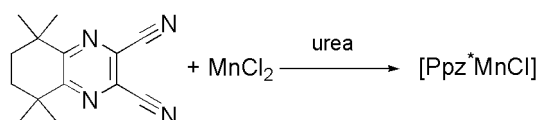
A mixture of PzDN* (300 mg, 1.248 mmol), MnCl$_2$.4H$_2$O (124 mg, 0.624 mmol) and urea (149 mg, 2.49 mmol) was heated at 220°C under an argon atmosphere for 30 minutes. The product was washed with pentane and diethyl ether (2x20 mL) then purified by column chromatography (CHCl$_3$, Al$_2$O$_3$). After removing the solvent, the product was obtained as a green solid.

Yield: 48 mg, 0.046 mmol, 15 %.

Elemental analysis: ($C_{56}H_{64}N_{16}MnCl$, 1051.61 g/mol)

Found (Calculated): C: 66.53%(63.96%), H: 7.85% (6.13%), N: 19.49% (21.31%).

UV/Vis. (CDCl$_3$): λ/nm = 674 (s), 611(sh), 489 (sh), 366 (m), 303(m).

MS (APCI-HRMS(+)): m/z = 1050.9475 [M]$^+$, calcd. $[C_{56}H_{64}N_{16}MnCl]^+$: 1050.9475.

4.5.12 Synthesis of [Ppz*Fe]
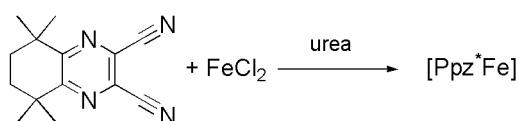
A mixture of PzDN* (300 mg, 1.248 mmol), FeCl$_2$.4H$_2$O (124 mg, 0.624 mmol) and urea (149 mg, 2.49 mmol) was heated at 220°C under an argon atmosphere for 30 minutes. The product was washed with diethyl ether (2x20 mL), and purified by column

chromatography (CHCl$_3$, Al$_2$O$_3$). After removing the solvent, the product was obtained as a green solid.

Yield: 102 mg, 0.100 mmol, 32 %.

Elemental analysis: (C$_{56}$H$_{64}$N$_{16}$Fe, 1017.06 g/mol)

Found (Calculated): C: 70.11%(66.12 %), H: 9.05%(6.35%), N: 17.50% (22.03%).

UV/Vis. (CHCl$_3$): λ/nm = 636 (s), 578 (sh), 452 (m).

MS(APCI-HRMS(+)):m/z = 1017.4919[MH]$^+$, calcd. for [C$_{56}$H$_{65}$N$_{16}$Fe]$^+$: 1017.4923.

4.5.13 Attempted synthesis of [(Ppz*Fe)$_2$N]
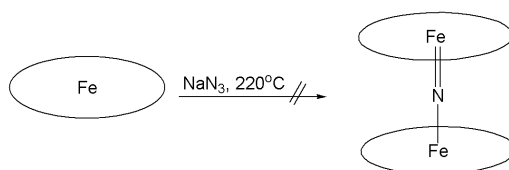
A mixture of [Ppz*Fe] (14 mg, 0.014 mmol), NaN$_3$ (700 mg, 10.77 mmol) and 1-CNP (20 mL) was heated at 220°C for 3 hours. Pentane (50 mL) was added to precipitate a non-colorful yellow – green product.

4.5.14 Synthesis of [Ppz*FeCl]
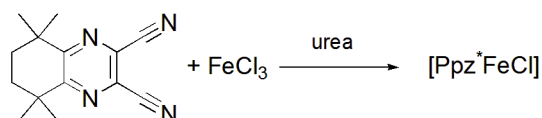
A mixture of PzDN* (300 mg, 1.248 mmol), FeCl$_3$.6H$_2$O (168 mg, 0.624 mmol) and urea (149 mg, 2.49 mmol) was heated at 220°C under an argon atmosphere for 30 minutes. The product was washed with diethyl ether (2x20 mL) and purified by column chromatography (CHCl$_3$, Al$_2$O$_3$). After removing the solvent, the product was obtained as a green solid.

Yield: 64 mg, 0.061 mmol, 19 %.

Elemental analysis: (C$_{56}$H$_{64}$N$_{16}$FeCl, 1052.51 g/mol)

Found (Calculated): C: 66.58% (63.90%), H: 8.18% (6.13%), N: 18.82% (21.29%).

UV/Vis. (CDCl$_3$): λ/nm = 878(w), 636 (s), 573 (sh), 418(sh), 305 (s).

MS(APCI-HRMS(+)):m/z=1052.4607[MH]$^+$,calcd. for [C$_{56}$H$_{65}$N$_{16}$FeCl]$^+$:1052.4623.

4.5.15 Synthesis of [Ppz*Co]
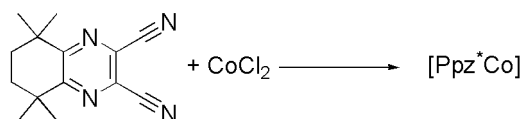
A mixture of PzDN* (300 mg, 1.248 mmol) and CoCl$_2$.6H$_2$O (148 mg, 0.624 mmol) was heated at 220°C under an argon atmosphere for 30 minutes. The product was washed with diethyl ether (2x20 mL) and purified by column chromatography (CHCl$_3$, Al$_2$O$_3$). After removing the solvent, the product was obtained as a blue solid.

Yield: 106 mg, 0.104 mmol, 33 %.

Elemental analysis: (C$_{56}$H$_{64}$N$_{16}$Co, 1020.15 g/mol)

Found (Calculated): C: 67.20% (65.93%), H: 7.87% (6.32%), N: 20.79% (21.97%).

IR: $\tilde{v}$/cm^{-1} = 2615(m), 2546(m), 2481(m), 2292(m), 2222(s), 2145(s), 2086(s), 2027(s), 1951(s), 1939(s), 858(m), 627(m), 558(m), 502(s), 425(s).

UV/Vis. (CHCl$_3$): λ/nm = 630 (s), 572 (sh), 328 (s).

MS(APCI-HRMS(+)):m/z= 1020.4901 [MH]$^+$, calcd. for [C$_{56}$H$_{65}$N$_{16}$Co]$^+$: 1020.4905.

4.5.16 Attempted synthesis of [Ppz*CoI]
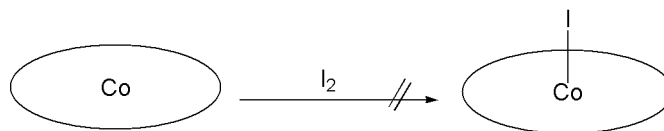
A mixture of [Ppz*Co] (170 mg, 0.167 mmol), I$_2$ (445 mg, 1.753 mmol) and KI solution (5 %, 100 mL) was refluxed overnight. No reaction took place.

4.5.17 Synthesis of [Ppz*Ni]
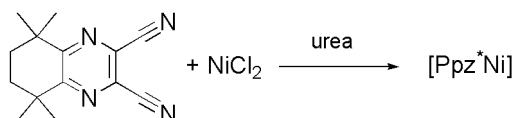
A mixture of PzDN* (300 mg, 1.248 mmol), NiCl$_2$.6H$_2$O (148 mg, 0.624 mmol) and urea (149 mg, 2.49 mmol) was heated at 220°C under an argon atmosphere for 30 minutes. The product was washed with diethyl ether (2x20 mL) and purified by column chromatography (CHCl$_3$, Al$_2$O$_3$). After removing the solvent, the desired product was obtained as a blue solid.

Yield: 266 mg, 0.261 mmol, 84 %.

Elemental analysis: (C$_{56}$H$_{64}$N$_{16}$Ni, 1019.91 g/mol)

Found (Calculated): C: 67.69% (65.95%), H: 8.08% (6.32%), N: 20.35% (21.97%).

IR: $\tilde{v}$/cm^{-1} = 2355 (w), 2255 (s), 2159 (vs), 2088 (s), 1996 (s), 1954 (vs), 773 (m), 666 (w), 627 (w), 547 (m), 503 (m), 483 (s), 430 (s), 419 (s).

UV/Vis. (CHCl$_3$): λ/nm = 630 (s), 604 (sh), 572 (w), 358 (w), 330 (m).

MS(APCI-HRMS(+)): m/z= 1019.4917[MH]$^+$, calcd. for [C$_{56}$H$_{65}$N$_{16}$Ni]$^+$: 1019.4926.

4.5.18 Synthesis of [Ppz*Cu]
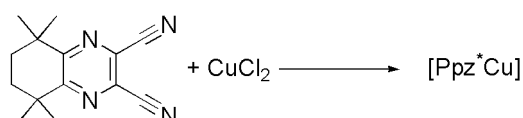
A mixture of PzDN* (300 mg, 1.248 mmol) and CuCl$_2$.2H$_2$O (106 mg, 0.624 mmol) was heated at 220°C under an argon atmosphere for 30 minutes. The product was washed with diethyl ether (2x20 mL) and purified by column chromatography (CHCl$_3$, Al$_2$O$_3$). After removing the solvent, the product was obtained as a blue solid.

Yield: 126 mg, 0.123 mmol, 39 %.

Elemental analysis: (C$_{56}$H$_{64}$N$_{16}$Cu, 1024.76 g/mol)

Found (Calculated): C: 68.80% (65.63%), H: 8.47% (6.29%), N: 18.67% (21.87%).

UV/Vis. (CHCl$_3$): λ/nm = 684 (sh), 638 (s), 580 (sh), 342 (m), 302(sh).

MS(APCI-HRMS(+)):m/z= 1024.4868[MH]$^+$, calcd. For [C$_{56}$H$_{65}$N$_{16}$Cu]$^+$: 1024.4869.

4.5.19 New synthetic method for [Ppz*Zn]
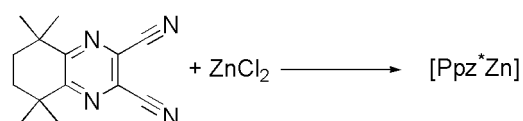
A mixture of PzDN* (300 mg, 1.248 mmol) and ZnCl$_2$ (85 mg, 0.624 mmol) was heated at 220°C under an argon atmosphere for 30 minutes. The product was washed with diethyl ether (2x20 mL) and purified by column chromatography (CHCl$_3$, Al$_2$O$_3$). After removing the solvent, the product was obtained as a blue solid.

Yield: 97 mg, 0.095 mmol, 30 %.

Elemental analysis: (C$_{56}$H$_{64}$N$_{16}$Zn, 1026.60 g/mol)

Found (Calculated): C: 65.12% (65.52%), H: 7.26% (6.28%), N: 21.33% (21.83%).

^{1}H-NMR (300 MHz, CHCl$_3$): δ/ppm = 1.90 (s, 16H, H_ε), 1.64 (s, 48H, $H_{\delta 1+2}$).

IR: $\tilde{v}$/cm^{-1} = 2443 (m), 2264 (m), 2185 (m), 2153 (s), 2052 (m), 1979 (m), 1954 (m), 1521 (w), 1101 (w), 942 (w), 851 (m), 648 (m), 508 (s), 445 (s), 413 (s).

UV/Vis. (CDCl$_3$): λ/nm = 642 (s), 614 (sh), 582 (s), 349 (s), 582 (s), 349 (s).

MS(APCI-HRMS(+)):m/z= 1025.4866[MH]$^+$, calcd. for [C$_{56}$H$_{65}$N$_{16}$Zn]$^+$: 1025.4864.

4.5.20 New synthetic method for Ppz*H$_2$
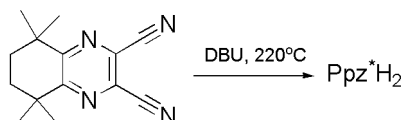
Method 1: A mixture of PzDN* (300 mg, 1.248 mmol) and DBU (0.5 mL) was heated at 220°C in 1-pentanol (1 mL) for 15 minutes. After cooling, pentane (100 mL) was added to precipitate a solid residue. The residue was purified using column chromatography (CHCl$_3$, Al$_2$O$_3$). After removing the solvent, the product was obtained as a green solid.

Yield: 72 mg, 0.075 mmol, 24 %.

MS (APCI-HRMS(+)): m/z = 963.5727 [MH]$^+$, calcd. for [C$_{56}$H$_{67}$N$_{16}$]$^+$: 963.5729.
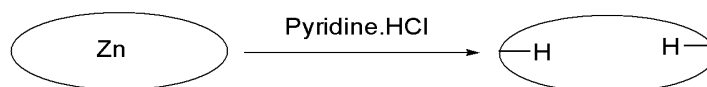
Method 2: A mixture of [Ppz*Zn] (72 mg, 0.0701 mmol), pyridine (5 mL) and pyridine-HCl (1.507 g, 13 mmol) was stirred overnight at 110°C under an argon atmosphere. Afterwards, the mixture was cooled down and H$_2$O (10 mL) was added. Finally, the precipitate was filtered, washed with water and dried under vacuum.

Yield: 57 mg, 0.0594 mmol, 85 %.

4.5.21 Synthesis of [Ppz*AlCl]
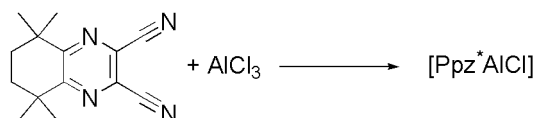
A mixture of PzDN* (300 mg, 1.248 mmol) and AlCl$_3$ (83 mg, 0.624 mmol) was heated at 220°C under an argon atmosphere for 30 minutes. The solid residue was washed with diethyl ether (2x20 mL) and purified by column chromatography (THF, Al$_2$O$_3$). After removing the solvent, the product was obtained as a blue-green solid.

Yield: 225 mg, 0.221 mmol, 71 %.

Elemental analysis: (C$_{56}$H$_{64}$N$_{16}$AlCl, 1023.65 g/mol)

Found (Calculated): C: 67.27% (65.71%), H: 7.97% (6.30%), N: 19.13% (21.89%).

¹H-NMR (300 MHz, CDCl₃): δ/ppm = 2.27 (s, 16H, H_ε), 1.43 (s, 48H, $H_{\delta1+2}$).

¹³C-NMR (75 MHz, CDCl₃): δ/ppm = 125.5, 59.6, 38.2, 32.0, 29.7, 22.7, 14.2.

UV/Vis. (CHCl₃): λ/nm = 642 (s), 614 (sh), 582 (w), 352 (m), 296 (m), 244 (m).

Fluorescence (CHCl₃): λ = 647 nm.

MS (APCI-HRMS(+)): m/z=1023.5083[MH]⁺, calcd. for [C₅₆H₆₅N₁₆AlCl]⁺:1023.5075.

4.5.22 Synthesis of [Ppz*AlF]
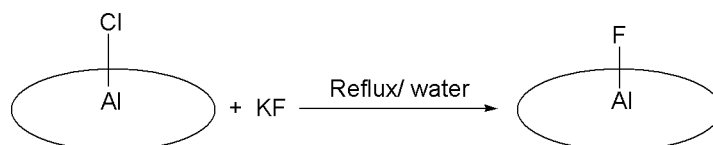
A mixture of [Ppz*AlCl] (100 mg, 0.099 mmol), KF (1.45 g, 24.96 mmol) and H₂O (100 mL) was refluxed overnight. After cooling, the blue solid was filtered, washed with water and dried under vacuum.

Yield: 94 mg, 0.094 mmol, 96 %.

Elemental analysis: (C₅₆H₆₄N₁₆AlF, 1007.19 g/mol)

Found (Calculated): C: 68.34% (66.78%), H: 8.23% (6.40%), N: 20.07% (22.25%).

¹H-NMR (300 MHz, CDCl₃): δ/ppm = 2.27 (s, 16H, H_ε), 1.43 (s, 48H, $H_{\delta1+2}$).

¹³C-NMR (75 MHz, CDCl₃): δ/ppm = 125.6, 68.1, 34.3, 30.4, 25.7, 21.3.

IR: $\tilde{v}$/cm⁻¹ = 431 (w), 699 (m), 797 (s), 1009 (s), 1080 (s), 1259 (s), 1456 (m), 2919 (m).

UV/Vis. (CHCl₃): λ/nm = 642 (s), 612 (w), 580 (w), 357 (s), 293 (m), 250 (m).

MS (APCI-HRMS(+)): m/z = 1007.5370[MH]⁺, calcd. for C₅₆H₆₅N₁₆AlF⁺: 1007.5372.

4.5.23 Attempted synthesis of [Ppz*AlOH]
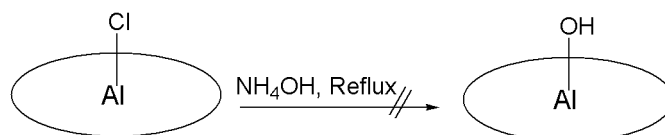
Attempt 1: A mixture of [Ppz*AlCl] (100 mg, 0.098 mmol), conc. NH₄OH (10 mL) and H₂O (50 mL) was refluxed overnight, then the solvent was removed by filtration. The product was characterized as [Ppz*AlCl].
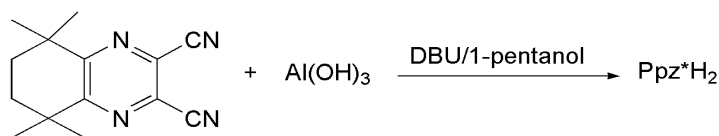
Attempt 2: A mixture of PzDN* (300 mg, 1.248 mmol), excess $Al(OH)_3$ (0.34 g, 3.33 mmol), DBU (0.5 mL) and 1-pentanol (2 mL) was heated for 60 minutes at 220°C. After cooling, pentane (20 mL) was added to precipitate a solid. This solid was washed with diethyl ether (2x20 mL) and purified by column chromatography ($CHCl_3$, Al_2O_3). After removing the solvent, the resulting blue product was characterized as Ppz*H_2.

Additional information:

When a similar mixture was heated overnight at 160°C, no reaction took place.
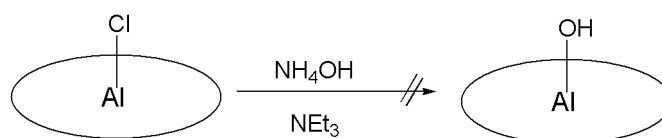
Attempt 3: A mixture of [Ppz*AlCl] (124 mg, 0.121 mmol), conc. NH_4OH (50 mL) and triethylamine (50 mL) was stirred for two days, then a solid was precipitated by adding pentane (200 mL). The solvent was removed by filtration and the obtained product was characterized as [Ppz*AlCl].

4.5.24 Attempted synthesis of [Ppz*AlSH]
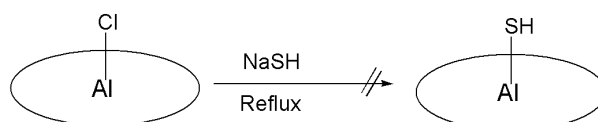
A mixture of [Ppz*AlCl] (100 mg, 0.098 mmol), NaSH (927 mg, 17.34 mmol) and toluene (100 mL) was refluxed overnight then the solvent was removed under reduced pressure and the product was characterized as [Ppz*AlCl].

Additional information:

When a similar mixture was refluxed for 3 h in acetone, the chromophore was destroyed.

4.5.25 Attempted synthesis of [Ppz*AlCH₃]
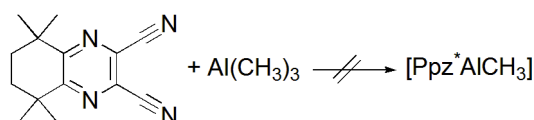
Attempt 1: A mixture of PzDN* (300 mg, 1.248 mmol) and Al(CH$_3$)$_3$ (60.16 mg, 0.08 mL, 0.834 mmol) was heated at 220°C under an argon atmosphere for 30 minutes. The product was washed with diethyl ether (2x30 mL) then purified by column chromatography (THF, Al$_2$O$_3$). The green product could not be identified by MS (APCI-HRMS(+)) measurements.
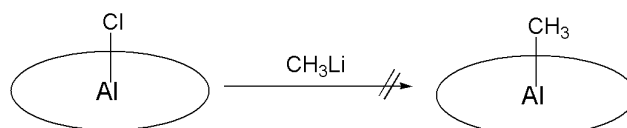
Attempt 2: A mixture of [Ppz*AlCl] (104 mg, 0.102 mmol), CH$_3$Li (2.45 mg, 0.112 mmol contained in 0.07 mL of 1.595 M in diethyl ether) and dry toluene (30 mL) was stirred under an argon atmosphere for 3 hours. The chromophore was destroyed.

Additional information

The same was obtained, when Et$_2$O was used as a solvent.
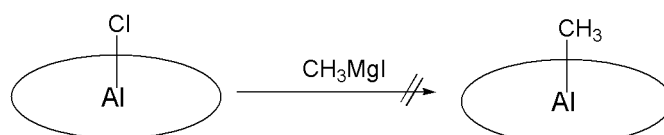
Attempt 3: A mixture of [Ppz*AlCl] (121 mg, 0.118 mmol), CH$_3$MgI (22.27 mg, 0.134 mmol contained in 0.06 mL of 2.218 M in diethyl ether) and dry THF (30 mL) was stirred for 3 hours under an argon atmosphere. This led to destruction of the chromophore.

Additional information

When the experiment was performed in dry toluene at 120°C, no reaction took place.

4.5.26 Attempted synthesis of [Ppz*AlC$_2$H$_5$]
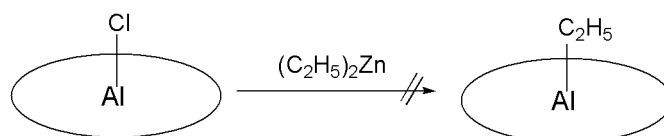
A mixture of [Ppz*AlCl] (100 mg, 0.098 mmol), (C$_2$H$_5$)$_2$Zn (12.07 mg, 0.0977 mmol contained in 0.110 g of toluene solution) and dry diethyl ether (30 mL) was stirred for 3 h under an argon atmosphere. The chromophore was destroyed.

4.5.27 Attempted synthesis of [Ppz*AlC₆H₅]
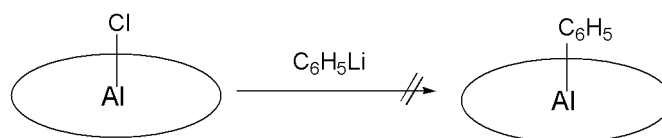
A mixture of [Ppz*AlCl] (164 mg, 0.160 mmol), C_6H_5Li (13.45 mg, 0.16 mmol contained in 0.08 mL of 2 M in dibutyl ether) and dry toluene (30 mL) was stirred at 120°C for 3 h under an argon atmosphere. The chromophore was destroyed.

4.5.28 Attempted synthesis of [Ppz*AlNMe₂]
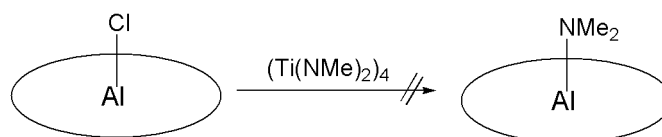
A mixture of [Ppz*AlCl] (100 mg, 0.098 mmol), $Ti(NMe_2)_4$ (48.8 mg, 0.214 mmol, 0.05 mL) and dry diethyl ether (30 mL) was stirred for 3 hours under an argon atmosphere. The solvent was removed under vacuum and the product was characterized as [Ppz*AlCl].

Additional information

When the experiment was performed in dry toluene at 100°C, no reaction took place.

4.5.29 Attempted synthesis of [Ppz*AlOP(O)(OH)₂] or [(Ppz*AlO)₂P(O)(OH)]
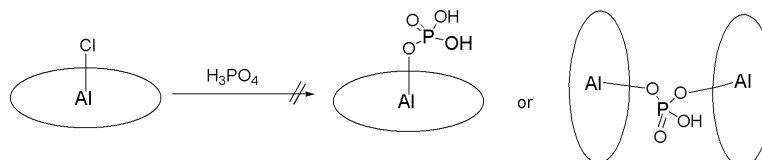
[Ppz*AlCl] (197 mg, 0.192 mmol) was stirred in H_3PO_4 (85 %, 25 mL) at 110°C for 24 h. Then, the product was precipitated by adding water (100 mL). After filtration, the product was washed with Na_2CO_3 solution and water. The product was characterized as [Ppz*AlCl].

Additional information:

When the experiment was performed overnight under refluxing conditions, the chromophore was destroyed.

173

4.5.30 Synthesis of [Ppz*GaCl]
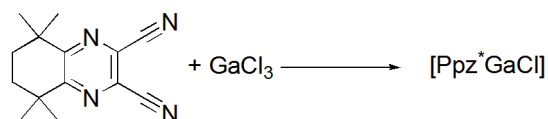
A mixture of PzDN* (300 mg, 1.248 mmol) and GaCl$_3$ (109 mg, 0.624 mmol) was heated at 220°C under an argon atmosphere for 30 minutes. The obtained solid residue was washed with diethyl ether (2x20 mL) and purified by column chromatography (THF, Al$_2$O$_3$). After removing the solvent, the product was obtained as a green solid.

Yield: 138 mg, 0.130 mmol, 42 %.

Elemental analysis: (C$_{56}$H$_{64}$N$_{16}$GaCl, 1066.39 g/mol)

Found (Calculated): C: 63.04% (63.07%), H: 7.35% (6.05%), N: 19.47% (21.02%).

^{1}H-NMR (300 MHz, CDCl$_3$): δ/ppm = 2.08 (s, 16H, H_ε), 1.84 (s, 48H, $H_{\delta 1+2}$)

^{13}C-NMR (75 MHz, CDCl$_3$): δ/ppm = 151.6, 135.9, 128.3, 125.6, 34.2, 30.4, 21.3.

UV/Vis. (CHCl$_3$): λ/nm = 648 (s), 622 (sh), 586 (w), 442 (sh), 352 (m), 278 (s), 244 (s).

Fluorescence (CHCl$_3$): λ = 652 nm.

MS(APCI-HRMS(+)): m/z=1067.4498[MH]$^+$, calcd. for [C$_{56}$H$_{65}$N$_{16}$GaCl]$^+$:1067.4515.

4.5.31 Attempted synthesis of [Ppz*GaF]
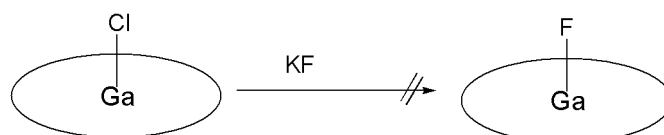
A mixture of [Ppz*GaCl] (112 mg, 0.105 mmol) and KF (1.64 g, 28.23 mmol) and H$_2$O (100 mL) was refluxed overnight. The green solid was filtered and characterized as [Ppz*GaCl].

4.5.32 Attempted synthesis of [Ppz*GaCH$_3$]
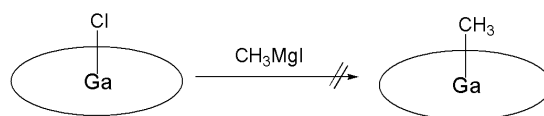
Attempt 1: A mixture of [Pz*GaCl] (230 mg, 0.216 mmol), CH$_3$MgI (110.6 mg, 0.665 mmol contained in 0.3 mL of 2.218 M in diethyl ether) and dry toluene (30 mL) was stirred overnight at 100°C under an argon atmosphere. The solvent was removed under reduced pressure. After washing with pentane, the product was identified as [Ppz*GaCl].

Additional information:

When the experiment was performed in dry THF at room temperature, the chromophore was destroyed.
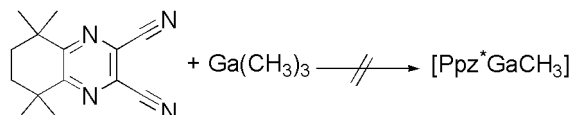
Attempt 2: A mixture of PzDN* (300 mg, 1.248 mmol) and Ga(CH$_3$)$_3$ (79.24 mg, 0.690 mmol, 0.07 mL) was heated for 30 minutes at 220°C under an argon atmosphere. The obtained solid residue was washed with diethyl ether (2x20 mL) and purified by column chromatography (THF, Al$_2$O$_3$). The resulting pale green product could not be identified by either ^{1}H-NMR or MS (APCI-HRMS(+)) measurements.
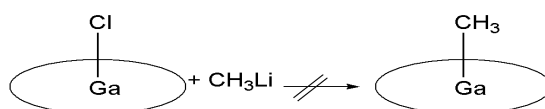
Attempt 3: A mixture of [Ppz*GaCl] (186 mg, 0.174 mmol), CH$_3$Li (3.52 mg, 0.16 mmol, contained in 0.1 mL of 1.595 M in dimethyl ether) and dry toluene (30 mL) was stirred overnight under an argon atmosphere. The chromophore was destroyed.

4.5.33 Synthesis of [Ppz*InCl]
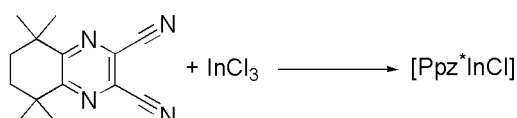
A mixture of PzDN* (300 mg, 1.248 mmol) and InCl$_3$ (138 mg, 0.624 mmol) was heated at 220°C under an argon atmosphere for 30 minutes. After cooling, the solid residue was added to CH$_2$Cl$_2$ (200 mL) and filtered off to remove the insoluble part. The filtrate was concentrated and washed with methanol until the washing methanol became colorless. The green product was dried under vacuum.

Yield: 44 mg, 0.040 mmol, 13 %.

Elemental analysis: (C$_{56}$H$_{64}$N$_{16}$InCl, 1111.48 g/mol)

Found (Calculated): C: 58.36% (60.50%), H: 6.08% (5.82%), N: 19.94% (20.17%).

^{1}H-NMR (300 MHz, CDCl$_3$): δ/ppm = 2.29 (s, 16H, H_ε), 1.93 (s, 24H, $H_{\delta 1}$), 1.83 (s, 24H, $H_{\delta 2}$).

^{13}C-NMR (75 MHz, CDCl$_3$): δ/ppm = 164.6, 150.4, 146.5, 39.4, 34.0, 30.7, 30.4.

UV/Vis. (CHCl$_3$): λ/nm = 648 (s), 621 (sh), 590 (m), 356 (s), 298 (m), 258 (m).

Fluorescence (CHCl$_3$): λ = 652 nm.

MS (APCI-HRMS(+)):m/z=1111.4293[MH]$^+$,calcd. for [C$_{56}$H$_{65}$N$_{16}$InCl]$^+$:1111.4300.

4.5.34 Attempted synthesis of [Ppz*InF]
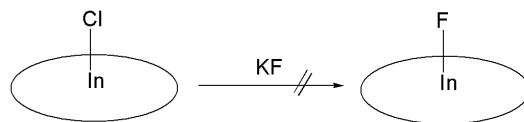
A mixture of [Ppz*InCl] (93 mg, 0.0836 mmol), KF (1.60 g, 27.54 mmol) and H$_2$O (100 mL) was refluxed overnight. Then, the green solid was filtered and characterized as [Ppz*InCl].

4.5.35 Synthesis of [Ppz*SiCl$_2$]
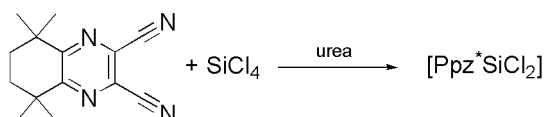
A mixture of PzDN* (300 mg, 1.248 mmol), SiCl$_4$ (148 mg, 0.1 mL, 0.871 mmol) and urea (149 mg, 2.49 mmol) was heated at 220°C under an argon atmosphere for 30 minutes. The product was washed with diethyl ether (2x20 mL) and purified by column chromatography (CHCl$_3$, Al$_2$O$_3$). After removing the solvent, the desired product was obtained as a blue-green solid.

Yield: 88 mg, 0.081 mmol, 27 %.

^{1}H-NMR (300 MHz, CDCl$_3$): δ/ppm = 2.25 (s, 16H, H$_\varepsilon$), 1.97 (s, 48H, H$_{\delta 1+2}$).

UV/Vis. (CDCl$_3$): λ/nm = 652 (s), 590 (w), 357 (m), 296 (m), 244 (m).

MS (APCI-HRMS(+)) : m/z = 1059.4719[MH]$^+$, calcd. for [C$_{56}$H$_{65}$N$_{16}$SiCl$_2$]$^+$: 1059.4730.

4.5.36 Attempted synthesis of [Ppz*SiF$_2$]
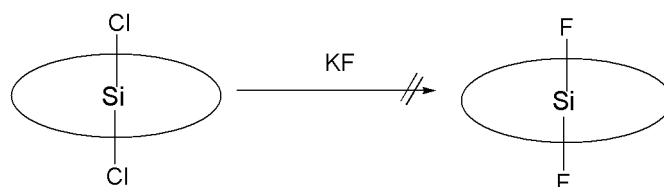
A mixture of [Ppz*SiCl$_2$] (113 mg, 0.107 mmol), KF (2.92 g, 50.3 mmol) and H$_2$O (50 mL) was refluxed overnight. No reaction took place.

4.5.37 Synthesis of [Ppz*Si(Oi-Pr)₂]

A mixture of isopropanol (50 mL) and [Ppz*SiCl₂] (114 mg, 0.108 mmol) was refluxed overnight. After removing the solvent under reduced pressure, the product was obtained as a blue - green solid.

Yield: 105 mg, 0.104 mmol, 89 %.

UV/Vis. (CHCl₃): λ/nm = 644(s), 606(m), 588(m), 384(m), 346(s), 320(s), 257(s).

MS (APCI-HRMS(+)): m/z = 1107.6333 [MH]⁺, calcd. for $[C_{56}H_{65}N_{16}Si(OC_3H_7)_2]^+$: 1107.6336.

4.5.38 Attempted synthesis of [Ppz*Si(CH₃)₂]
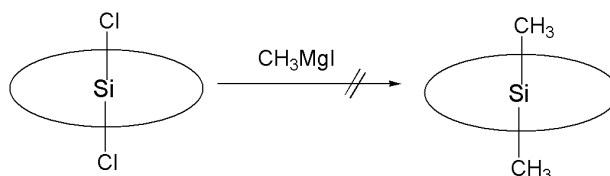
Attempt 1: A mixture of [Ppz*SiCl₂] (176 mg, 0.166 mmol), CH₃MgI (89.54 mg, 0.586 mmol contained in 0.38 mL of 2.218 M solution in diethyl ether) and THF (20 mL) was stirred overnight at room temperature under an argon atmosphere. This led to destruction of the chromophore.

Additional information

When the experiment was performed in dry toluene, the same result was obtained.
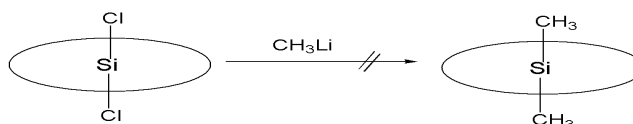
Attempt 2: A mixture of [Ppz*SiCl₂] (112 mg, 0.106 mmol), CH₃Li (5.26 mg, 0.239 mmol contained in 0.15 mL of 1.595 M solution in diethyl ether) and dry toluene (20 mL) was stirred overnight under argon. This led to destruction of the chromophore.

177
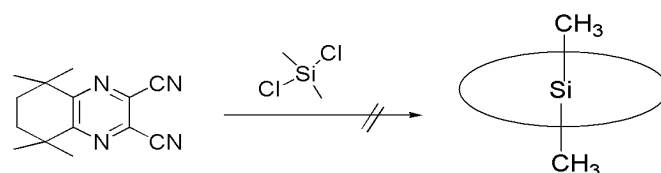
Attempt 3: A mixture of PzDN* (300 mg, 1.248 mmol), $(CH_3)_2SiCl_2$ (106 mg, 0.1 mL, 0.824 mmol) and urea (149 mg, 2.49 mmol) was heated at 220°C for 30 minutes under an argon atmosphere. The product was washed with diethyl ether (2x20 mL) and purified by column chromatography ($CHCl_3$, Al_2O_3). The pale green product could not be identified by either ^1H-NMR or MS (APCI-HRMS(+)) measurements.

4.5.39 Attempted synthesis of [Ppz*Si(C₆H₅)₂]
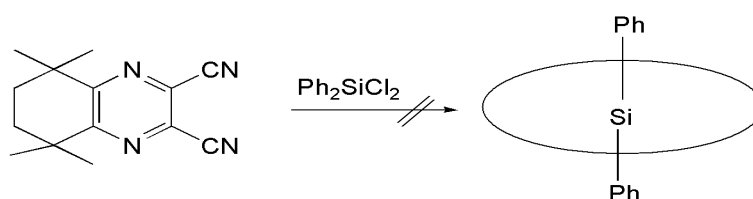
A mixture of PzDN* (300 mg, 1.248 mmol), $(C_6H_5)_2SiCl_2$ (180.6 mg, 0.15 mL, 0.713 mmol) and urea (149 mg, 2.49 mmol) was heated at 220°C for 30 minutes under an argon atmosphere. The product was washed with diethyl ether (2x20 mL) and purified by column chromatography ($CHCl_3$, Al_2O_3). The pale green product could not be identified by either ^1H-NMR or MS (APCI-HRMS(+)) measurements.

4.5.40 Synthesis of [Ppz*Ge(OH)₂]
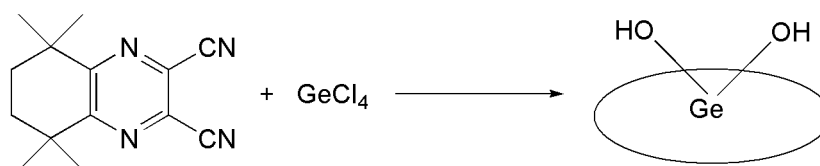
A mixture of PzDN* (300 mg, 1.248 mmol), $GeCl_4$ (150.4 mg, 0.08 mL, 0.701 mmol) and urea (149 mg, 2.49 mmol) was heated at 220°C for 30 minutes under an argon atmosphere. The product was washed with diethyl ether (2x20 mL) and purified by column chromatography ($CHCl_3$, Al_2O_3). After removing the solvent, the product was obtained as a blue-green solid.

Yield: 92 mg, 0.083 mmol, 28.221 %.

Elemental analysis: ($C_{56}H_{64}N_{16}Ge(OH)_2$, 1067.87 g/mol)

Found (Calculated): C: 58.82% (62.99%), H: 7.51% (6.23%), N: 17.94% (20.99%).

^1H-NMR (300 MHz, $CDCl_3$): δ/ppm = 2.24 (s, 16H, H_ε), 1.96 (s, 48H, $H_{\delta1+2}$), 3.33 (bs, 2H, Ge(OH)₂) .

^{13}**C-NMR** (75 MHz, CDCl$_3$): δ/ppm = 165.7, 164.9, 145.4, 39.7, 34.2, 30.9, 29.5.

UV/Vis. (CHCl$_3$): λ/nm = 636(s), 610(sh), 577(w), 354(m).

MS (APCI-HRMS(+)) : m/z = 1065.4883 [MH+CH$_3$-H$_2$O]$^+$, calcd. for [C$_{56}$H$_{65}$N$_{16}$GeOCH$_3$]$^+$: 1065.4892.

4.5.41 Attempted synthesis of [Ppz*Mg]
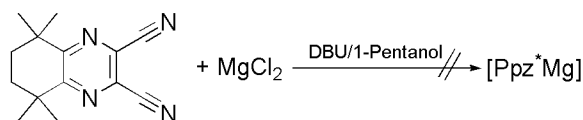
A mixture of PzDN* (300 mg, 1.248 mmol), MgCl$_2$.6H$_2$O (127 mg, 0.624 mmol), DBU (0.5 mL) and 1-pentanol (3 mL) was stirred for 20 minutes at 220°C under an argon atmosphere. Then, the mixture was cooled to 160°C and stirred overnight at this temperature. After cooling, pentane (20 mL) was added to precipitate a brown solid. The solid was isolated and purified by column chromatography (CHCl$_3$, Al$_2$O$_3$). The product could not be identified by either ^{1}H-NMR or MS (APCI-HRMS(+)) measurements.

4.5.42 Attempted synthesis of [Ppz*ScCl]
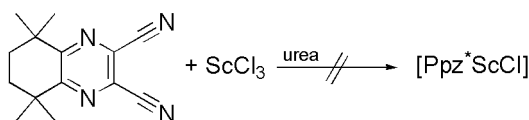
Attempt 1: A mixture of PzDN* (300 mg, 1.248 mmol), ScCl$_3$ (94 mg, 0.624 mmol), urea (149 mg, 2.49 mmol) and 1-CNP (2 mL) was heated overnight at 160°C under an argon atmosphere. After cooling, pentane (20 mL) was added to precipitate a dark solid. The solid was purified by column chromatography (CHCl$_3$, Al$_2$O$_3$). The obtained pale green product could not be identified by either ^{1}H-NMR or MS (APCI-HRMS(+)) measurements.

Attempt 2: A mixture of PzDN* (300 mg, 1.248 mmol), ScCl$_3$ (94 mg, 0.624 mmol) and urea (149 mg, 2.49 mmol) was heated at 220°C for 30 minutes under an argon atmosphere. Then, the product was washed with diethyl ether (2x20 mL) and purified by column chromatography (CHCl$_3$, Al$_2$O$_3$). The pale green product could not be identified by either ^{1}H-NMR or MS (APCI-HRMS(+)) measurements.
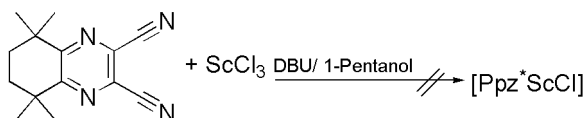
Attempt 3: A mixture of PzDN* (300 mg, 1.248 mmol), ScCl$_3$ (94 mg, 0.624 mmol), DBU (0.5 mL) and 1-pentanol (3 mL) was heated for 60 minutes at 220°C under an argon

atmosphere. After cooling to 160°C, stirring was continued overnight at this temperature then pentane (20 mL) was added to precipitate a brown solid. The solid was purified by column chromatography (CHCl$_3$, Al$_2$O$_3$). The product could not be identified by either ^{1}H-NMR or MS (APCI-HRMS(+)) measurements.

4.5.43 Attempted synthesis of [Ppz*ZrCl$_2$]
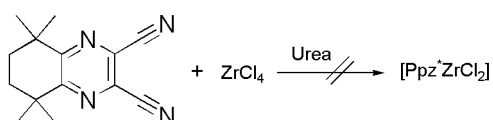
Attempt 1: A mixture of PzDN* (300 mg, 1.248 mmol), ZrCl$_4$ (145 mg, 0.624 mmol) and urea (149 mg, 2.49 mmol) was heated at 220°C for 30 minutes under an argon atmosphere. The product was washed with diethyl ether (2x20 mL) and purified by column chromatography (CHCl$_3$, Al$_2$O$_3$). The pale green product could not be identified by either ^{1}H-NMR or MS (APCI-HRMS(+)) measurements.
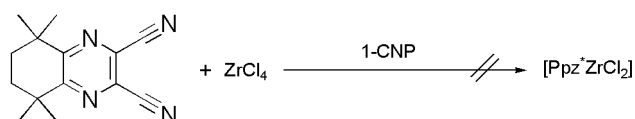
Attempt 2: A solution of PzDN* (300 mg, 1.248 mmol) in 1-CNP (2 mL) was heated at 220°C for an hour, then ZrCl$_4$ (145 mg, 0.624 mmol) was added and the solution was stirred at this temperature under an argon atmosphere for 30 minutes. After cooling, pentane (20 mL) was added to precipitate a dark residue. The residue was washed with diethyl ether (2x20 mL) and purified by column chromatography (CHCl$_3$, Al$_2$O$_3$). The pale green product could not be identified by either ^{1}H-NMR or MS (APCI-HRMS(+)) measurements.

4.5.44 Attempted synthesis of [Ppz*ZrBr$_2$]
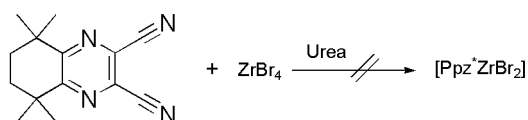
A mixture of PzDN* (300 mg, 1.248 mmol), ZrBr$_4$ (256 mg, 0.624 mmol) and urea (149 mg, 2.49 mmol) was heated at 220°C for 30 minutes under an argon atmosphere. The product was washed with diethyl ether (2x20 mL) and purified by column chromatography (CHCl$_3$, Al$_2$O$_3$). The pale green product could not be identified by either ^{1}H-NMR or MS (APCI-HRMS(+)) measurements.

4.5.45 Attempted synthesis of [Ppz*Mo]
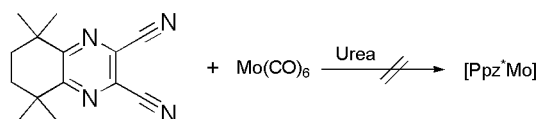
A mixture of PzDN* (300 mg, 1.248 mmol), $Mo(CO)_6$ (165 mg, 0.624 mmol) and urea (149 mg, 2.49 mmol) was heated at 220°C for 30 minutes under an argon atmosphere. The product was washed with diethyl ether (2x20 mL) and purified by column chromatography ($CHCl_3$, Al_2O_3). The pale green product could not be identified by either ^{1}H-NMR or MS (APCI-HRMS(+)) measurements.

4.5.46 Attempted synthesis of [Ppz*MoO]
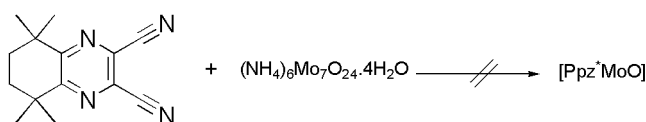
A mixture of PzDN* (300 mg, 1.248 mmol) and $(NH_4)_6Mo_7O_{24}.4H_2O$ (1.54 g, 1.248 mmol) was heated at 220°C for 30 minutes under an argon atmosphere. The obtained solid residue was washed with diethyl ether (2x20 mL) and purified by column chromatography ($CHCl_3$, Al_2O_3). The pale green product could not be identified by either ^{1}H-NMR or MS (APCI-HRMS(+)) measurements.

4.5.47 Attempted synthesis of [Ppz*MoN]
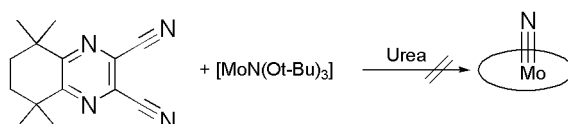
A mixture of PzDN* (300 mg, 1.248 mmol), $[MoN(Ot-Bu)_3]$ (206 mg, 0.624 mmol) and urea (149 mg, 2.49 mmol) was heated at 220°C for 30 minutes under an argon atmosphere. After cooling, the solid residue was washed with diethyl ether and dissolved in chloroform. No chromophore was obtained.

4.5.48 Attempted synthesis of [Ppz*W]
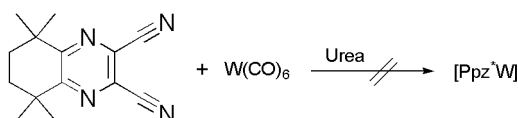
A mixture of PzDN* (300 mg, 1.248 mmol), $W(CO)_6$ (220 mg, 0.624 mmol) and urea (149 mg, 2.49 mmol) was heated at 220°C for 30 minutes under an argon atmosphere. The product was washed with diethyl ether (2x20 mL) and purified by column

chromatography (CHCl$_3$, Al$_2$O$_3$). The pale green product could not be identified by either ^{1}H-NMR or MS (APCI-HRMS(+)) measurements.

4.5.49 Attempted synthesis of [Ppz*WN]
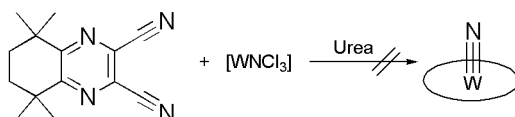
A mixture of PzDN* (300 mg, 1.248 mmol), WNCl$_3$ (189 mg, 0.624 mmol) and urea (149 mg, 2.49 mmol) was heated at 220°C for 30 minutes under an argon atmosphere. After cooling, the solid residue was washed with diethyl ether and dissolved in chloroform. No chromophore was obtained.

4.5.50 Attempted synthesis of [Ppz*W(Nt-Bu)Cl]
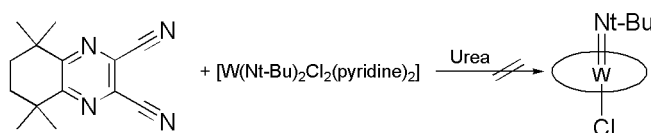
A mixture of PzDN* (300 mg, 1.248 mmol), [W(Nt-Bu)$_2$Cl$_2$(Py)$_2$] (346 mg, 0.624 mmol) and urea (149 mg, 2.49 mmol) was heated at 220°C for 30 minutes under an argon atmosphere. After cooling, the solid residue was washed with diethyl ether and dissolved in chloroform. No chromophore was obtained.

4.5.51 Attempted synthesis of [Ppz*WWPpz*]
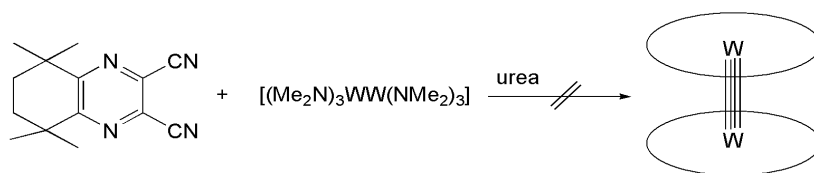
A mixture of PzDN* (300 mg, 1.248 mmol), [(MeN)$_3$WW(NMe$_2$)$_3$] (394 mg, 0.624 mmol) and urea (149 mg, 2.49 mmol) was heated at 220°C for 30 minutes under an argon atmosphere. After cooling, the solid residue was washed with diethyl ether and dissolved in chloroform. No chromophore was obtained.

4.5.52 Attempted synthesis of [Ppz*Re(Nt-Bu)Cl]
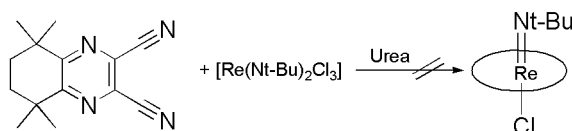
A mixture of PzDN* (300 mg, 1.248 mmol), [Re(Nt-Bu)$_2$Cl$_3$] (271 mg, 0.624 mmol) and urea (149 mg, 2.49 mmol) was heated at 220°C for 30 minutes under an argon atmosphere. After cooling, the solid residue was washed with diethyl ether and dissolved in chloroform. The product is not colorful.

4.5.53 Attempted synthesis of [Ppz*Cd]
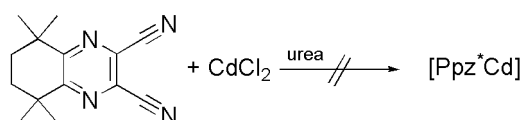
Attempt 1: A mixture of PzDN* (300 mg, 1.248 mmol), CdCl$_2$.H$_2$O (125 mg, 0.624 mmol) and urea (149 mg, 2.49 mmol) was heated at 220°C for 30 minutes under an argon atmosphere. The product was washed with diethyl ether (2x20 mL) and purified by column chromatography (CHCl$_3$, Al$_2$O$_3$). The pale green product could not be identified by either ^{1}H-NMR or MS (APCI-HRMS(+)) measurements.
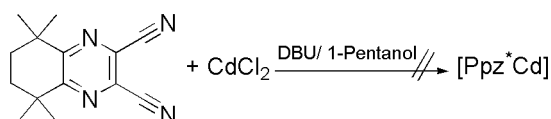
Attempt 2: A mixture of PzDN* (300 mg, 1.248 mmol), CdCl$_2$.H$_2$O (125 mg, 0.624 mmol), DBU (0.5 mL) and 1-pentanol (3 mL) was stirred for 20 minutes at 220°C under an argon atmosphere. After cooling to 160°C, the mixture was stirred overnight at this temperature. Afterwards, pentane (20 mL) was added to precipitate a brown solid. The solid was isolated and purified by column chromatography (CHCl$_3$, Al$_2$O$_3$). The obtained product could not be identified by either ^{1}H-NMR or MS (APCI-HRMS(+)) measurements.

4.5.54 Attempted synthesis of [Ppz*SnCl$_2$]
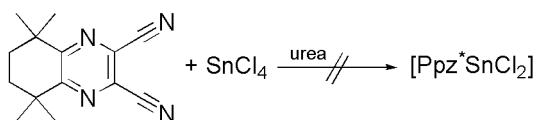
A mixture of PzDN* (355 mg, 1.477 mmol), SnCl$_4$.5H$_2$O (259 mg, 0.739 mmol) and urea (177 mg, 2.95 mmol) was heated at 220°C under an argon atmosphere for 30 minutes. The obtained solid residue was dissolved in chloroform. No chromophore was obtained.

4.5.55 Attempted synthesis of [Ppz*Pb]
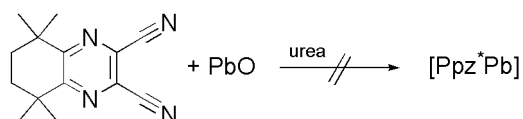
A mixture of PzDN* (300 mg, 1.248 mmol), PbO (139 mg, 0.624 mmol) and urea (149 mg, 2.49 mmol) was heated at 220°C under an argon atmosphere for 30 minutes. The product was washed with diethyl ether (2x20 mL) and purified by column chromatography (CHCl$_3$, Al$_2$O$_3$). The pale green product could not be identified by either ^{1}H-NMR or MS (APCI-HRMS(+)) measurements.

Additional information:

Using Pb(CH$_3$COO)$_2$.3H$_2$O as a metal template led to the same result.

4.6 Synthesis of Ppz# complexes

4.6.1 Synthesis of [Ppz#Co]
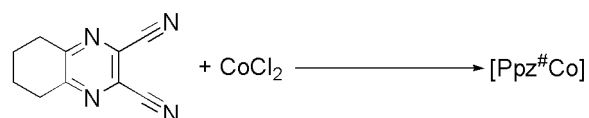
A mixture of PzDN# (350 mg, 1.900 mmol), CoCl$_2$.6H$_2$O (228 mg, 0.96 mmol) and urea (228 mg, 3.80 mmol) was heated at 220°C for 30 minutes under an argon atmosphere. The product was washed with ethanol (3x20 mL), water (3x20 mL) and chloroform until the solution became colorless. Finally, the residue was dissolved in pyridine (10 mL) and filtered through a short Al$_2$O$_3$ column ($\sim$ 5 cm). After removal of pyridine under reduced pressure, the product was obtained as a green solid.

MS (APCI-HRMS(+)): m/z = 796.2391 [MH]$^+$, calcd. for [C$_{40}$H$_{33}$N$_{16}$Co]$^+$: 796.2401.

4.6.2 Synthesis of [Ppz#Cu]
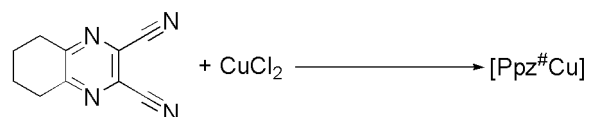
A mixture of PzDN# (328 mg, 1.780 mmol), CuCl$_2$.2H$_2$O (153 mg, 0.90 mmol) and urea (215 mg, 3.56 mmol) was heated at 220°C for 30 minutes under an argon atmosphere. The product was washed with ethanol (3x20 mL), water (3x20 mL) and chloroform until the solution became colorless. Finally, the residue was dissolved in pyridine (10 mL) and filtered through a short Al$_2$O$_3$ column ($\sim$ 5 cm). After removal of pyridine under reduced pressure, the product was obtained as a green solid.

MS (APCI-HRMS(+)): m/z = 800.2371 [MH]$^+$, calcd. For [C$_{40}$H$_{33}$N$_{16}$Cu]$^+$: 801.2365.

4.7 Attempted synthesis of [(CatPpz*)Zn]
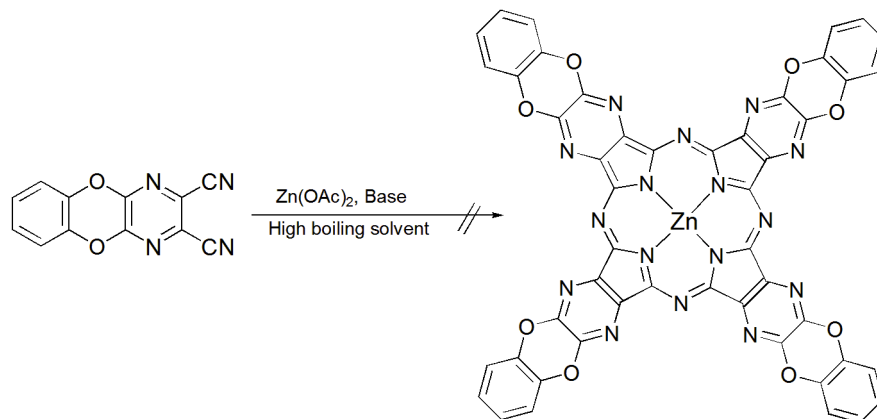
Although several attempts to prepare the zinc azaphthalocyanine compound [(CatPpz*)Zn] were performed (Table 31), the obtained products are not colorful and could not be characterized by either EI mass spectrometry or UV / Vis. spectroscopy.

Table 31: Testing conditions for attempted synthesis of [(CatPpz*)Zn].

Number	CatPzDN*	Zn(OAc)$_2$.2H$_2$O	Base	Solvent	Temperature	Duration
1	100 mg, 0.423 mmol, 2.0 eq	47 mg, 0.211 mmol, 1.0 eq	Urea	Quinoline(1mL)	160°C	20h
2	200 mg, 0.847 mmol, 2.0 eq	93 mg, 0.423 mmol, 1.0 eq	Urea	-	220°C	25 min.
3	200 mg, 0.847 mmol, 2.0 eq	93 mg, 0.423 mmol, 1.0 eq	DBU	1-Octanol(1mL)	160°C	18h
4	50 mg, 0.212 mmol, 2.0 eq	23 mg, 0.106 mmol, 1.0 eq	Urea	1-CNP(1mL)	160°C	20h

4.8 New synthetic procedures for [PcTiS][320]

4.8.1 Successful strategies
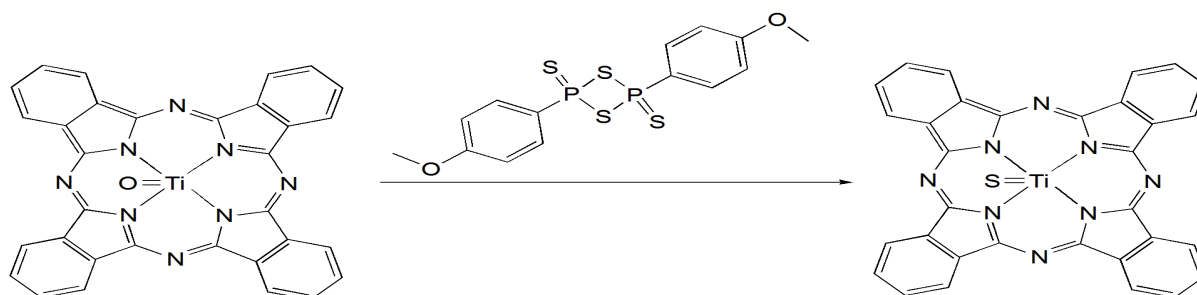
Method 1: A mixture of [PcTiO] (1 g, 1.7 mmol) and Lawesson's reagent (1.41 g, 3.5 mmol) was refluxed in dry toluene (20 mL) for 8 hours then the solution was cooled to room temperature and stirred overnight. The resulting dark green product was washed with toluene and THF and dried under vacuum.

Yield: 0.833 g (1.4 mmol, 81 %).

MS(APCI-HRMS(+)): m/z=591.1182[MH]$^+$, calcd. for [C$_{32}$H$_{17}$N$_8$TiS]$^+$: 591.0614.
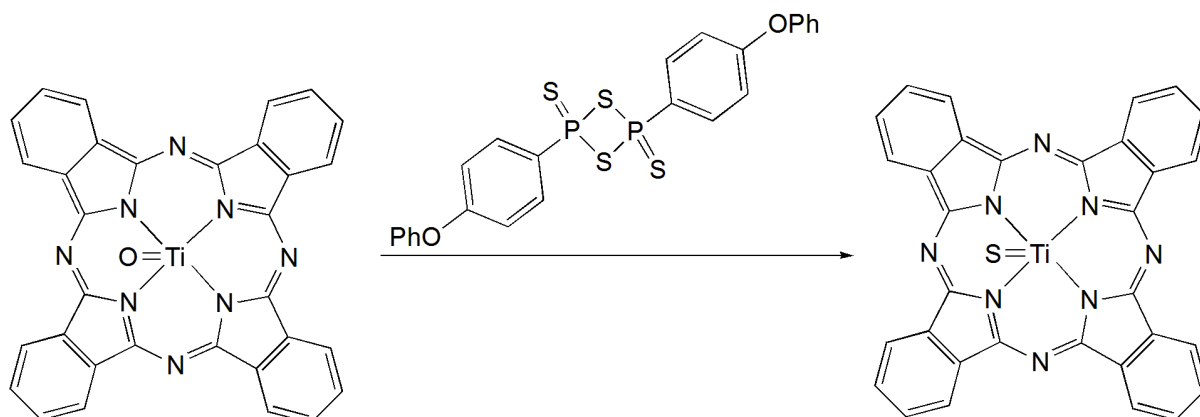
Method 2: A mixture of [PcTiO] (1 g, 1.7 mmol) and 2,4-bis(4-phenoxyphenyl)-1,3,2,4-dithiadiphosphetan-2,4-disulphide (3.69 g, 7.0 mmol) was refluxed in dry toluene for 9 hours, then the solution was stirred overnight at 100 °C. The resulting dark green product was washed with THF and dried at 250°C under vacuum.

Yield: quantitative.

IR: $\tilde{v}$/cm^{-1} = 495 (w), 732 (m), 1001 (b), 1240 (m).

MS (APCI-HRMS(+)) m/z = 591.1169 [MH]$^+$, calcd. for [C$_{32}$H$_{17}$N$_8$TiS]$^+$: 591.0614.

MS (LDI-TOF): m/z = 592.45 [C$_{32}$H$_{16}$N$_8$TiS]$^+$.

4.8.2 Unsuccessful strategies
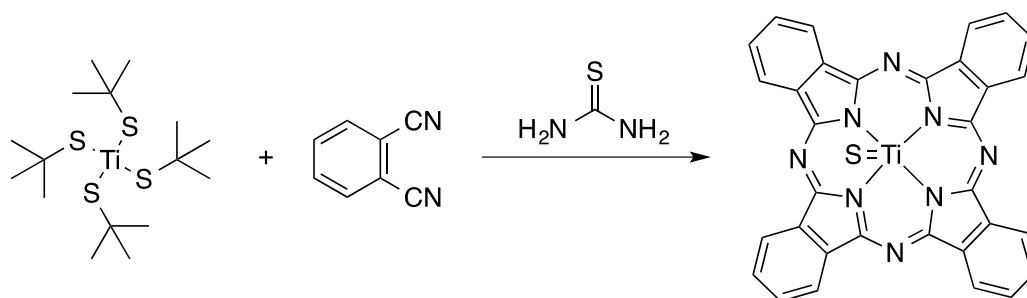
Method 1: A mixture of PDN (0.112 g, 0.9 mmol), Ti(S-tert-butyl)$_4$ (0.349 g, 0.9 mmol) and thiourea (0.131 g, 1.7 mmol) was heated at 220 °C for 30 minutes under nitrogen. To the product, a mixture of DCM (50 mL) and TFA (5 mL) was added and the mixture was filtered under nitrogen to remove the insoluble black residue. Removing the solvent under reduced pressure resulted in formation of an unidentified green product.

Additional information:

Performing the experiment in 1-octanthiol for 6 h at 150°C resulted in formation of an unidentified brown product.
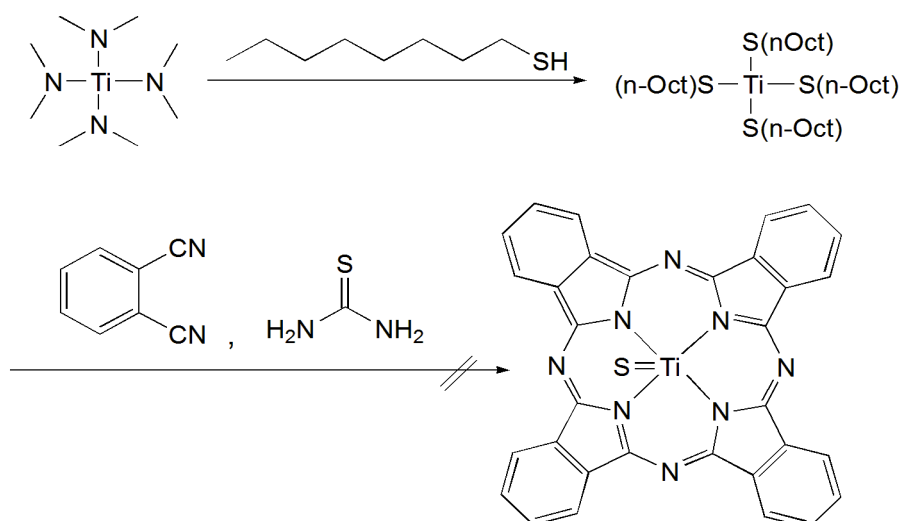
Method 2: To a solution of Ti(NMe$_2$)$_4$ (3 g, 13.37 mmol) in pentane (30 mL) at 25 °C, 1-octanthiol (40 mL, 214.1 mmol) was added. Immediately after the addition, the solution became dark red then the excess pentane was removed under vacuum. To the product, PDN (3.127 g, 24.4 mmol) and thiourea (0.929 g, 12.2 mmol) were added then the mixture was heated at 150 °C for 6 hours under nitrogen. After cooling to room temperature, ethanthiol (20 mL) was added and the mixture was refluxed for 30 minutes. The dark brown product was filtered, washed with toluene, ethanthiol and pentane and dried under vacuum. The product could not be identified by either (APCI-HRMS(+)) or UV/Vis. measurements.

4.8.3 Synthesis of [PcTiSe][320]
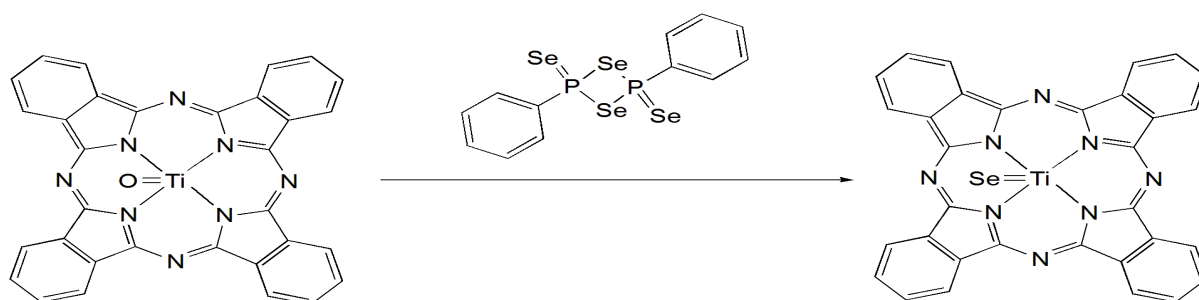
A mixture of [PcTiO] (1 g, 1.7 mmol) and Woollin's reagent (3.692 g, 6.9 mmol) was refluxed in dry toluene (100 mL) for 9 hours. Then, the solution was stirred overnight at 100°C. The resulting dark green product was washed with refluxing toluene and dried under vacuum.

Yield: quantitative.

IR: $\tilde{v}$/cm^{-1} = 526 (w), 685 (w), 723 (w), 890 (s), 948 (m), 1066 (w), 1141 (s), 1324 (s).

MS (LDI-TOF): *m/z* = 639.35 [C$_{32}$H$_{16}$N$_8$TiSe]$^+$.

UV/Vis (CNP): λ/nm = 693 (s), 363 (s).

4.9   Crystallographic Results

The crystal structure analyses were carried out at the Department of Chemistry, Philipps-Universität Marburg on a Stoe IPDS 2 area detector system using MoKα radiation (λ = 71.073 pm) at 100 K. Stoe IPDS software[183] was used for integration and data reduction. Structure solution and refinement were done using the WinGX program[184] suite using SHELX-86[185] and SHELX-97.[186] In the case of [Pc*Co], heavily disordered solvent molecules could not be modeled adequately. Thus the SQUEEZE routine of the PLATON program package[187] was used to remove the corresponding delocalized electron density from the data sets. Molecular graphics were produced with Diamond 3.0a.[188] In most cases, the hydrogen atoms and any solvent molecules have been removed for clarity. Ellipsoids are shown at 50% probability.

4.9.1   1,1,4,4-Tetramethyl-6,7-dibromotetraline

Crystallographer	Christian Prinzisky	
Habitus, colour	block, translucent light colourless	
Crystal size	0.494 x 0.432 x 0.150 mm^3	
Crystal system	Monoclinic	
Space group	P 21/c	Z = 4
Unit cell dimensions	a = 8.2765(4) Å	α= 90°.
	b = 9.0010(4) Å	β= 94.110(2)°.
	c = 18.2323(7) Å	γ = 90°.
Volume	1354.75(10) Å^3	
Empirical formula	C$_{14}$ H$_{18}$ Br$_2$	
Formula weight	346.10	
Density (calculated)	1.697 Mg/m^3	
Absorption coefficient	5.956 mm^{-1}	
F(000)	688	
Reflections collected	17790	
Independent reflections	2460 [R(int) = 0.0634]	
Completeness to theta = 25.000°	99.9 %	
Observed reflections	2203[II > 2(I)]	
Reflections used for refinement	2460	
Absorption correction	Semi-empirical from equivalents	
Max. and min. transmission	0.7452 and 0.2846	
Largest diff. peak and hole	0.718 and -0.518 e.Å^{-3}	
Refinement	Full-matrix least-squares on F^2	
Data / restraints / parameters	2460 / 0 / 149	
Goodness-of-fit on F^2	1.071	
R index (all data)	wR2 = 0.0686	
R index conventional [I>2sigma(I)]	R1 = 0.0263	

4.9.2   2-Bromo-3,3,6,6-hexamethylcyclohexanone

Crystallographer	Christian Prinzisky	
Habitus, colour	plate-like, colourlessg	
Crystal size	0.350 x 0.120 x 0.020 mm^3	
Crystal system	monoclinic	
Space group	P 21/c	Z = 4
Unit cell dimensions	a = 8.6550(3) Å	α= 90°.
	b = 12.7860(4) Å	β= 111.3530(10)°.
	c = 10.3443(3) Å	γ = 90°.
Volume	1066.15(6) Å^3	
Cell determination	130 peaks with Theta 5.4 to 25.5°.	
Empirical formula	C10 H17 Br O	
Formula weight	233.14	
Density (calculated)	1.453 Mg/m^3	
Absorption coefficient	3.811 mm^{-1}	
F(000)	480	
Reflections collected	21513	
Independent reflections	2320 [R(int) = 0.0415]	
Completeness to theta = 25.000°	99.9 %	
Observed reflections	2147[II > 2(I)]	
Reflections used for refinement	2320	
Absorption correction	Semi-empirical from equivalents	
Max. and min. transmission	0.7455 and 0.5298	
Largest diff. peak and hole	0.405 and -0.426 e.Å^{-3}	
Refinement	Full-matrix least-squares on F^2	
Data / restraints / parameters	2320 / 0 / 113	
Goodness-of-fit on F^2	1.066	
R index (all data)	wR2 = 0.0445	
R index conventional [I>2sigma(I)]	R1 = 0.0174	

4.9.3 [Pc*VO].4CHCl$_3$

Crystallographer	Dr. Klaus Harms & Christian Prinzisky	
Habitus, colour	prism, green	
Crystal size	0.29 x 0.07 x 0.05 mm^3	
Crystal system	Monoclinic	
Space group	P 1 21/c 1	Z = 2
Unit cell dimensions	a = 11.8492(12) Å	α= 90°.
	b = 23.456(2) Å	β= 90.054(6)°.
	c = 12.8910(14) Å	γ = 90°.
Volume	3582.9(6) Å^3	
Cell determination	111 peaks with Theta 2.5 to 25.0°.	
Empirical formula	C$_{68}$ H$_{76}$ Cl$_{12}$ N$_8$ O V	
Formula weight	1497.71	
Density (calculated)	1.388 Mg/m^3	
Absorption coefficient	0.634 mm^{-1}	
F(000)	1550	
Reflections collected	60066	
Independent reflections	6299 [R(int) = 0.1067]	
Completeness to theta = 25.00°	99.9 %	
Observed reflections	4814[I>2(I)]	
Reflections used for refinement	6299	
Absorption correction	Semi-empirical from equivalents	
Max. and min. transmission	0.7455 and 0.5704	
Largest diff. peak and hole	0.913 and -0.734 e.Å^{-3}	
Refinement	Full-matrix least-squares on F^2	
Data / restraints / parameters	6299 / 86 / 468	
Goodness-of-fit on F^2	1.119	
R index (all data)	wR2 = 0.1564	
R index conventional [I>2sigma(I)]	R1 = 0.0704	

4.9.4 [Pc*Co]

Crystallographer	Christian Prinzisky	
Habitus, colour	block-like, blue	
Crystal size	0.140 x 0.130 x 0.090 mm^3	
Crystal system	triclinic	
Space group	P -1	Z = 1
Unit cell dimensions	a = 10.4590(5) Å	α= 70.742(2)°.
	b = 13.4426(6) Å	β= 67.879(2)°.
	c = 13.6434(6) Å	γ = 70.993(2)°.
Volume	1632.45(13) Å^3	
Cell determination	124 peaks with Theta 3.6 to 23.2°.	
Empirical formula	$C_{64} H_{72} Co N_8$	
Formula weight	1012.22	
Density (calculated)	1.030 Mg/m^3	
Absorption coefficient	0.303 mm^{-1}	
F(000)	539	
Reflections collected	7076	
Independent reflections	7076 [R(int) = ?]	
Completeness to theta = 25.000°	99.5 %	
Observed reflections	5849[II > 2(I)]	
Reflections used for refinement	7076	
Absorption correction	Semi-empirical from equivalents	
Max. and min. transmission	1.0000 and 0.9454	
Largest diff. peak and hole	0.846 and -0.391 e.Å^{-3}	
Refinement	Full-matrix least-squares on F^2	
Data / restraints / parameters	7076 / 0 / 339	
Goodness-of-fit on F^2	1.118	
R index (all data)	wR2 = 0.1331	
R index conventional [I>2sigma(I)]	R1 = 0.0484	

4.9.5 [Pc*Ni].4CHCl$_3$

Crystallographer	Lars Hendrik Finger	
Habitus, colour	needle, green	
Crystal size	0.37 x 0.07 x 0.04 mm^3	
Crystal system	Monoclinic	
Space group	P 21/c	Z = 2
Unit cell dimensions	a = 11.727(4) Å	α= 90°.
	b = 22.985(7) Å	β= 90.240(12)°.
	c = 12.931(4) Å	γ = 90°.
Volume	3485.5(19) Å^3	
Cell determination	3687 peaks with Theta 2.4 to 24.5°.	
Empirical formula	C$_{68}$ H$_{76}$ Cl$_{12}$ N$_8$ Ni	
Formula weight	1489.48	
Density (calculated)	1.419 Mg/m^3	
Absorption coefficient	0.786 mm^{-1}	
F(000)	1544	
Reflections collected	32273	
Independent reflections	6135 [R(int) = 0.1617]	
Completeness to theta = 25.00°	99.9 %	
Observed reflections	3815[I>2(I)]	
Reflections used for refinement	6135	
Absorption correction	Semi-empirical from equivalents	
Max. and min. transmission	0.7455 and 0.4738	
Largest diff. peak and hole	1.023 and -0.699 e.Å^{-3}	
Refinement	Full-matrix least-squares on F^2	
Data / restraints / parameters	6135 / 0 / 411	
Goodness-of-fit on F^2	1.018	
R index (all data)	wR2 = 0.1813	
R index conventional [I>2sigma(I)]	R1 = 0.0693	

193

4.9.6   [Pc*Cu].4CHCl$_3$

Crystallographer	Christian Prinzisky	
Habitus, colour	prism, blue-green	
Crystal size	0.27 x 0.04 x 0.04 mm^3	
Crystal system	Monoclinic	
Space group	P 21/c	Z = 2
Unit cell dimensions	a = 11.7760(11) Å	α= 90°.
	b = 23.2066(13) Å	β= 90.314(8)°.
	c = 12.9591(12) Å	γ = 90°.
Volume	3541.4(5) Å^3	
Cell determination	9350 peaks with Theta 1.7 to 25.1°.	
Empirical formula	C$_{68}$ H$_{76}$ Cl$_{12}$ Cu N$_8$	
Formula weight	1494.31	
Density (calculated)	1.401 Mg/m^3	
Absorption coefficient	0.808 mm^{-1}	
F(000)	1546	
Reflections collected	18719	
Independent reflections	6210 [R(int) = 0.1497]	
Completeness to theta = 25.00°	99.8 %	
Observed reflections	2970[I>2(I)]	
Reflections used for refinement	6210	
Absorption correction	Semi-empirical from equivalents	
Max. and min. transmission	1.0047 and 0.8394	
Largest diff. peak and hole	0.609 and -1.903 e.Å^{-3}	
Refinement	Full-matrix least-squares on F^2	
Data / restraints / parameters	6210 / 0 / 411	
Goodness-of-fit on F^2	0.904	
R index (all data)	wR2 = 0.2082	
R index conventional [I>2sigma(I)]	R1 = 0.0735	

4.9.7 [Ppz*VO(H₂O)].8DCM

Crystallographer	Lars Hendrik Finger	
Habitus, colour	plate, blue	
Crystal size	0.370 x 0.120 x 0.100 mm^3	
Crystal system	tetragonal	
Space group	P 4/n m m	Z = 2
Unit cell dimensions	a = 26.3873(17) Å	α= 90°.
	b = 26.3873 Å	β= 90°.
	c = 13.3566(11) Å	γ = 90°.
Volume	9300.1(14) Å^3	
Cell determination	122 peaks with Theta 2.3 to 17.8°.	
Empirical formula	C$_{128}$ H$_{161}$ Cl$_{32}$ N$_{32}$ O$_{12}$ V$_2$	
Formula weight	3576.17	
Density (calculated)	1.277 Mg/m^3	
Absorption coefficient	0.617 mm^{-1}	
F(000)	3678	
Reflections collected	109297	
Independent reflections	5551 [R(int) = 0.1120]	
Completeness to theta = 25.240°	99.9 %	
Observed reflections	3874[II > 2(I)]	
Reflections used for refinement	5551	
Absorption correction	Semi-empirical from equivalents	
Max. and min. transmission	0.7455 and 0.6408	
Largest diff. peak and hole	2.045 and -1.108 e.Å^{-3}	
Refinement	Full-matrix least-squares on F^2	
Data / restraints / parameters	5551 / 14 / 323	
Goodness-of-fit on F^2	1.050	
R index (all data)	wR2 = 0.3584	
R index conventional [I>2sigma(I)]	R1 = 0.1146	

4.9.8 [Ppz*MnCl].5CHCl₃

Crystallographer	Christian Prinzisky	
Habitus, colour	plate-like, metallic dark blue-black	
Crystal size	0.280 x 0.250 x 0.050 mm^3	
Crystal system	tetragonal	
Space group	P 42/n	Z = 4
Unit cell dimensions	a = 17.5096(10) Å	α= 90.0000(10)°.
	b = 17.5096(10) Å	β= 90.0000(10)°.
	c = 24.5917(15) Å	γ = 90.0000(10)°.
Volume	7539.5(10) Å^3	
Cell determination	127 peaks with Theta 3.1 to 21.6°.	
Empirical formula	$C_{61} H_{69} Cl_{16}$ Mn N_{16}	
Formula weight	1655.40	
Density (calculated)	1.458 Mg/m^3	
Absorption coefficient	0.792 mm^{-1}	
F(000)	3388	
Reflections collected	39709	
Independent reflections	8200 [R(int) = 0.1168]	
Completeness to theta = 25.000°	99.7 %	
Observed reflections	5171[II > 2(I)]	
Reflections used for refinement	8200	
Absorption correction	Semi-empirical from equivalents	
Max. and min. transmission	1.000 and 0.845	
Largest diff. peak and hole	0.911 and -0.730 e.Å^{-3}	
Refinement	Full-matrix least-squares on F^2	
Data / restraints / parameters	8200 / 48 / 534	
Goodness-of-fit on F^2	1.136	
R index (all data)	wR2 = 0.2301	
R index conventional [I>2sigma(I)]	R1 = 0.0826	

4.9.9 [Ppz*AlF(OH₂)]

Crystallographer	Christian Prinzisky	
Habitus, colour	block, black	
Crystal size	0.284 x 0.121 x 0.118 mm^3	
Crystal system	Monoclinic	
Space group	P 21/c	Z = 4
Unit cell dimensions	a = 19.810(5) Å	α= 90°.
	b = 23.975(5) Å	β= 105.703(5)°.
	c = 15.377(5) Å	γ = 90°.
Volume	7031(3) Å^3	
Cell determination	9148 peaks with Theta 1.4 to 27.1°.	
Empirical formula	$C_{61.14}$ $H_{77.92}$ Al Cl_3 F N_{16} $O_{1.81}$	
Formula weight	1218.28	
Density (calculated)	1.151 Mg/m^3	
Absorption coefficient	0.196 mm^{-1}	
F(000)	2577	
Reflections collected	43343	
Independent reflections	14914 [R(int) = 0.1439]	
Completeness to theta = 25.00°	99.9 %	
Observed reflections	3802[I>2(I)]	
Reflections used for refinement	14914	
Absorption correction	Semi-empirical from equivalents	
Max. and min. transmission	0.9724 and 0.9597	
Largest diff. peak and hole	1.021 and -0.292 e.Å^{-3}	
Refinement	Full-matrix least-squares on F^2	
Data / restraints / parameters	14914 / 36 / 826	
Goodness-of-fit on F^2	0.861	
R index (all data)	wR2 = 0.3423	
R index conventional [I>2sigma(I)]	R1 = 0.1078	

197

5 References

[1]   M. Hanack, H. Heckmann, R. Polley, in Houben-Weyl, Methods of Organic Chemistry, F: *Aromatic and Heteroaromatic Large Rings*, Vol. 4, Thieme, Stuttgart, **1997**, pp. 717-842.

[2]   K. J. Balkus, C. C. Leznoff, A. B. P. Lever, *Phthalocyanines, Properties and Applications* Wiley-VCH, New York, **1989**.

[3]   N. B. McKeown, in *Science of Synthesis*, Vol 17, Thieme Stuttgart, **2003**.

[4]   A. Braun, J. Tcherniac, *Ber. Dtsch. Chem. Ges.*, **1907**, 40, 2709-2714.

[5]   H. de Diesbach, E. von der Weid, *Helv. Chim. Acta*, **1927**, 10, 886-888.

[6]   R. P. Linstead, A. R. Lowe, *J. Chem. Soc.*, **1934**, 1016-1017.

[7]   S. N. Brumfield, V. W. Foltz, C. M. McGhee, A. L. Thomas, *J. Org. Chem.*, **1962**, 27, 2266-2267.

[8]   R. M. Christie, D. D. Deans, *Perkin Trans.*, **1989**, 2, 193-198.

[9]   M. Gorsch, H. Homborg, *Z. anorg. allg. Chem.*, **1998**, 624, 634-641.

[10]   A. Meller, A. Ossko, *Monatsh. Chem.*, **1972**, 103, 150-155.

[11]   V. W. Day, T. J. Marks, W. A. Wachter, *J. Am. Chem. Soc.*, **1975**, 97, 4519-4527.

[12]   N. Ishikawa, *J. Porphyrins Phthalocyanines*, **2001**, 5, 87-101.

[13]   G.A. Corker, B. Grant, N. J. Clecak, *J. Electrochem. Soc.*, **1979**, 126, 1339-1343.

[14]   M-T Riou, M. Auregan, C. Clarisse, *J. Electroanal. Chem.*, **1985**, 187, 349-354.

[15]   M. L'Her, Y. Cozien, J. Courtot-Coupez, *C. R. Acad. Sci. Paris Se´r. II*, **1985**, 11, 487-509.

[16]   A . Chang, J-C. Marchon, *Inorg. Chim. Acta*, **1981**, 53, L241-L243.

[17]   J-J Andre´, K. Holczer, P. Petit, M-T. Riou, C. Clarisse, R. Even, M. Fourmigue, J. Simon, *Chem. Phys. Lett.*, **1985**, 115, 463-466.

[18]   P. Turek, P. Petit, J-J. Andre´, J. Simon, R. Even, B. Boudjema, G. Guillaud, M. Maitrot, *J. Am. Chem. Soc.*, **1987**, 109, 5119-5122.

[19]   M. Maitrot, G. Guillaud, B. Boudjema, J-J. Andre´, H. Strzelecka, J. Simon, R. Even, *Chem. Phys. Lett.*, **1987**, 133, 59-62.

[20]   P. Petit, K. Holczer, J-J. Andre´, *J. Phys.*, **1987**, 48, 1363-1367.

[21]   Z. Belarbi, C. Sirlin, J. Simon, J-J. Andre´, *J. Phys. Chem.*, **1989**, 93, 8105-8110.

[22]   J. Yao, H. Yonehara, C. Pac, *Bull. Chem. Soc. Jpn.*, **1995**, 68, 1001-1005.

[23]   A. B. P. Lever, in *Advances in inorganic chemistry and radiochemistry* (Eds.: H. J. Eleméus, A. G. Sharpe), Academic Press, New York, **1981**.

[24]   L. H. Vogt, A. Zalkin, D. H. Templeton, *Inorg. Chem.,* **1967**, 6, 1725-1730.

[25]   V. L. Goedken, G. Dessy, C. Ercolani, V. Fares, L. Gastaldi, *Inorg. Chem.*, **1985**, 24, 991-995.

[26]   W. Darwish, S. Schlecht, A. Schaper, M. Fröba, K. Harms, W. Massa, J. Sundermeyer, *Z. anorg. allg. Chem.*, **2009**, 635, 1215-1224.

[27]   K. Schweiger, H. Hückstädt, H. Homborg, *Z. anorg. allg. Chem.*, **1997**, 623, 1853-1854.

[28]   J. Mack, N. Kobayashi, *Chem. Rev.,* **2011**, 111, 281-321.

[29] K. M. Kadish, K. Smith, M. R. Guilard, *The Porphyrin Handbook* Vol. 20, Elsevier Science, San Diego, California, USA, 2003.

[30] G. de la Torre, P. Vazquez, F. Agullo-Lopez, T. Torres, *J. Mater. Chem.*, **1998**, 8, 1671-1683.

[31] N. Kobayashi, R. Kondo, S. Nakajima, T. Osa, *J. Am. Chem. Soc.*, **1990**, 112, 9640-9641.

[32] C. C. Leznoff, T. W. Hall, *Tetrahedron Lett.* **1982**, 23, 3023-3026.

[33] J. G. Young, W. Onyebuagu, *J. Org. Chem.*, **1990**, 55, 2155-2159.

[34] K. J. M. Nolan, M. Hu, C. C. Leznoff, *Synlett*, **1997**, 5, 593-594.

[35] E. A. Ough, M. J. Stillman, K. A. M. Creber, *Can. J. Chem.*, **1993**, 71, 1898-1909.

[36] J. R. Lakowicz, *Principles of fluorescence spectroscopy*, Plenum Press, New York, **1983**.

[37] G. G. Guilbault, *Practical fluorescence*, M. Dekker: New York, **1990**.

[38] P. G. Varley, *Methods in molecular biology*, Clifton, N.J., **1994,** 22, 203-218.

[39] Dewey, T. G. *Biophysical and biochemical aspects of fluorescence spectroscopy*, Plenum Press, New York, **1991**.

[40] L. C. Hwang, T. Wohland, *ChemPhysChem*, **2004**, 5, 549-551.

[41] S. A. Soper, H. L. Nutter, R. A. Keller, L. M. Davis, E. B. Shera, *Photochem.Photobiol.*, **1993**, 57, 972-977.

[42] M. Hof, R. Hutterer, V. Fidler, *Fluorescence spectroscopy in biology : advanced methods and their applications to membranes, proteins, DNA, and cells*, Springer: Berlin, New York, **2005**.

[43] S. A. Soper, D. Williams, *Analytical Chemistry*, **1995**, 67, 3427-3432.

[44] S. A. Soper, C. Owens, S. Lassiter, Y. Xu, *Topics in Fluorescence Spectroscopy*, **2003**, 1-68.

[45] B. N. G. Giepmans, S.R. Adams, M. H. Ellisman, R. Y. Tsien, *Science*, **2006**, 312, 217-224.

[46] G. G. Guilbault, *Fluorescence : theory, instrumentation, and practice*, M. Dekker: New York, **1967**.

[47] R. S. Becker, *Theory and interpretation of fluorescence and phosphorescence*, Wiley Interscience: New York, **1969**.

[48] B. Valeur, *Molecular fluorescence: principles and applications*, Wiley-VCH: Weinheim, **2002**.

[49] R. P. Linstead, E. G. Noble, J. M. Wright, *J. Chem. Soc.,* **1937**, 911-921.

[50] A. R. Katritzky, D. Zhang, K. Kirichenko, *J. Org. Chem.*, **2005**, 70, 3271-3274.

[51] J. M. Khurana, B. M. Kandpal, *Tetrahedron Lett.*, **2003**, 44, 4909-4912.

[52] R. Zibuck, D. Seebach, *Helv. Chim. Acta*, **1988**, 71, 237-240.

[53] S. Makhseed, F. Ibrahim, C. G. Bezzu, N. B. McKeown, *Tetrahedron Lett.*, **2007**, 48, 7358-7361.

[54] E. G. Gal'pern, E. A. Luk'yanets, M. G. Gal'pern, *Russ. Chem. Bull.*, **1973**, 22, 1925-1929.

[55] D. Dini, M. Hanack, H.-J. Egelhaaf, J. C. Sancho-García, J. Cornil, *J. Phys. Chem. B*, **2005**, 109, 5425-5432.

[56] G. Winter, H. Heckmann, P. Haisch, W. Eberhardt, M. Hanack, L. Lüer, H.-J. Egelhaaf, D. Oelkrug, *J. Am. Chem. Soc.,* **1998**, 120, 11663-11673.

[57] F Mitzel, S. FitzGerald., A. Beeby, R. Faust, *Eur. J. Org. Chem.,* **2004**, 2004, 1136-1142.

[58] G. Guillaud, J. Simon, J.P. Germain, *Coord. Chem. Rev.*, **1998**, 180, 1433-1484.

[59]   M. Bouvet, K. Kadish, K. M. Smith, R. Guilard, *The Porphyrin Handbook*, Vol. 19 Boston, **2003**, 37-98.

[60]   M. A. Loi, H. Neugebauer, P. Denk, C. J. Brabeck, N. S. Sariciftci, A. Gouloumis, P. Vazquez, T. Torres, *J. Mater. Chem.*, **2003**, 13, 700-704.

[61]   D. M. Guldi, A. Gouloumis, P. Vazquez, T. Torres, *Chem. Commun.*, **2002**, 2056-2058.

[62]   Y. H. Gursel, B. F. Senkal, M. Kandaz, F. Yakuphanoglu, *Polyhedron*, **2009**, 28, 1490-1496.

[63]   M. Durmus, S. Y. Ilot, V. Ahsen, *New J. Chem.*, **2006**, 30(5), 675-678.

[64]   J. W. Perry, K. Mansour, I. Y. S. Lee, X. L. Wu, P. V. Bedworth, C. T. Chen, D. Ng, S. R. Marder, P. Miles, T. Wada, M. Tian, H. Sasabe, *Science*, **1996**, 273(5281), 1533-1536.

[65]   M. Hanack, T. Schneider, M. Barthel, J. S. Shirk, S. R. Flom, R. G. S. Pong, *Coord. Chem. Rev.*, **2001**, 219-221, **2001**, 235-258.

[66]   Y. Chen, M. Hanack, Y. Araki, O. Ito, *Chem. Soc. Rev.*, **2005**, 34, 517-529.

[67]   J. Simon, P. Bassoul, *Desing of Molecular Materials, Supramolecular Engineering*, John Wiley Sons. Ltd, West Sussex, **2000**.

[68]   S. R. Flom, in *The Porphyrin Handbook*, Vol. 19, (Eds.: K. Kadish, K.M. Smith, R. Guilard), Boston, **2003**, pp. 179-189.

[69]   M. N. Yarasir, M. Kandaz, B. F. Senkal, A. Koca, B. Salih, *Polyhedron*, **2007**, 26, 5235-5242.

[70]   L. C. Penning, T. M. Dubbelman, *Anti-Cancer Drugs*, **1994**, 5, 139-146.

[71]   J. G. Moser, *Photodynamic Tumor Therapy: 2nd and 3rd Generation Photosensitizers*, Harwood Academic, Amsterdam, **1998**.

[72]   J. W. Hoffman, F. Zeeland, S. Turker, *J. Med. Chem.*, **2007**, 50(7), 1485-1494.

[73]   H. Kolarova, P. Nevrelova, R. Bajgar, *Toxicol. in Vitro*, **2007**, 21, 249-253.

[74]   T. Dougherty, *J Clin Laser Med Surg.*, **2002**, 20, 3-7.

[75]   C. Sibata, V. Colussi, N. Oleinick, T. Kinsella, *Expert Opin Pharmacother*, **2001**, 2, 917-927.

[76]   R. R. Allison, C. H. Sibata, *Photodiagnosis and Photodynamic Therapy*, **2010**, 7, 61-75.

[77]   T. Dougherty, M. Cooper, T. Mang, *Lasers Surg Med.*, **1990**, 10, 485-488.

[78]   S. Moriwaki, J. Misawa, Y. Yoshinari, I. Yamada, M. Takigawa, Y. Tokura, *Photodermatol Photoimmunol Photomed*, **2001**, 17, 241-243.

[79]   A. Peaston, M. Leach, R. Higgins, *J Am Vet Med Assoc.*, **1993**, 202(8), 1261-1265.

[80]   D. Dolmans, D. Fukumura, R. Jain, *Nat Rev Cancer*, **2003**, 3(5), 380-387.

[81]   E. Lukyanets, *J. Porphyrins Phthalocyanines*, **1999**, 3(6-7), 424-432.

[82]   L. Uspenskii, L. Chistov, E. Kogan, V. Loshchenov, I. A. Ablitsov, V. Rybin, *Khirurgiia (Mosk)*, **2000**, 2, 38-40.

[83]   V. Sokolov, E. Stranadko, N. Zharkova, R. Iakubovskaia, E. Filonenko, T. Astrakhankina, *Vopr Onkol*, **1995**, 41(2), 134-138.

[84]   E. Stranadko, M. Garbuzov, V. Zenger, A. Nasedkin, N. Markichev, M. Riabov, *Vestn Otorinolaringol.*, **2001**, 3, 36-39.

[85]   E. Filonenko, V. Sokolov, V. Chissov, E. Lukyanets, G. Vorozhtsov, *Photodiagnosis Photodyn Ther.*, **2008**, 5(3), 187-190.

[86]   J. Miller, E. Baron, H. Scull, A. Hsia, J. Berlin, T. McCormick, *Toxicol Appl Pharmacol.*, **2007**, 224(3), 290-299.

[87]   G. De Mori, Z. Fu, E. Viola, X. Cai, C. Ercolani, M. P. Donzello, K. M. Kadish, *Inorg. Chem.*, **2011**, 50, 8225-8237.

[88] D. Atilla, M. Durmus, A. G. Gurek, V. Ahsen, T. Nyokong, *Dalton Trans.,* **2007**, 1235-1243.

[89] D. R. Coulter, V. M. Miskowski, J. W. Perry, T. H. Wei, E. W. Van Stryland, A. D. J. Hagan, *SPIE proc.*, **1989**, 1105, 42-51.

[90] J. S. Shirk, R. G. S. Pong, S. R. Flom, H. Heckmann, M. Hanack, *J. Phys. Chem. A*, **2000**, 104 (7), 1438-1449.

[91] M. Garcia-Iglesias, J.J. Cid, J.-H. Yum, A. Forneli, P. Vazquez, M. K. Nazeeruddin, E. Palomares, M. Grätzel, T. Torres, *Energy Environ. Sci*., **2011**, 4, 189-194.

[92] D. A. Li, M. A. Ratner, T. J. Marks, *J. Am. Chem. Soc.*, **1988**, 110, 1707-1715.

[93] E. Karmann, J. –P. Meyer, D. Schlettwein, N. I. Jaeger, M. Anderson, A. Schmidt, N. R. Armstrong, *Mol. Cry. Liq. Cryst.,* **1996**, 283, 283.

[94] Z. Bao, A. J. Lovinger, J. Brown, *J. Am. Chem. Soc.*, **1998**, 120, 207-208.

[95] a) P. M. Kuznesof, R. S. Nohr, K. J. Whynne, *J. Macromole. Sci. Chem.*, **1981**, A16, 229. b) R. S. Nohr, K. J. Whynne, *J. Chem. Soc., Chem. Commun.*, **1981**, 1210-1211. c) K. J. Whynne, *Inorg. Chem.*, **1985**, 24, 1339-1343.

[96] K. J. Whynne, R. S. Nohr, *Mol. Cryst. Liq. Cryst.*, **1983**, 81, 243.

[97] P. Brant, R. S. Nohr, K. J. Whynne, D. C. Weber, *Mol. Cryst. Liq. Cryst.* **1982**, 81, 225.

[98] C. D. Dimitrakopoulos, P. R. L. Malenfant, *Adv. Mater.*, **2002**, 14, 99-117.

[99] M. Hanack, M. Lang, *Adv. Mater.*, **1994**, 6, 819-833.

[100] N. Lior, *Energy*, **2008**, 33, 842-857.

[101] S. S. Penner, J. Haraden, S. Mates, *Energy*, **1992**, 17, 883-899.

[102] http://en.wikipedia.org/wiki/Renewable_energy.

[103] D. Y. Goswami, *Advances in Solar Energy: An Annual Review of Research and Development*, **2003,** 15.

[104] C. Brabec, U. Scherf, V. Dyakonov, *Organic PhotoVoltaics: Materials, Device Physics, and Manufacturing Technologies*, Wiley- VCH: **2008**.

[105] V. Petrova-Koch, R. Hezel, A. Goetzberger, *High-Efficient Low-Cost PhotoVoltaics*, Springer Series in Optical Sciences, **2009**.

[106] S.-S. Sun, N. S. Sariciftci, *Organic PhotoVoltaics: Mechanisms, Materials, and Devices*, Marcel Dekker, **2005**.

[107] A. Smee, *Elements of Electro-Biology*, Longman, Brown, Green, and Longmans: London, **1849**.

[108] D. M. Chapin, C. S. Fuller, G. L. Pearson, *J. Appl. Phys.*, **1954**, 25, 676-677.

[109] M. A. Green, K. Emery, Y. Hishikawa, W. Warta, *Prog. Photovolt. Res. Appl.*, **2011**, 19, 84-92.

[110] A. F. Hollemann, E. Wiberg, *Lehrbuch der Anorganischen Chemie*, Vol. 101, de Gruyter, Berlin, New York, **1995**.

[111] A. W. Hains, Z. Liang, M. A. Woodhouse, B. A. Gregg, *Chem. Rev.,* **2010**, 110, 6689-6735.

[112] C. W. Tang, *Appl. Phys. Lett.*, **1986**, 48, 183-185.

[113] J.-L. Brédas, J. E. Norton, J. Cornil, V. Coropceanu, *Acc. Chem. Res.*, **2009**, 42, 1691-1699.

[114] I. Bruder, A. Ojala, C. Lennartz, S. Sundarraj, J. Schöneboom, R. Sens, J. Hwang, P. Erk, J. Weis, *Sol. Energy Mater. Sol. Cells*, **2010**, 94, 310-316.

[115] I. Bruder, J. Schöneboom, R. Dinnebier, A. Ojala, S. Schäfer, R. Sens, P. Erk, J. Weis, *Org. Electron.*, **2010**, 11, 377-387.

[116] S. Pfuetzner, J. Meiss, A. Petrich, M. Riede, K. Leo, *Appl. Phys. Lett.*, **2009**, 94, 223307.

[117] B. O'Regan, M. Grätzel, *Nature*, **1991**, 353, 737-740.

[118] A. Hagfeldt, M. Grätzel, *Chem. Rev.*, **1995**, 95, 49-68.

[119] M. Grätzel, *MRS Bull.*, **2005**, 30, 23-27.

[120] Y. Chiba, A. Islam, Y. Watanabe, R. Komiya, N. Koide, L. Han, *Jpn. J. Appl. Phys.*, **2006**, 45, 638-640.

[121] M. K. Nazeeruddin, F. De Angelis, S. Fantacci, A. Selloni, G. Viscardi, P. Liska, S. Ito, B. Takeru, M. Grätzel, *J. Am. Chem. Soc.*, **2005**, 127, 16835-16847.

[122] C. Li, M. Liu, N. G. Pschirer, M. Baumgarten, K. Müllen, *Chem. Rev.*, **2010**, 110, 6817–6855.

[123] M. K. Nazeeruddin, R. Humphry-Baker, M. Grätzel, D. Wohrle, G. Shnurpfeil, G. Schneider, A. Hirth, N. Trombach, *J. Porphyrins Phthalocyanines*, **1999**, 3, 230-237.

[124] J. He, G. Benko, F. Korodi, T. Polivka, R. Lomoth, B. Akermak, L. Sun, A. Hagfeldt, V. Sundstrom, *J. Am. Chem. Soc.*, **2002**, 124, 4922-4932.

[125] E. Palomares, M. V. Martinez-Diaz, S. A. Haque, T. Torres, J. R. Durrant, *Chem. Commun.*, **2004**, 2112-2113.

[126] S. Eu, T. Katoh, T. Umeyama, Y. Matano, H. Imahori, *Dalton Trans.*, **2008**, 5746-5754.

[127] S. Mori, M. Nagata, Y. Nakahata, K. Yasuta, R. Goto, M. Kimura, M. Taya, *J. Am. Chem. Soc.*, **2010**, 132, 4054-4055.

[128] G. Pozzi, S. Quici, M.C. Raffo, C.A. Bignozzi, S. Caramori, M. Orlandi, *J.Phys. Chem. C*, **2011**, 115, 3777-3788.

[129] M. Garcia-Iglesias, J.-H. Yum, R. Humphry-Baker, S.M. Zakeeruddin, P. Pechy, P. Vazquez, E. Palomares, M. Graetzel, M. K. Nazeeruddin, T. Torres, *Chem. Sci.*, **2011**, 2, 1145-1150.

[130] J. O. Morley, M. H. Charlton, *J. Phys. Chem.*, **1995**, 99, 1928-1934.

[131] M. Stillman, J. Mack, N. Kobayashi, *J. Porphyrins Phthalocyanines*, **2002**, 6, 296-300.

[132] N. Kobayashi, H. Konami, *J. Porphyrins Phthalocyanines*, **2001**, 5, 233-255.

[133] P. C. Minor, M. Gouterman, A. B. P. Lever, *Inorg. Chem.* **1985**, 24, 1894-1900.

[134] M. Gouterman, G. H. Wagniere, L. C. Snyder, *J. Mol. Spectrosc.*, **1963**, 11, 108-127.

[135] S. P. Keizer, J. Mack, B. A. Bench, S. M. Gorun, M. J. Stillman, *J. Am. Chem. Soc.*, **2003**, 125, 7067-7085.

[136] D. Huang, E. S. Liu, S. L. Yang, N. S. Chen, J. L. Huang, J. P. Duan, Y. Chen, *Spectroscopy and Spectral Analysis*, **2000**, 20, 95-98.

[137] M. J. Cook, A. J. Dunn, S. D. Howe, A. J. Thomson, K. J. Harrison, *Journal of the Chemical Society-Perkin Transactions*, **1988**, 1, 2453-2458.

[138] D. R. Tackley, G. Dent, W. E. Smith, *Phys. Chem. Chem. Phys.*, **2001**, 3, 1419-1426.

[139] A. Rosa, E. J. Baerends, *Inorg. Chem.*, **1994**, 33, 584-595.

[140] N. B. Mckeown, *The Porphyrin Handbook* (Kadish, K. M.; Smith, K. M.; Guilard, R., Eds.), Academic Press: Boston **2003**, 15, 61-124.

[141] R. F. Devlin, W. B. Dandliker, P. O. G. Arrhenius, *U.S. Patent 6,060,598*, **2000**.

[142] X. Y. Li, D. K. P. Ng, *Tetrahedron Lett.*, **2001**, 42, 305-309.

[143] R. P. Hammer, C. V. Owens, S. H. Hwang, C. M. Sayes, S. A. Soper, *Bioconj. Chem.*, **2002**, 13, 1244-1252.

[144] A. Ogunsipe, T. Nyokong, *J. Porphyrins Phthalocyanines*, **2005**, 9, 121-129.

[145] G. T. Walker, J. G. Nadeau, C. P. Linn, R. F. Devlin, W. B. Dandliker, *Clin. Chem.*, **1996**, 42, 9-13.

[146] D. C. Schindele, B. V. Pepich, G. E. Renzoni, K. L. Fearon, N. H. Andersen, T. H. Stanton, *U.S. Patent 5,494,793,* **1996**.

[147] W. M. Sharman, J. E. van Lier, C. M. Allen, *Adv. Drug Delivery Rev.*, **2004**, 56, 53-76.

[148] M. D. Savellano, T. Hasan, *Clin. Cancer Res.*, **2005**, 11, 1658-1668.

[149] R. Hudson, R. W. Boyle, *J. Porphyrins Phthalocyanines*, **2004**, 8, 954-975.

[150] R. Pérez-Soler, *The Oncologist*, **2004**, 9, 58-67.

[151] F. Meric-Bernstam, M.-C. Hung, *Clin. Cancer Res.*, **2006**, 12, 6326-6330.

[152] J.–P. Spano, C. Lagorce, D. Atlan, G. Milano, J. Domont, R. Bnamouzig, A. Attar, J. Benichou, A. Martin, J.–F. Morere, M. Raphael, F. Penault-Llorca, J.–L. Breau, R. Fagard, D. Khayat, P. Wind, *Ann. of Oncol.*, **2005**, 16, 102-108.

[153] G. Galizia, E. Iieto, F. Ferraraccio, F. De Vita, P. Castellano, M. Orditura, V. Imperatore, A. La Mura, G. La Manna, M. Pinto, G. Catalano, C. Pignatelli, F. Ciardiello, *Ann. of Surg. Oncol.*, **2006**, 13, 823-835.

[154] U. Dougherty, A. Sehdev, S. Cerda, R. Mustafi, N. Little, W. Yuan, S. Jagadeeswaran, A. Chumsangsri, J. Delgado, M. Tretiakova, L. Joseph, J. Hart, E. E. Cohen, L. Aluri, A. Fichera, M. Bissonnette, *Clin. Cancer Res.*, **2008**, 14, 2253-2262.

[155] J. Loeffler-Ragg, I. Schwentner, G. M. Sprinzl, H. Zwierzina, *Expert Opin. Investig. Drugs*, **2008**, 17, 1517-1531.

[156] G. Molema, *Acta Biochim. Polonica*, **2005**, 52, 301-310.

[157] K. Y. Dane, L. A. Chan, J. J. Rice, P. S. Daugherty, *J. Immun. Meth.*, **2006**, 309, 120-129.

[158] C. Frochot, B. D. Stasio, R. Vanderesse, M.-J. Belgy, M. Dodeller, F. Guillemin, M.-L. Viriot, M. Barberi-Heyob, *Bioorganic Chem.*, **2007**, 35, 205-220.

[159] S. X. Song, D. Liu, J. L. Peng, Y. Sun, Z. H. Li, J. R. Gu, Y. H. Xu, *Int. J. Pharmac.*, **2008**, 363, 155-161.

[160] S. Song, D. Liu, J. Peng, H. Deng, Y. Guo, L. X. Xu, A. D. Miller, Y. Xu, *FASEB J.*, **2009**, 23, 1396-1404.

[161] Z. Li, R. Zhao, X. Wu, Y. Sun, M. Yao, J. Li, Y. Xu, J. Gu, *FASEB J.*, **2005**, 19, 1978-1985.

[162] B. G. Ongarora, K. R. Fontenot, X. Hu, I. Sehgal, S. D. Satyanarayana-Jois, d. G. H. Vicente, *J. Med. Chem.*, **2012**, 55 (8), 3725-3738.

[163] Arnida; N. Nishiyama, N. Kanayama, W-D. Jang, Y. Yamasaki, K. Kataoka, *J. Controlled Release*, **2006**, 115(2), 208-215.

[164] T. Suzuki, M. Oishi, Y. Nagasaki, *J. Photopoyml. Sci. and Technol.*, **2009**, 22(4), 547-550.

[165] M. Bai, P-C. Lo, J. Ye, C. Wu, W-P. Fong, K. P. Ng Dennis, *Org. & Biomol. Chem.* **2011**, 9(20), 7028-7032.

[166] H. Li, F. R. Fronczek, M. G. H. Vicente, *Tetrahedron Lett.*, **2011**, 52, 6675-6678.

[167] J. Fang, T. Sawa, T. Akaike, K. Greish, H. Maeda, *Int. J. Cancer.* **2004**, 109, 1-8.

[168] K. Ichikawa, T. Hikita, N. Maeda, Y. Takeuchi, Y. Namba, N. Oku, *Biol. Pharm. Bull.*, **2004**, 27, 443-444.

[169] R. Argazzi, N. Y. M. Iha, H. Zabri, F. Odobel, C. A. Bignozzi, *Coord. Chem. Rev.*, **2004**, 248, 1299-1316.

[170] M. K. Nazeeruddin, S. M. Zakeeruddin, J.-J. Lagref, P. Liska, P. Comte, C. Barolo, G. Viscardi, K. Schenk, M. Grätzel, *Coord. Chem. Rev.*, **2004**, 248, 1317-1328.

[171] A. S. Polo, M. K. Itokazu, N. Y. M. Iha, *Coord. Chem. Rev.*, **2004**, 248, 1343-1361.

[172] G. J. Meyer, *Inorg. Chem.*, **2005**, 44, 6852-6864.

[173] N. Robertson, Angew. Chem., **2006**, 45, 2338-2345.

[174] P. Xie, F. Guo, *Curr. Org. Chem.*, **2007**, 11, 1272-1286.

[175] G. C. Vougioukalakis, A. I. Philippopoulos, T. Stergiopoulos, O. Falaras, *Coord. Chem. Rev.*, **2011**, 255, 2602– 2621.

[176] K. Hara, T. Sato, R. Katoh, A. Furube, Y. Ohga, A. Shinpo, S. Suga, K. Sayama, H. Sugihara, H. Arakawa, *J. Phys. Chem. B*, **2003**, 107, 597-606.

[177] C. A. Bignozzi, R. Argazzi, R. Boaretto, E. Busattoa, S. Carli, F. Ronconia, S. Caramori, *Coord. Chem. Rev.*, **2013**, 257, 1472–1492.

[178] W. L. Armarego, D. D. Perrin, *Purification of Laboratory Chemicals*, Vol. 4, Elsevier, Burlington, **1996**.

[179] Wilhelm Eckert, Ferdinand Quind, *US 2,200,689*, **1940**.

[180] K. A. Bronislavovich, K. O. Iosifovich, K. O. Iosifovich, E. S. Valentinova, *RU 2,269,536 C1*, **2006**.

[181] K. Takaki, Y. Yamasaki , *EP1418207 A1*, **2004**.

[182] H. E. Gottlieb, V. Kotlyar, A. Nudelman, *J. Org. Chem.*, **1997**, 62, 7512-7515.

[183] Stoe X-AREA and X-RED; Stoe & Cie GmbH: Darmstadt, Germany, **2001**.

[184] J. L. Farrugia, *J. Appl. Crystallogr.* **1999**, 32, 837–838.

[185] G. M. Sheldrick, *Shelxs-86*, Universität Göttingen, Göttingen, **1986**.

[186] G. M. Sheldrick, *Shelxl-97*, Universität Göttingen, Göttingen, **1997**.

[187] A. L. Spek, *PLATON*, A Multipurpose Crystallographic Tool, Utrecht University, Utrecht, The Netherlands, **2011**.

[188] K. Brandenburg, *Diamond Ver. 3.0a*, Crystal Impact GbR, Bonn, **2005**.

[189] S. A. Mikhalenko, L. I. Solov'eva, E. A. Luk'yanets, *J. Gen. Chem. USSR*, **1988**, 58, 2618-2619.

[190] S. A. Mikhalenko, L. I. Solov'eva, E. A. Luk'yanets, *J. Gen. Chem. USSR*, **1991**, 61, 996-1003.

[191] D. D. Coffman, E. L. Jenner, R.D. Lipscomb, *J. Am. Chem. Soc.*, **1958**, 80, 2864-2872.

[192] P. Jones, G. B. Villeneuve, C. Fei, J. DeMarte, A. J. Haggarty, K. T. Nwe, D. A. Martin, A.-M. Lebuis, J. M. Finkelstein, B. J. Gour-Salin, T. H. Chan, B. R. Leyland-Jones, *J. Med. Chem.*, **1998**, 41, 3062-3077.

[193] E. Seikel, B. Oelkers, O. Burghaus, J. Sundermeyer, *Inorg. Chem.*, **2013**, 52, 4451-4457.

[194] D. G. Rodriguez, T. Torres, D. M. Guldi, J. Rivera, M. A. Herranz, L. Echegoyen, *J. Am. Chem. Soc.*, **2004**, 126, 6301-6313.

[195] a)T. Suzuki, Y. Nagate, K. Mitsuhashi, *J. Heterocycl. Chem.*, **1986**, 23, 1419-1421. b) E. H. Morkved, L. T. Holmass, H. Kjosen, G. Hvistendahl, *Acta Chem. Scand.*, **1996**, 50, 1153-1156.

[196] E. Seikel, B. Oelkers, J. Sundermeyer, *Inorg. Chem.*, **2012**, 51, 2709-2717.

[197] E. Seikel, M. Grau, R. Käsmarker, B. Oelkers, J. Sundermeyer, *Inorg. Chem. Acta*, **2011**, 374, 119-126.

[198] Elizabeth Seikel, *Dissertation*, Philipps Universität Marburg, **2012.**

[199] P. Tau, T. Nyokong, *Polyhedron*, **2006**, 25, 1802-1810.

[200] J. Mark, M. J. Stillman, *J. Am. Chem. Soc.*, **1994**, 116, 1292-1304.

[201] P. Tau, T. Nyokong, *Dalton Transactions*, **2006**, 4482–4490.

[202] M. J. Stillman and T. Nyokong, in *Phthalocyanines: Properties and Applications*, (C. C. Leznoff, A. B. P. Lever), Vol. 1, chapter 3, VCH, New York, USA, **1989**.

[203] E. A. Ough, T. Nyokong, K. A. M. Creber, M. J. Stillman, *Inorg. Chem.*, **1988**, 27, 2724.

[204] K. Ejsmont, R. Kubiak, *Acta Crystallogr. C*, **1998**, 54, 1844-1846.

[205] P. A. Barrett, C. E. Dent, R. P. Linstead, *J. Chem. Soc.*, **1936**, 1719-1736.

[206] C Baffert, S. W. Feldberg, A. M. Bond, D-.L. Longb, L. Croni, *Dalton Trans.* **2007**, 4599–4607.

[207] N. P. Rodrigues, J. Obirai, T. Nyokong, F. Bedioui, *Electroanalysis*, **2005**, 17, 186.

[208] J. Obirai, T. Nyokong, *Electrochimica Acta*, **2005**, 50, 5427-5434.

[209] C. C. Leznoff, L. S. Black, A. Hiebert, P. W. Causey, D. Christendat, A.B.P. Lever, *Inorg. Chim. Acta*, **2006**, 359, 2690–2699.

[210] B. Agboola, K. I. Ozoemena, P. Westbroek, T. Nyokong, *Electrochimica Acta*, **2007**, 52, 2520–2526.

[211]A. Koca, A. R. Ozkaya, M. Selcukoglu, E. Hamuryudan, *Electrochimica Acta*, **2007**, 52, 2683–2690.

[212] Z. Odabas, H. Kara, A. R. Ozkaya, M. Bulut, *Polyhedron*, **2012**, 39, 38–47.

[213] J. Obirai, N. P. Rodrigues, F. Bedioui, T. Nyokong, *J. Porphyrins Phthalocyanines*, **2003**, 7, 508-520.

[214] G. Mbambisa, P. Tau, E. Antunes, T. Nyokong, *Polyhedron*, **2007**, 26, 5355–5364

[215] D. W. Smith, R. J. P. Williams, *Struct. Bonding (Berlin)*, **1970**, 7, 1-45.

[216] T. Yamamoto, T. Nozawa, N. Kobayashi, M. Hatano, *Bull. Chem. Soc. Jpn.*, **1982**, 55, 3059-3063.

[217] N. Kobayashi, M. Koshiyama, T. Osa, *Chem. Lett.*, **1983**, 163-166.

[218] L. K. Lee, N. H. Sabelli, P. R. LeBreton, *J. Chem. Phys.*, **1982**, 86, 3926-3931.

[219] N. Kobayashi, M. Koshiyama, K. Funayama, T. Osa, H. Shirai, K. Hanabusa, *J. Chem. Soc., Chem. Commun.*, **1983**, 913-914.

[220] R. Li, D. Qi, J. Jiang, Y. Bian, *J. Porphyrins Phthalocyanines*, **2010**, 14, 421–437.

[221] Y. Zhang, P. Ma, P. Zhu, X. Zhang, Y. Gao, D. Qi, Y. Bian, N. Kobayashid, J. Jiang, *J. Mater. Chem.*, **2011**, 21, 6515-6524.

[222] H. Onay, B. Esat, R. Öztürk, *Polyhedron.* **2010**, 29, 1314–1316.

[223] R. Taube, *Z. Chem.*, **1963**, 3, 194-195.

[224] G. Zanotti, N. Angelini, A. M. Paoletti, G. Pennesi, G. Rossi, A. A. Bonapasta, G. Mattioli, A. D. Carlo, T. M. Brown, A. Lembo, A. Reale, *Dalton Trans.*, **2011**, 40, 38-40.

[225] T. Ikeuchi, H. Nomoto, N. Masaki, M. J. Griffith, S. Mori, M. Kimura, *Chem. Commun.*, **2014**, 50, 1941-1943.

[226] A. N. Komissarov, D. A. Makarov, O. A. Yuzhakova, L. P. Savvina, N. A. Kuznetsova, O. L. Kaliya, E. A. Lukyanets, V. M. Negrimovsky, *Macroheterocycles*, **2012**, 5(2), 169-174.

[227] N. W. Polaske, H.-C. Lin, A. Tang, M. Mayukh, L. E. Oquendo, J. T. Green, E. L. Ratcliff, N. R. Armstrong, S. Scott Saavedra, D. V. McGrath, *Langmuir,* **2011**, 27, 14900–14909.

[228] H.-C. Lin, N. W. Polaske, L. E. Oquendo, M. Gliboff, K. M. Knesting, D. Nordlund, D. S. Ginger, E. L. Ratcliff, B. M. Beam, N. R. Armstrong, D. V. McGrath, S. S. Saavedra, *J. Phys. Chem. Lett.*, **2012**, 3, 1154–1158.

[229] M. Barthel, M. Hanack, *J. Porphyrins Phthalocyanines,* **2000**, 4, 635-638.

[230] W. Darwish, E. Seikel, R. Käsmarker, K. Harms, J. Sundermeyer, *Dalton Trans.,* **2011**, 40, 1787-1794.

[231] M. Barthel, D. Dini, S. Vagin, M. Hanack, *Eur. J. Org. Chem.*, **2002**, 2002, 3756-3762.

[232] W.-F. Law, R. C. W. Liu, J. Jiang, D. K. P. Ng, *Inorg. Chim. Acta*, **1997**, 256, 147-150.

[233] O. V. Dolotova, N. I. Bundina, O. L. Kaliya, E. A. Lukyanets, *J. Porphyrins Phthalocyanines*, **1997**, 1, 355-366.

[234] O. Dolotova, A. Konarev, K. Volkov, V. Negrimovsky, O. L. Kaliya, *J. Porphyrins Phthalocyanines*, **2012**, 16, 946.

[235] C. H. Griffith, M. Griffiths, S. Walker, P. Goldstein, *Mol. Cryst. Liq. Cryst.*, **1976**, 33, 149-170.

[236] R. F. Ziolo, C. H. Griffiths, J. M. Troup, *J. Chem. Soc., Dalton Trans.*, **1980**, 2300-2302.

[237] L. Lapok, M. Lener, O. Tsaryova, S. Nagel, C. Keil, R. Gerdes, D. Schlettwein, S. M. Gorun, *Inorg. Chem.*, **2011**, 50, 4086–4091

[238] Y. Xu, S. Shi, *Appl. Magn. Reson.*, **1996**, 11, 1-6.

[239] L. J. Boucher, in *Coordination Chemistry of Macrocyclic Compounds*. (G. A. Melson), Plenum, New York, **1979**, p. 527.

[240] J. Janczak, *Acta Cryst.*, **2004**, C60, m330-m332

[241] R. Mason, G. A. Williams, P. E. Fielding, *J . Chem. Soc. Dalton Trans.*, **1979**, 676-683.

[242] C. G. Barraclough, R. L. Martin, S. Mitra, R. C. Sherwood, *J. Chem. Phys.*, **1970**, 53, 1638-1645.

[243] H. Miyoshi, H. Ohya-nishiguchi, Y. Deguchi, *Bull. Chem. Soc. Jpn.*, **1973**, 46(9), 2724-2728.

[244] J. M. Robertson, I. Woodward, *J. Chem. Soc.*, **1937**, 219-230.

[245] J. M. Robertson, *J. Chem. Soc.*, **1935**, 615-621.

[246] C. J. Brown, *J. Chem. Soc. A*, **1968**, 2488-2493.

[247] J. R. Hall, H. E. Hook, *Solid state physics*, Chichester: Wiley **1994**.

[248] R. A. Levy, *Principles of Solid State Physics*, Academic Press. **1968**.

[249] I. L. Duarte, M. Wang, R. H. Baker, M. Ince, M. V. M. Diaz, M. K. Nazeeruddin, T. Torres, M. Grätzel, *Angew. Chem.*, **2012**, 51, 1895 –1898.

[250] M. Kandaz, M. N.U. Yarasir, A. Koca, O. Bekaroglu, *Polyhedron*, **2012**, 21, 255–263

[251] A.B.P. Lever, E.L. Milaeva, E. Speier, in The Phthalocyanines Properties and Applications, Vol. 3, (C.C. Leznoff, A.B.P. Lever), VCH Publishers, New York, **1993**, p. 42.

[252] I. Yilmaz, A. Gürek, V. Ahsen, *Polyhedron*, **2005**, 24, 791–798

[253] A.B.P. Lever, E.R. Milaeva, G. Speier, in *Phthalocyanines: Properties and Applications*, Vol. 3, (C.C. Leznoff, A.B.P. Lever), VCH Publishers, Weinheim, **1993**, pp. 1-69.

[254] A. A. Esenpınar, A. R. Özkaya, M. Bulut, *J. Org. Chem.*, **2011**, 696, 3873-3881.

[255] A. A. Esenpınar, A. R. Özkaya, M. Bulut, *J. Porphyrins Phthalocyanines*, **2009**, 13, 739-746.

[256] I. Yılmaz, M. Kandaz, A.R. Özkaya, A. Koca, *Monats. Chem.*, **2002**, 133, 609-647.

[257] M. Kandaz, A. R. Özkaya, A. Koca, *Transition Met. Chem.*, **2004**, 29, 847-854.

[258] I. Yilmaz, M. Kocak, *Polyhedron*, **2004**, 23, 1279-1285.

[259] M. Selcukoglu, E. Hamuryudan, *Dyes and Pigments*, **2007**, 74, 17-20.

[260] B. Agboola, K. I. Ozoemena, T. Nyokong, *Polyhedron*, **2009**, 28, 2831-2838.

[261] B. Agboola, K. I. Ozoemena, T. Nyokong, *Electrochimica Acta*, **2006**, 51, 4379-4387.

[262] M. Arıcı, D. Arıcan, A. L. Ugur, A. Erdogmuş, A. Koca, *Electrochimica Acta*, **2013**, 87, 554– 566.

[263] V. P. Chauke, Y. Arslanoglu, T. Nyokong, *Polyhedron*, **2011**, 30, 2132–2139.

[264] I. Özcesmeci, A. Koca, A. Gül, *Electrochimica Acta*, **2011**, 56, 5102–5114.

[265] J. Obirai, T. Nyokong, *Electrochimica Acta*, **2005**, 49, 1417-1428.

[266] J. Obirai, T. Nyokong, *Electrochimica Acta*, **2005**, 50, 3296-3304.

[267] A. R. Ozkaya, A. G. Gfirek, A. Gal, O. Bekarolu, *Polyhedron*, **1997**, 16(I1), 1877-1883.

[268] M. N. Yarasir, M. Kandaz, A. Koca, B. Salih, *Polyhedron*, **2007**, 26, 1139–1147.

[269] A. B. P. Lever, S. R. Pickens, P. C. Minor, S. Licoccia, B. S. Ramaswany, K. Magnell, *J. Am. Chem. Soc.*, **1981**, 103, 6800-6806.

[270] R. Li, X. Zhang, I. P. Zhu, D. K. P. Ng, N. Kobayashi, J. Jiang, *Inorg. Chem.*, **2006**, 45, 2327.

[271] A.B.P. Lever, E.R. Milaeva, G. Speier, in *Phthalocyanines: Properties and Applications*, 3, (C.C. Leznoff, A.B.P. Lever), VCH, New York, **1996**.

[272] M. L'Her, A. Pondaven, in *The Porphyrin Handbook*, Vol. 16, (K.M. Kadish, K.M. Smith, R. Guilard), Academic Press, Boston, **2003**, p. 117.

[273] I. Yilmaz, S. Arslan, S. Guney, I. Becerik, *Electrochimica Acta*, **2007**, 52, 6611–6621

[274] J. Silver, P. Lukes, P. Hey, M.T. Ahmet, *J. Mater. Chem.*, **1991**, 1 (5), 881.

[275] A. Koca, A. R. Ozkaya, Y. Arslanoglu, E. Hamuryudan, *Electrochimica Acta*, **2007**, 52 3216–3221.

[276] P. Tau, T. Nyokong, *Electrochimica Acta*, **2007**, 52, 3641–3650.

[277] S. E. Maree, *Dissertation*, Rhoods University, **2001**.

[278] J. Obirai, T. Nyokong, *Journal of Electoanalytical Chemistry*, **2004**, 573, 77-85.

[279] M. P. Donzello, R. Agostinetto, S. S. Ivanova, M. Fujimori, Y. Suzuki, H. Yoshikawa, J. Shen, K. Awaga, C. Ercolani, K. M. Kadish, P. A. Stuzhin, *Inorg. Chem.*, **2005**, 44, 8539, 8551.

[280] J. Cleary, L. E. Bromberg, E. Magner, *Langmuir*, **2003**, 19, 9162.

[281] A. J. Cunningham, A. L. Underwood, *Biochem.*, **1967**, 6, 266–271.

[282] H. T. Tien, *J. Phys. Chem.*, **1984**, 88, 3172–3174.

[283] P. M. Allemand, A. Koch, F. Wudl, Y. Rubin, F. Diederich, M. M. Alvarez, S. J. Anz, R. L. Whetten, *J. Am. Chem. Soc.*, **1991**, 113, 1050–1051.

[284] H. A. Azab, L. Banci, M. Borsari, C. Luchinat, M. Sola, M. S. Viezzoli, *Inorg. Chem.*, **1992**, 31, 4649–4655.

[285] N. Anicet, A. Anne, J. Moiroux, J. M. Saveant, *J. Am. Chem. Soc.*, **1998**, 120, 7115–7116.

[286] J. Zhang, A. M. Bond, *Analyst*, **2005**, 130, 1132–1147.

[287] E. I. Rogers, D. S. Silvester, D. L. Poole, L. Aldous, C. Hardacre, R. G. Compton, *J. Phys. Chem. C*, **2008**, 112, 2729–2735.

[288] G. Gritzner, *Pure Appl. Chem.*, **1990**, 62, 1839–1858.

[289] A. M. Bond, T. L. E. Henderson, D. R. Mann, T. F. Mann, W. Thormann, C. G. Zoski, *Anal. Chem.*, **1988**, 60, 1878–1882.

[290] M. I. Montenegro, D. J. Pletcher, *Electroanal. Chem. Interfacial Electrochem.*, **1986**, 200, 371–374.

[291] K. M. Kadish, C. H. Su, *J. Am. Chem. Soc.*, **1983**, 105, 177–180.

[292] N. Ito, T. Saji, S. Aoyagui, *J. Organomet. Chem.*, **1983**, 247, 301–305.

[293] J. Wang, *Analytical Electrchemistry, 1st Ed., VCH*, New York, **1994**, 1.

[294] T. Nyokong, *S. Afr. J. Chem.*, **1995**, 23, 48.

[295] N. S .Neghmouche, T. Lanez, *Recent Trends in Physical Chemistry: An International Journal*, **2013**, 1(1), 1-3.

[296] T. Morikita, T. Yamamoto, *J. Organomet. Chem*. **2001**, 809, 637–639.

[297] A. B. Sorokin, S. Mangematin and C. Pergrale, *J. Mol. Catal. A*, **2002**, 267, 182–183.

[298] L. A. Bottomley, J.-N. Gorce, V. L. Goedken, C. Ercolani, *Inorg. Chem.*, **1985**, 24, 3733.

[299] A. B. Sorokin, E. V. Kudrik, D. Bouchu, *Chem. Commun.*, **2008**, 2562–2564.

[300] D. Wohrle, Macromol. *Rapid Commun.*, **2001**, 22, 68.

[301] H. Wei-Ywan, C. Jian-Long, H. Li-Qing, *Bulletin de la societe chimique de France*, **1986**, 6, 881-884.

[302] M. Shigeyasu, S. Masakichi, F. Yasuo, T. Takashi, *Synthesis*, **1982**, 12, 1021-1023.

[303] F. Takashi, H. Toshikazu, O. Yoshiki, *Tetrahedron letters*, **1992**, 33(39), 5823-5826.

[304] J. N. Moorthy, K. Senapati, N. Singhal, *Tetrahedron Letters*, **2009**, 50, 2493–2496.

[305] G. W. Coates, D. R. Moore, *Angew. Chemie*, **2004**, 43, 6618 - 6639.

[306] X. -B. Lu, D. J. Darensbourg, *Chem. Soc. Rev.*, **2012**, 41, 1462–1484.

[307] Y. Chen, M. Hanack, W. J. Blau, D. Doni, Y. Liu, Y. Lin, J. Bai, *J. Mater. Sci.*, **2006**, 41, 2169-2185.

[308] J. P. Linsky, T. R. Paul, R.S. Nohr, M. E. Kenney, *Inorg. Chem.*, **1980**, 19, 3131-3135.

[309] K. J. Wynne, *Inorg. Chem.*, **1984**, 23(26), 4658-4663.

[310] Ogunsipe, A.; Nyokong, T. J. Mol. Struct. **2004**, 689, 89-97.

[311] N. Kobayashi, A.B.P. Lever, *J. Am. Chem. Soc.*, **1987**, 109, 7433-7441.

[312] H. Isago, *Chem. Commun.* **2003**, 1864-1865.

[313] N. A. Kuznetsova, D. A. Makarov, O. A. Yuzhakova, L. I. Solovieva, O. L. Kaliya, *J. Porphyrins Phthalocyanines*, **2010**, 14, 968-947.

[314] N. Alharbi, A. Diaz-Moscoso, G. J. Tizzard, S. J. Coles, *Tetrahedron*, **2014**, 70, 7370-7379.

[315] H. Ripperger, *Journal für Pratische Chemie* , **2014**, 329(6), 1039-1044.

[316] R. J. Blagg, L. Ungur, F. Tuna, J. Speak, P. Comar, D. Collison, W. Wernsdorfer, E. J. L. Mclnnes, L. F. Chibotaru, R. E. P. Winpenny, *Nature Chemistry*, **2013**, 5, 673-678.

[317] I. P. Gray, P. Bhattacharyya, A. M. Z. Slawin, J. D. Woollins, *Chem. Eur. J.* **2005**, 11, 6221 – 6227.

[318] J. Cheon, J. E. Gozum, G. S. Girolami, *Chem. Mater.,* **1997**, 9(8), 6221 – 6227.

[319] I. Chen, *Journal of Molecular Spectroscopy,* **1967**, 23, 144 – 148.

[320] Marius Klein, Master Research Project AC-MPR-2, Marburg 2015.

[321] T. Kavitha, A. Kulandaisamy, P. Thillaiarasu, *International Journal of ChemTech Research*, **2012**, 4(4), 1571– 1581.

[322] D. M. Roundhill, *Modern Inorganic Chemistry, Photochemistry and Photophysics of Metal Complexes,* ISBN 0-306-44694-4*, PLENUM, New York*, **1994**.

[323] Wael Darwish, *Dissertation*, Philipps Universität Marburg, **2006.**

[324] R. C. Pettersen, *Acta Cryst.*, **1969**, B25, 2527-2539.

[325] S. C. Manna, S. Mistri, A. D. Jana, *CrystEngComm.*, **2012**, 14, 7415– 7422.

[326] K. J. Wynne, *Inorg. Chem.* , **1985**, 24, 1339– 1343.

[327] B. Aßmann, H. Homborg, *Z. allg. Chem.,* **2012**, 622, 766– 770.

[328] J. A. Cissell, T. P. Vaid, A. L. Rheingold, *Inorg. Chem.* , **2006**, 45, 2367– 2369.

[329] F. Würthner, T. E. Kaiser, C. R. Saha-Möller, *Angew. Chem. Int. Ed.* **2011**, 50, 3376–3410.

[330] D. Wöhrle, G. Schnurpfeil, S. Makarov, O. Suvorova, *Chemie Unserer Zeit*, **2012**, 46, 12-24.

[331] M. K. Engel, in The Porphyrin Handbook, Vol. 20: *Phthalocyanines: Structural Characterization* (Eds.: K. M. Kadish, K. M. Smith, R. Guilard), Elsevier Science, San Diego, **2003**, 1-88.